Washington University in St. Louis
Washington University Open Scholarship

All Theses and Dissertations (ETDs)

January 2011

Increasing Energy Efficiency of HVAC Systems in Buildings Using Phase Change Material

Jared Daiber
Washington University in St. Louis

Follow this and additional works at: https://openscholarship.wustl.edu/etd

Recommended Citation
Daiber, Jared, "Increasing Energy Efficiency of HVAC Systems in Buildings Using Phase Change Material" (2011). *All Theses and Dissertations (ETDs)*. 465.
https://openscholarship.wustl.edu/etd/465

This Thesis is brought to you for free and open access by Washington University Open Scholarship. It has been accepted for inclusion in All Theses and Dissertations (ETDs) by an authorized administrator of Washington University Open Scholarship. For more information, please contact digital@wumail.wustl.edu.

WASHINGTON UNIVERSITY IN ST. LOUIS

School of Engineering and Applied Science

Department of Mechanical Engineering and Materials Science

Thesis Examination Committee:

Ramesh K. Agarwal

David Peters

Kenneth Jerina

INCREASING ENERGY EFFICIENCY OF HVAC SYSTEMS IN BUILDINGS USING PHASE CHANGE MATERIAL

by

Jared T. Daiber

A thesis presented to the School of Engineering and Applied Science

At Washington University in St. Louis in partial fulfillment of the

requirements for the degree of

MASTER OF SCIENCE

May 2011

St. Louis, Missouri

ABSTRACT OF THE THESIS

Increasing Energy Efficiency of HVAC Systems in Buildings Using Phase Change Material

by

Jared T. Daiber

Master of Science in Mechanical Engineering

Washington University in St. Louis, 2011

Research Advisor: Dr. Ramesh K. Agarwal

Using Computational Fluid Dynamics (CFD), four different cooling systems used in modern office and residential environments are modeled in order to gain insight into the relative energy consumptions and thermal comfort levels involved. Utilizing convection and radiation technologies, full-scale models of an outward facing office room are created to compare arrangements for (a) a Variable Air Volume (VAV) all overhead air system, (b) a combined VAV and hydronic radiant system, (c) a Displacement Ventilation (DV) all-air raised floor system, and (d) a combined DV and hydronic radiant system. The room model used for each computation consists of one isothermal wall (simulating the exterior wall of the building) and adiabatic conditions for the remaining five surfaces, which simulate the interior walls of the room. The exterior wall changes temperature as a function of time, simulating the temperature changes on the exterior wall of a building throughout a 24 hour period. Two sets of computations were conducted, both utilizing the same exterior wall temperature condition. The first set utilized a glass window and plastic shade configuration for the exterior wall to compare the 4 cooling schemes. The second set of computations utilized a different configuration for the exterior wall to examine the effect of a phase change material (PCM) on the cooling energy requirements. Results show superior thermal comfort levels as well as substantial energy savings can be accrued using the displacement ventilation with a chilled ceiling system (d) over the conventional mixing ventilation system (a). The results also show that the addition of a PCM layer to the exterior wall could significantly decrease the cooling energy requirements.

Acknowledgements

Thanks to Dr. Ramesh Agarwal for his help and guidance throughout my endeavors in the CFD lab, and helping me to better understand the research mindset. Thanks to Lee Chusak for his help and experience in working out the many difficulties involved in tackling a computational modeling problem.

Jared T. Daiber

Washington University in St. Louis

May 2011

Table of Contents

List of Tables

List of Figures

Chapter 1: Introduction

1.1 Motivation

Concerns for the future of our planet's environment in recent years have shifted the focus of a large portion of research and design efforts to accommodate the need for more energy sensible lifestyles. These concerns arise mainly from the increasing amounts of damage done to our environment by the release of carbon dioxide and other greenhouse gas emissions. By targeting the building sector, which is the overall largest energy consuming sector in the US (Figure 1), the most significant impact can be made by any success in energy efficiency; therefore a relatively small decrease in energy usage in the building sector becomes significantly more effective due to its large scale use of energy. Buildings are by far the biggest consumer of electricity (Figure 2), and almost half of all the electricity generated in the United States comes from the combustion of coal (Figure 3). Coal combustion is an extremely harmful process to the environment, due to the production of greenhouse gases such as carbon dioxide, and this process produces over a third of the carbon dioxide produced from energy sources in the US (Figure 4). In order to decrease this output of greenhouse gases, there is a need to cut back on the amount of energy consumed in buildings in the US, and in order to achieve this reduction we need to address one of the biggest areas of energy consumption in buildings, which is the Heating, Ventilation, and Air Conditioning (HVAC) system. "With the consolidation of the demand for thermal comfort, HVAC systems (and its associated energy consumption) have become an unavoidable asset, accounting for almost half the energy consumed in buildings." [Perez-Lombard 2008(12)]

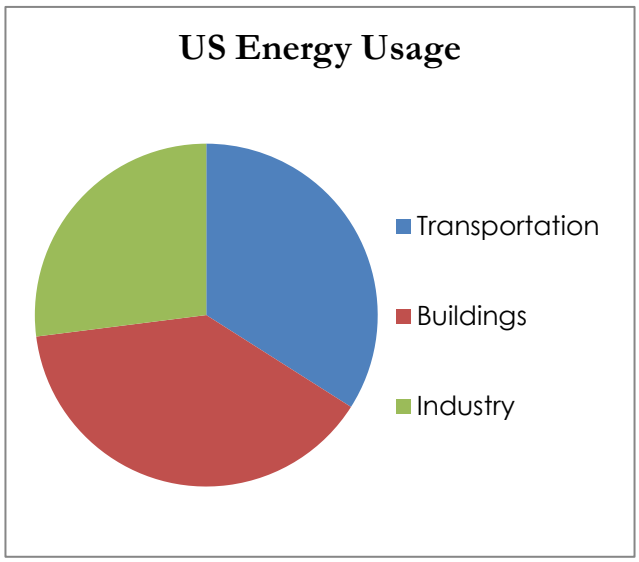

Figure 1: US Energy Usage by Sector [Building Energy Codes Program(13)]

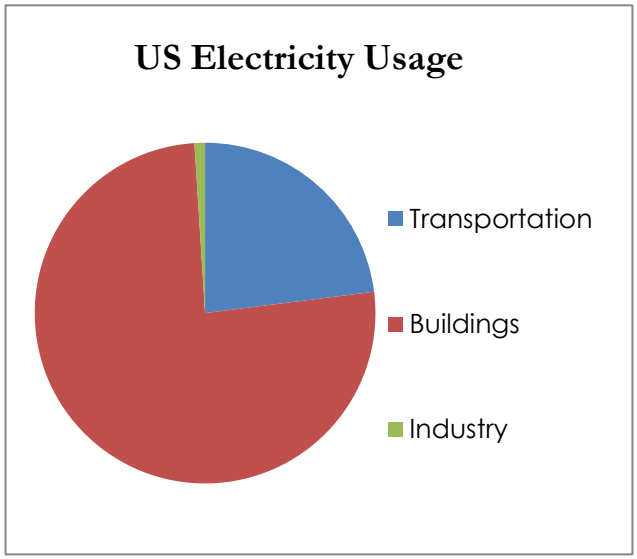

Figure 2: Electricity Use in the US by Sector [Architecture 2030 (16)]

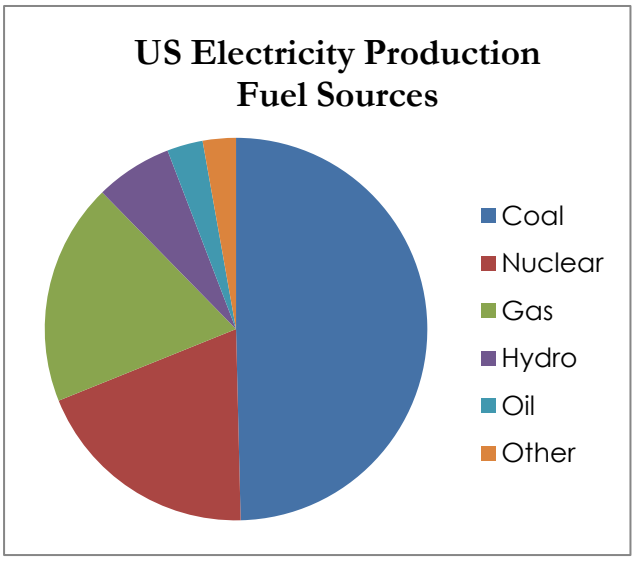

Figure 3: Electricity Production by Fuel Source [Clean Energy (14)]

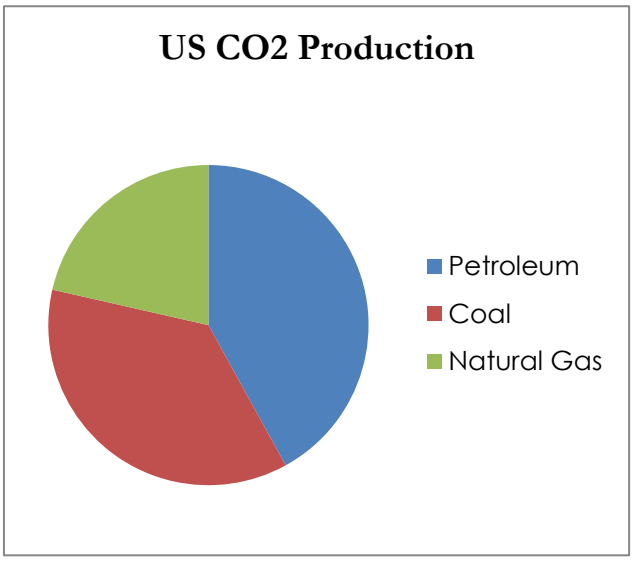

Figure 4: US Carbon Dioxide Production by Fuel Source [Energy Information Administration (15)]

1.2 Improving HVAC Efficiency

HVAC systems are integral to a building's ability to maintain a confortable space for a wide variety of usages, and thus are tailored to meet different needs for thermal control. Buildings with different purposes and in different climates require different amounts of heating and cooling, in addition to specific humidification requirements. Therefore it isn't possible to create one system to apply universally to every type of building, even within a geographical region. Some of the factors that affect overall heating and cooling loads in a building include the environment inside the building (equipment, people, etc.), the construction of the building itself, and the climate (or external environment). In terms of the construction of the building, increased insulation in the wall can decrease the peak heating and cooling demand by increasing the time it takes for the external conditions to affect the interior of the building. Thus the type of construction and the material used can affect the size of the HVAC system; a smaller HVAC system may be allowed in well-constructed buildings with high grade insulation. When considering cooling systems, building orientation can also affect the load on the system. Due to the orientation of the sun during the day, the east and west walls receive the most direct sunlight, therefore by limiting the amount of west and east facing wall area, and especially the number of windows on these walls, the cooling load can be significantly decreased. In addition to HVAC loads, indoor lighting can be a major consumer of electricity, and therefore "by introducing daylighting control, as a measure of saving lighting electricity energy, significant savings in cooling energy are also obtained." [Korolija 2011(17)]

1.3 Scope of the Thesis

1.3.1 Objectives of the Thesis

The main objective of the research conducted in this thesis is to compare the energy efficiency of four different ventilation systems by employing the tools of Computational Fluid Dynamics and Heat Transfer. In particular, a typical office room of 12' (length) x 12' (width) x 9'6" (height) is considered to analyze the energy efficiency of: (a) standard Variable Air Volume (VAV) system, (b) a VAV system with radiant cooling (hydronic system), (c) the Distributed Ventilation (DV) system, and (d) a DV system with radiant cooling (using a radiation slab with chilled water in the room's ceiling). The VAV system, and the VAV system with radiant cooling are also studied with the inclusion of a Phase Change Material (PCM) layer in the external wall treatment (which is made of a glass layer and a curtain) to evaluate the effects of the PCM layer on the energy efficiency of the two ventilation systems. These two objectives are described in greater detail in sections 1.3.2, and 1.3.3 below.

In the CFD calculations using FLUENT, we solve the Unsteady Reynolds Averaged Navier-Stokes (URANS) equations. These equations require the choice of a turbulence model to describe the turbulent eddy viscosity. The choice of the turbulence model does affect the accuracy of the solution. In addition, because of the low speed nature of the flow in this problem, we employ the incompressible form of the equations. However, the effects of buoyancy are important to consider in such flows, which can be modeled by the Boussinesq approximation within the incompressible formulation. Another objective of this thesis is to investigate the effect of the choice of turbulence model and the Boussinesq

approximation on the solution accuracy. These two objectives are described in greater detail in sections 1.3.4 and 1.3.5 below.

1.3.2 Study of Various Cooling Systems for a 3-D Model of an Office Room without Phase Change Material

The Computational Fluid Dynamics software FLUENT is employed to study the fluid flow and heat transfer inside a typical office room of dimensions 12' (length) x 12' (width) x 9'6" (height). Four cooling systems are studied to evaluate their energy efficiency and thermal comfort. These systems include (a) a variable air volume (VAV) overhead system, (b) a combined VAV and hydronic radiant cooling system (variable air volume system with a chilled ceiling), (c) a displacement ventilation (DV) all-air raised floor system, and (d) a combined DV and hydronic radiant cooling system (displacement ventilation with a chilled ceiling). In the computations it is assumed that the 3-D model of the room consists of one wall with specified temperature which varies during a 24-hour period (simulating the exterior wall of the building) and adiabatic conditions for the remaining five surfaces, which simulate the interior walls of the room. The exterior wall changes temperature as a function of time, simulating the temperature changes on the exterior wall of a building during a 24 hour period for a particular location and day of the year. We employ the temperature curve given by the American Society of Heating, Refrigeration and Air Conditioning Engineers (ASHRAE) for St. Louis during a typical summer day in July. The construction of the external wall of the room consists of a 1" glass window, followed by a 1" air space, followed by a 1/32" plastic shade to represent a standard window treatment. The results of calculations of flow fields and heat transfer for these four cases are given in Chapter 5. Chapter 5 also compares the energy efficiency of the four cooling systems.

1.3.3 Study of Various Cooling Systems for a 3-D Model of an Office Room with Phase Change Material

Two of the four cooling systems mentioned in section 1.3.2 are recomputed by including a layer of Phase Change Material (PCM) between the 1" air space and the 1/32" plastic shade in the window treatment. The PCM layer is made of material which melts at some higher temperature and then freezes at a lower temperature (some types of commercial PCMs include Rubitherm, Outlast, etc.). Thus the phase change material changes phase from solid to liquid and vice-versa in a material specific temperature band. During the melting phase, it absorbs energy at a higher temperature and in the solidification phase, it releases energy at a lower temperature. Thus during the hotter part of the day, it can absorb energy and not transmit it inside the room, and during the cooler part of the day, it can release energy inside the room. Thus PCM can be very effective in reducing the cooling loads and thereby improve the energy efficiency. For the calculations with the PCM layer, we employ the ASHRAE SolAir calculation procedure which approximates all the heat transfer from convection, conduction and radiation on the surface of a building with an equivalent temperature. We consider the SolAir temperature for Sioux Falls, SD in our calculations. We employ two different types of PCM layers in our analysis and compare the effectiveness of the different PCM layers (different in material and thickness) for energy efficiency. The results showing the influence of a PCM layer on heat transfer and energy efficiency are given in Chapter 6. We also compare the energy efficiency of the different PCM cases tested.

1.3.4 Turbulence Model

The two most commonly used turbulence models for the computation of low speed flows are the one-equation Spalart-Allmaras (S-A) model, and the two-equation models: k-ε, k-ω, and Shear Stress Transport (SST). In order to evaluate the relative accuracy of one- and two-equation turbulence models, we consider the S-A model and the realizable k-ε model. The computations are performed for the VAV case (without a PCM layer) on the same grid, and using the same numerical algorithm. The results of these computations are given in Chapter 3. Based on these results, it is concluded that there is not much difference (≈ 1%) in the calculations using the two models. Although the computations with the k-ε model require more computational time (since two equations are solved instead of one), it was concluded that this is a better model because of the three-dimensional nature of the computational domain with significant vortical flow.

1.3.5 Buoyancy Model

Although it is fairly obvious that the varying air density in the room affects the fluid motion and should be included in the analysis, it was decided to evaluate its effect relative to a constant density approximation. This changing air density affects the air buoyancy, and this buoyancy effect was modeled using the Boussinesq approximation in the vertical direction. Again the overhead ventilation system with Variable Air Volume (VAV) was considered for this comparison between the Boussinesq approximation for density versus the constant density approximation. The results of this comparison are given in Chapter 4. As a result of these comparisons, it was decided to use the Boussinesq approximation in all the calculations reported in this thesis.

Chapter 2: Ventilation Systems Literature Survey

2.1 Variable Air Volume (VAV) Ventilation

One of the primary considerations in the construction of a modern office or residential building is the total cost; the life cycle cost analysis is rarely conducted. As a result, the energy costs during the life of the building due to the choice of HVAC system are also rarely considered. This situation is slowly changing due to the efforts of ASHRAE and the Leadership in Energy and Environmental Design (LEED), however most of the focus concerning the energy efficiency of an HVAC system remains on limiting the amount of unconditioned air infiltrating the building space through cracks in the outer construction and on utilizing building materials with high thermal insulation. While these steps are important, more effort is needed to be focused on selecting and deploying a ventilation system that can deliver the conditioned air more efficiently. The majority of currently deployed HVAC systems are VAV systems which employ all-air overhead ventilation. The performance of a VAV system relies on the turbulent mixing of existing room air with conditioned air which is not an efficient way to condition the air. As a result, a large quantity of conditioned air is introduced at one location in the ceiling at a higher velocity, and the system depends on the high volume and speed of the air for it to get distributed sufficiently throughout the room.

The typical internal heat loads observed in an office room consist of heat plumes created from occupants, lights, and office equipment; conventional offices and industrial building designs use this criterion for ventilation rather than to provide adequate air for

respiration for the inhabitants. This is due to the fact that ASHRAE standards require about 7.5 liter/sec per person for respiration, while typical air changes needed for thermal comfort in an office require at least ten times this amount [Linden(1)]. Despite this apparent inefficiency, this type of HVAC system is common due to the low initial construction and maintenance costs. Despite the low initial cost of VAV ventilation, it is now recognized that considerable progress towards increasing the energy efficiency of buildings can be made by considering alternatives to this generally developed HVAC system.

2.2 Displacement Ventilation (DV)

DV systems are widely considered to be superior to the standard VAV systems for several reasons. Displacement Ventilation consists of a conditioned air delivery system in which ventilated air is dispersed at low speeds along the floor and absorbs heat from various internal sources such as lights, equipment and people causing this air to rise to the top, where it displaces the air near the ceiling, forcing it out of the ventilation outlets. This type of system results in more efficient air changes, because the air is generally moving up as it gains heat resulting in less turbulence and making it more effective at removing contaminants than conventional turbulent mixing VAV ventilation. This increased efficiency allows the same ASHRAE ventilation criteria to be met with less air overall, requiring about half as much airflow rate when compared to standard VAV system [Ürge-Vorsatz (2)]. One of the largest sources of efficiency in an HVAC system can result by allowing the use of slightly warmer supply air, which allows for smaller and less powerful air conditioning equipment to be deployed. This decreases both the initial cost of the system as well as the electricity

requirements for operating the HVAC system. This feature increases the attractiveness of DV systems, since they are able to operate with about 5° C higher supply air temperature than VAV systems for the same thermal comfort level, reducing the chilling load significantly. All these effects can result in reduced energy requirement for cooling and ventilation by about 30-60% for DV systems, depending on the climate of the region, which determines the outdoor air temperatures and the humidity [Bourassa(3); Howe(4)].

2.3 Radiant Cooling Systems

The last cooling scheme to be analyzed in this thesis is the hydronic radiant cooling system which can be added to either the VAV or DV systems described in sections 2.1 and 2.2 respectively to significantly increase the cooling efficiency. This increase in efficiency is a result of the fact that this system uses chilled water to radiate cooling into the room; it is well known that a water chilled container is much more efficient at transferring colder energy from one location to another through radiation than the mixing of cold air with existing hot air. Furthermore, the effectiveness of using water to cool a room is amplified by the fact that cold water can be supplied at about 16-20º C compared to the temperature of 5-7º C needed chill the air in air-only systems. This results in an additional decrease in the size of equipment needed, leading to a reduced operating power demand and initial cost. In some cases water doesn't even have to be chilled specifically for the purpose of running through the radiant cooling system, but can also be used to chill the air required before being pumped into the radiant cooling slab.

Although a radiant cooling system alone cannot meet the HVAC requirements for a room since it cannot ventilate the space, it can reduce a significant portion of the cooling load for the air system. This allows a reduction in the amount of air cooling required to not more than the ventilation needs; instead of recirculating up to 80% of the return air from the room and introducing 20% fresh outdoor air, more outdoor air can be used because it doesn't need to be cooled as much before entering the room. This allows for a much healthier airspace in the room, because contaminants in the air get removed from the system more quickly [Harvey (5)].

2.4 Phase Change Materials

In recent years it has been proposed that one way of reducing the cooling loads on HVAC systems is the inclusion of Phase Change Materials (PCM) in the construction of the building. A PCM is a material which is constructed with specific temperatures at which it melts and solidifies, changing phase from solid to liquid, and vice versa. This enables it to absorb significant amounts of energy in the liquid phase at higher external temperatures, thereby preventing the energy from outside to enter the room and heat it up during the day. However, in the evening when the outside temperatures are lower, the PCM material begins to solidify, releasing the stored energy in the melting phase inside the room, thereby raising the temperature inside the room to a comfortable level. The energy absorbed by the PCM as it melts at higher temperatures and then released as it solidifies at lower temperatures reduces the peak demand on the HVAC system during the day. When a PCM reaches its

melting temperature, it can effectively absorb a large amount of heat while remaining at a nearly constant temperature, preventing most of that heat from being transferred into the room. Most PCMs are capable of storing 5 to 14 times more heat per unit volume than conventional energy storage materials such as concrete, rock and even water [Sharma (18)]. This behavior of PCM reduces the cooling load on the HVAC system, thereby requiring a smaller system for cooling; HVAC systems are typically designed to satisfy the largest cooling demand on the hottest day of the year. Thus, the use of PCM allows for the installation of a smaller, more energy efficient and less costly HVAC system.

Chapter 3: Evaluation of One- and Two-Equation Turbulence Models for a 3-D Room with a VAV System

3.1 Turbulence Models

The choice of a turbulence model can have a significant influence on the accuracy of the CFD solution. For 3-D flows in complex geometries, it is generally agreed that at least a two-equation turbulence model should be employed since it determines the length and time scales in the entire domain by using the physical quantities such as turbulent kinetic energy (k) and turbulent dissipation (ε), each of which is modeled by a transport equation. In contrast, a one-equation turbulence model such as the Spalart-Allmaras (S-A) model requires a guess of the length scale in order to determine the eddy viscosity which is required for solving the Unsteady Reynolds-Averaged Navier-Stokes equations (URANS). In this chapter, we present results of calculations for the flow field inside a 3-D model of a room with a VAV ventilation system using the one-equation S-A model and the two-equation realizable k-ε model. Here we only present the overall result for the energy efficiency; the detailed flow field calculations for this system with realizable k-ε model are given in Chapter 5.

3.2 Results

The computations for the VAV system for a model 3-D room were performed using the S-A model and the realizable k-ε model for two consecutive 24-hour cycles each. During the second 24-hour cycle, all the transient effects due to initial conditions had died down and the results were recorded. The energy removed from the room to maintain the temperature inside the room within the controller band was calculated by the following equation:

$$\int \dot{m} * C_p * (T_{outlet-vent} - T_{cold-jet}) dt \tag{3.1}$$

The energy removed from the room by a ventilation system is an excellent indicator of its efficiency. Figure 5 shows the total amount of energy removed from the room by the VAV system using two different turbulence models. A time step of 10 seconds was used in the computations, therefore 8640 time steps are equivalent to a 24 hour period.

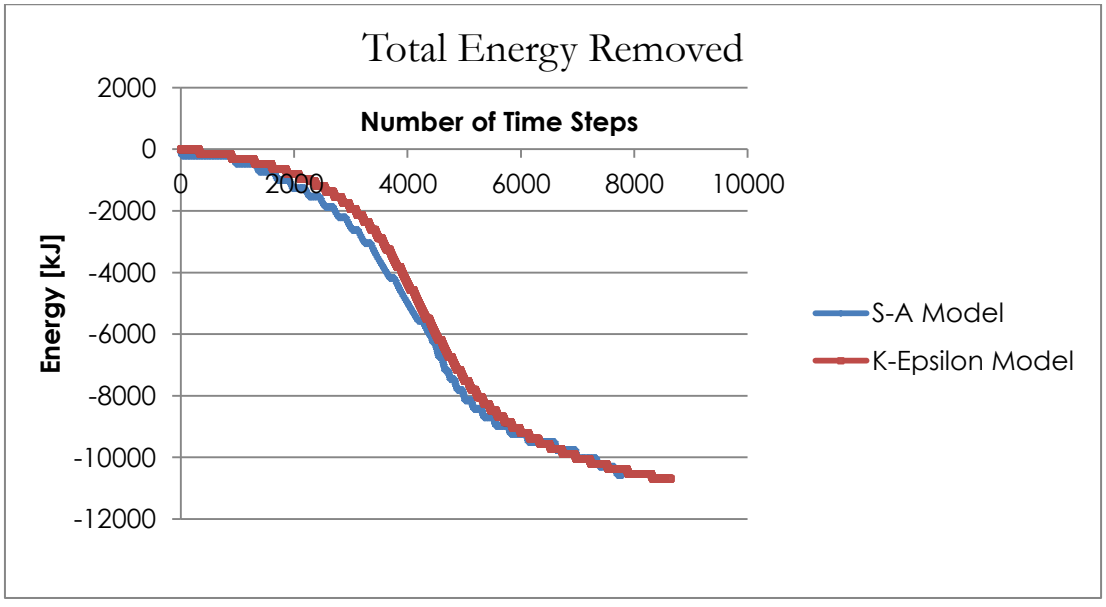

Figure 5: Energy Removed by the VAV System Using S-A and k-ε Models

Figure 5 shows that there is very little difference between the results for the energy removed from the room using two different turbulence models; the difference between the two results is less than 1%. This result is very encouraging. Although both the S-A and k-ε models appear to be equally accurate and the S-A model is computationally more efficient, we choose to use the generally accepted wisdom and employ the realizable k-ε model in all the computations reported in this thesis in Chapters 4 and 5. However, we take advantage of these findings and use the increased computational efficiency of the S-A turbulence model for the analysis of the 3-D room with an added PCM layer in Chapter 6.

Chapter 4: Evaluation of Two Density Models for a 3-D Room with a VAV System

4.1 Boussinesq Approximation

Although the flow inside an office room is of very low velocity, it is driven by natural convection. Therefore the inclusion of the effect of buoyancy in a CFD simulation can be very important. The effects of buoyancy can be modeled by employing the Boussinesq approximation in the momentum equation in the vertical direction (the direction of gravity's effects). In this chapter, we evaluate the influence of buoyancy by considering the 3-D model room with a VAV ventilation system. We perform two calculations, one with constant density throughout and the other with density variation using the Boussinesq approximation. The results of these calculations are given in the following section.

4.2 Results

The computations for the VAV system were performed using the constant density throughout the room for one, and by employing the Boussinesq approximation for density variation for the other. The computations were performed for two consecutive 24-hour cycles for each case. During the second 24-hour cycle, all the transient effects due to initial conditions had died down and the results were recorded. By calculating the energy required by the ventilation system, we can assess its energy efficiency. The energy input into the

system was calculated using equation 4.1 below; it represents the amount of energy required to keep the room within the band of comfortable temperatures monitored by the temperature controller.

$$\int \dot{m} * C_p * (T_{outside} - T_{cold-jet}) dt \tag{4.1}$$

Figure 6 shows the total amount of energy input for cooling the air entering the room in order to keep the temperature within the comfortable range maintained by the temperature controller.

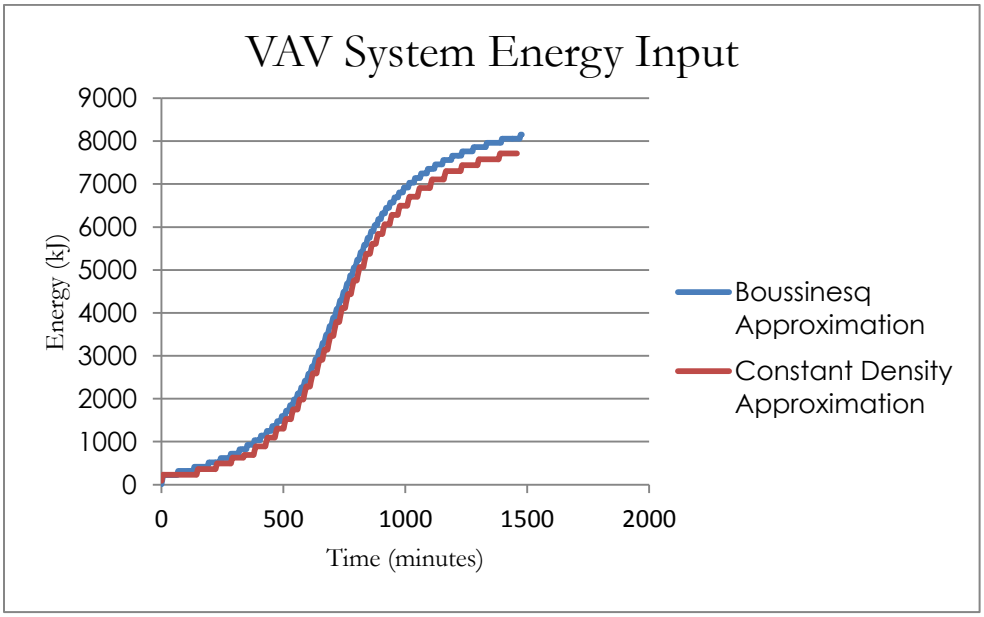

Figure 6: Comparison of Energy Input into the Room with a VAV System Using a Constant Density Approximation and the Boussinesq Approximation

Figure 6 shows that the calculation for total energy input using the constant density approximation has a 5.38% lower value than that obtained by using the Boussinesq approximation. This is a significant difference. However, it is an expected result; the influence of the buoyancy is to increase the thermal load on the system. Considering the physical realism of the model represented by the Boussinesq approximation, all the calculations reported in this thesis employ this model.

Chapter 5: 3-D Ventilation System Models and Analyses

5.1 Computational Solver

Using two ANSYS computer codes, GAMBIT [ANSYS Inc.] and FLUENT [ANSYS Inc.], four different HVAC systems are modeled for the same room geometry. GAMBIT was used to create the geometry of the room to be modeled, as well as to generate the mesh inside the room. GAMBIT allows the user to specify the type of mesh (structured, unstructured, or hybrid), as well as its topology and distribution. This program also allows the specification of various types of boundary conditions on different surfaces surrounding the room; some surfaces are designated as adiabatic walls, isothermal walls, or mass flow inlets and outlets. The areas which are not designated with a boundary condition are labeled as either a fluid or a solid and are used in the computation of the behavior of the system. This mesh is then exported for use by a CFD code, such as FLUENT.

FLUENT is a general-purpose CFD code which solves the Unsteady Reynolds-Averaged Navier-Stokes (URANS) equations using the finite-volume method on a collocated grid. Using a versatile interface, this program is capable of modeling fluid flow and heat transfer in and around complex geometries in both two and three dimensions. It can perform both steady and unsteady simulations. FLUENT also has the capability of solving incompressible and compressible flows for inviscid, laminar, or a turbulent fluid. For URANS equations, the effects of turbulence can be modeled by employing a wide variety of

turbulent eddy viscosity models, including the one-equation Spalart-Allmaras (S-A), and two-equation k-ω and k-ε (standard, RNG, Realizable) models.

5.2 3-D Model of an Office Room

For the purpose of comparing the four different ventilation systems, the same 3-D model of an office room was employed in the numerical simulations. In all cases, the initial starting values of temperature, T_0=288.16 K, and density, ϱ_0= 1.225 kg/m^3, were employed. The Discrete-Ordinate method for the radiation calculation was also employed. The governing equations were solved using the First-Order-Upwind scheme and the pressure was calculated using the PRESTO! scheme. The SIMPLE algorithm was employed for coupling the velocity and pressure. The k-ε (RNG) model, which uses two equations to calculate the turbulent eddy viscosity, was used in all computations. The Boussinesq approximation for density was utilized to simulate the buoyancy effects. For each case, the solution process was initiated using the initial conditions and the solution was computed at various time steps for a 24-hour cycle. This solution was then used to calculate the flow field for a second 24-hour ASHRAE cycle and the results were recorded. The solution for the second cycle was utilized for analysis because it was free of transient effects due to the initial conditions.

5.2.1 Temperature Controller

In order to monitor and maintain the temperature control in the room, a temperature controller was developed to operate like a thermostat; it was designed to maintain the temperature in the room within a band of temperatures deemed comfortable,

i.e. between 72.4F and 76.0F (295.6K and 297.6K). The controller was included as a point in the mesh that read the temperature 3" in front of the rear wall and at the midpoint between the floor and the ceiling, and the two side walls. This was done to simulate realistic placement of the thermostat inside of the room. The controller was setup such that if the temperature reached the upper set point in the controller, the mass flow inlets would turn on and drive the temperature down to the lower set point, at which the air jets would turn off. Figure 8 shows the behavior of the temperature controller as it cycles the mass flow inlets inside the room. A Constant mass flux boundary condition was specified at the mass flow inlets.

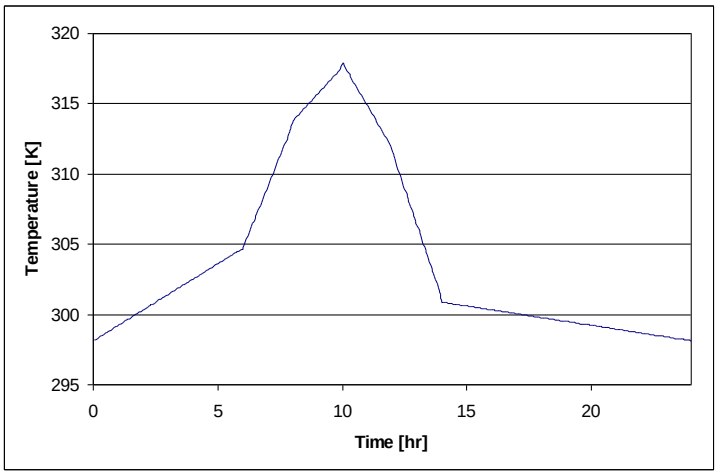

Figure 7: External Wall Temperature Wave Form

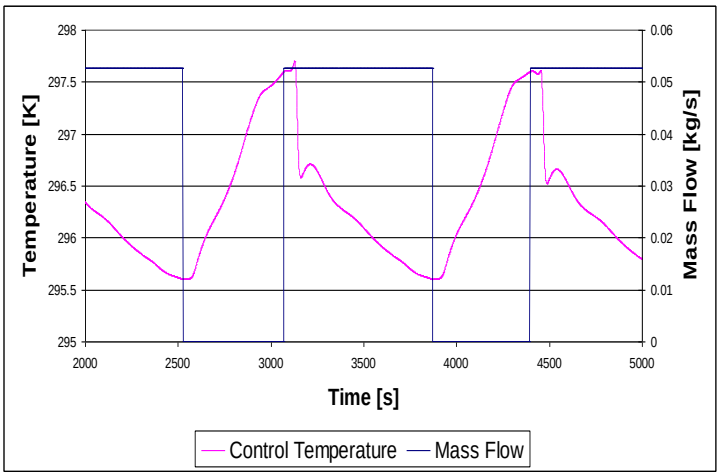

Figure 8: Temperature Controller Behavior

5.2.2 Exterior Wall Modeling

To simulate an externally exposed office room, an external wall temperature wave form was employed in the simulation. For all four ventilation systems considered, an ASHRAE TETD curve was coded into FLUENT as a User Defined Function (UDF); this curve is depicted in Figure 7 [Donnelly(9)]. In addition, the exterior wall was modeled as a traditional glazed window construction with a window shade. The materials, layer thicknesses and their properties are given in Table 1. These thicknesses accurately model the heat transfer that takes places as the outermost surface is heated by the sun. In our model room, the exterior wall is taken to be a window with the above mentioned window treatment. The exterior wall construction is shown in Figure 9.

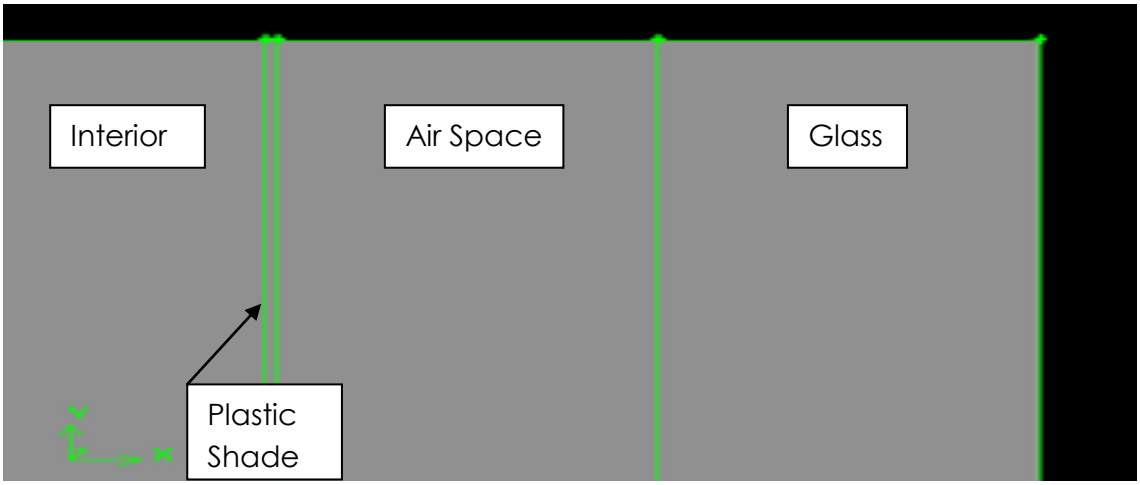

Figure 9: External Wall Construction and Window Treatment

Table 1: Exterior Wall Construction for Ventilation System Analysis

Material	Thickness [in]	Cp [J/kg-K]	ϱ [kg/m3]	k [W/m-K]
Glass	1	840	2500	0.0405
Air	1	1006.43	1.225	0.0242
Plastic Shade	1/32	1670	905	0.12

5.3 Models for Various 3-D Ventilation Systems

5.3.1 Variable Air Volume System (Case 1)

The first CFD simulation case was performed to simulate the conventional Variable Air Volume (VAV) ventilation system inside a 12' (length) x 12' (width) x 9'6" (height) room. A 3-D Cartesian mesh inside the room was generated by GAMBIT with a uniform grid of 3" spacing as shown in Figure 10. The exterior wall layers were meshed with each layer having 3 nodes across its thickness. The blue rectangle represents the cold air inlet, placed near the exterior wall which is facing away from the reader in Figure 10. This vent is placed close to the exterior wall in order to most efficiently cool the heat entering the room from the hot exterior wall. The red rectangle represents the air outlet for the warm air leaving the room. All the simulations employ a mass flow rate of 0.0528 kg/s, an air temperature of 288.706 K (60F) and a time step of 10 seconds.

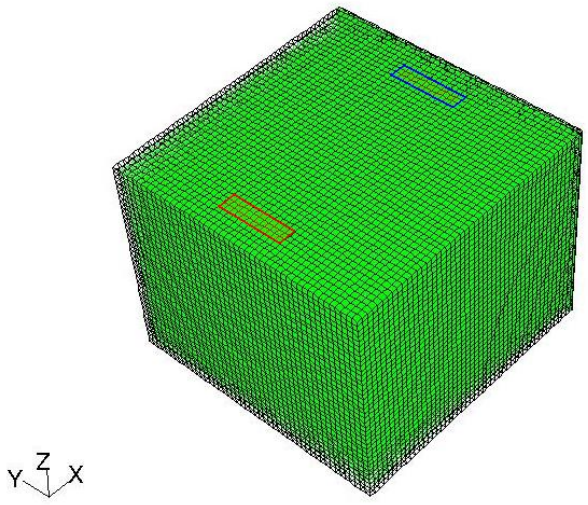

Figure 10 : Case 1 – View of 3-D Mesh

Despite the steep flow gradients near the walls, the grid spacing of 3" is sufficient to capture the flow field with reasonable accuracy. The mesh has a cell count of 87,552 and a node count of 110,322. The air inlet vent in this case was sized based on the HVAC requirements. The inlet and outlet dimensions of the vents are 9" x 36" (0.2286m x 0.9144m) spaced 12" (0.3048m) away from the rear wall as shown in Figure 11, which gives an area of 2.25 ft^2 (0.2090 m^2) for each vent. The room volume is 1,368 ft^3 (38.74 m^3). By meeting the guidelines of four air changes per hour [Harvey (5)], this vent size gives a flow velocity of 40.54 ft/min (0.206 m/sec). All the walls, including the hot external wall and the internal walls of the room are considered gray and diffuse with an absorption coefficient of 0.85. The air has an absorption coefficient of 0.17 to account for the water vapor [Donnelly (9)].

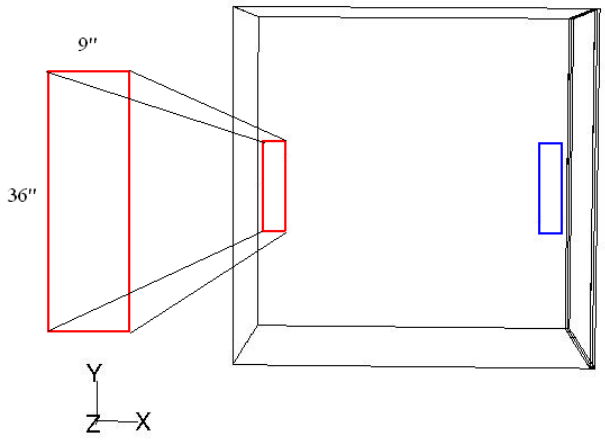

Figure 11 : Case 1 - Vent Sizes

5.3.2 Variable Air Volume System with Radiant Cooling (Case 2)

This case was created to simulate the conventional Variable Air Volume (VAV) ventilation system with radiant cooling. The vents of Case 2 are of the same size and are located at the same positions as those of Case 1. Case 2 has the addition of a radiation slab which provides the chilled ceiling effect. This slab measures 6'(length) x 6'(width) x 6"(height), and is placed 6" below the ceiling of the room. The plan view of the room ceiling is depicted from above in Figure 12.

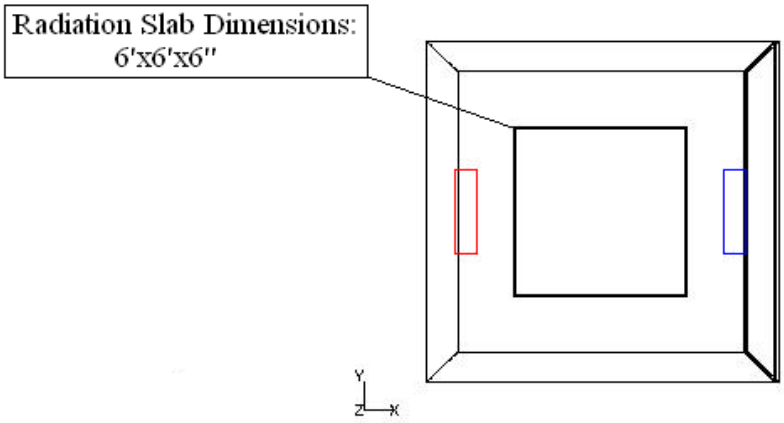

Figure 12: Case 2 - Plan View of the Ceiling with Radiation Slab and Vents

The mesh for this case varies slightly from Case 1 due to the inclusion of the radiation slab. Consequently the room volume for Case 2 is also slightly smaller than Case 1 (Case 2 room = 1,350 ft^3 (38.228 m^3)). A 3-D Cartesian mesh inside the room for this case was generated by GAMBIT, with a uniform grid spacing of 3" as shown in Figure 13. The exterior wall layers were meshed with each layer having 3 nodes across its thickness. Despite the steep flow gradients near the walls, this mesh spacing is sufficient to capture the flow field with reasonable accuracy. The mesh has a cell count of 97,344 and a node count of 109,793.

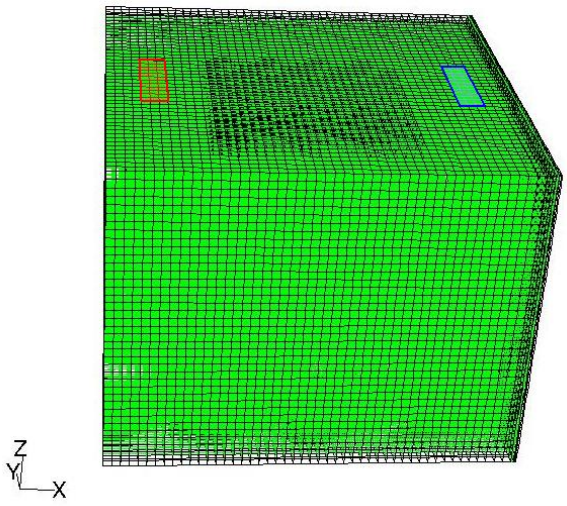

Figure 13: Case 2 – View of 3-D Mesh

For this case, the Discrete-Ordinate radiation model was employed for heat transfer calculations due to radiation. This effect adds another term $q_{radiation}$ to the total surface heat flux from a given surface. FLUENT calculates the values for $q_{radiation}$ and $q_{convection}$ for the chilled ceiling. The radiation block is made of weathered stainless steel with external emissivity of 0.85. The hot external wall and the internal walls all have the same properties as for Case 1. As the external wall heats up the room, low temperature radiation is

transmitted from the chilled slab to the room air and walls. Note that after the radiation transfer of lower temperature to air and the walls of the room, the portion of the heat that is not absorbed is diffusely reflected into the air and to the other walls.

5.3.3 Distributed Ventilation System (Case 3)

This case was created to simulate a Distributed Ventilation (DV) system. Figure 14 shows the schematic of the plan view of the room for Case 3 with the two outlet vents in the ceiling and six inlet vents on the floor.

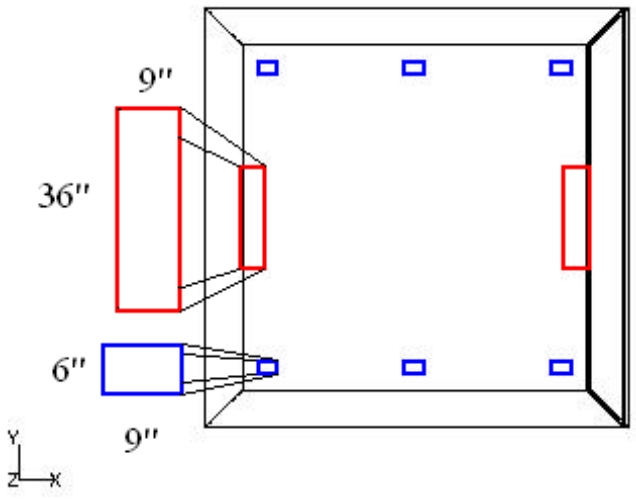

Figure 14: Case 3 – Plan View of Six Inlet Vents on the Floor and Two Outlet Vents on the Ceiling and their Sizes and Placements

The inlet vents for Case 3 are designed to have the same total inlet vent area as in Case 1 and 2. There are six inlet vents on the floor. Hence, the Case 3 inlet vents are 6" x 9", which gives an area of 2.25 ft^2 (0.209 m^2) for six vents. Since there is no change in the total inlet vent area compared to Case 1, Case 3 also meets the ASHRAE guidelines of air movement in the room. The six inlet vents are placed on the floor near the adiabatic walls.

The outlet vent area of Case 3 is double the size of the outlet vent area of Case 1. Each outlet vent is of the size, 9" x 36" (0.2286m x 0.9144m) spaced 12", giving an area of 4.5 ft^2 (0.418 m^2)) for the 2 outlet vents. Case 3 has a room volume of 1,368 ft^3 (38.74 m^3).

A 3-D Cartesian mesh inside the room was generated by GAMBIT, with a uniform grid spacing of 3" as shown in Figure 15. The exterior wall layers were meshed with each layer having 3 nodes across its thickness. This mesh has a cell count of 100,320 and a node count of 112,233.

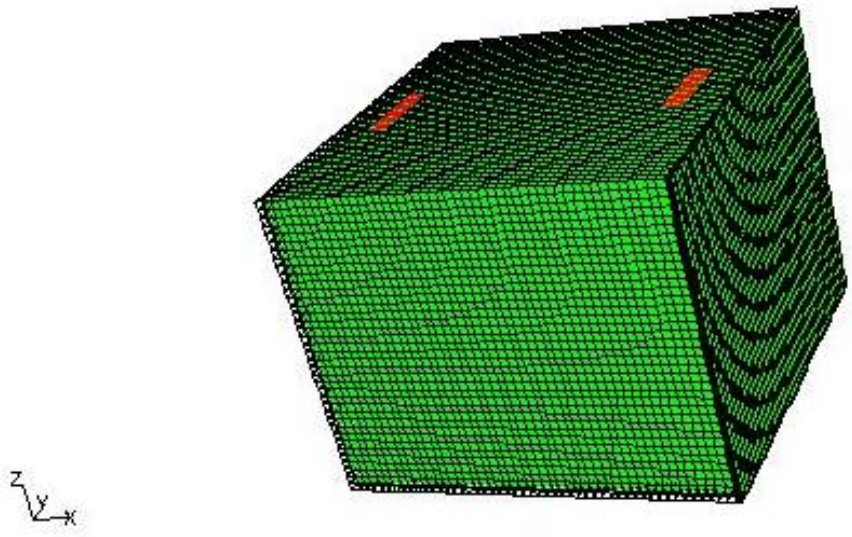

Figure 15 : Case 3 – View of 3-D Mesh

5.3.4 Distributed Ventilation System with Radiant Cooling (Case 4)

This case was created to simulate a Distributed Ventilation (DV) system with radiant cooling. There are no changes in the size or placement of the inlet or outlet vents from Case 3, therefore Case 4 also meets the ASHRAE guidelines of air movement in the room. Case 4 has the addition of a 6'(length) x 6'(width) x 6"(height) radiation slab which provides the chilled ceiling effect similar to Case 2. Also as in Case 2, the radiation slab is placed 6"

below the ceiling in the center of the room. The plan view of the inlet and outlet vents and the radiation slab is shown in Figure 16 and the 3-D view is shown in Figure 17.

Similar to Cases 1, 2 and 3, a 3-D Cartesian mesh for Case 4 was generated by GAMBIT, with a uniform grid spacing of 3", which is shown in Figure 18. The exterior wall layers were meshed with each layer having 3 nodes across its thickness. The Case 4 mesh varies slightly from Case 3, since the radiation slab is included in Case 4. Consequently the volume for Case 4 is also slightly smaller than that for Case 3 (Case 4 Room Volume = 38.228 m^3). The mesh has a cell count of 99,120 and a node count of 111,681. The same radiation model used in Case 2 is utilized in Case 4. Figure 18 shows the mesh inside the room. The hot external wall can be seen on the right side of this figure.

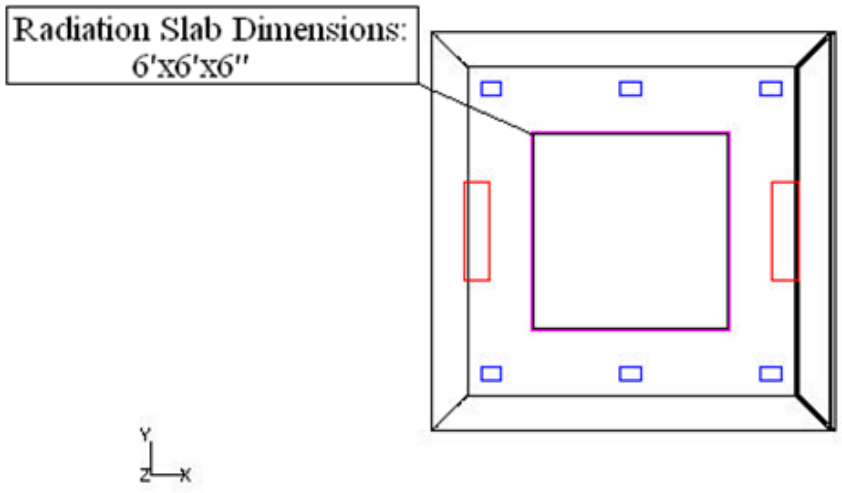

Figure 16: Case 4 – Plan View of Six Inlet Vents on the Floor; Two Outlet Vents in the Ceiling and the Radiation Slab on the Ceiling

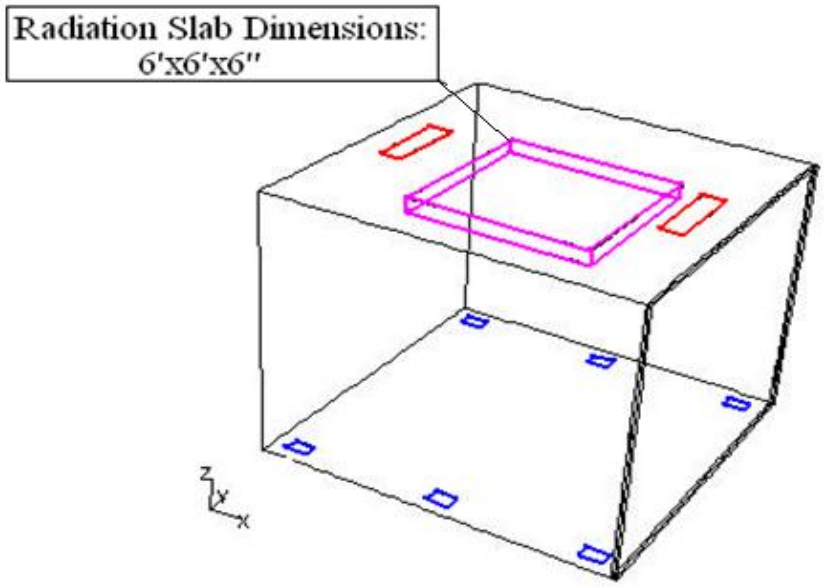

Figure 17: Case 4 – 3-D View of the Six Inlet Vents in the Floor; Two Outlet Vents and the Radiation Slab on the Ceiling

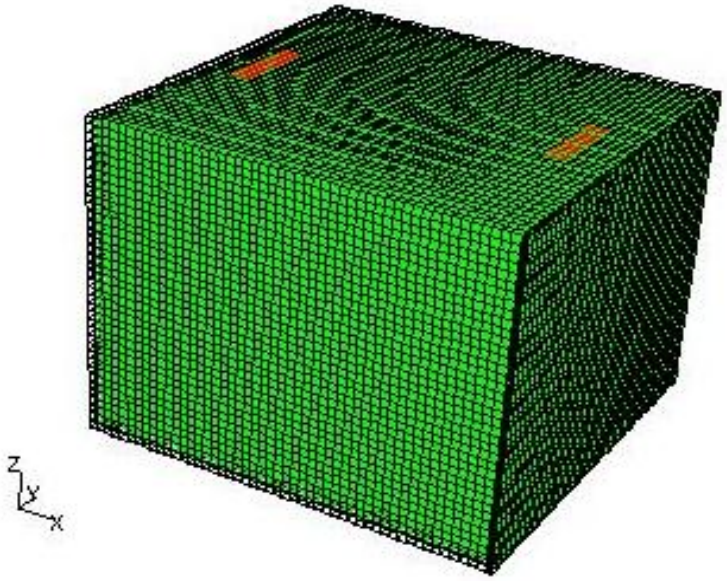

Figure 18: Case 4 - 3-D Mesh Inside the Room

5.4 CFD Simulation Results for 3-D Ventilation Systems

5.4.1 Presentation Format of Computed Data

In order to gain insight into the nature of fluid motion and heat transfer in each of the four ventilation systems under consideration, detailed results are recorded and presented at four different times within a 24-hour time period at T1 = 3:45 AM, T2 = 9:20 AM, T3 = 2:53 PM, and T4 = 8:27 PM. In order to present the data for each case, several planes inside the model room are considered; the contours of temperature in these cross-sectional planes are presented. Figure 19 shows the orientation of these planes with respect to the x, y, and z coordinate directions. The temperature, x-, y-, and z- components of velocity, turbulent kinetic energy (k), and turbulent dissipation rate (ε) are plotted to compare the changes in these quantities during a 24-hour period at time T1, T2, T3, and T4 for the four ventilation systems.

In Figure 19, the planes A1, A2 and A3 represent the y-z planes at three different x-locations, each a quarter of the room width apart from each other (3'). Planes B1, B2 and B3 represent the x-z planes at three different y-locations, each a quarter of the room length apart from each other (3'). Lastly, the C1, C2, and C3 planes represent the x-y planes at three different z-locations, each a quarter of the room height apart from each other (2' 4.5").

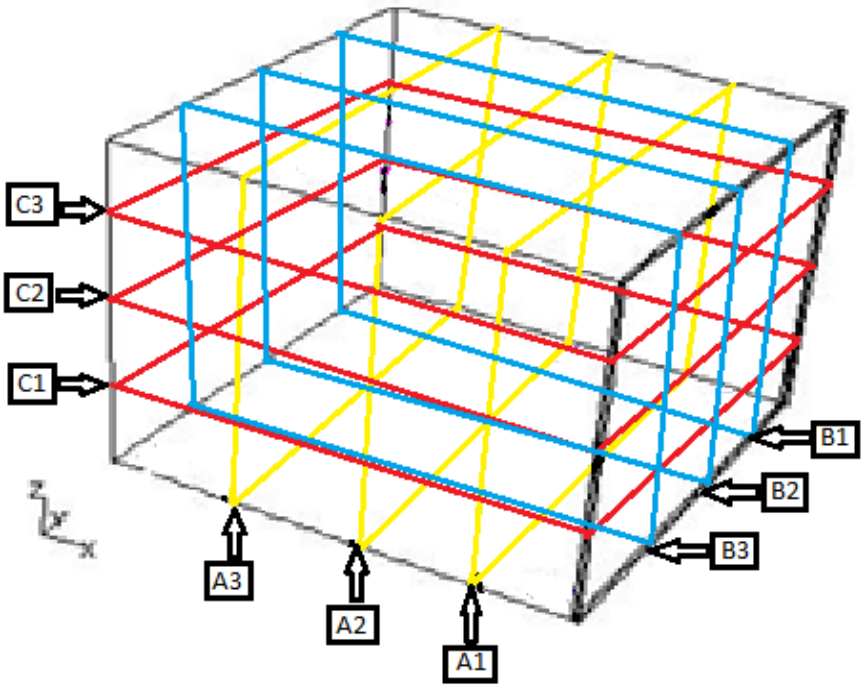

Figure 19: Presentation Format for the Computed Data

5.4.2 Case 1: Variable Air Volume Overhead Ventilation System

The calculations for Case 1 were performed using the Boussinesq approximation for density, the k-ε realizable turbulence model, and a first order upwind scheme in FLUENT. Computations were performed for two 24-hour time cycles. A time step of 10 seconds was employed in each iteration. A 24 hour time period is equivalent to 8640 time steps. The details of the geometry, mesh, boundary conditions, and mass flow rate into the room for this case are described in sections 5.2 and 5.3 of this chapter. A total of 197622 iterations were required to complete the two 24-hour cycles for Case 1. The solutions obtained during the second 24-hour cycle are free of transient effects due to the initial conditions. Figure 20 shows the convergence history of various flow variables and governing equations. In particular, it represents the change in the residuals during the iterative process.

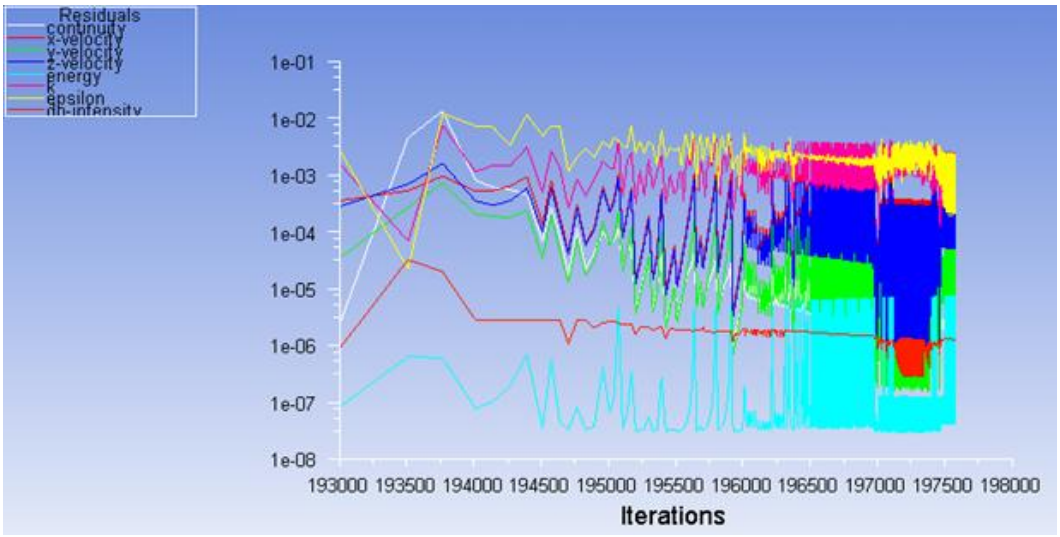

Figure 20: Case 1 – Residual History of Various Flow Variables and Governing Equations During the Iterative Process

Figure 21 shows the contours of temperature distributions in the different planes at T1 = 3:45 AM. T1 corresponds to a low temperature on the ASHRAE curve (Figure 7). As a result, the vents are not required to circulate the air inside the room, and the temperature remains nearly constant. These contours also show that the temperature is slightly cooler near the ceiling of the room. Figure 22 depicts the velocity contours in different planes of the room as described in Figure 19. These velocities are all very low because the vents have not been active at time T1, and have not been active for a long period of time before T1 because of the existing cooler temperature in the room. This figure does show that there is some circulation in the room. Also, the velocity is highest near the ceiling between the inlet and outlet vents of the VAV system. There is very little movement of air in the middle of the room.

Figure 23 shows the line plots of temperature distributions inside the room along various lines in planes A1-A3, B1-B3, and C1-C3 (shown in Figure 19). These plots show

that the solution satisfies the adiabatic wall conditions in the room except for the exterior wall where a constant temperature boundary condition is imposed corresponding to the external temperature at T1. In addition we note from Figure 23 that the temperature is warmer near the floor and cools towards the ceiling. This is a quantitative description of what is shown in the contour plots of Figure 21. These line plots also show that there is very little variation in the temperature inside the room; it varies between 295 and 296 K. Figures 24-26 show the line plots of various velocity components inside the room. These plots show, as expected, that the no slip condition is correctly imposed at the walls; all velocity components go to zero as they approach the walls. All of these velocities are very small in magnitude, which is a quantitative description of the contour plots shown in Figure 22. Figure 27 shows the turbulent kinetic energy line plots along various cross-sectional lines inside the room, which is indicative of the relative turbulence intensity in various parts of the room. The values of k are very small because of low flow velocities. As expected, the turbulent intensity is greater in the middle of the room than near the walls. Figure 28 shows the line plots of the turbulent dissipation rate along various cross-sectional lines inside the room. In contrast to k, the values of epsilon peak near the walls because of the large dissipation of turbulence. The value of epsilon is fairly constant across the room in all directions, except near the walls.

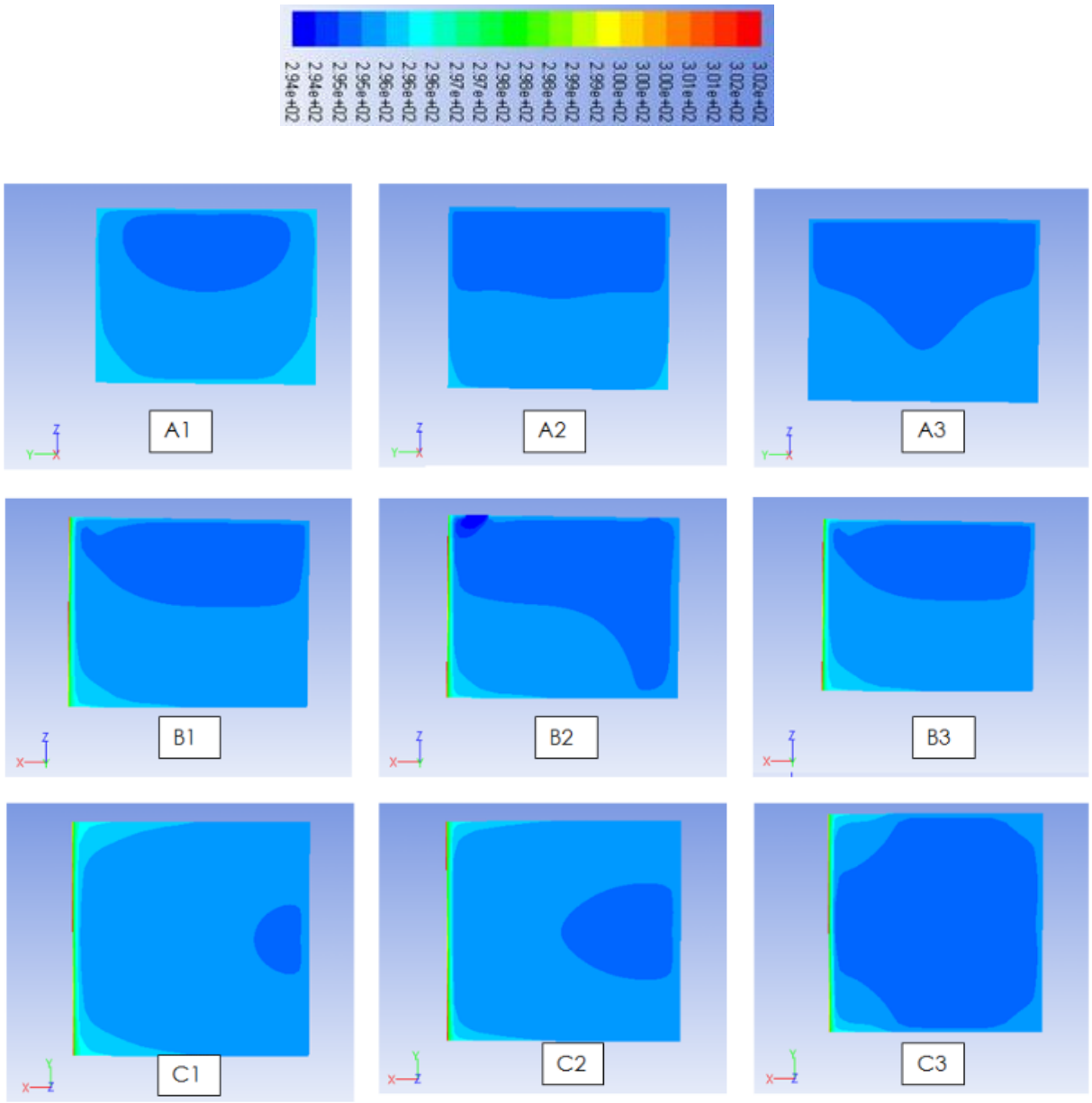

Figure 21: Case 1 - Temperature Contours in Different Planes of Figure 19 at Time T1 = 3:45 AM

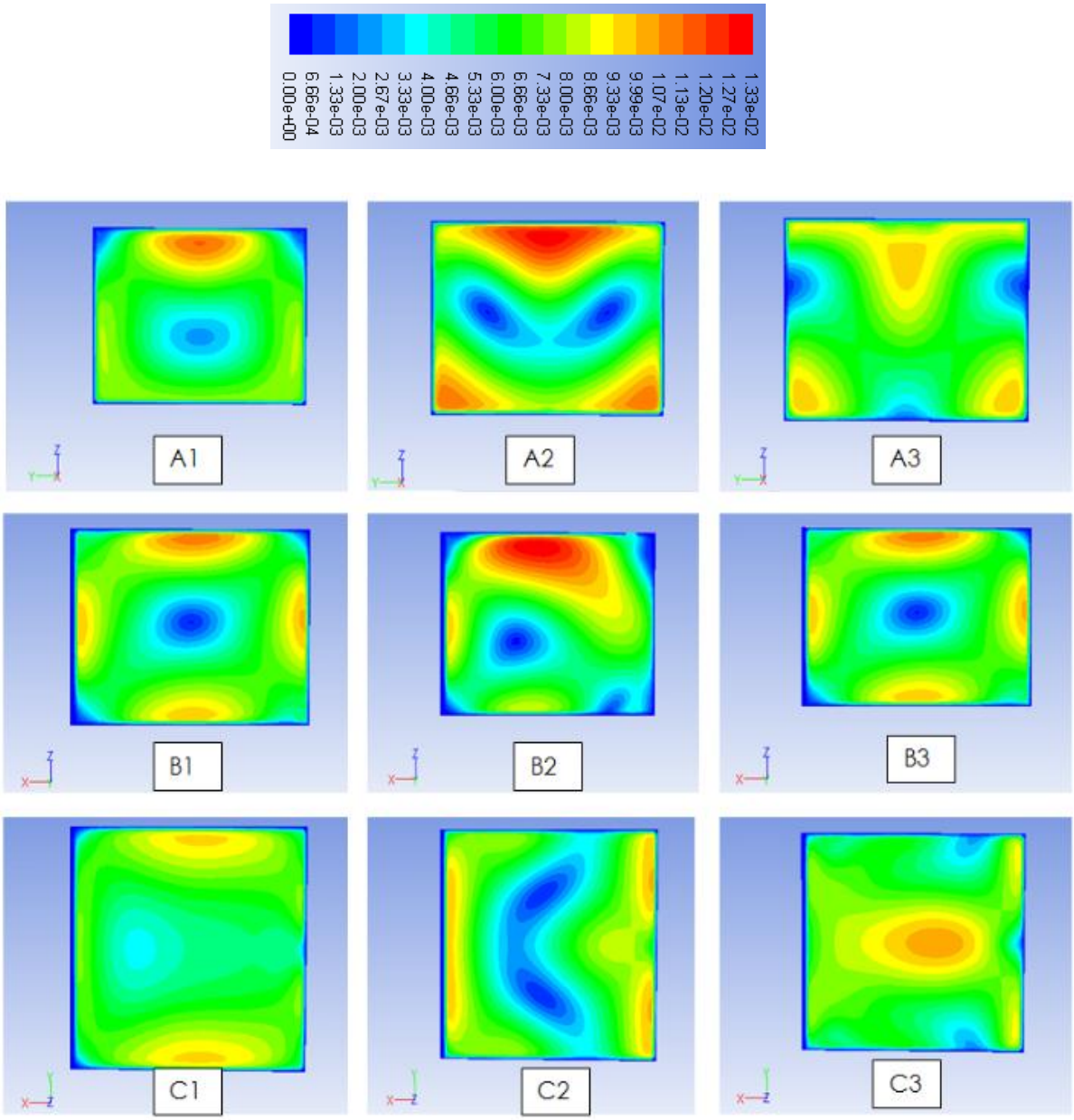

Figure 22: Case 1 - Velocity Contours in Different Planes of Figure 19 at Time T1 = 3:45 AM

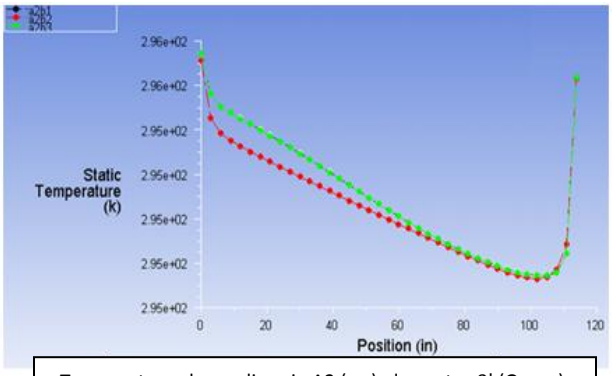

Temperature along z-lines in A2 (y-z) plane at y=3' (Green), y=6'(Red) and y=9'(Black)

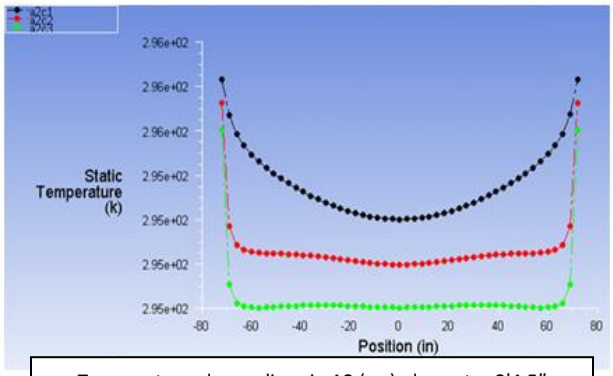

Temperature along y-lines in A2 (y-z) plane at z=2'4.5" (Black), z=4'9" (Red) and z=7'1.5" (Green)

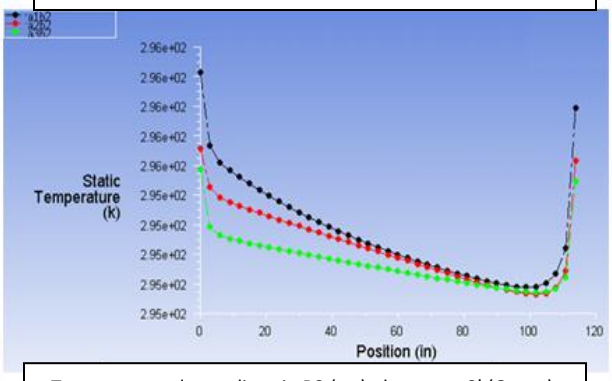

Temperature along z-lines in B2 (x-z) plane at x=3' (Green), x=6'(Red) and x=9'(Black)

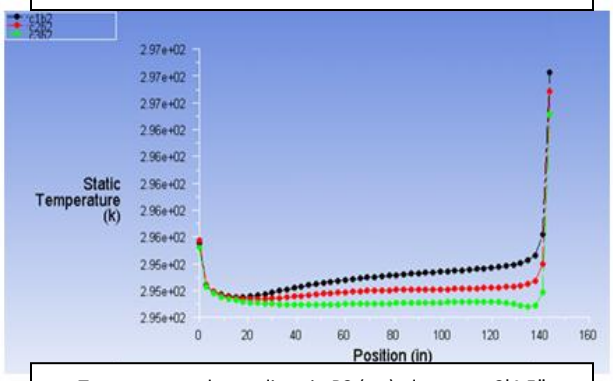

Temperature along x-lines in B2 (x-z) plane at z=2'4.5" (Black), z=4'9" (Red) and z=7'1.5" (Green)

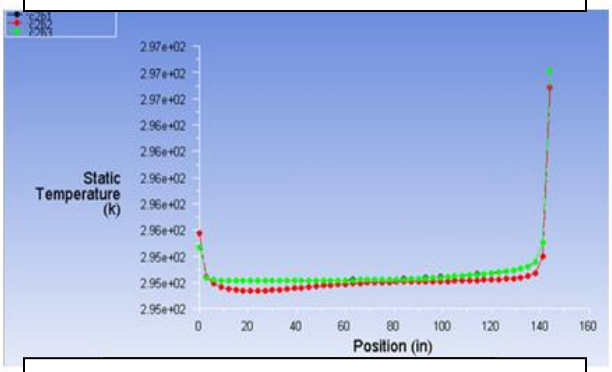

Temperature along x-lines in C2 (x-y) plane at y=3' (Green), y=6'(Red) and y=9'(Black)

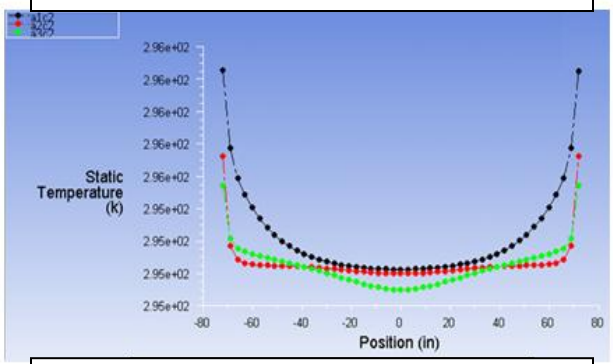

Temperature along y-lines in C2 (x-y) plane at x=3' (Green), x=6'(Red) and x=9'(Black)

Figure 23: Case 1 - Temperature Line Plots at Time T1 = 3:45 AM

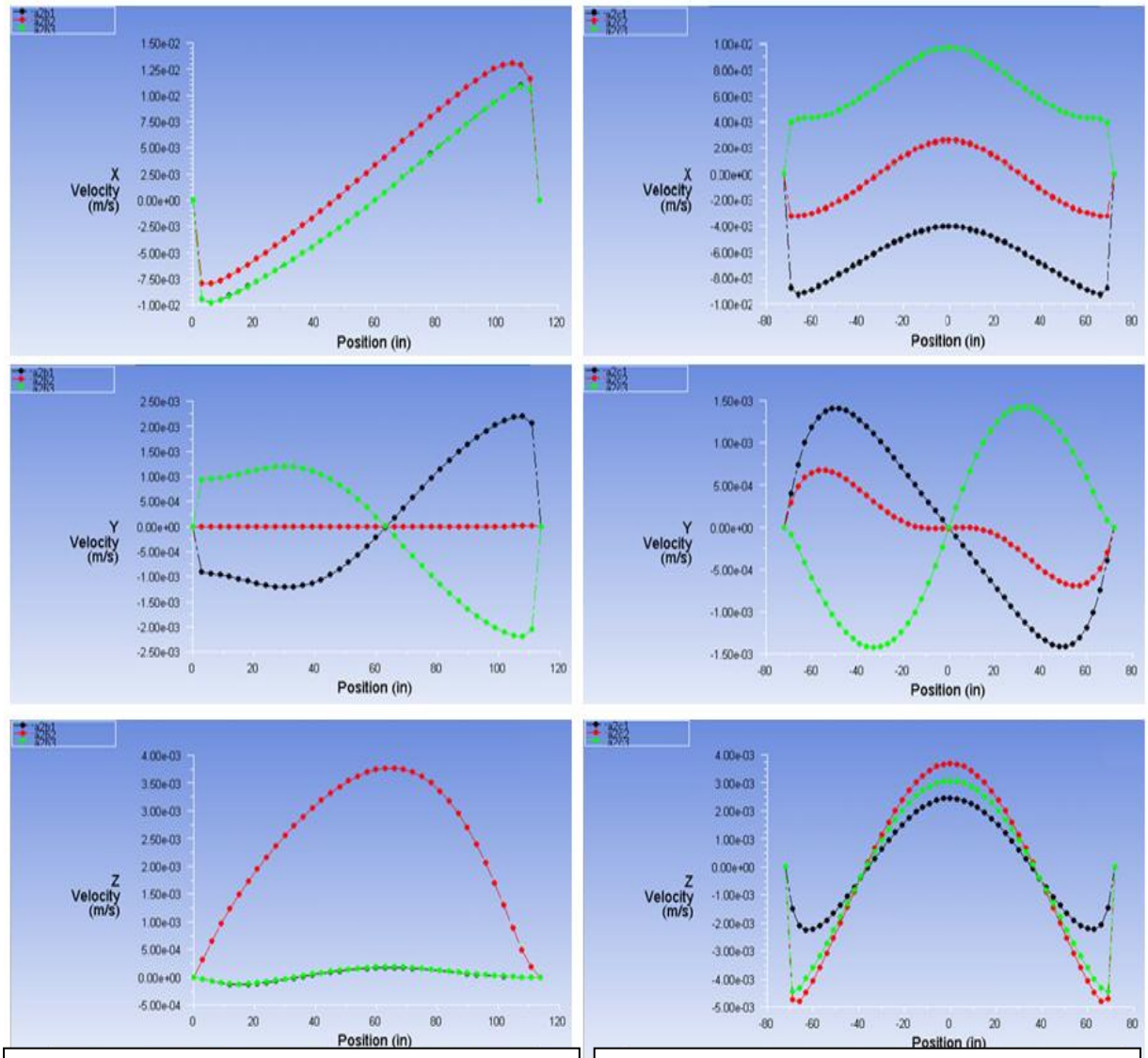

X, Y and Z Velocity Components along z-lines in A2 (y-z) plane at y=3' (Green), y=6' (Red), and y=9' (Black)

X, Y and Z Velocity Components along y-lines in A2 (y-z) plane at z=2'4.5" (Black), z=4'9" (Red), and z=7'1.5" (Green)

Figure 24: Case 1 - Velocity Components in the A2 Plane at Time T1 = 3:45 AM

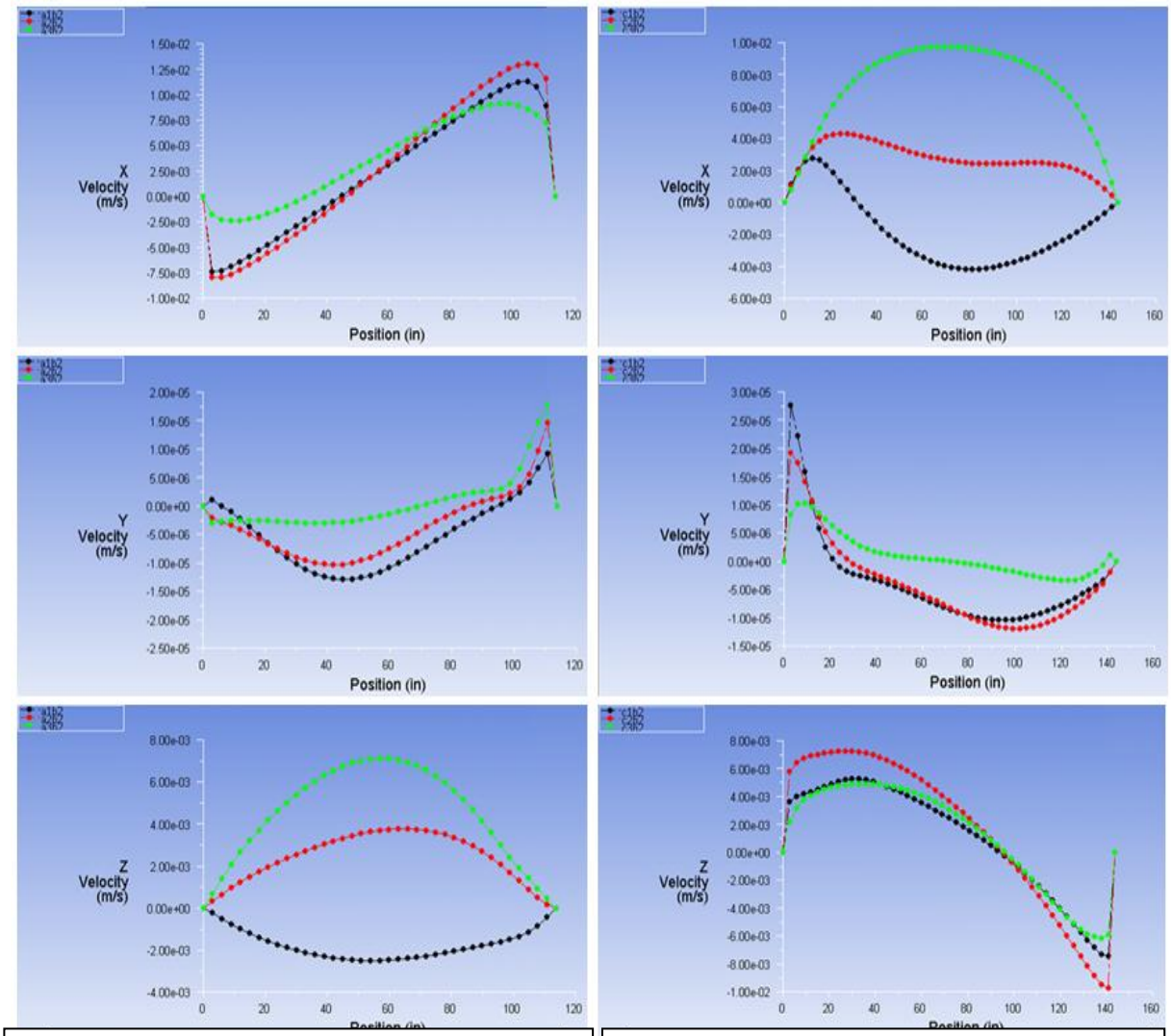

X, Y and Z Velocity Components along z-lines in B2(x-z) plane at x=3' (Green), x=6' (Red), and x=9' (Black)

X, Y and Z Velocity Components along x-lines in B2 (x-z) plane at z=2'4.5" (Black), z=4'9" (Red), and z=7'1.5" (Green)

Figure 25: Case 1 - Velocity Components in the B2 Plane at Time T1 = 3:45 AM

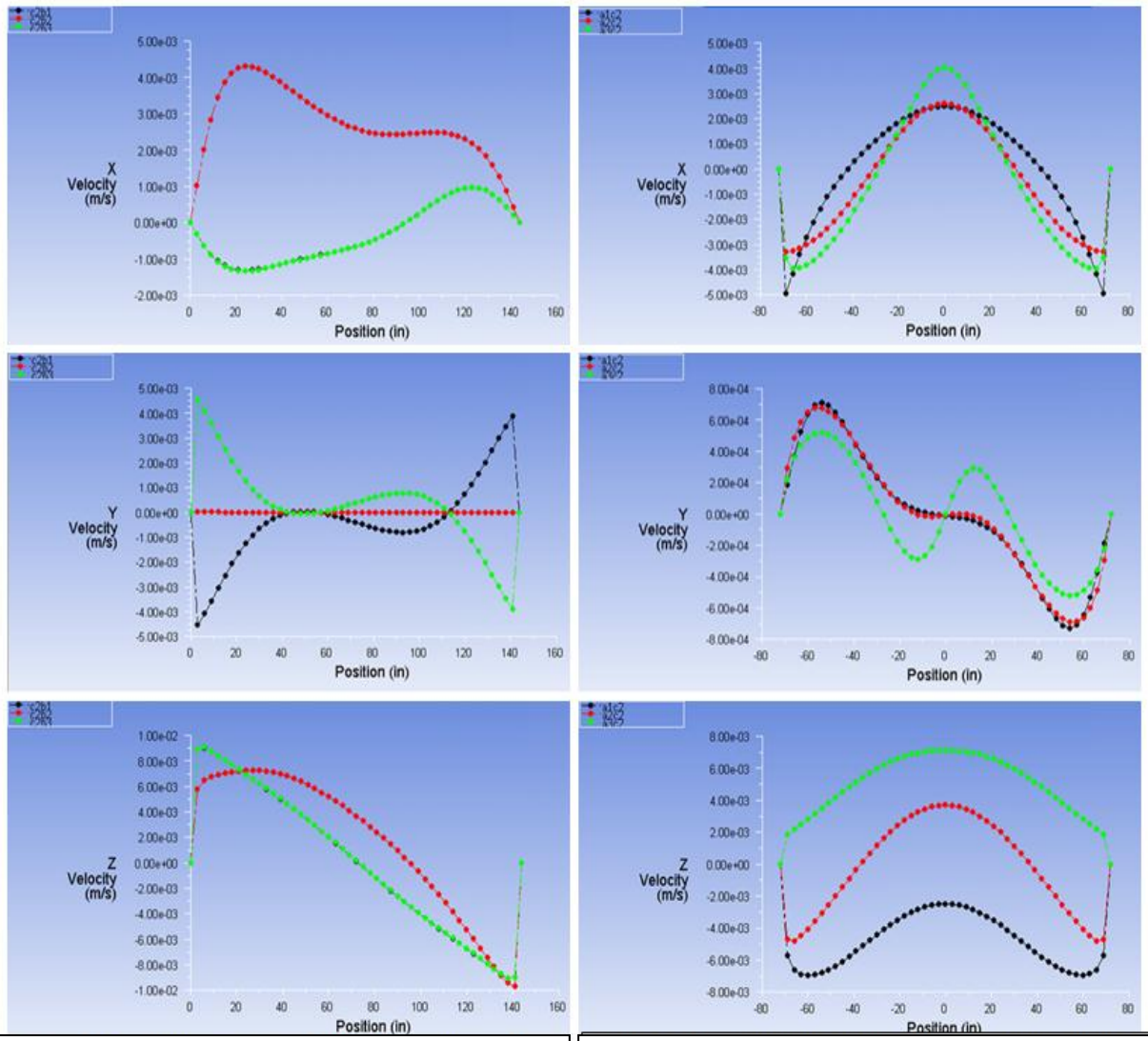

X, Y and Z Velocity Components along x-lines in C2 (x-y) plane at y=3' (Green), y=6' (Red), and y=9' (Black)

X, Y and Z Velocity Components along y-lines in C2 (x-y) plane at x=3' (Green), x=6' (Red), and x=9' (Black)

Figure 26: Case 1 - Velocity Components in the C2 Plane at Time T1 = 3:45 AM

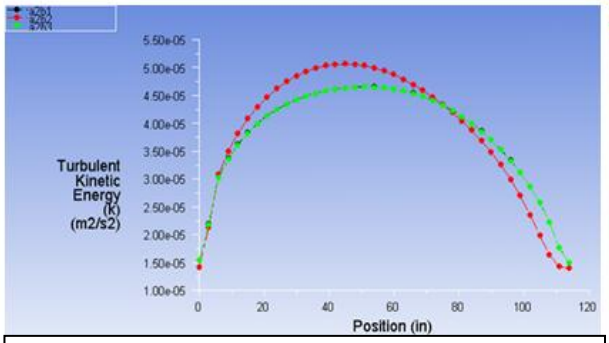

Turbulent Kinetic Energy along z-lines in A2 (y-z) plane at y=3' (Green), y=6'(Red) and y=9'(Black)

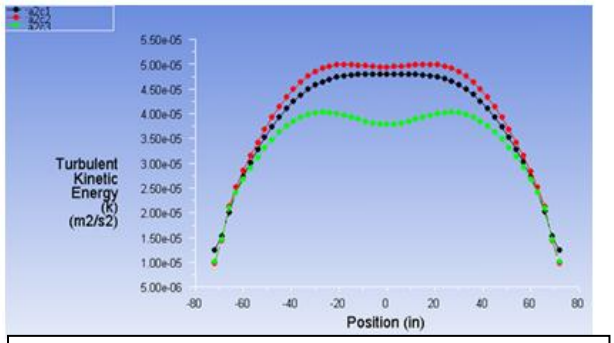

Turbulent Kinetic Energy along y-lines in A2 (y-z) plane at z=2'4.5" (Black), z=4'9" (Red) and z=7'1.5" (Green)

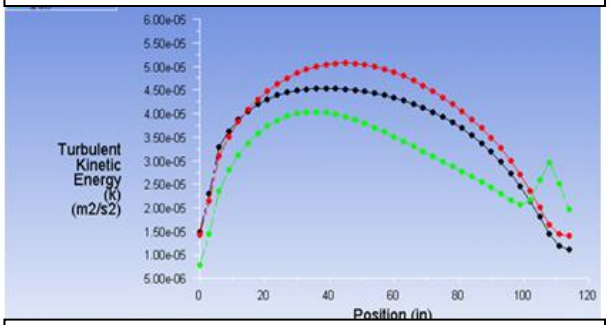

Turbulent Kinetic Energy along z-lines in B2 (x-z) plane at x=3' (Green), x=6'(Red) and x=9'(Black)

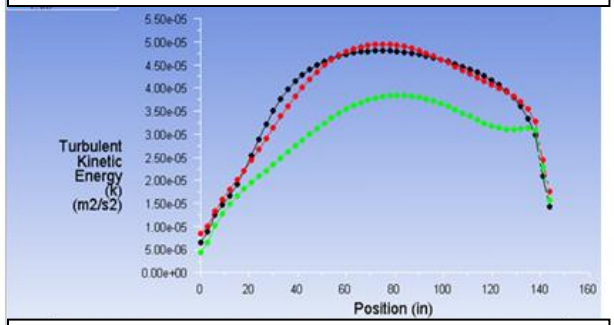

Turbulent Kinetic Energy along x-lines in B2 (x-z) plane at z=2'4.5" (Black), z=4'9" (Red) and z=7'1.5" (Green)

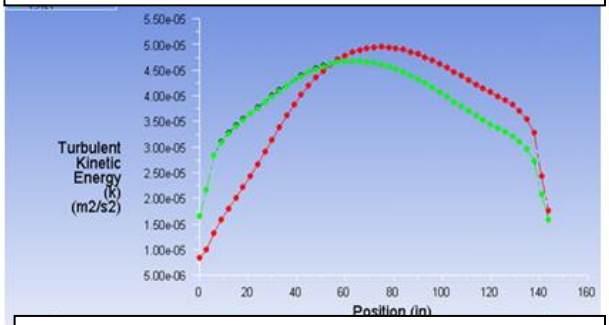

Turbulent Kinetic Energy along x-lines in C2 (x-y) plane at y=3' (Green), y=6'(Red) and y=9'(Black)

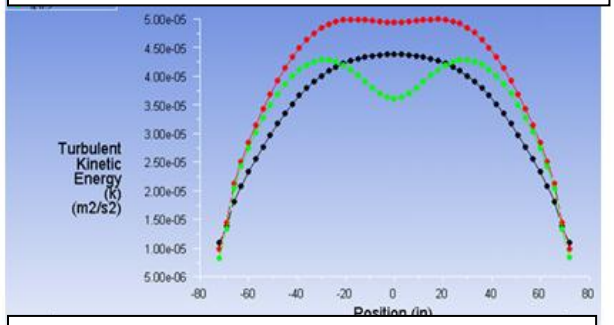

Turbulent Kinetic Energy along y-lines in C2 (x-y) plane at x=3' (Green), x=6'(Red) and x=9'(Black)

Figure 27: Case 1 - Turbulent Kinetic Energy Line Plots at Time T1 = 3:45 AM

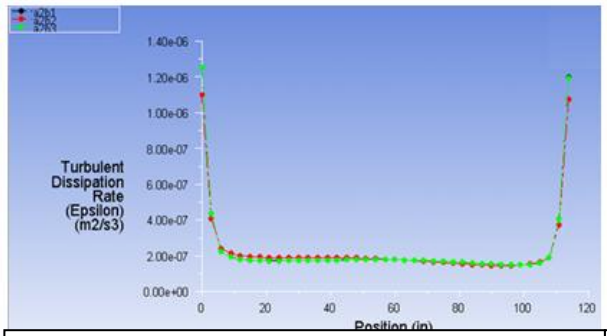

Turbulent Dissipation Rate along z-lines in A2 (y-z) plane at y=3' (Green), y=6'(Red) and y=9'(Black)

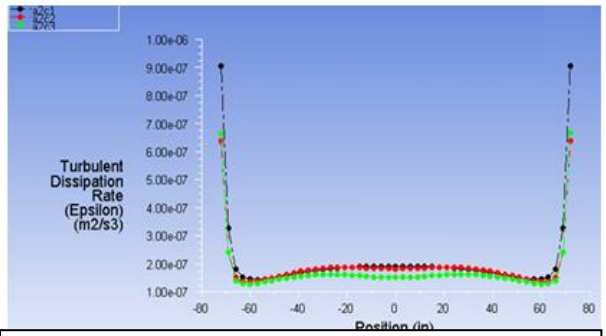

Turbulent Dissipation Rate along y-lines in A2 (y-z) plane at z=2'4.5" (Black), z=4'9" (Red) and z=7'1.5" (Green)

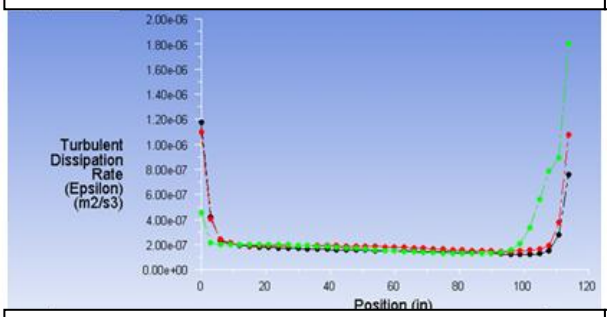

Turbulent Dissipation Rate along z-lines in B2 (x-z) plane at x=3' (Green), x=6'(Red) and x=9'(Black)

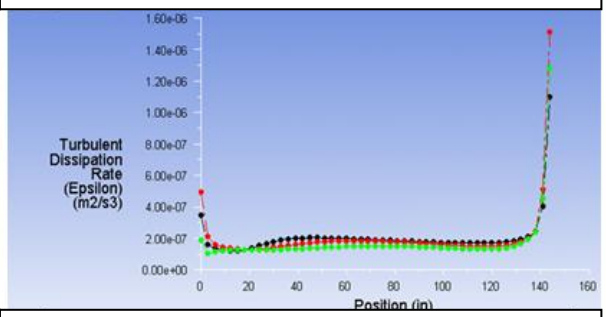

Turbulent Dissipation Rate along x-lines in B2 (x-z) plane at z=2'4.5" (Black), z=4'9" (Red) and z=7'1.5" (Green)

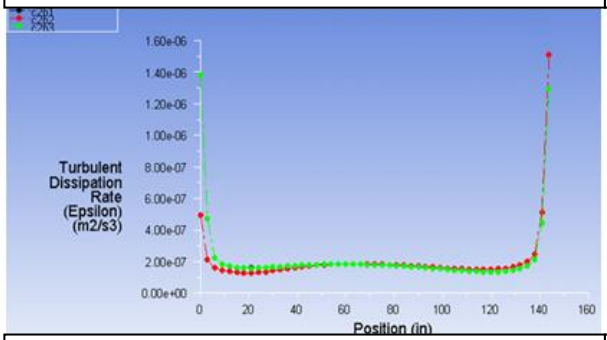

Turbulent Dissipation Rate along x-lines in C2 (x-y) plane at y=3' (Green), y=6'(Red) and y=9'(Black)

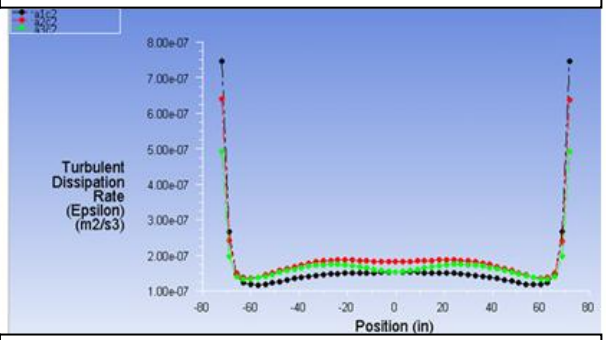

Turbulent Dissipation Rate along y-lines in C2 (x-y) plane at x=3' (Green), x=6'(Red) and x=9'(Black)

Figure 28: Case 1 - Turbulent Dissipation Rate Line Plots at Time T1 = 3:45 AM

Next, we present results at time T2 = 9:20 AM. The key to interpreting the results in the various planes (A1-A3, B1-B3, C1-C3) and along the various lines in these planes inside the room is the same as described before for Figures 21-28 at T1 = 3:45 AM. At T2 = 9:20 AM, the outside temperature is higher as shown in the ASHRAE temperature curve (Figure 7). The air inside the room is therefore warmer than at T1 = 3:45 AM. Figure 29 shows the temperature contours inside the room in A1-A3, B1-B3, and C1-C3 planes. At time T2 = 9:20 AM we can observe the effects of the cold air coming from the inlet vent in the B2 plane. We note from the A1 plane that the cold air significantly affects the area near the exterior wall, however its effect diminishes as we move through the A2 and A3 planes towards the back of the room. As a result the air is much colder near the hot exterior wall due to the vent placement, and the rear of the room is slightly warmer. Figure 30 shows the velocity contours in different planes of the room at time T2 = 9:20 AM. We notice the high air velocity from the inlet and outlet vents in the B2 plane near the ceiling as expected, however this fast moving air doesn't spread very far into the room, which agrees with our observation from Figure 29 that there is a lack of cold air distribution in the room.

Figure 31 shows the line plots of temperature distribution inside the room, which show somewhat higher temperatures than those at time T1 = 3:45 AM as expected. These temperature line plots show that the adiabatic temperature boundary condition is satisfied on the five interior walls, and that the highest temperature occurs at the exterior wall. The temperature line plots in planes A1-A3, and B1-B3 show that the cold air initially is near the floor and begins to rise as it gains heat, as expected physically. The temperature line plots in the C2 plane show that the temperature is fairly constant in the rear of the room, however it

suddenly decreases as the area near the vent is approached. It begins to rise again as the hot exterior wall is approached.

Figures 32-34 show the line plots of velocity in various planes inside the room, which are fairly similar to those in Figures 24-26 at time T1 = 3:45 AM. Figure 34 shows that the z-component of velocity matches the form that would be expected with the velocity becoming negative indicating that this region is affected by the inlet vent. Figure 35 shows the line plots of turbulent kinetic energy in various planes inside the room. The turbulent kinetic energy(k) is quite high near the hot exterior wall as expected due to high air velocity, and is nearly zero elsewhere. Figure 36 shows the line plots of the turbulent dissipation rate in various planes inside the room. The behavior of both k and ε is as expected since the temperature increases at time T2 = 9:20 AM.

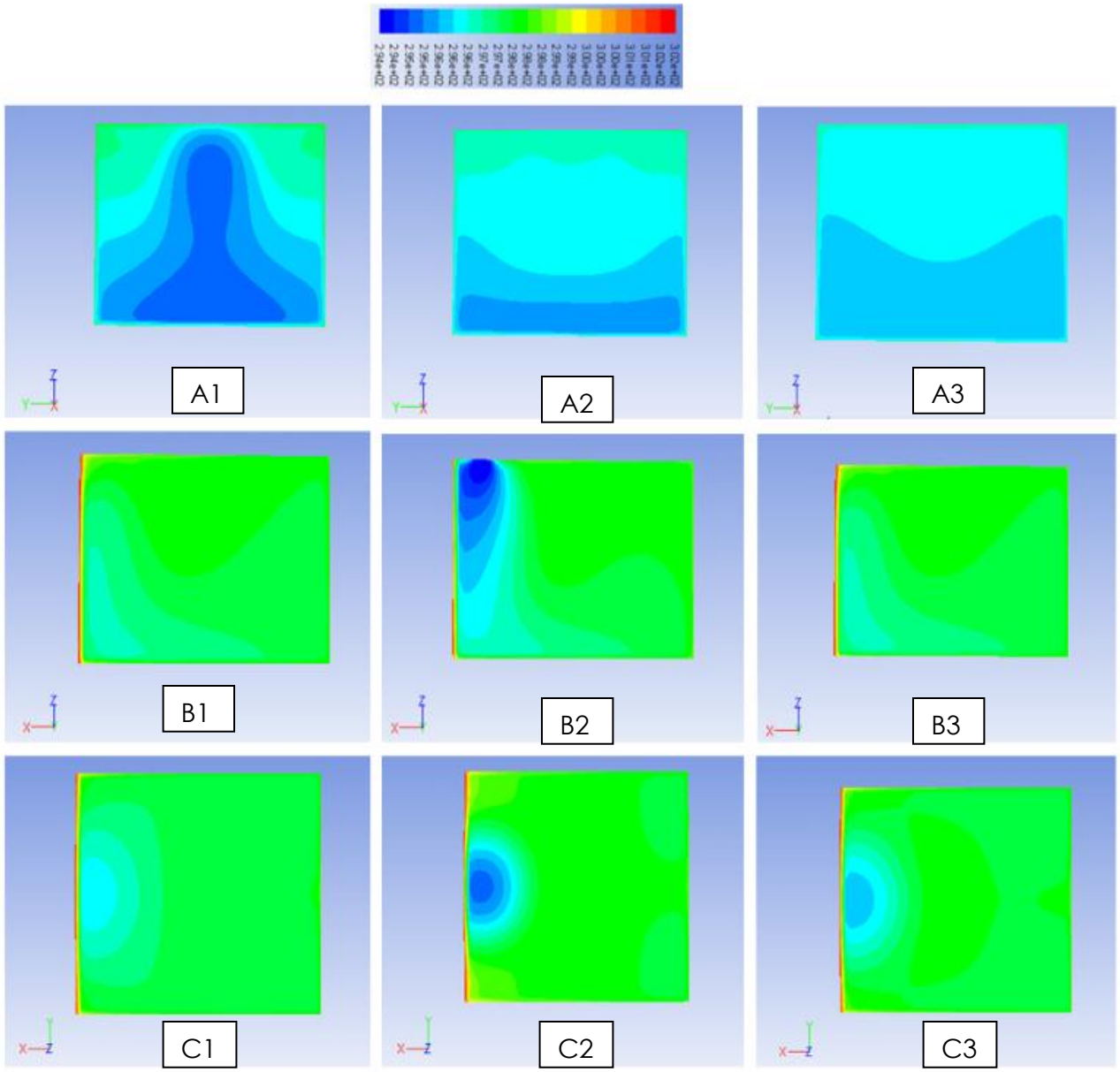

Figure 29: Case 1 - Temperature Contours in Different Planes of Figure 19 at Time T2 = 9:20 AM

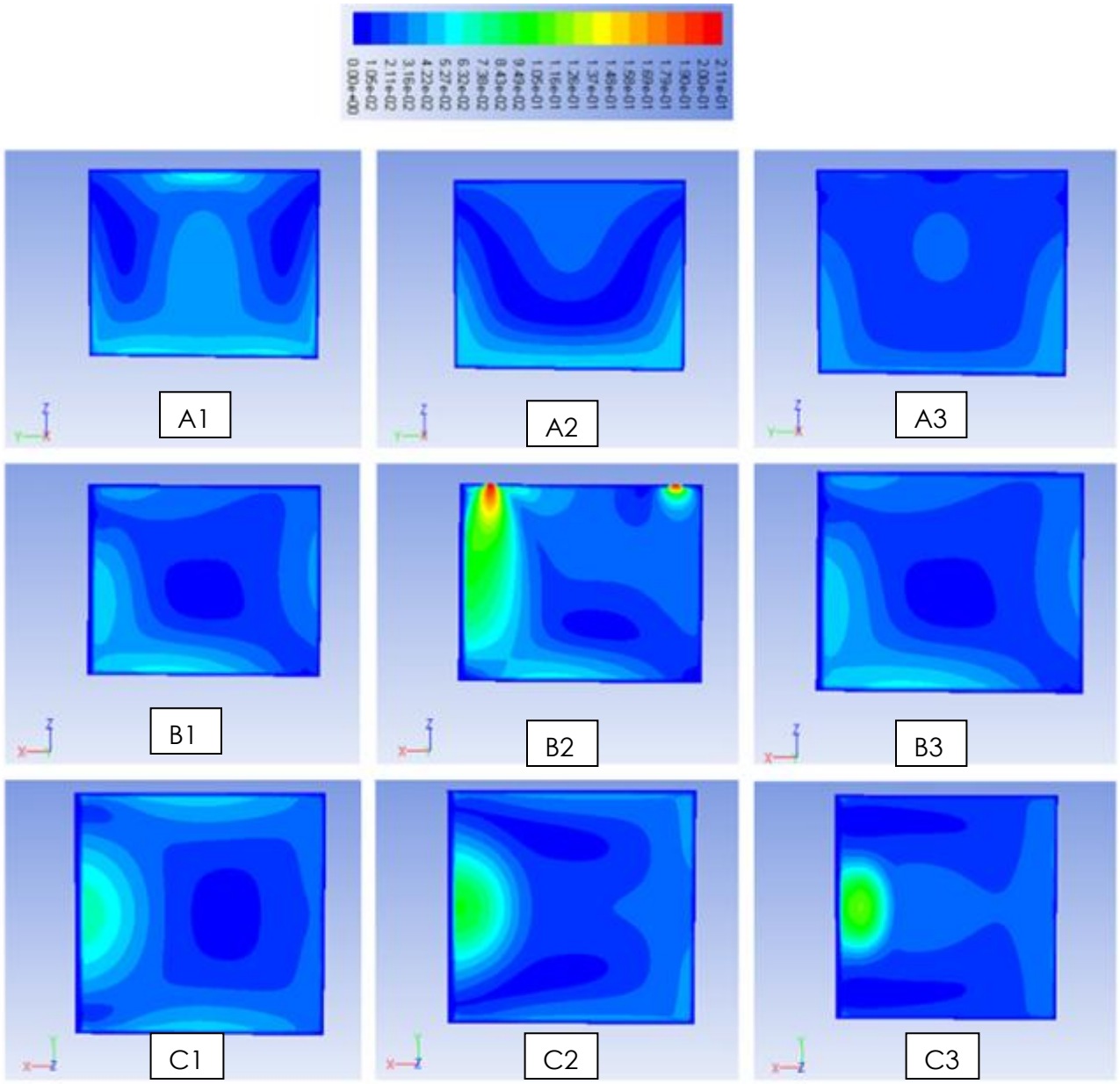

Figure 30: Case 1 - Velocity Contours in Different Planes of Figure 19 at Time T2 = 9:20 AM

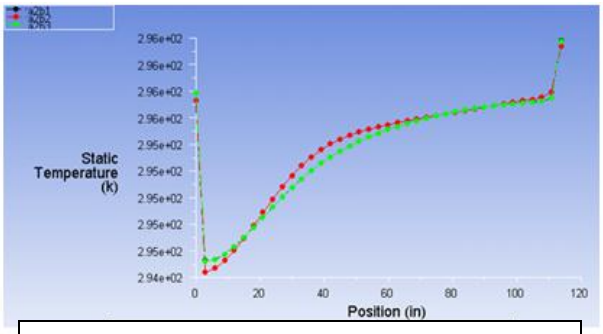

Temperature along z-lines in A2 (y-z) plane at y=3' (Green), y=6'(Red) and y=9'(Black)

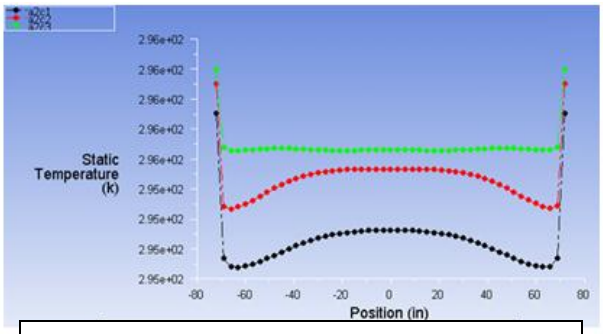

Temperature along y-lines in A2 (y-z) plane at z=2'4.5" (Black), z=4'9" (Red) and z=7'1.5" (Green)

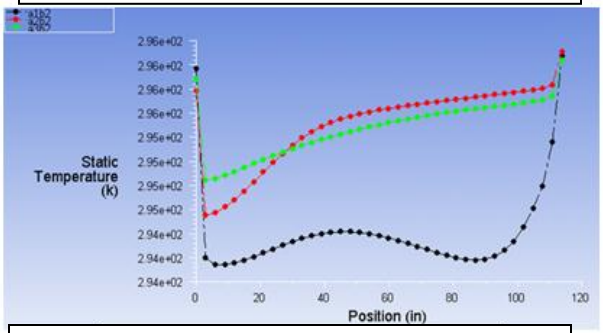

Temperature along z-lines in B2 (x-z) plane at x=3' (Green), x=6'(Red) and x=9'(Black)

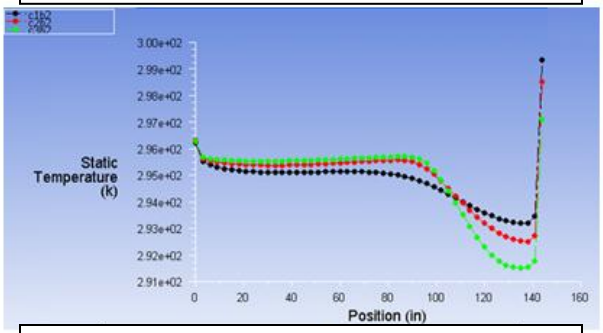

Temperature along x-lines in B2 (x-z) plane at z=2'4.5" (Black), z=4'9" (Red) and z=7'1.5" (Green)

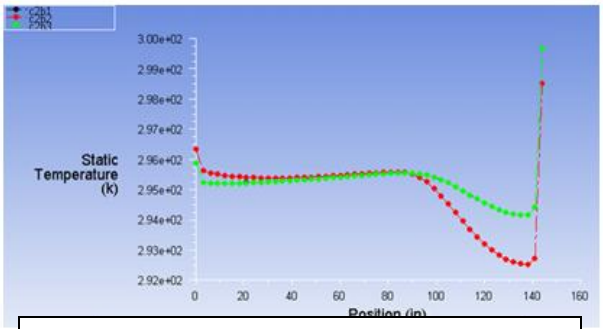

Temperature along x-lines in C2 (x-y) plane at y=3' (Green), y=6'(Red) and y=9'(Black)

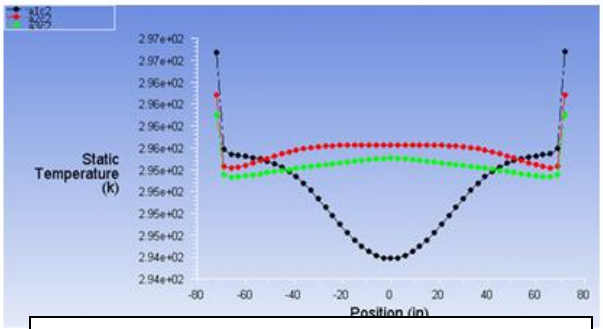

Temperature along y-lines in C2 (x-y) plane at x=3' (Green), x=6'(Red) and x=9'(Black)

Figure 31: Case 1 – Temperature Line Plots at Time T2 = 9:20 AM

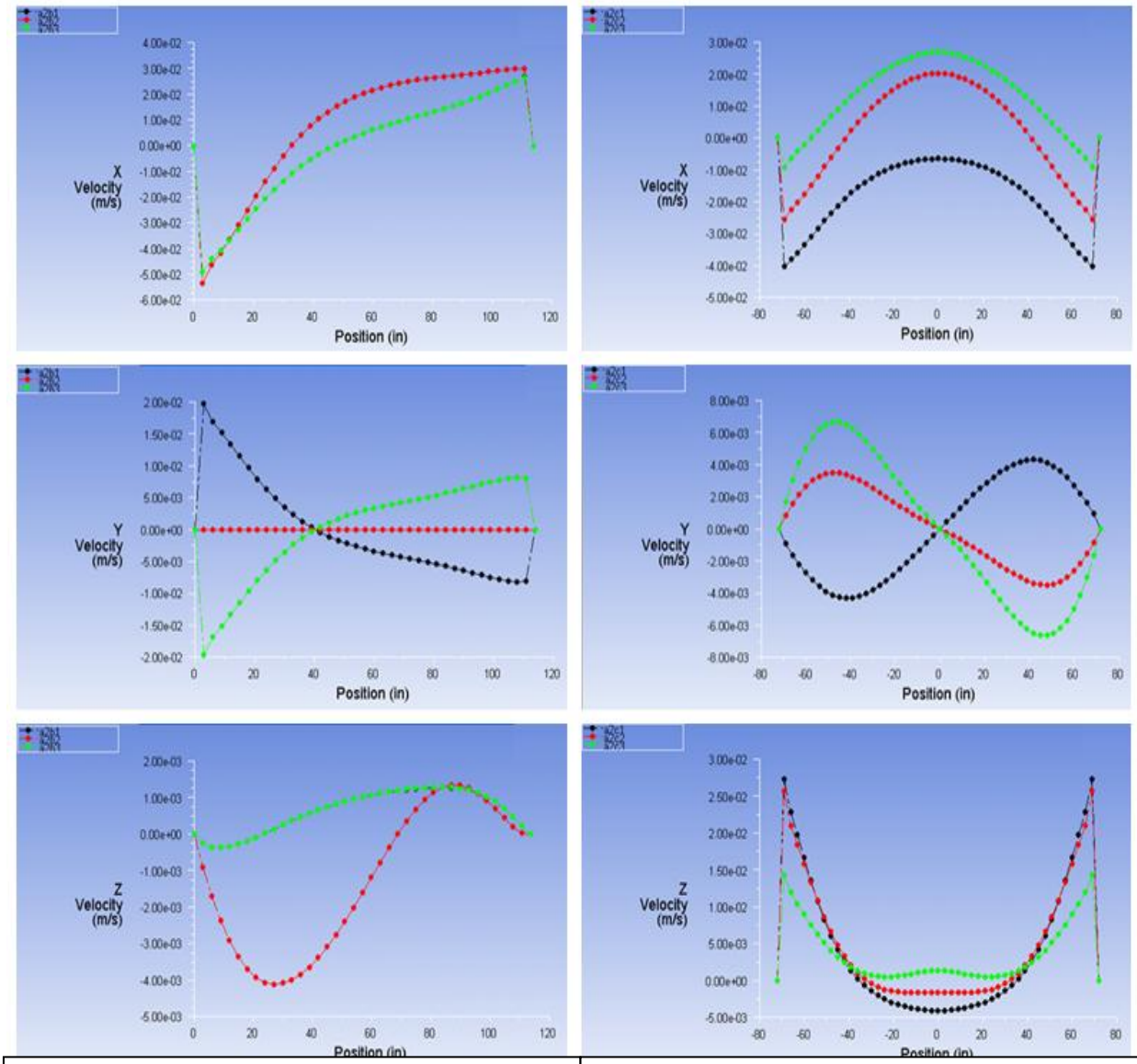

X, Y and Z Velocity Components along z-lines in A2 (y-z) plane at y=3' (Green), y=6' (Red), and y=9' (Black)	X, Y and Z Velocity Components along y-lines in A2 (y-z) plane at z=2'4.5" (Black), z=4'9" (Red), and z=7'1.5" (Green)

Figure 32: Case 1 - Velocity Components in the A2 Plane at Time T2 = 9:20 AM

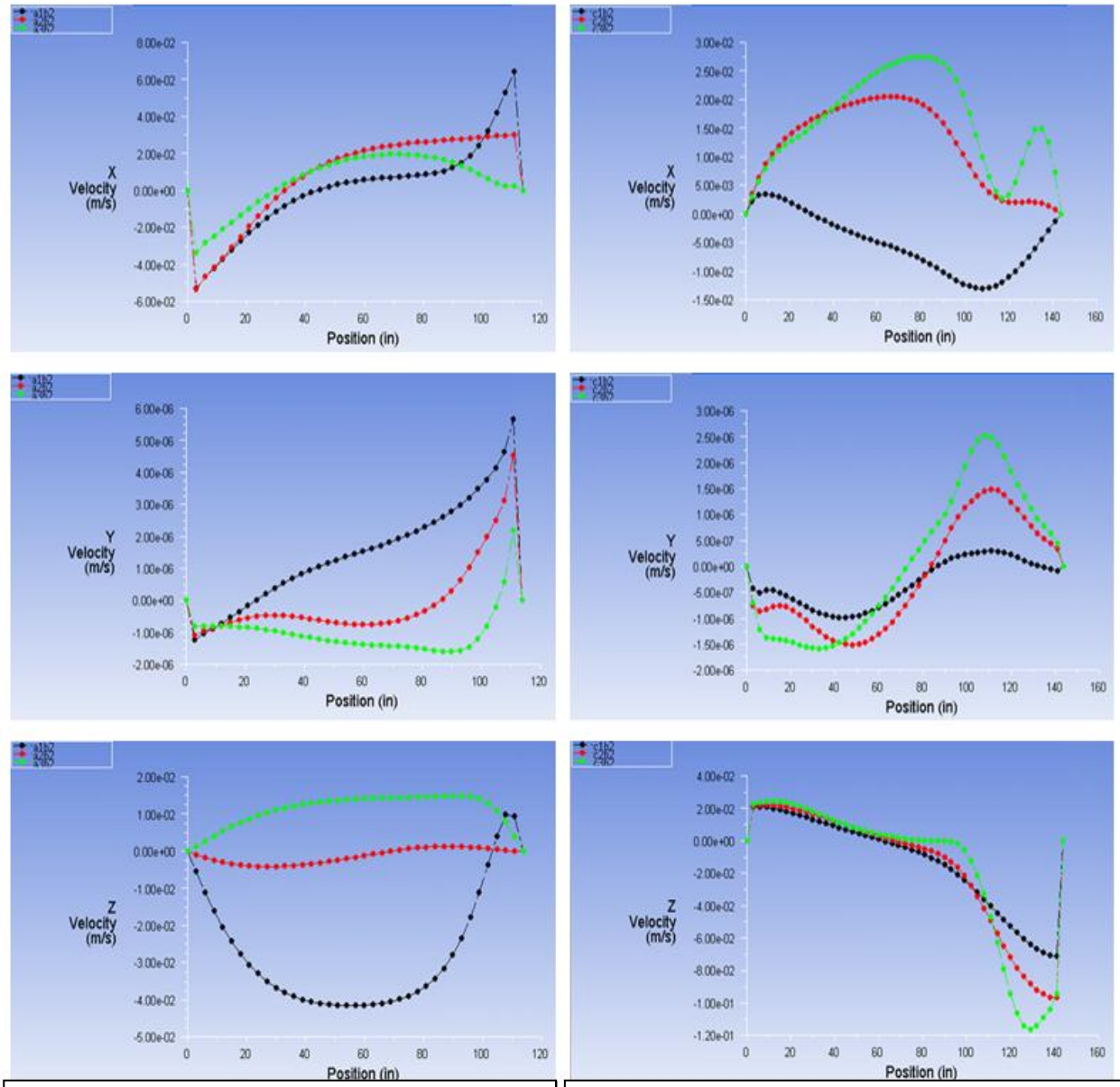

X, Y and Z Velocity Components along z-lines in B2(x-z) plane at x=3' (Green), x=6' (Red), and x=9' (Black)	X, Y and Z Velocity Components along x-lines in B2 (x-z) plane at z=2'4.5" (Black), z=4'9" (Red), and z=7'1.5" (Green)

Figure 33: Case 1 - Velocity Components in the B2 Plane at Time T2 = 9:20 AM

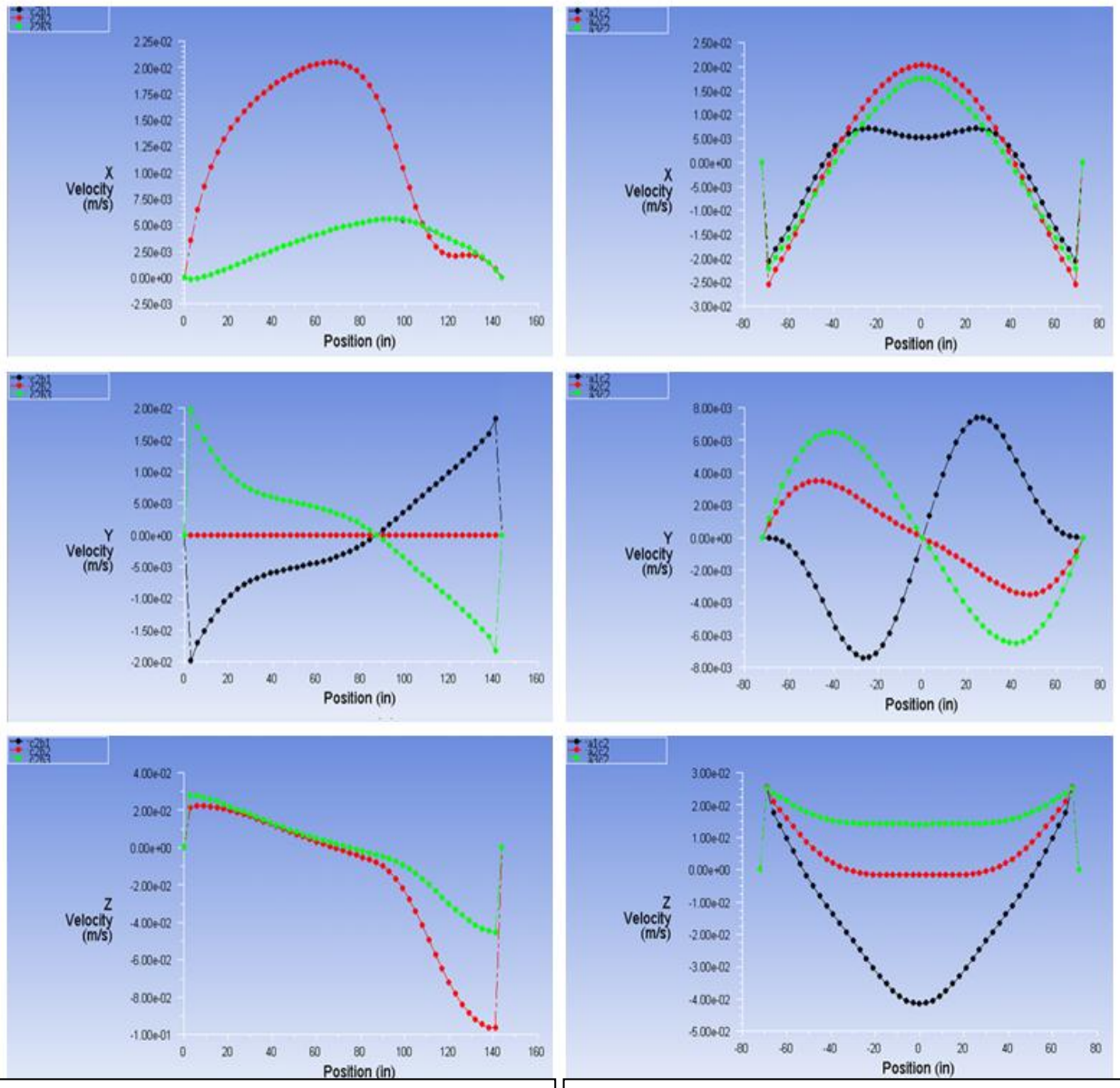

X, Y and Z Velocity Components along x-lines in C2 (x-y) plane at y=3' (Green), y=6' (Red), and y=9' (Black)	X, Y and Z Velocity Components along y-lines in C2 (x-y) plane at x=3' (Green), x=6' (Red), and x=9' (Black)

Figure 34: Case 1 - Velocity Components in the C2 Plane at Time T2 = 9:20 AM

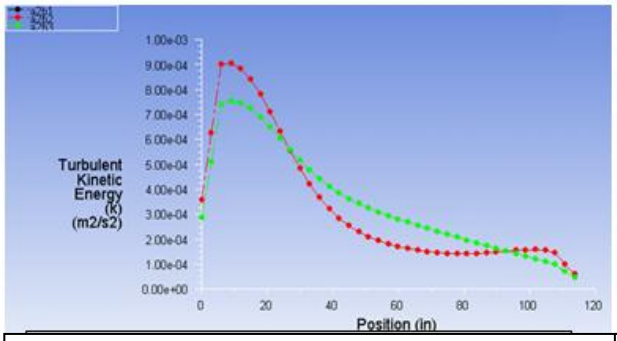

Turbulent Kinetic Energy along z-lines in A2 (y-z) plane at y=3' (Green), y=6'(Red) and y=9'(Black)

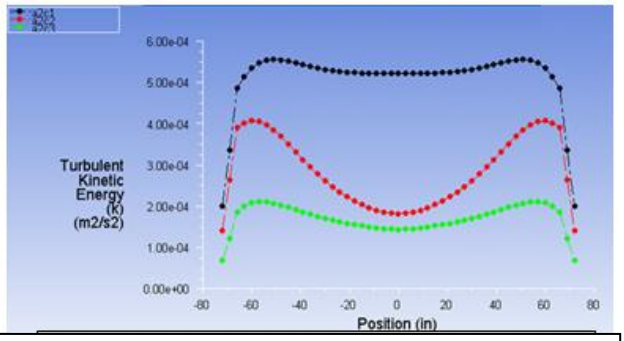

Turbulent Kinetic Energy along y-lines in A2 (y-z) plane at z=2'4.5" (Black), z=4'9" (Red) and z=7'1.5" (Green)

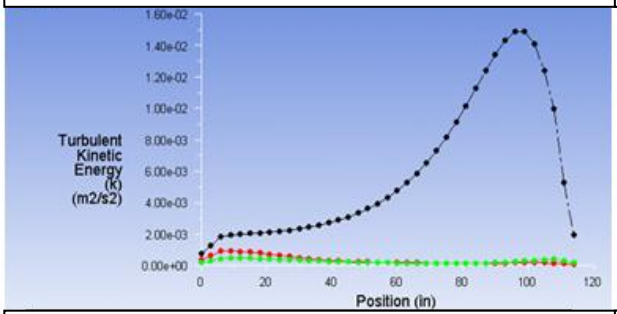

Turbulent Kinetic Energy along z-lines in B2 (x-z) plane at x=3' (Green), x=6'(Red) and x=9'(Black)

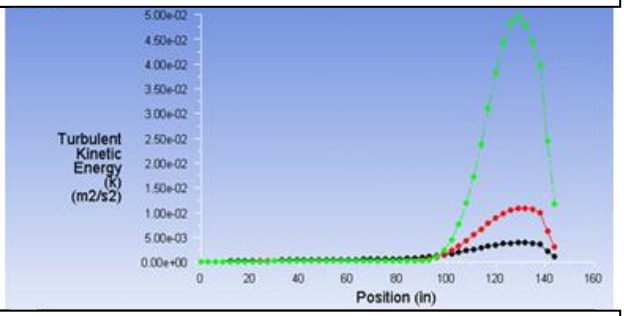

Turbulent Kinetic Energy along x-lines in B2 (x-z) plane at z=2'4.5" (Black), z=4'9" (Red) and z=7'1.5" (Green)

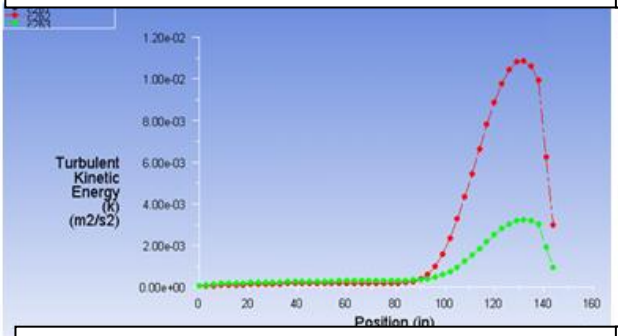

Turbulent Kinetic Energy along x-lines in C2 (x-y) plane at y=3' (Green), y=6'(Red) and y=9'(Black)

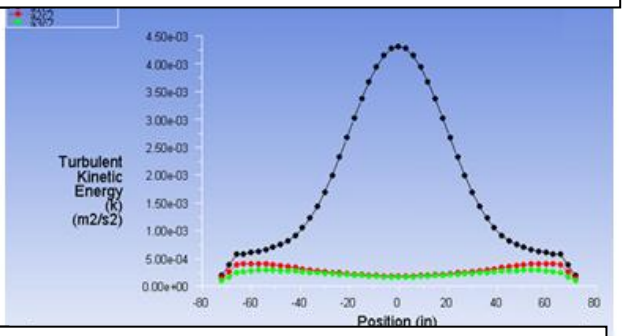

Turbulent Kinetic Energy along y-lines in C2 (x-y) plane at x=3' (Green), x=6'(Red) and x=9'(Black)

Figure 35: Case 1 - Turbulent Kinetic Energy Line Plots at Time T2 = 9:20 AM

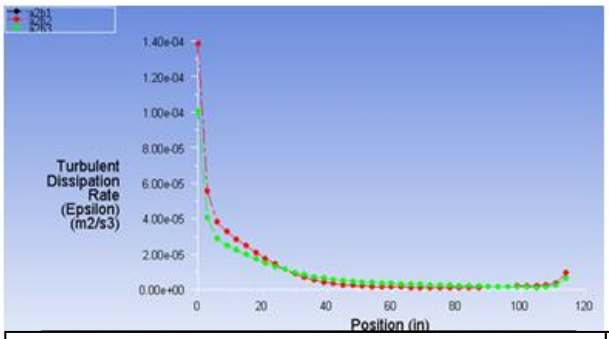

Turbulent Dissipation Rate along z-lines in A2 (y-z) plane at y=3' (Green), y=6'(Red) and y=9'(Black)

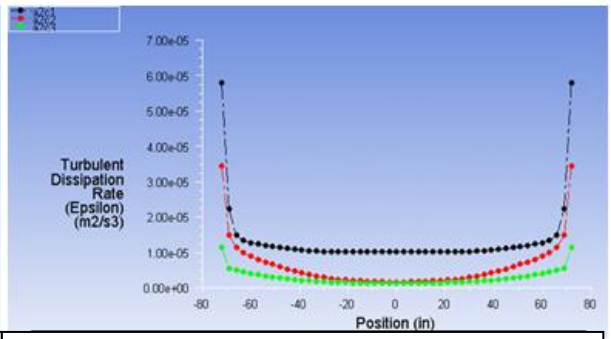

Turbulent Dissipation Rate along y-lines in A2 (y-z) plane at z=2'4.5" (Black), z=4'9" (Red) and z=7'1.5" (Green)

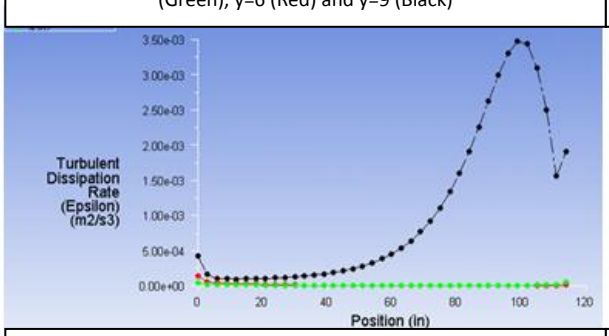

Turbulent Dissipation Rate along z-lines in B2 (x-z) plane at x=3' (Green), x=6'(Red) and x=9'(Black)

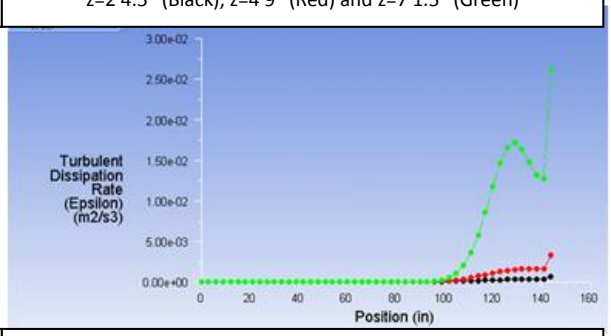

Turbulent Dissipation Rate along x-lines in B2 (x-z) plane at z=2'4.5" (Black), z=4'9" (Red) and z=7'1.5" (Green)

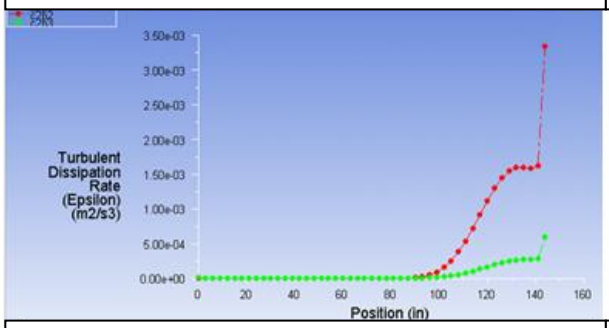

Turbulent Dissipation Rate along x-lines in C2 (x-y) plane at y=3' (Green), y=6'(Red) and y=9'(Black)

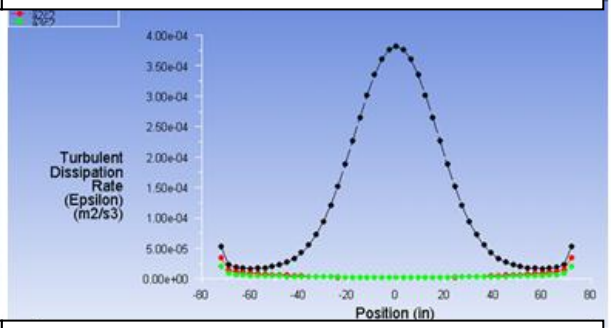

Turbulent Dissipation Rate along y-lines in C2 (x-y) plane at x=3' (Green), x=6'(Red) and x=9'(Black)

Figure 36: Case 1 - Turbulent Dissipation Rate Line Plots at Time T2 = 9:20 AM

Next, we present results at time T3 = 2:53 PM. The key to interpreting the results in the various planes (A1-A3, B1-B3, and C1-C3) and along the various lines in these planes inside the room is the same as described before for Figures 21-28 at time T1=3:45 AM. At T3 = 2:53 PM the outside temperature is just past its peak as shown in the ASHRAE curve (Figure 7). Figure 37 shows the temperature contours inside the room in planes (A1-A3, B1-B3, and C1-C3). The temperature in the room is nearly constant.

Figure 38 shows the velocity magnitude contours in the different planes of the room as described in Figure 19. These contours show increased velocity along the floor and the ceiling of the room due to the circulation of air caused by the rising warm air. Figure 39 shows the line plots of the temperature distributions inside the room along the lines in planes A1-A3, B1-B3, and C1-C3 shown in Figure 19. These line plots show that the solution satisfies the adiabatic wall conditions in the room except for the exterior wall where a constant temperature boundary condition is imposed corresponding to the external temperature at time T3. Figures 40-42 show the line plots of the velocity components in the room. These plots show that the velocity components go to zero as they approach the walls. These line plots are a quantitative description of the contour plots shown in Figure 38. Figure 43 shows the turbulent kinetic energy line plots along the various cross-sectional lines inside the room; they are indicative of the relative turbulence intensity in various parts of the room. As expected, the turbulent intensity is greater in the middle of the room than near the walls. Figure 44 shows line plots of the turbulent dissipation rate (ε) along various cross-sectional lines inside the room. In contrast to k, the value of epsilon peaks near the walls because of large dissipation of turbulence, and is fairly constant across the room in all directions except near the walls.

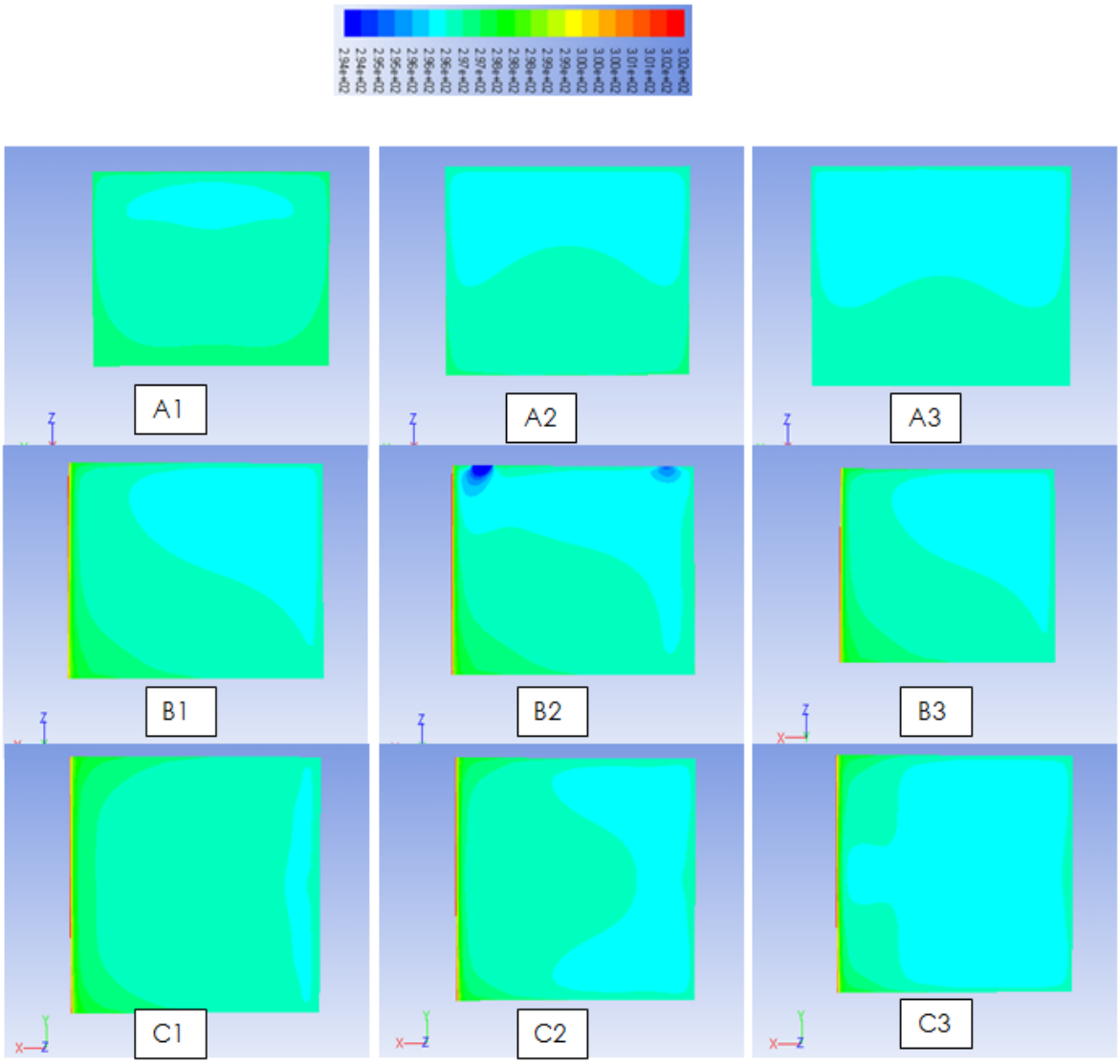

Figure 37: Case 1 - Temperature Contours in Different Planes of Figure 19 at Time T3 = 2:53 PM

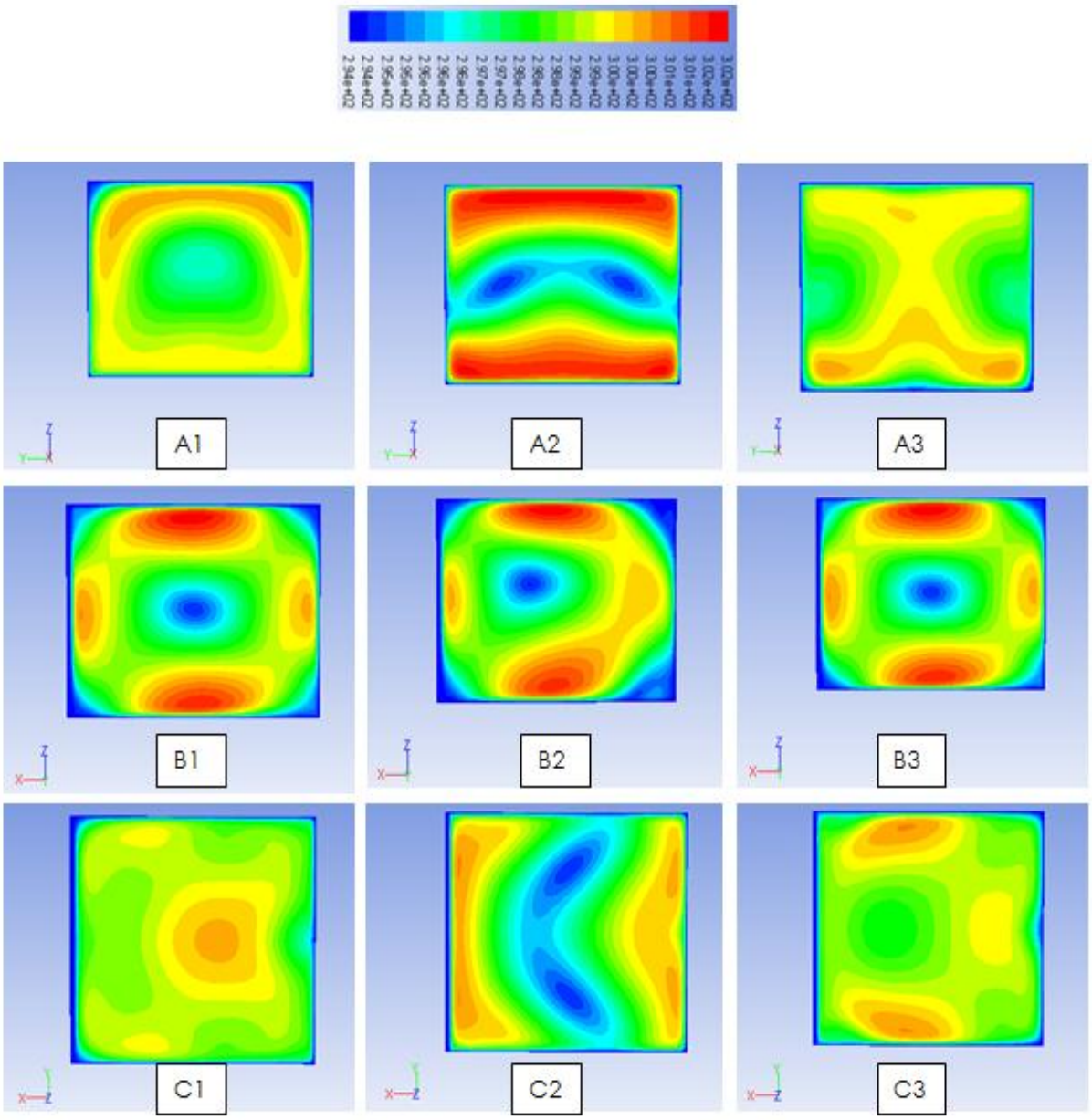

Figure 38: Case 1 - Velocity Contours in Different Planes of Figure 19 at Time T3 = 2:53 PM

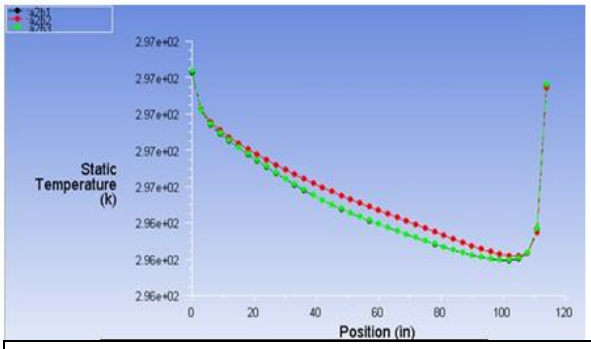

Temperature along z-lines in A2 (y-z) plane at y=3' (Green), y=6'(Red) and y=9'(Black)

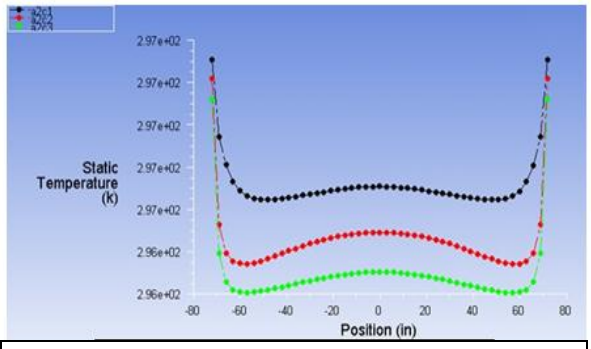

Temperature along y-lines in A2 (y-z) plane at z=2'4.5" (Black), z=4'9" (Red) and z=7'1.5" (Green)

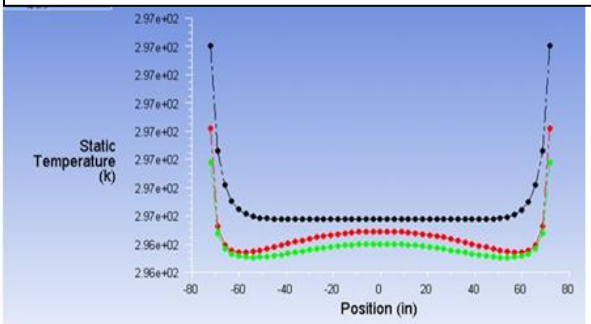

Temperature along z-lines in B2 (x-z) plane at x=3' (Green), x=6'(Red) and x=9'(Black)

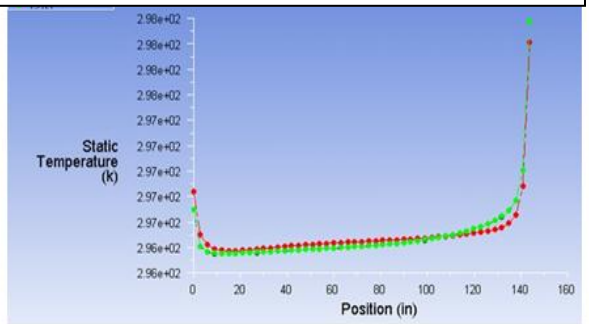

Temperature along x-lines in B2 (x-z) plane at z=2'4.5" (Black), z=4'9" (Red) and z=7'1.5" (Green)

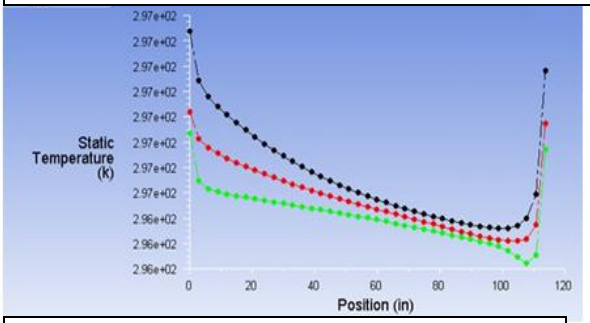

Temperature along x-lines in C2 (x-y) plane at y=3' (Green), y=6'(Red) and y=9'(Black)

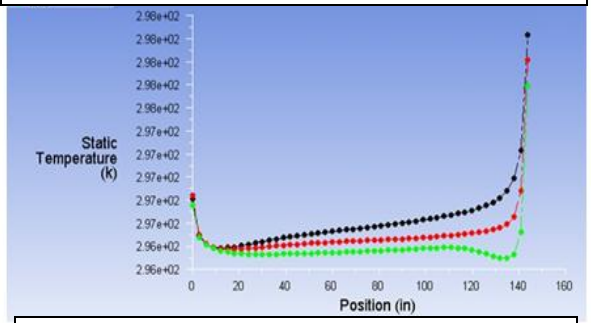

Temperature along y-lines in C2 (x-y) plane at x=3' (Green), x=6'(Red) and x=9'(Black)

Figure 39: Case 1 – Temperature Line Plots at Time T3 = 2:53 PM

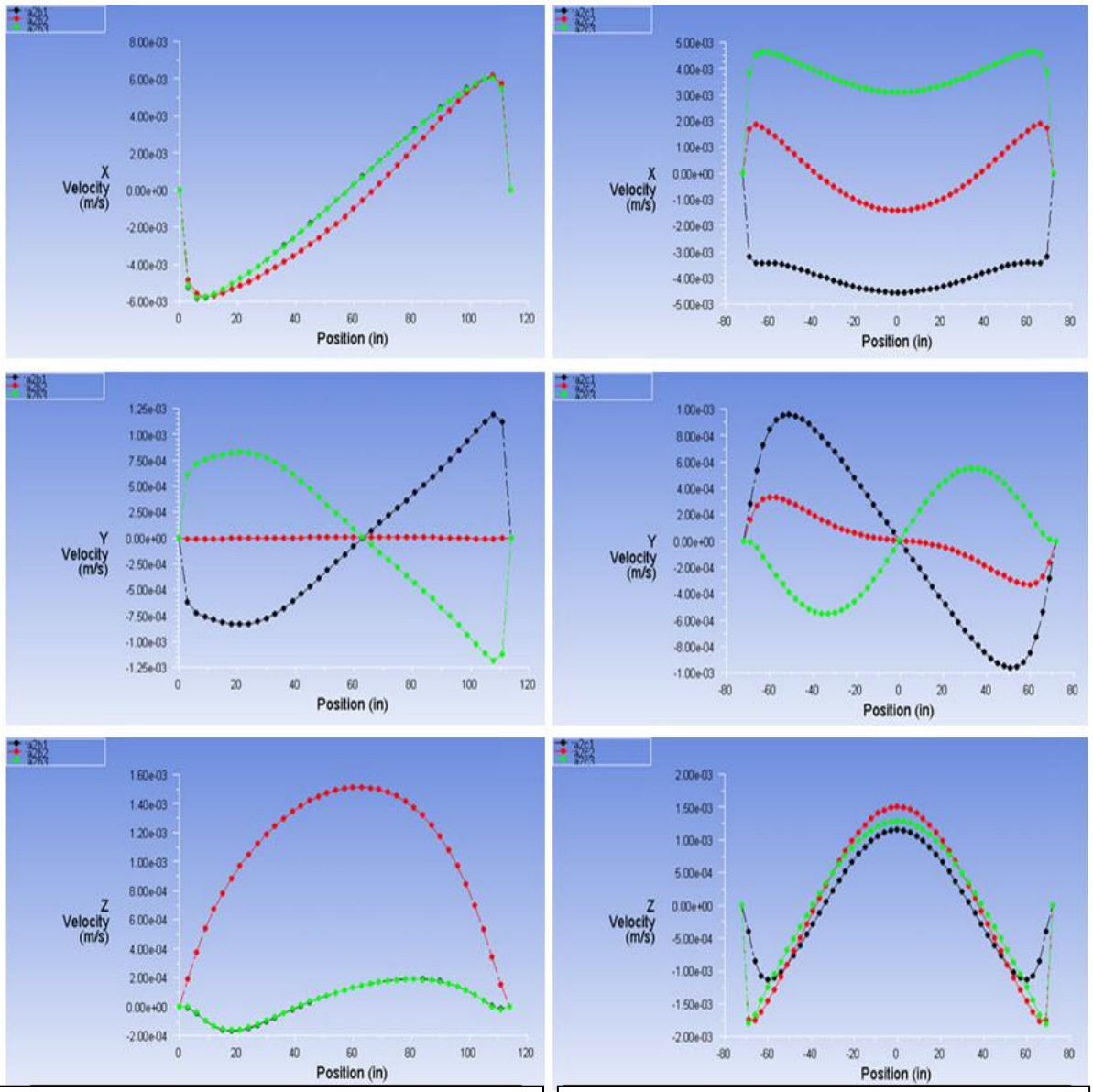

X, Y and Z Velocity Components along z-lines in A2 (y-z) plane at y=3'(Green), y=6'(Red), and y=9'(Black)

X, Y and Z Velocity Components along y-lines in A2 (y-z) plane at z=2'4.5" (Black), z=4'9" (Red), and z=7'1.5" (Green)

Figure 40: Case 1 - Velocity Components in the A2 Plane at Time T3 = 2:53 PM

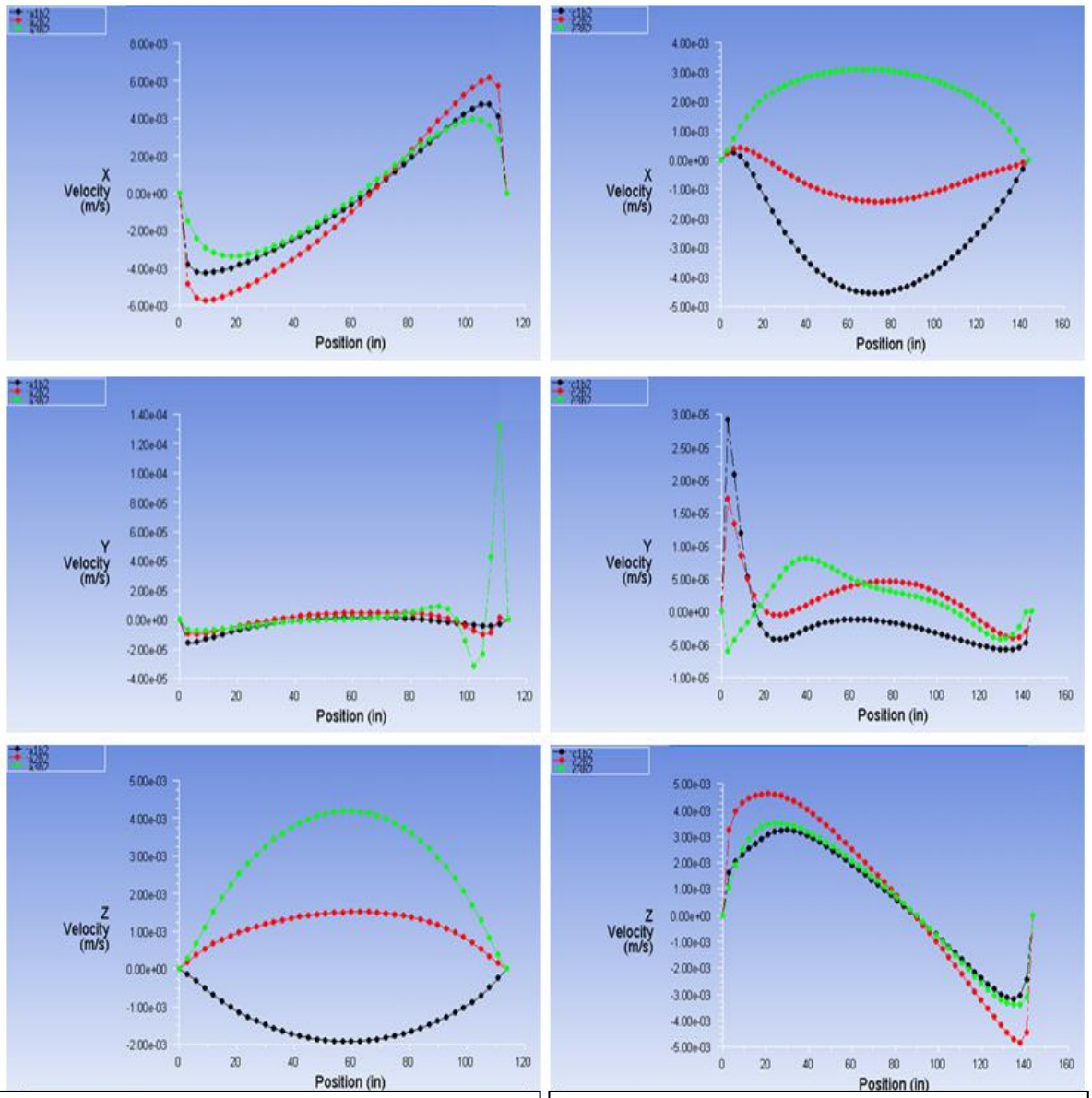

X, Y and Z Velocity Components along z-lines in B2(x-z) plane at x=3'(Green), x=6'(Red), and x=9'(Black)	X, Y and Z Velocity Components along x-lines in B2 (x-z) plane at z=2'4.5" (Black), z=4'9" (Red), and z=7'1.5"(Green)

Figure 41: Case 1 - Velocity Components in the B2 Plane at Time T3 = 2:53 PM

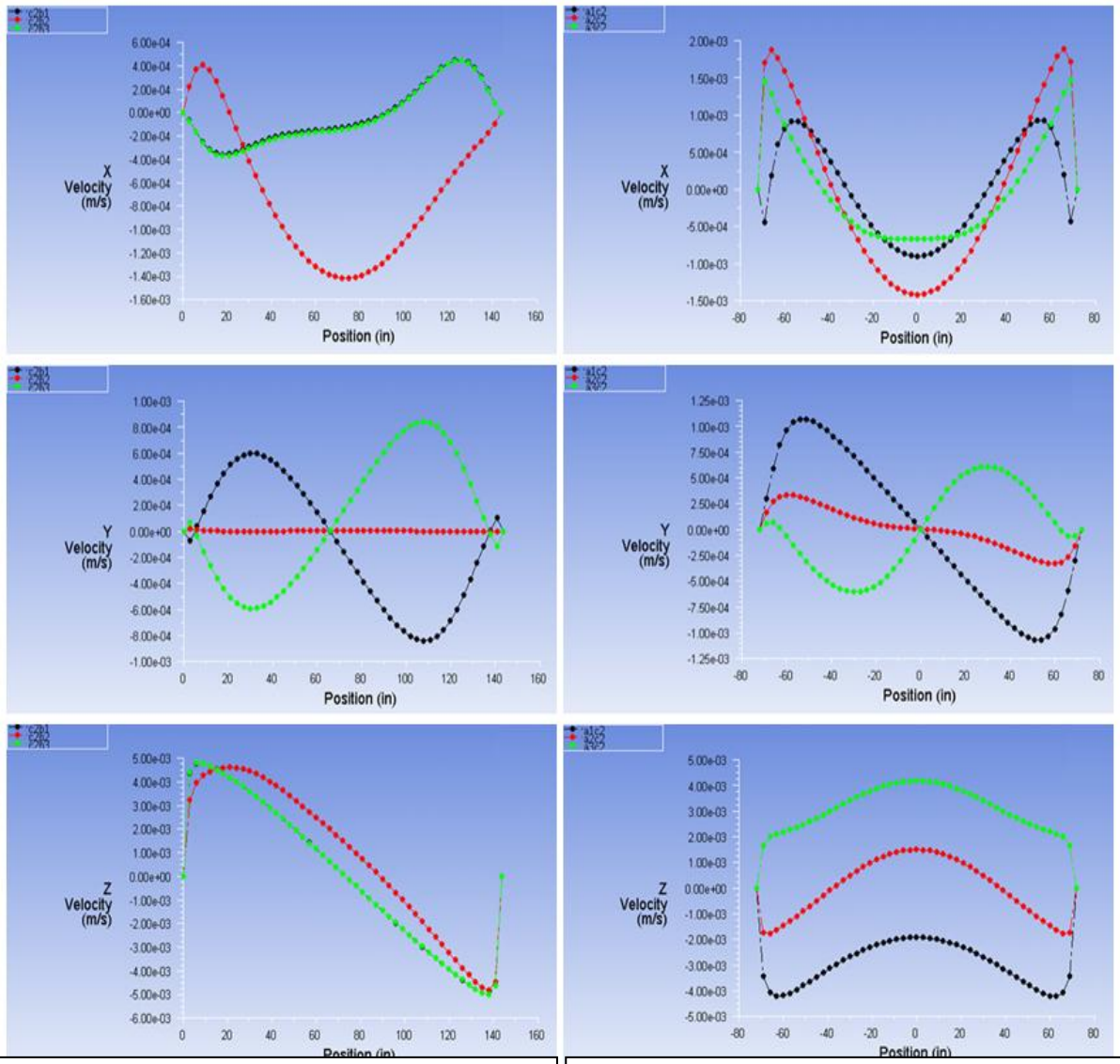

X, Y and Z Velocity Components along x-lines in C2 (x-y) plane at y=3' (Green), y=6' (Red), and y=9' (Black)

X, Y and Z Velocity Components along y-lines in C2 (x-y) plane at x=3' (Green), x=6' (Red), and x=9' (Black)

Figure 42: Case 1 - Velocity Components in the C2 Plane at Time T3 = 2:53 PM

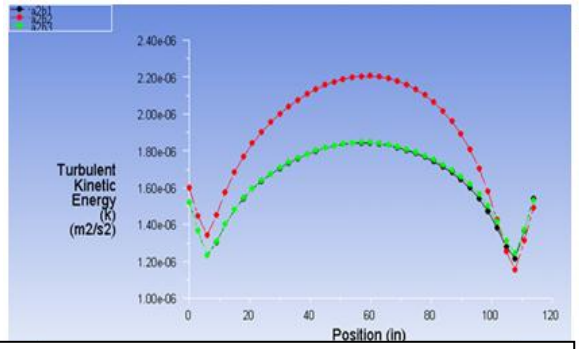

Turbulent Kinetic Energy along z-lines in A2 (y-z) plane at y=3' (Green), y=6'(Red) and y=9'(Black)

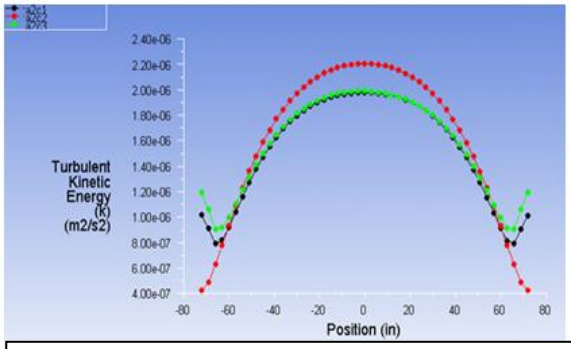

Turbulent Kinetic Energy along y-lines in A2 (y-z) plane at z=2'4.5" (Black), z=4'9"(Red) and z=7'1.5"(Green)

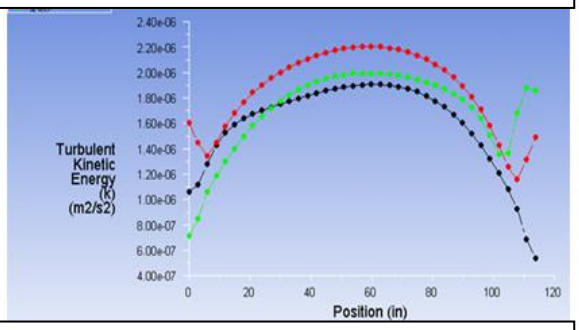

Turbulent Kinetic Energy along z-lines in B2 (x-z) plane at x=3' (Green), x=6'(Red) and x=9'(Black)

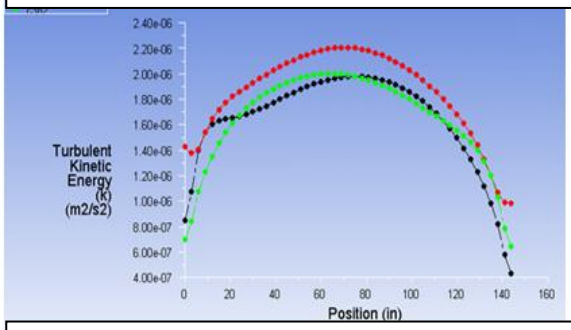

Turbulent Kinetic Energy along x-lines in B2 (x-z) plane at z=2'4.5" (Black), z=4'9"(Red) and z=7'1.5"(Green)

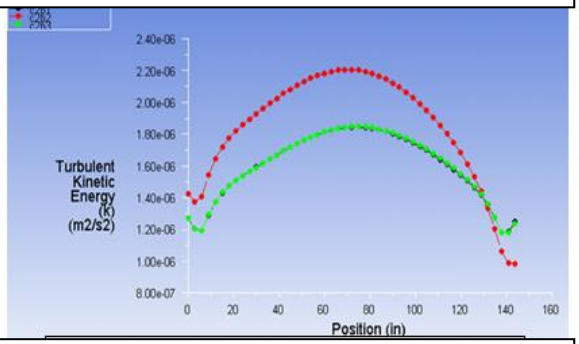

Turbulent Kinetic Energy along x-lines in C2 (x-y) plane at y=3' (Green), y=6'(Red) and y=9'(Black)

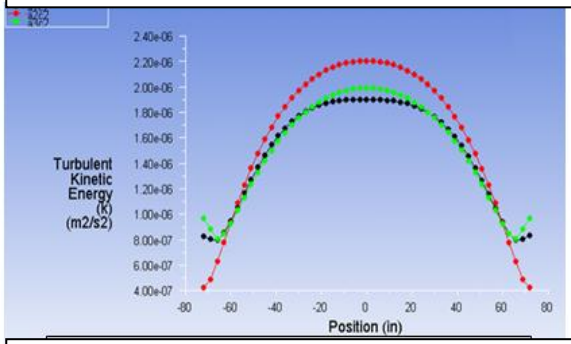

Turbulent Kinetic Energy along y-lines in C2 (x-y) plane at x=3' (Green), x=6'(Red) and x=9'(Black)

Figure 43: Case 1 - Turbulent Kinetic Energy Line Plots at Time T3 = 2:53 PM

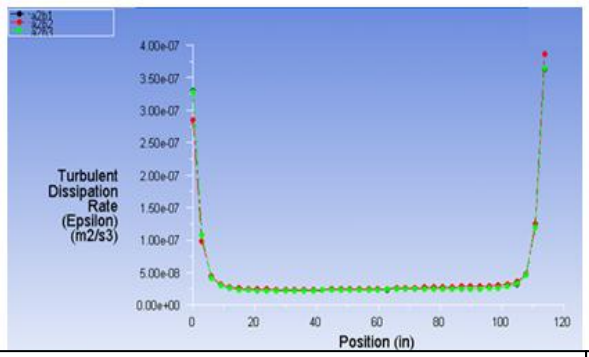

Turbulent Dissipation Rate along z-lines in A2 (y-z) plane at y=3' (Green), y=6'(Red) and y=9'(Black)

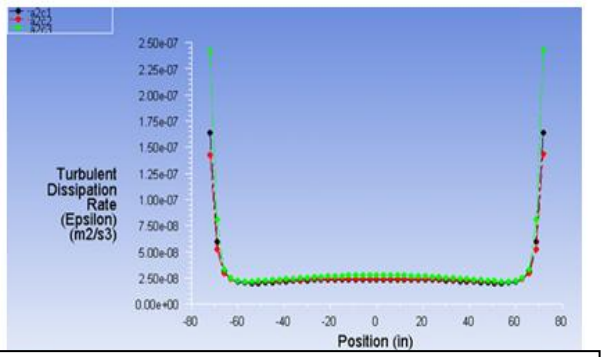

Turbulent Dissipation Rate along y-lines in A2 (y-z) plane at z=2'4.5" (Black), z=4'9"(Red) and z=7'1.5"(Green)

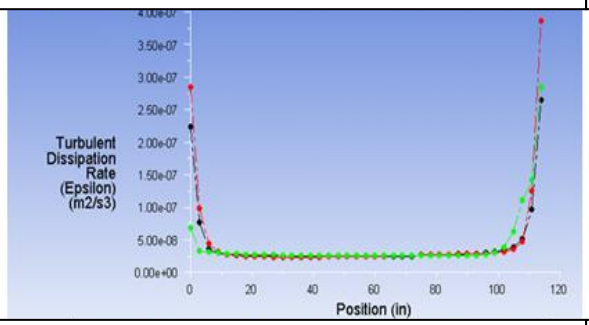

Turbulent Dissipation Rate along z-lines in B2 (x-z) plane at x=3' (Green), x=6'(Red) and x=9'(Black)

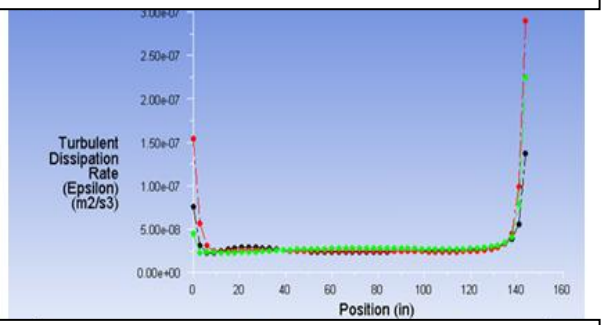

Turbulent Dissipation Rate along x-lines in B2 (x-z) plane at z=2'4.5" (Black), z=4'9"(Red) and z=7'1.5"(Green)

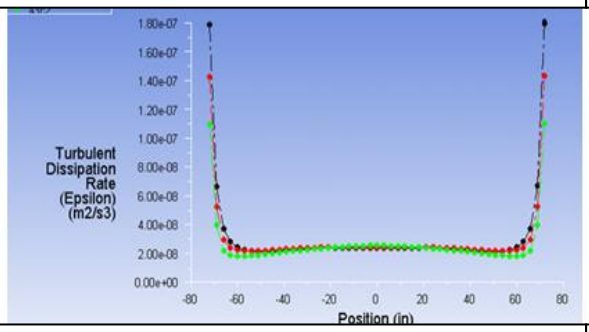

Turbulent Dissipation Rate along x-lines in C2 (x-y) plane at y=3' (Green), y=6'(Red) and y=9'(Black)

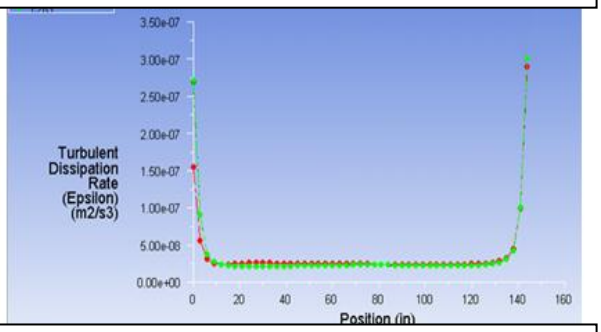

Turbulent Dissipation Rate along y-lines in C2 (x-y) plane at x=3' (Green), x=6'(Red) and x=9'(Black)

Figure 44: Case 1 - Turbulent Dissipation Rate Line Plots at Time T3 = 2:53 PM

The final data set for Case 1 is generated at T4 = 8:27 PM. This time corresponds to another low temperature outside the room as shown on the ASHRAE curve (Figure 7). Figure 45 shows the contours of temperature distributions in different planes (A1-A3, B1-B3, and C1-C3). The lack of heat from the hot external wall results in a nearly constant room temperature. Figure 46 shows the velocity contours in different planes of the room depicted in Figure 19. These velocities are very low because the low constant temperature doesn't require any cooling from the ventilation system. Figure 47 shows various line plots of temperature distribution inside the room in planes A1-A3, B1-B3, and C1-C3 shown in Figure 19. These plots show that the solution satisfies the adiabatic wall conditions in the room except for the exterior wall where a constant temperature boundary condition is imposed corresponding to temperature at time T4.

Figures 48-50 show various velocity components inside the room. These line plots show that the no slip condition is correctly imposed at the walls; all the velocity components go to zero at the walls. Figure 51 shows the turbulent kinetic energy line plots along various cross-sectional lines inside the room; they indicate the relative turbulence intensity in various parts of the room. The values of k are very small because of the very low flow velocities. As expected, the turbulent intensity is greater in the middle of the room than near the walls. Figure 52 shows line plots of the turbulent dissipation rate along various cross-sectional lines inside the room. In contrast to k, the values of epsilon peak near the walls because of the large dissipation of turbulence there. The value of epsilon is fairly constant across the room in all directions except near the wall.

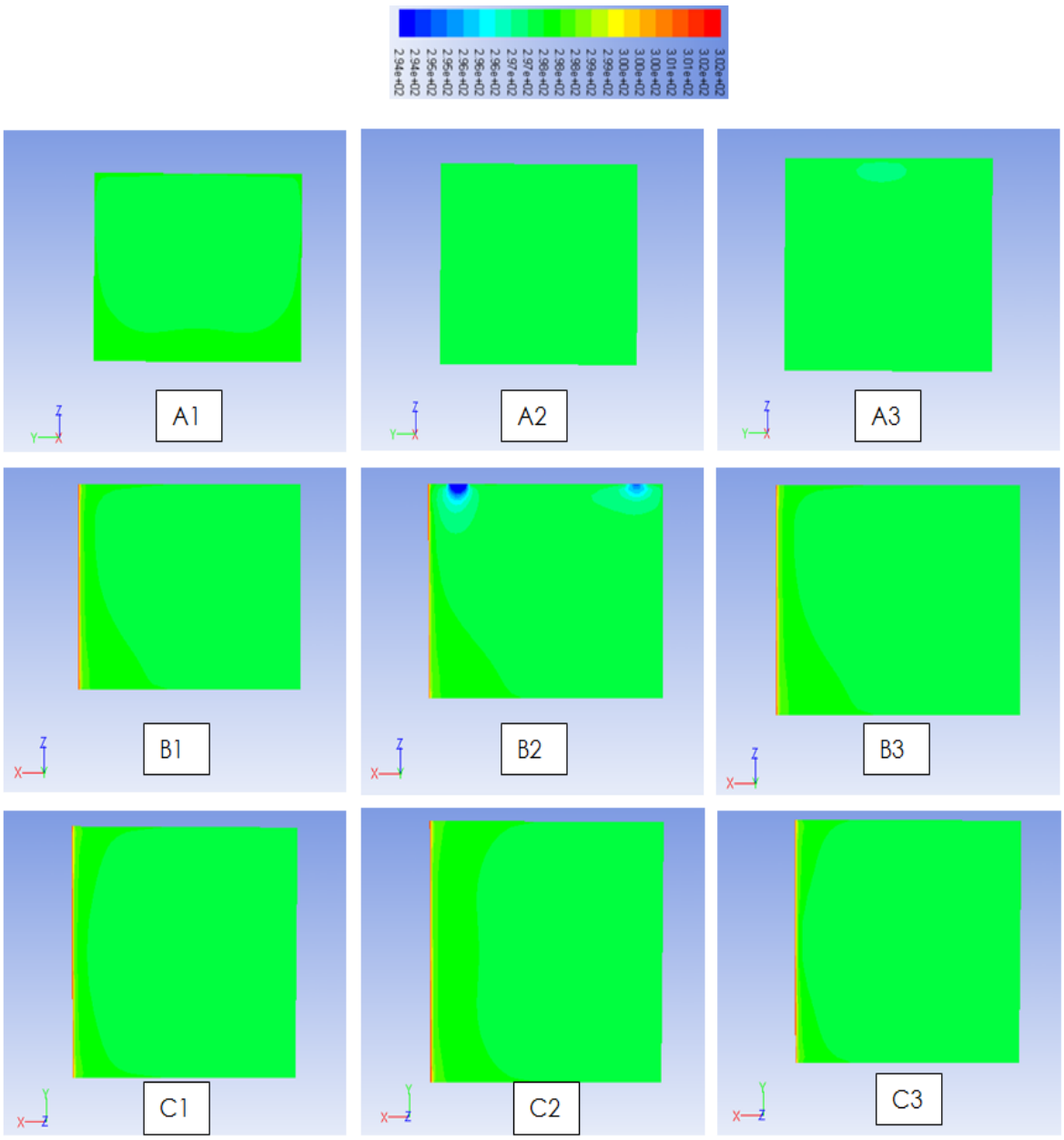

Figure 45: Case 1 - Temperature Contours in Different Planes of Figure 19 at Time T4 = 8:27 PM

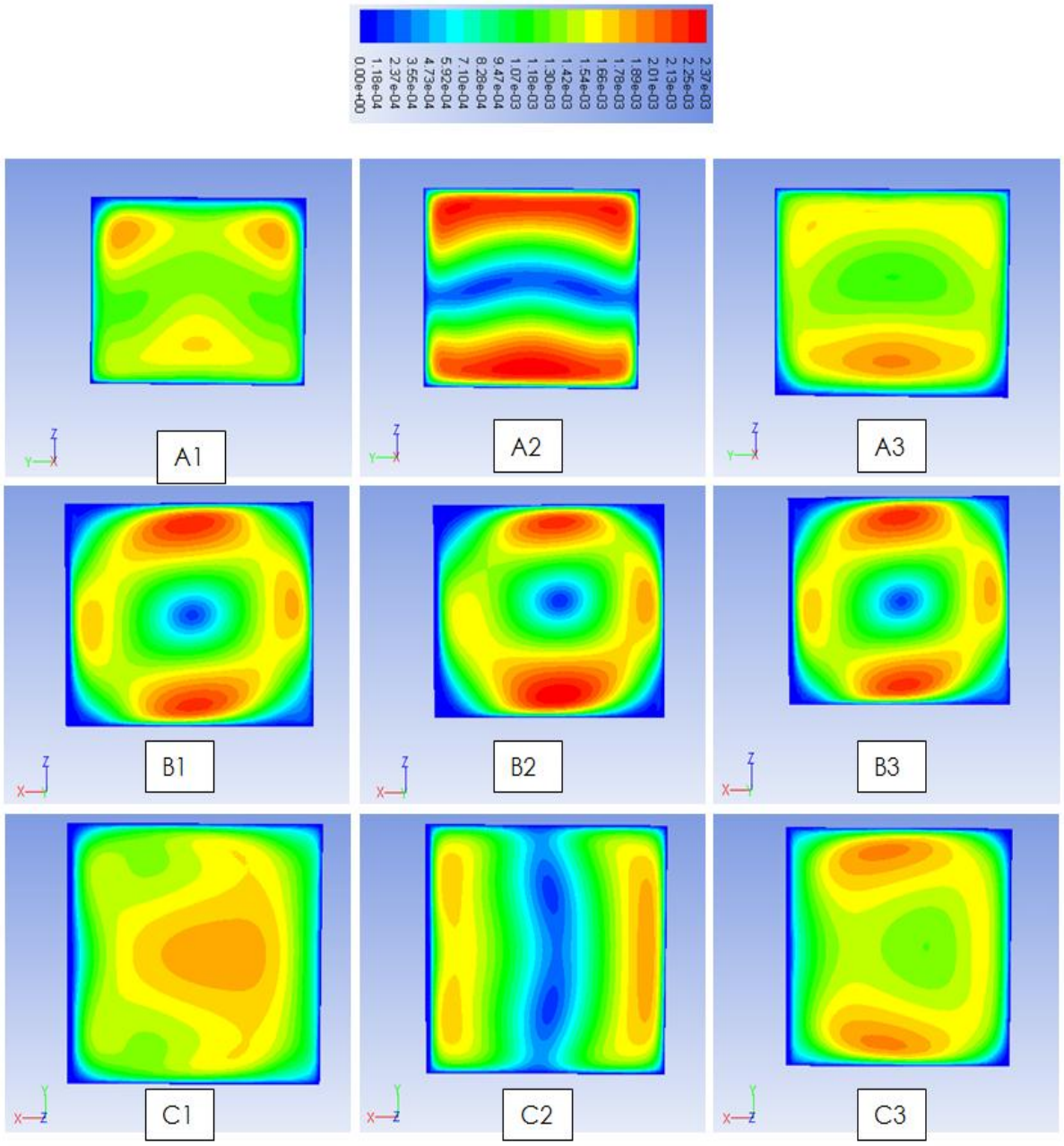

Figure 46: Case 1 - Velocity Contours in Different Planes of Figure 19 at Time T4 = 8:27 PM

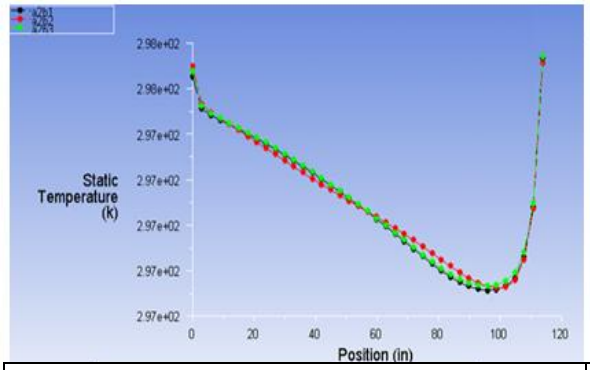

Temperature along z-lines in A2 (y-z) plane at y=3' (Green), y=6'(Red) and y=9'(Black)

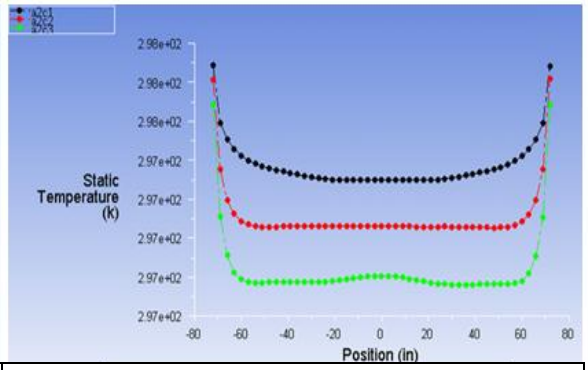

Temperature along y-lines in A2 (y-z) plane at z=2'4.5" (Black), z=4'9"(Red) and z=7'1.5"(Green)

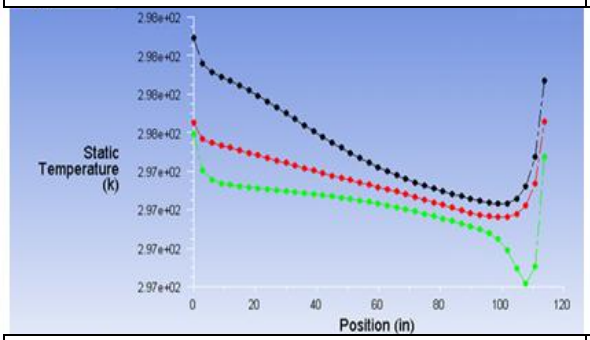

Temperature along z-lines in B2 (x-z) plane at x=3' (Green), x=6'(Red) and x=9'(Black)

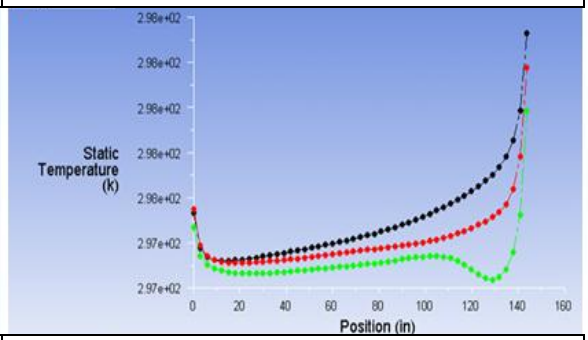

Temperature along x-lines in B2 (x-z) plane at z=2'4.5" (Black), z=4'9"(Red) and z=7'1.5"(Green)

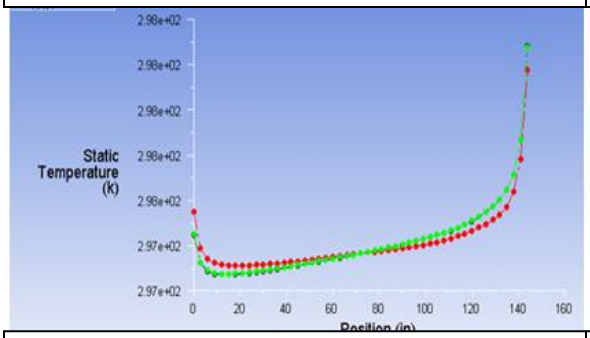

Temperature along x-lines in C2 (x-y) plane at y=3' (Green), y=6'(Red) and y=9'(Black)

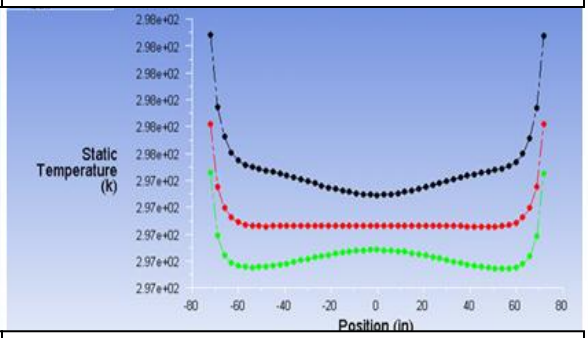

Temperature along y-lines in C2 (x-y) plane at x=3' (Green), x=6'(Red) and x=9'(Black)

Figure 47: Case 1 – Temperature Line Plots at Time T4 = 8:27 PM

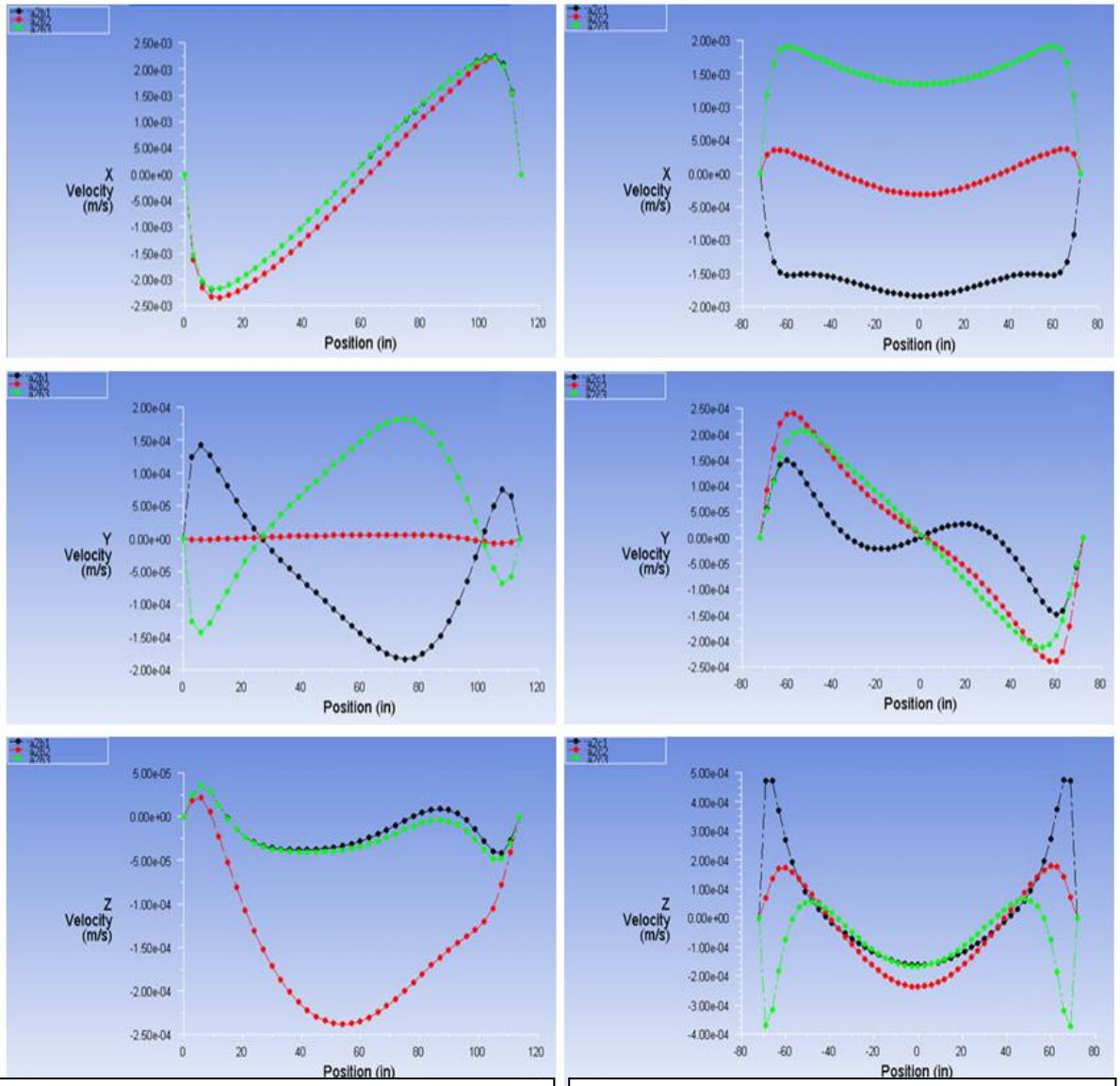

X, Y and Z Velocity Components along z-lines in A2 (y-z) plane at y=3'(Green), y=6'(Red), and y=9'(Black)

X, Y and Z Velocity Components along y-lines in A2 (y-z) plane at z=2'4.5" (Black), z=4'9" (Red), and z=7'1.5" (Green)

Figure 48: Case 1 - Velocity Components in the A2 Plane at Time T4 = 8:27 PM

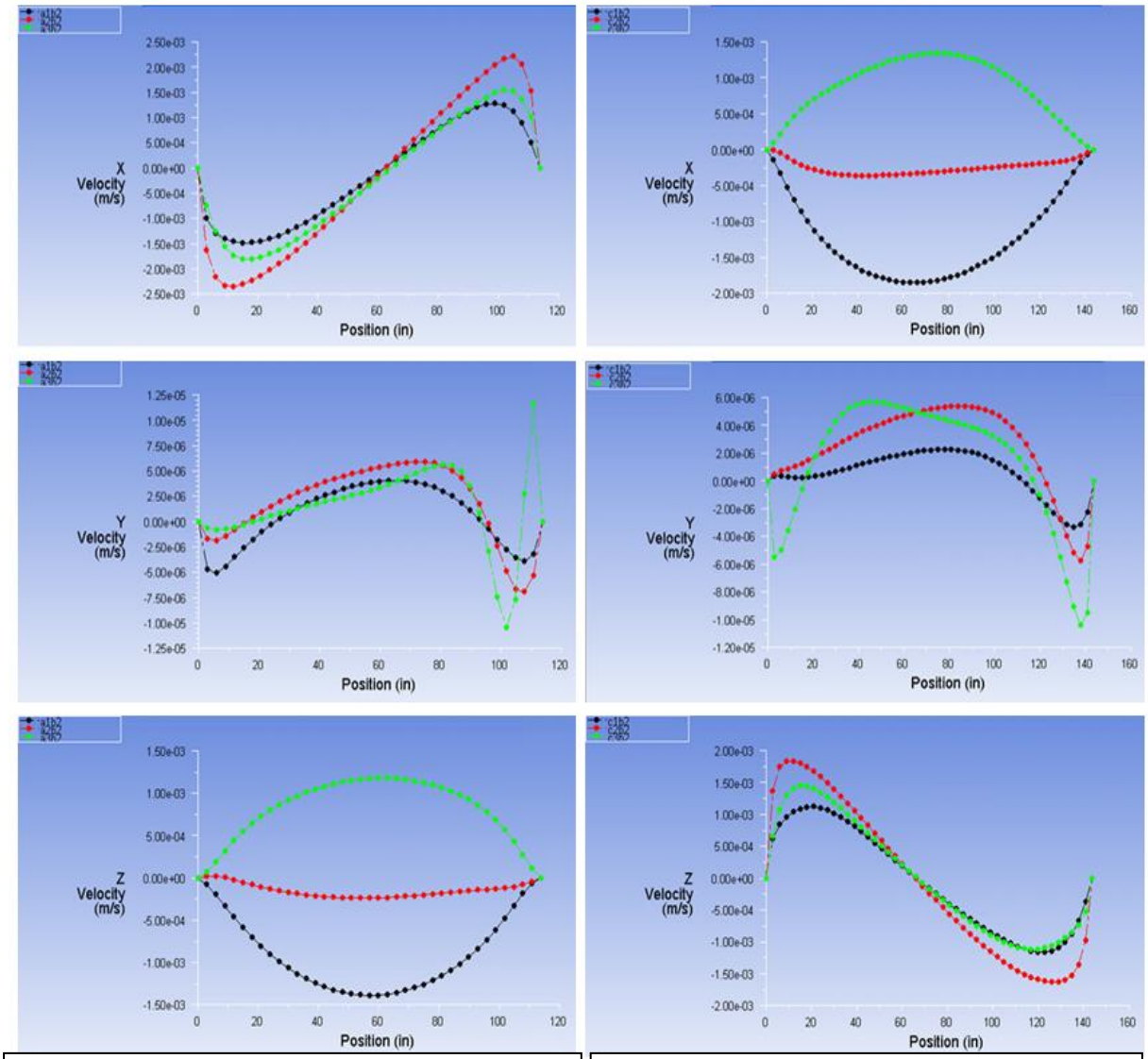

X, Y and Z Velocity Components along z-lines in B2(x-z) plane at x=3'(Green), x=6'(Red), and x=9'(Black)	X, Y and Z Velocity Components along x-lines in B2 (x-z) plane at z=2'4.5" (Black), z=4'9" (Red), and z=7'1.5"(Green)

Figure 49: Case 1 - Velocity Components in the B2 Plane at Time T4 = 8:27 PM

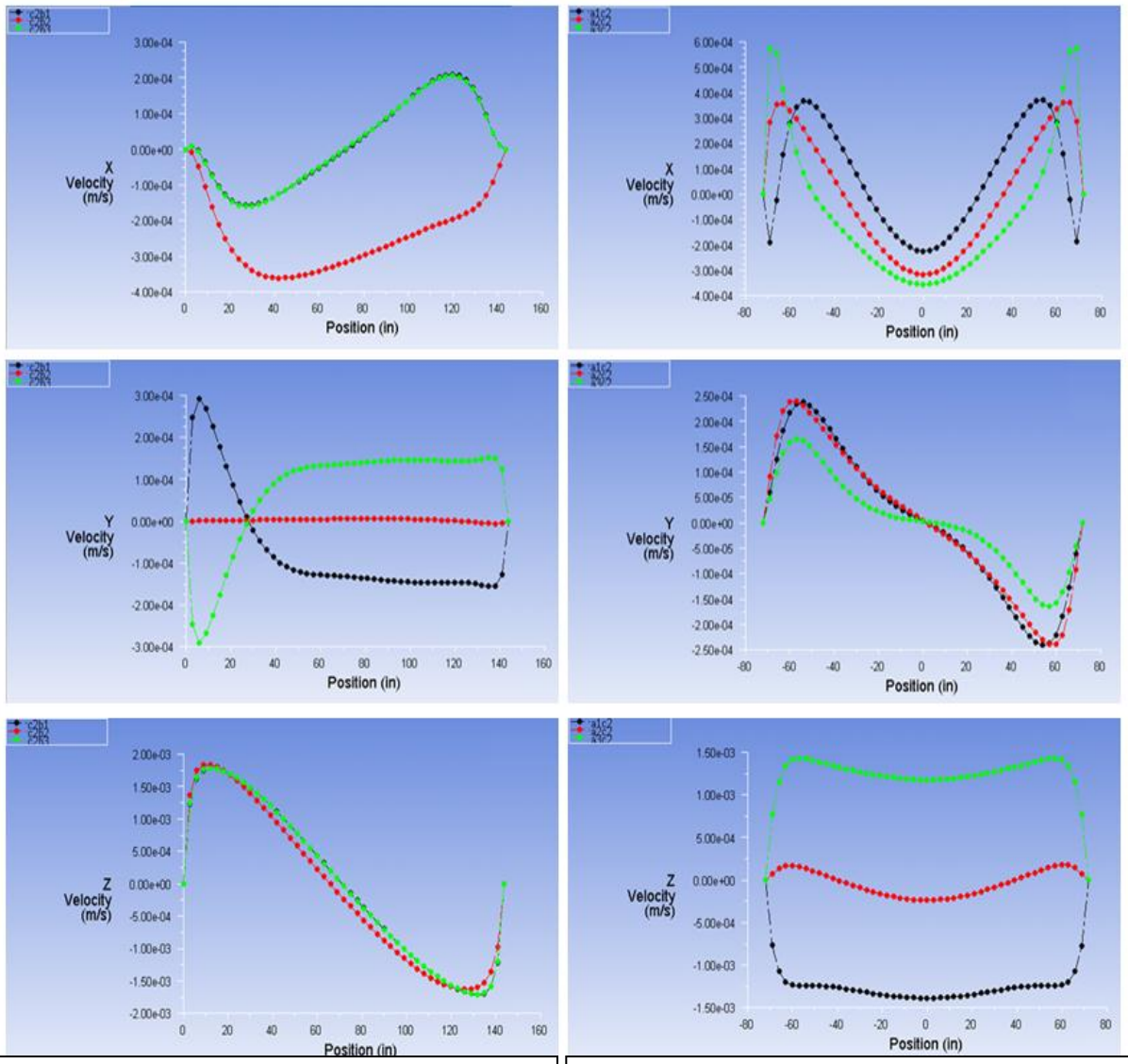

X, Y and Z Velocity Components along x-lines in C2 (x-y) plane at y=3' (Green), y=6' (Red), and y=9' (Black)	X, Y and Z Velocity Components along y-lines in C2 (x-y) plane at x=3' (Green), x=6' (Red), and x=9' (Black)

Figure 50: Case 1 - Velocity Components in the C2 Plane at Time T4 = 8:27 PM

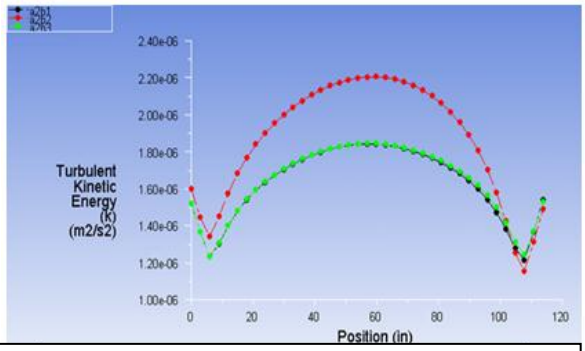

Turbulent Kinetic Energy along z-lines in A2 (y-z) plane at y=3' (Green), y=6'(Red) and y=9'(Black)

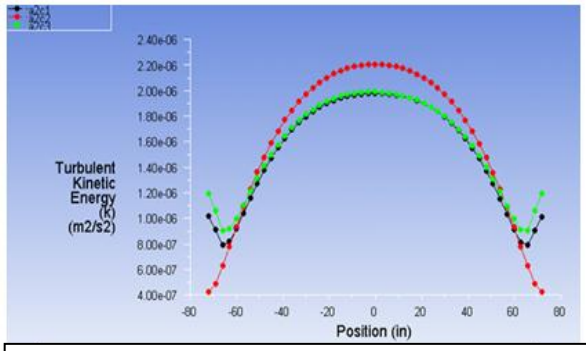

Turbulent Kinetic Energy along y-lines in A2 (y-z) plane at z=2'4.5" (Black), z=4'9"(Red) and z=7'1.5"(Green)

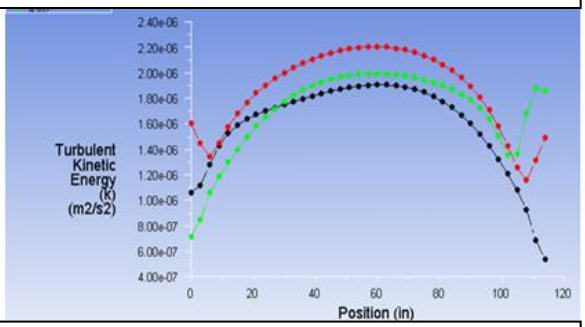

Turbulent Kinetic Energy along z-lines in B2 (x-z) plane at x=3' (Green), x=6'(Red) and x=9'(Black)

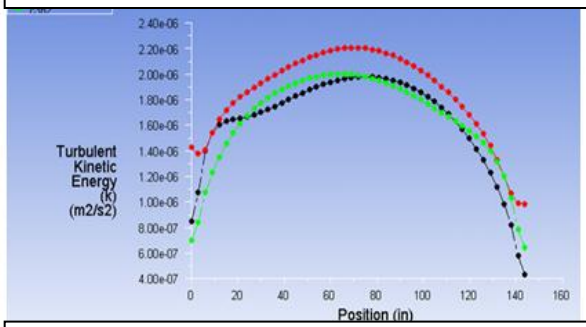

Turbulent Kinetic Energy along x-lines in B2 (x-z) plane at z=2'4.5" (Black), z=4'9"(Red) and z=7'1.5"(Green)

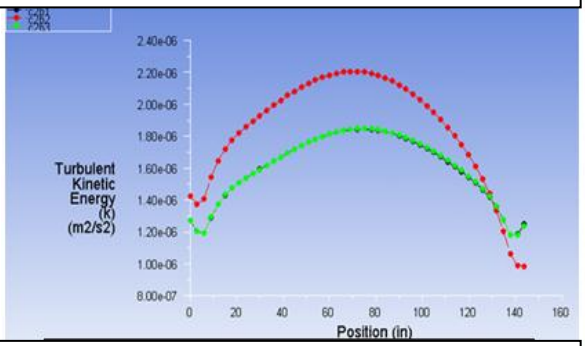

Turbulent Kinetic Energy along x-lines in C2 (x-y) plane at y=3' (Green), y=6'(Red) and y=9'(Black)

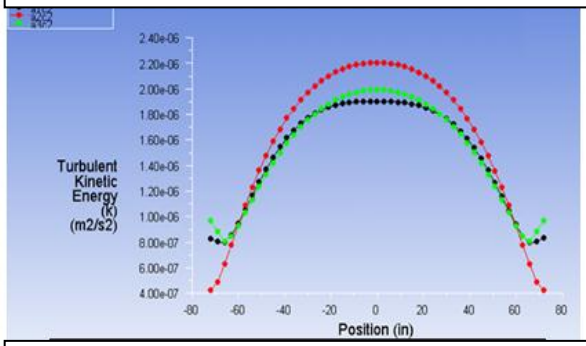

Turbulent Kinetic Energy along y-lines in C2 (x-y) plane at x=3' (Green), x=6'(Red) and x=9'(Black)

Figure 51: Case 1 - Turbulent Kinetic Energy Line Plots at Time T4 = 8:27 PM

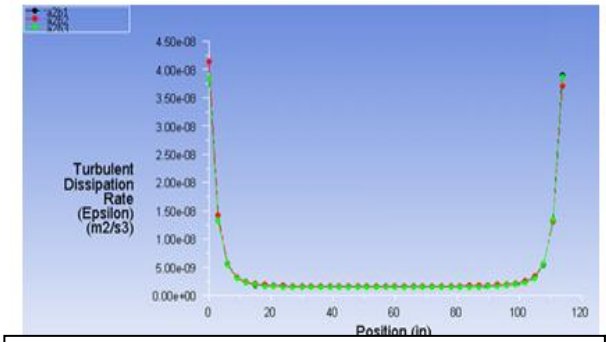

Turbulent Dissipation Rate along z-lines in A2 (y-z) plane at y=3' (Green), y=6'(Red) and y=9'(Black)

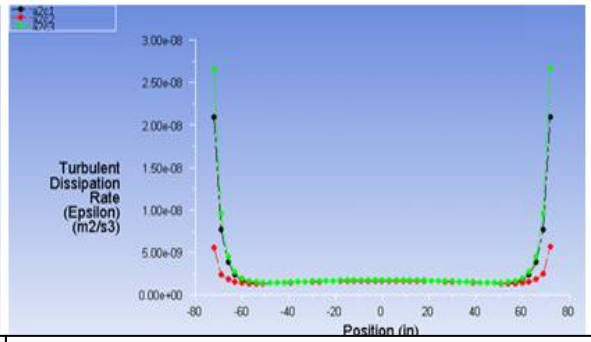

Turbulent Dissipation Rate along y-lines in A2 (y-z) plane at z=2'4.5" (Black), z=4'9"(Red) and z=7'1.5"(Green)

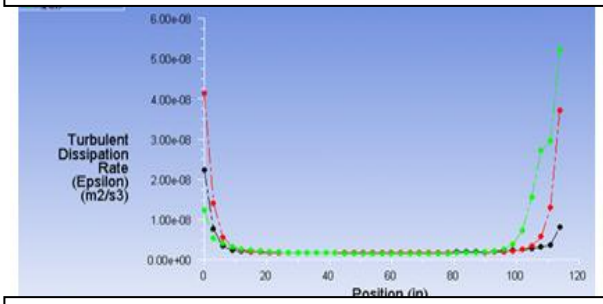

Turbulent Dissipation Rate along z-lines in B2 (x-z) plane at x=3' (Green), x=6'(Red) and x=9'(Black)

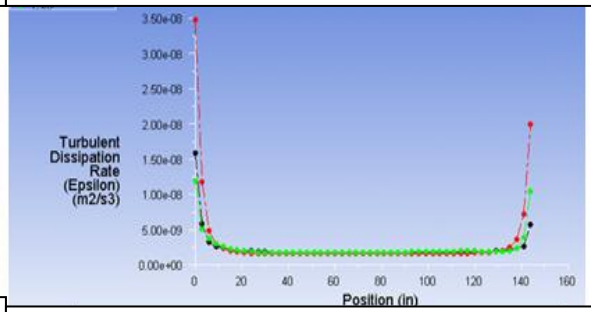

Turbulent Dissipation Rate along x-lines in B2 (x-z) plane at z=2'4.5" (Black), z=4'9"(Red) and z=7'1.5"(Green)

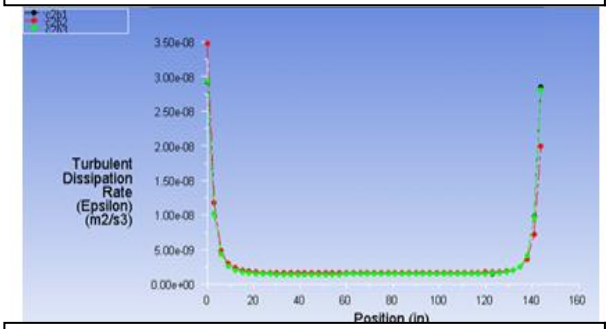

Turbulent Dissipation Rate along x-lines in C2 (x-y) plane at y=3' (Green), y=6'(Red) and y=9'(Black)

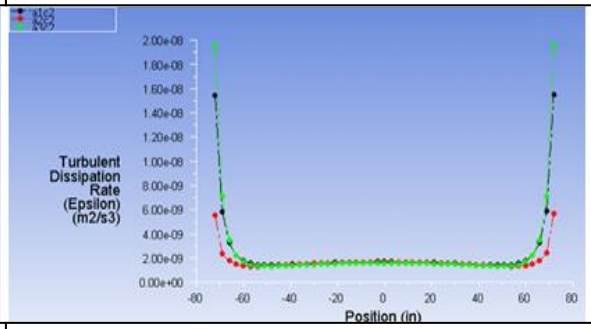

Turbulent Dissipation Rate along y-lines in C2 (x-y) plane at x=3' (Green), x=6'(Red) and x=9'(Black)

Figure 52: Case 1 - Turbulent Dissipation Rate Line Plots at Time T4 = 8:27 PM

5.4.3 Case 2: Variable Air Volume System with Radiant Cooling

The calculations for Case 2 were performed using the Boussinesq approximation for density, the k-ε realizable turbulence model, and a first order upwind scheme in FLUENT. Computations were performed for two 24-hour time cycles. A time step of 10 seconds was employed for each iteration. Thus, 8640 time steps were required to cover a 24-hour period. The details of the geometry, mesh, boundary conditions, and mass flow rate into the room for this case are described in sections 5.2 and 5.3. A total of 99240 iterations were required to complete the two 24-hour cycles for Case 2. The solutions obtained during the second 24-hour cycle are free of transient effects due to the initial conditions. Figure 53 shows the convergence history of various flow variables and governing equations. In particular, it represents the change in the residuals during the iterative process.

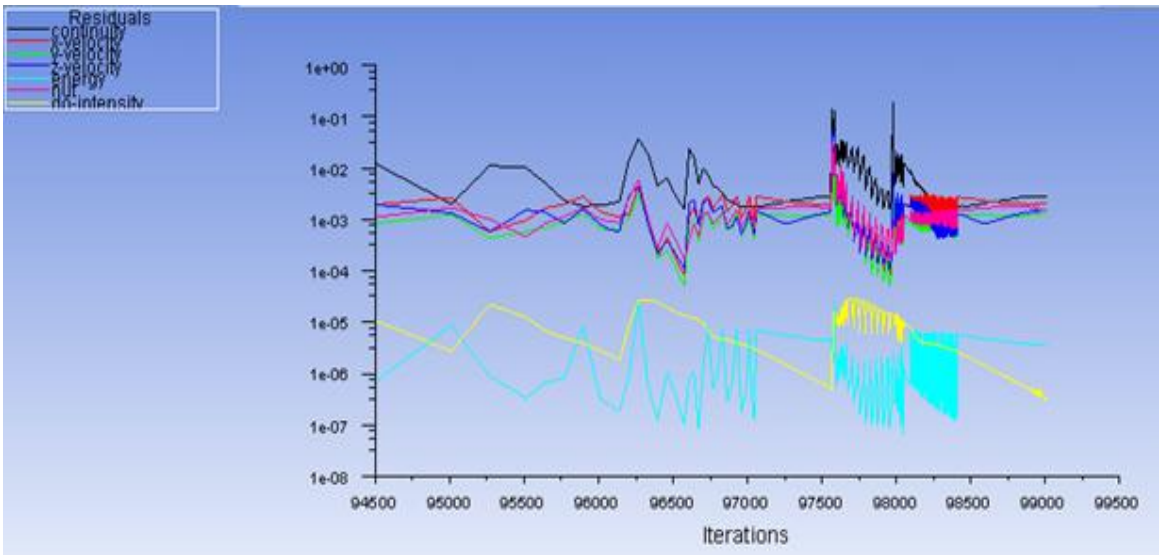

Figure 53: Case 2 - Residual History of Various Flow Variables and Governing Equations During the Iterative Process

Figure 54 shows the contours of temperature distributions in the different planes at T1 = 3:45 AM. T1 corresponds to a low temperature on the ASHRAE curve (Figure 7). As a result, the vents are not required to circulate the air inside the room, and the temperature remains nearly constant except in the area above the radiation slab where the air is much cooler. This area has a lower temperature than the rest of the room due to its proximity to the slab. Figure 55 depicts the velocity contours in different planes of the room as described in Figure 19. These velocities are slightly different than those of Case 1 due to the presence of the radiation slab, but are all still very low because the vents have not been active at time T1, and have not been active for a long period of time before time T1 because of the existing cooler temperature. This figure does show that there is some circulation in the room. Also, the velocity is highest in the middle of the room.

Figure 56 shows the line plots of temperature distributions inside the room along various lines in planes A1-A3, B1-B3, and C1-C3 as shown in Figure 19. These plots show that the solution satisfies the adiabatic wall conditions in the room except at the exterior wall where a constant temperature boundary condition is imposed corresponding to the external temperature at time T1. In addition we note from Figure 56 that the temperature is much cooler near the radiation slab in the ceiling as expected. This is a quantitative description of what is shown in the contour plots of Figure 54. These line plots also show that there is very little variation in the temperature inside the room that isn't near the radiation slab.

Figures 57-59 show the line plots of various velocity components inside the room. These plots show, as expected, that the no slip condition is correctly imposed at the walls; all velocity components go to zero as they approach the walls. All of these velocities are very

small in magnitude, which is a quantitative description of the contour plots shown in Figure 55. Figure 60 shows the turbulent kinetic energy line plots along various cross-sectional lines inside the room, which is indicative of the relative turbulence intensity in various parts of the room. The values of k are very small because of low flow velocities except near the ceiling around the radiation slab where the restricted area leads to slightly elevated turbulence. As expected, the turbulent intensity is generally greater in the middle of the room than near the walls, and near the radiation slab. Figure 61 shows the line plots of the turbulent dissipation rate along various cross-sectional lines inside the room. In contrast to k, the values of epsilon are nearly zero due to the very low air velocity. The value of epsilon is fairly constant across the room in all directions with values on the order of 10^{-12}.

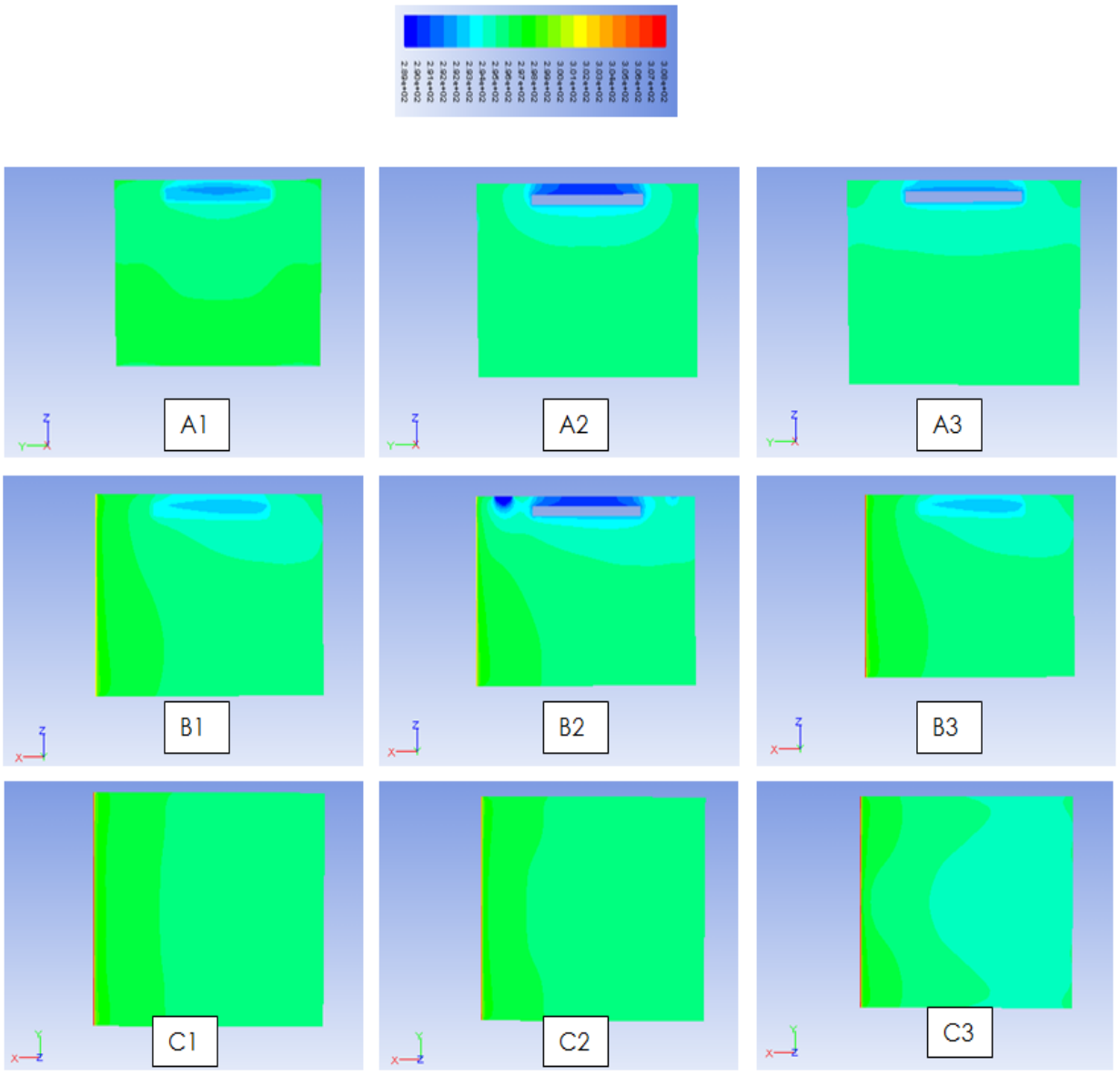

Figure 54: Case 2 - Temperature Contours in Different Planes of Figure 19 on Time T1 = 3:45 AM

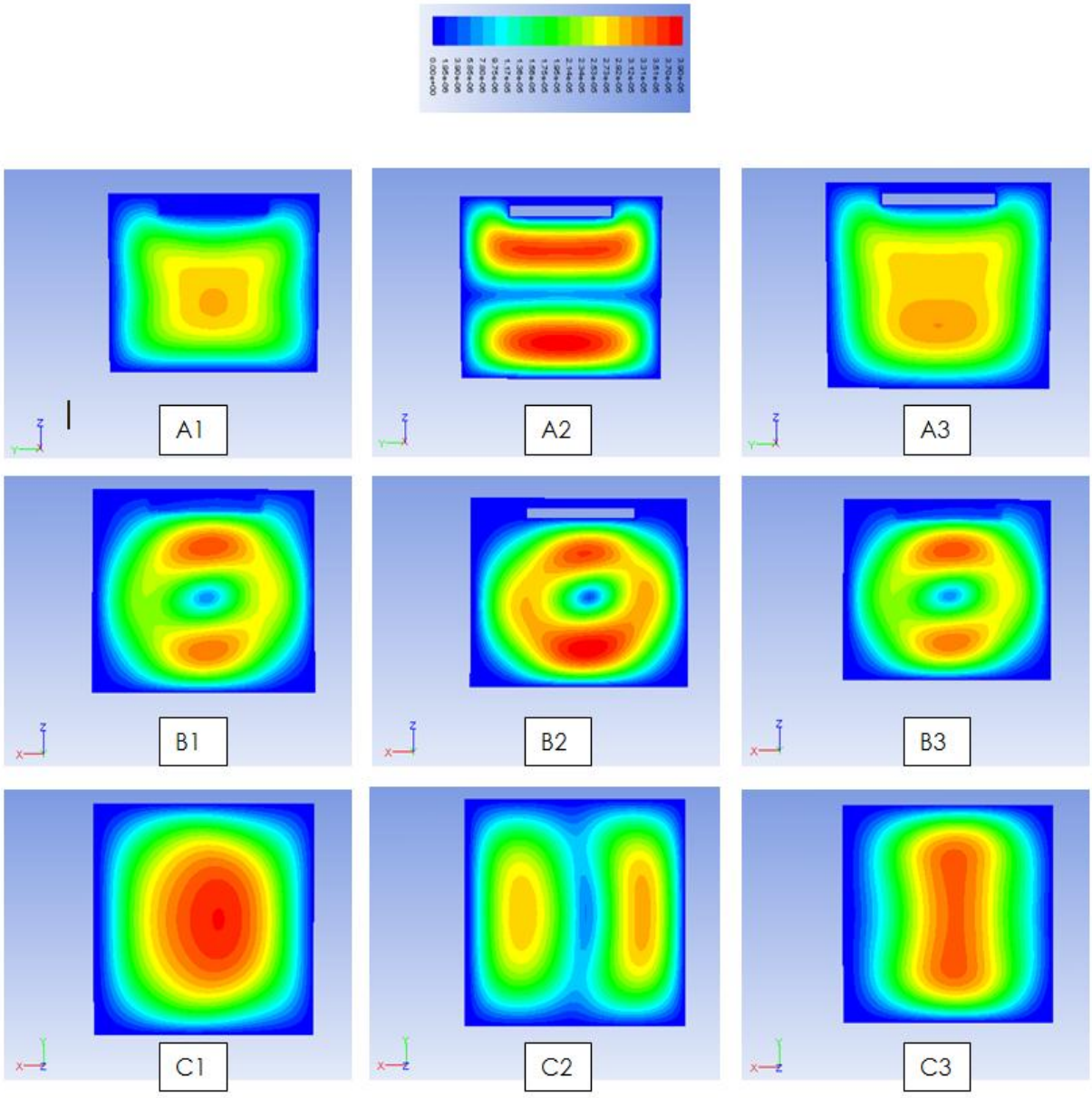

Figure 55: Case 2 - Velocity Contours in Different Planes of Figure 19 at Time T1 = 3:45 AM

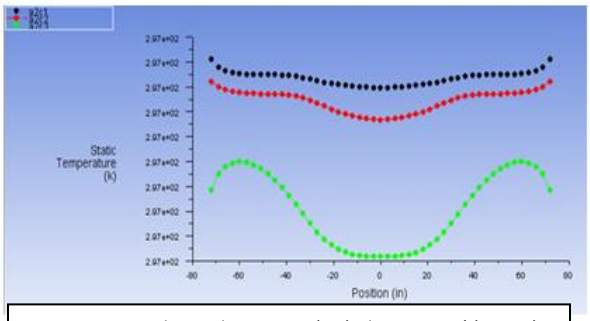

Temperature along z-lines in A2 (y-z) plane at y=3' (Green), y=6'(Red) and y=9'(Black)

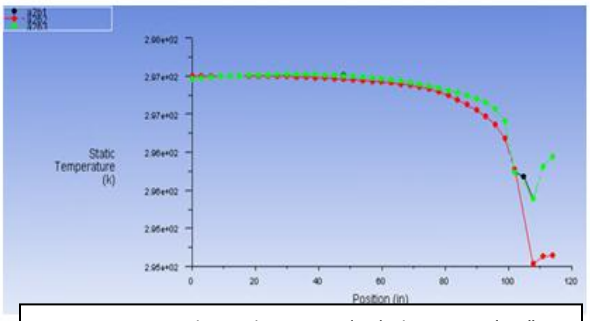

Temperature along y-lines in A2 (y-z) plane at z=2'4.5" (Black), z=4'9"(Red) and z=7'1.5"(Green)

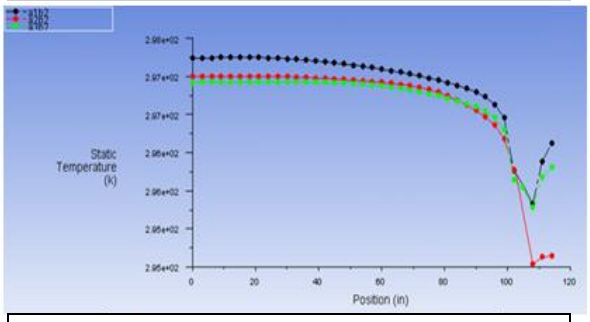

Temperature along z-lines in B2 (x-z) plane at x=3' (Green), x=6'(Red) and x=9'(Black)

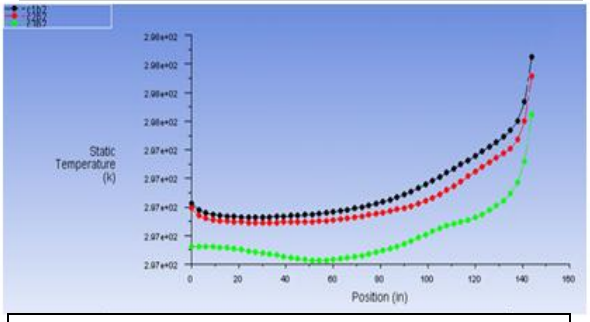

Temperature along x-lines in B2 (x-z) plane at z=2'4.5" (Black), z=4'9"(Red) and z=7'1.5"(Green)

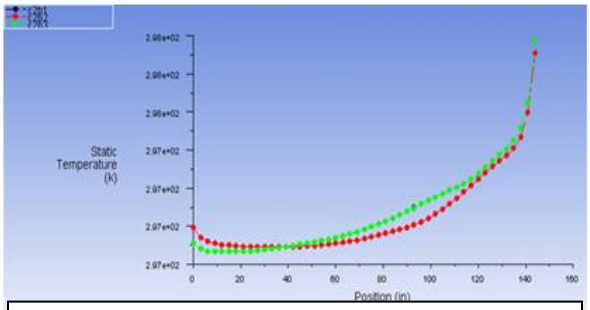

Temperature along x-lines in C2 (x-y) plane at y=3' (Green), y=6'(Red) and y=9'(Black)

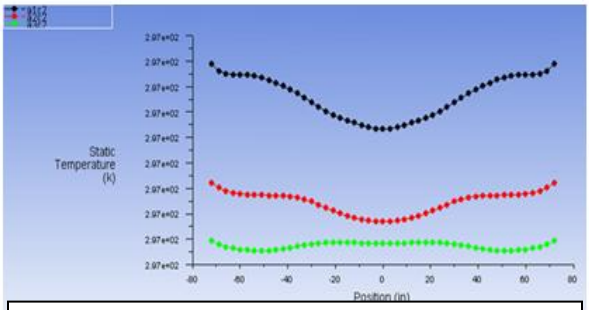

Temperature along y-lines in C2 (x-y) plane at x=3' (Green), x=6'(Red) and x=9'(Black)

Figure 56: Case 2 - Temperature Line Plots at Time T1 = 3:45 AM

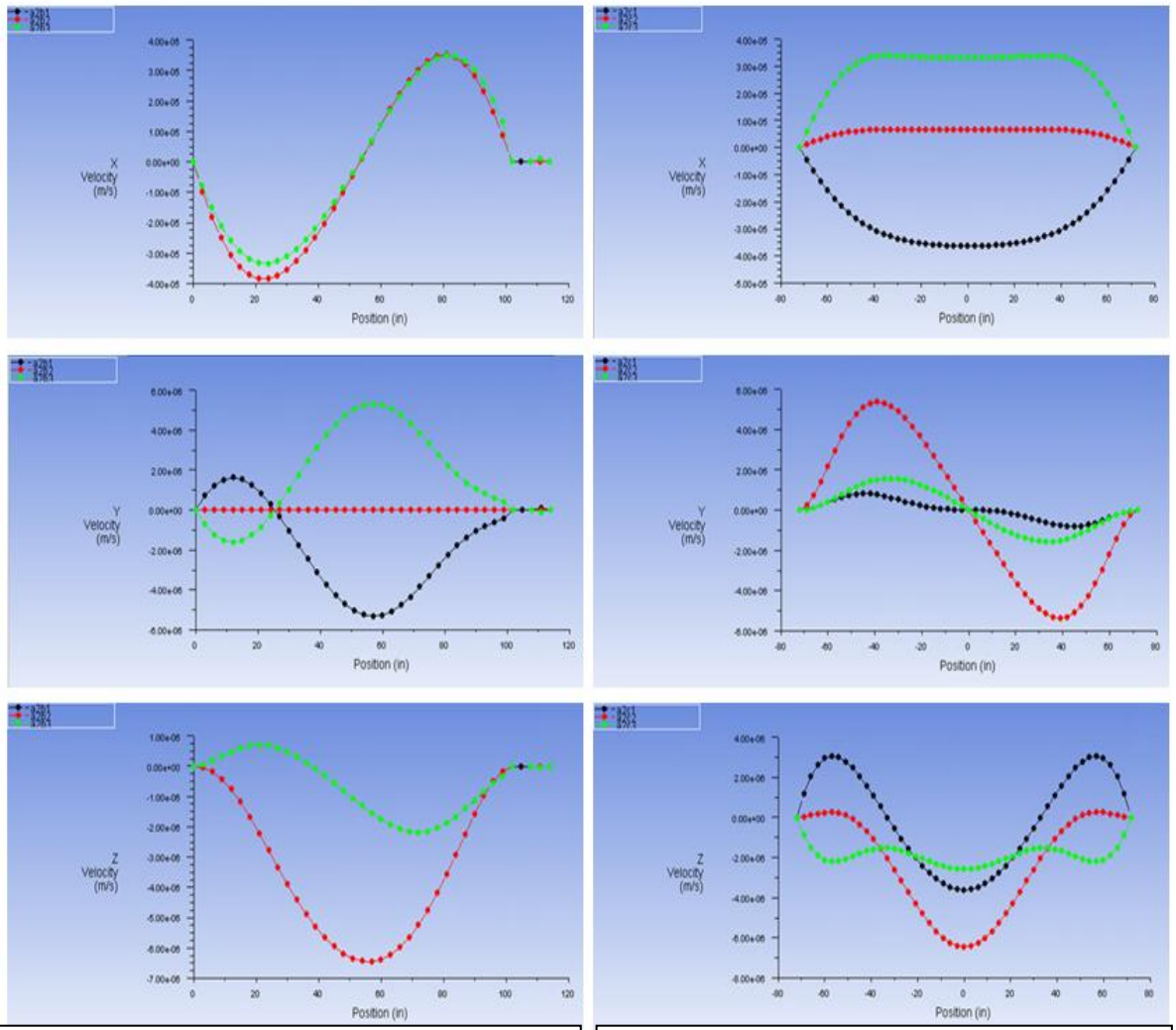

X, Y and Z Velocity Components along z-lines in A2 (y-z) plane at y=3'(Green), y=6'(Red), and y=9'(Black)	X, Y and Z Velocity Components along y-lines in A2 (y-z) plane at z=2'4.5" (Black), z=4'9" (Red), and z=7'1.5" (Green)

Figure 57: Case 2 - Velocity Components in the A2 Plane at Time T1 = 3:45 AM

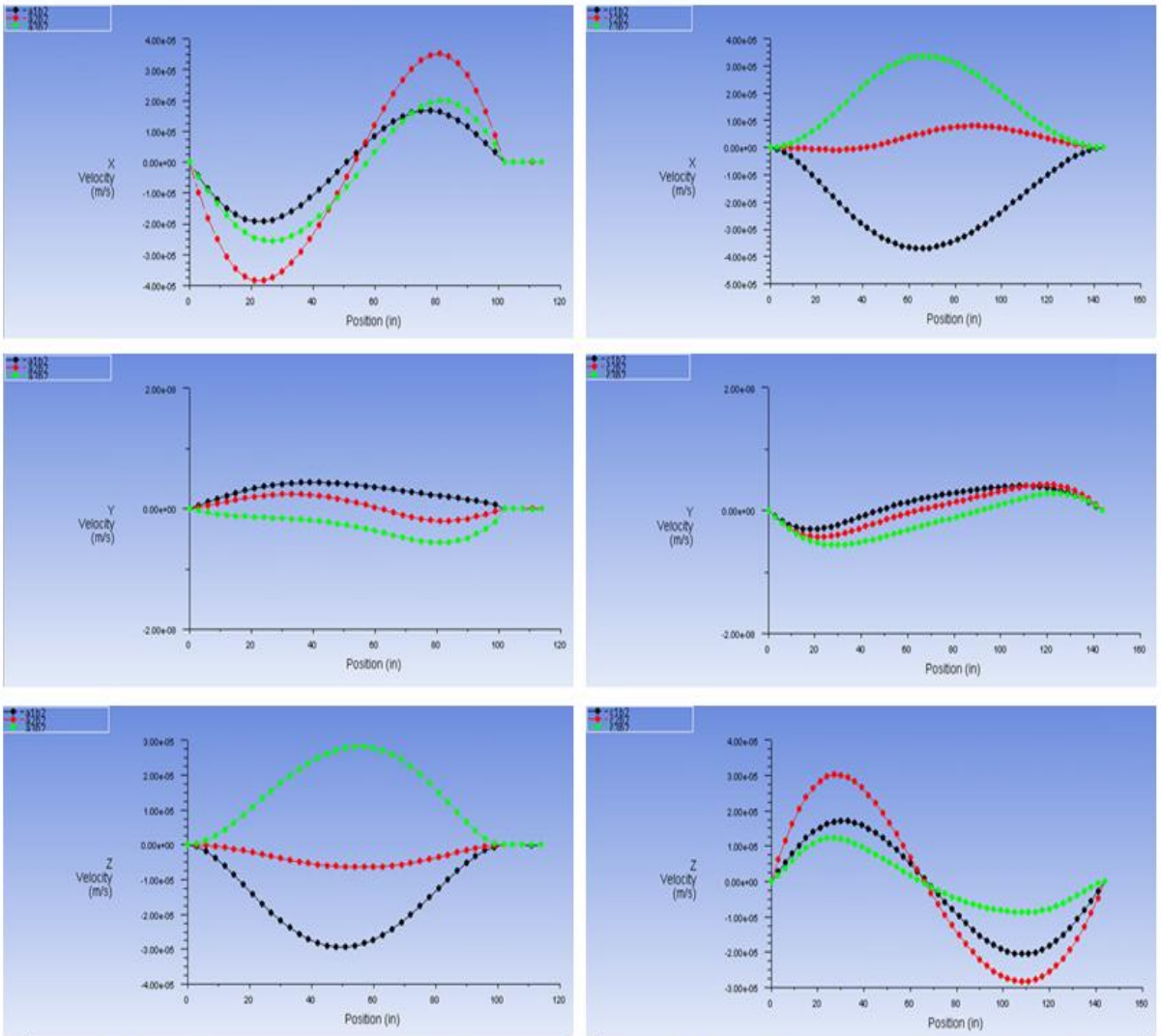

X, Y and Z Velocity Components along z-lines in B2(x-z) plane at x=3'(Green), x=6'(Red), and x=9'(Black)	X, Y and Z Velocity Components along x-lines in B2 (x-z) plane at z=2'4.5" (Black), z=4'9" (Red), and z=7'1.5"(Green)

Figure 58: Case 2 - Velocity Components in the B2 Plane at Time T1 = 3:45 AM

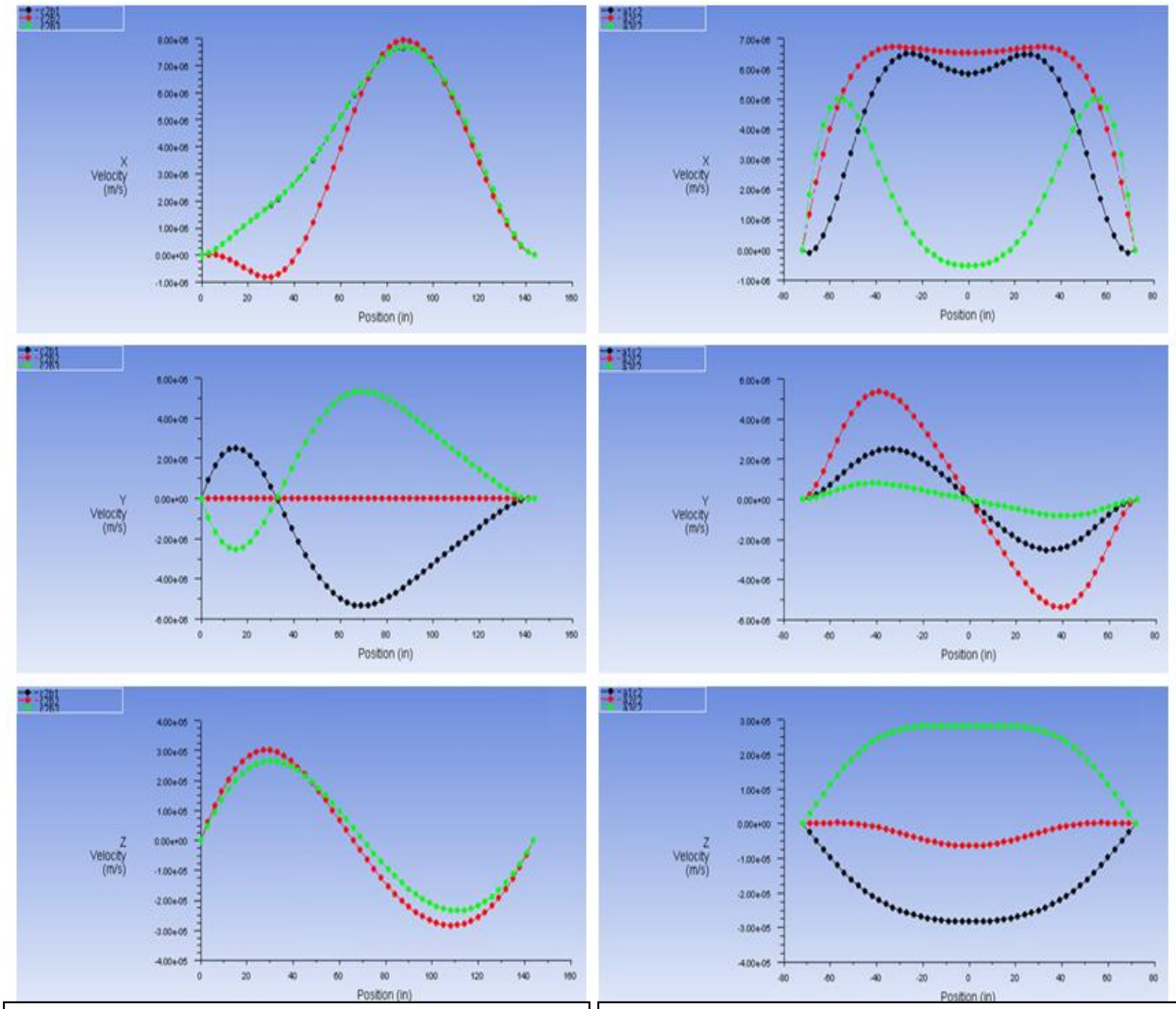

X, Y and Z Velocity Components along x-lines in C2 (x-y) plane at y=3' (Green), y=6' (Red), and y=9' (Black)	X, Y and Z Velocity Components along y-lines in C2 (x-y) plane at x=3' (Green), x=6' (Red), and x=9' (Black)

Figure 59: Case 2 - Velocity Components in the C2 Plane at Time T1 = 3:45 AM

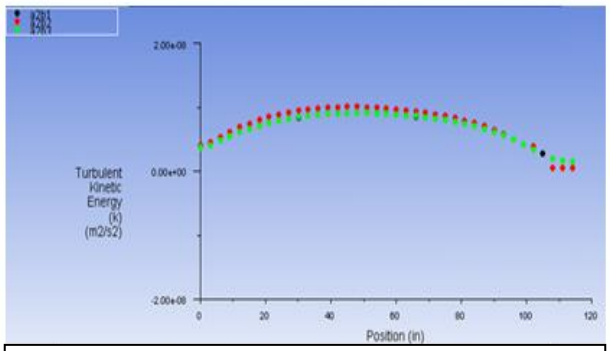

Turbulent Kinetic Energy along z-lines in A2 (y-z) plane at y=3' (Green), y=6'(Red) and y=9'(Black)

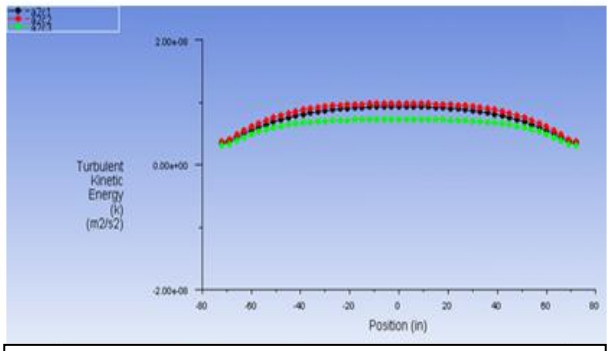

Turbulent Kinetic Energy along y-lines in A2 (y-z) plane at z=2'4.5" (Black), z=4'9"(Red) and z=7'1.5"(Green)

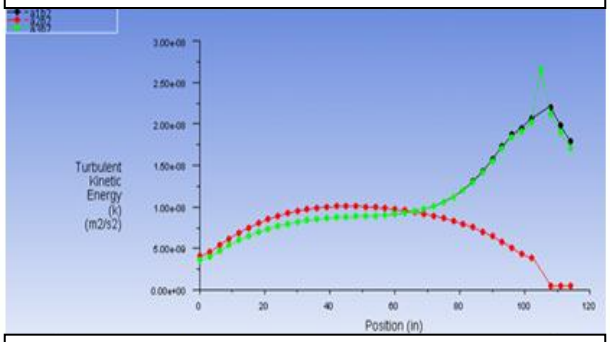

Turbulent Kinetic Energy along z-lines in B2 (x-z) plane at x=3' (Green), x=6'(Red) and x=9'(Black)

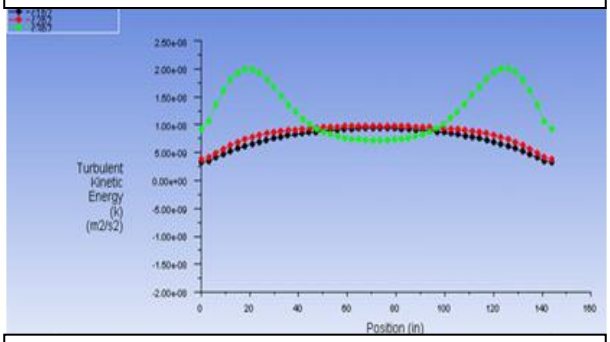

Turbulent Kinetic Energy along x-lines in B2 (x-z) plane at z=2'4.5" (Black), z=4'9"(Red) and z=7'1.5"(Green)

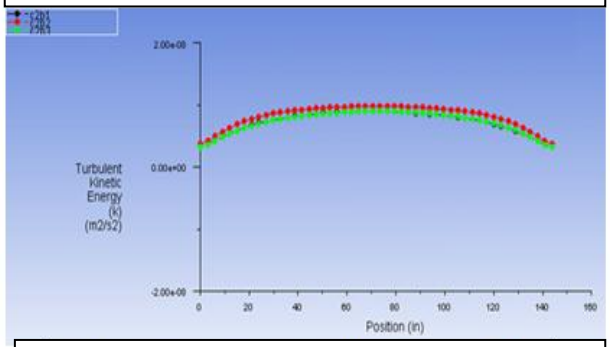

Turbulent Kinetic Energy along x-lines in C2 (x-y) plane at y=3' (Green), y=6'(Red) and y=9'(Black)

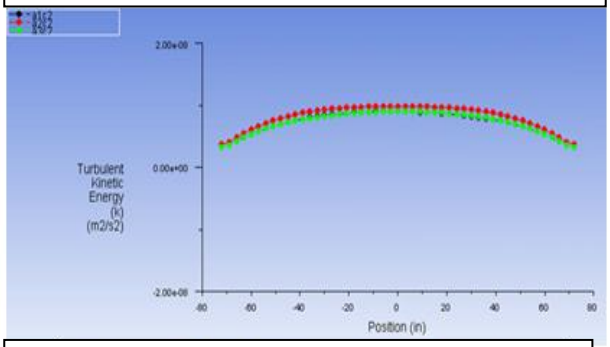

Turbulent Kinetic Energy along y-lines in C2 (x-y) plane at x=3' (Green), x=6'(Red) and x=9'(Black)

Figure 60: Case 2 - Turbulent Kinetic Energy Line Plots at Time T1 = 3:45 AM

Value range from 2.18706e-012 to 7.33026e-012

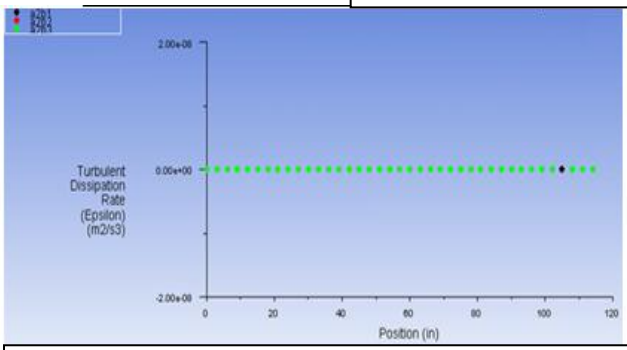

Turbulent Dissipation Rate along z-lines in A2 (y-z) plane at y=3' (Green), y=6'(Red) and y=9'(Black)

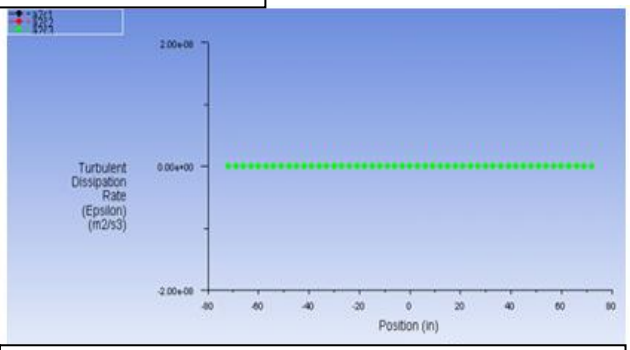

Turbulent Dissipation Rate along y-lines in A2 (y-z) plane at z=2'4.5" (Black), z=4'9"(Red) and z=7'1.5"(Green)

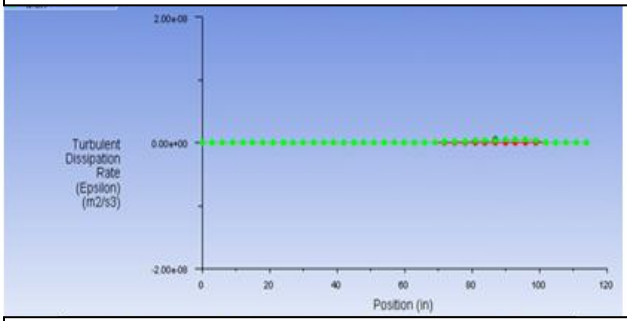

Turbulent Dissipation Rate along z-lines in B2 (x-z) plane at x=3' (Green), x=6'(Red) and x=9'(Black)

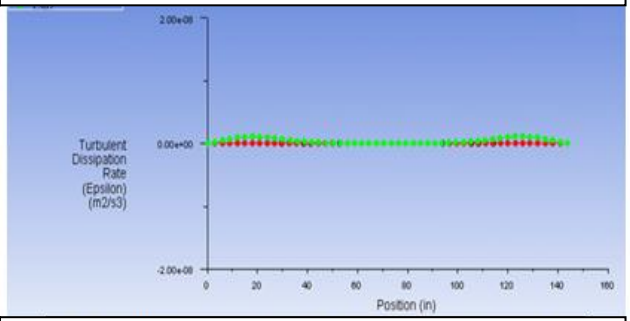

Turbulent Dissipation Rate along x-lines in B2 (x-z) plane at z=2'4.5" (Black), z=4'9"(Red) and z=7'1.5"(Green)

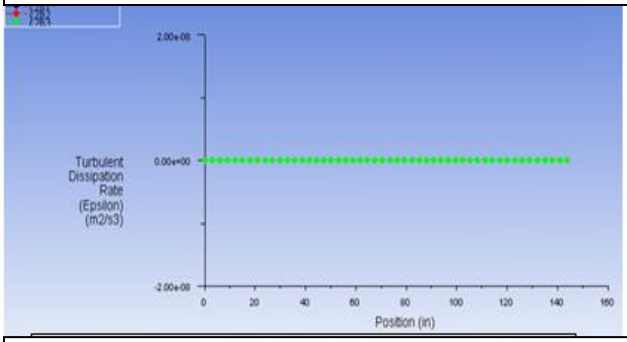

Turbulent Dissipation Rate along x-lines in C2 (x-y) plane at y=3' (Green), y=6'(Red) and y=9'(Black)

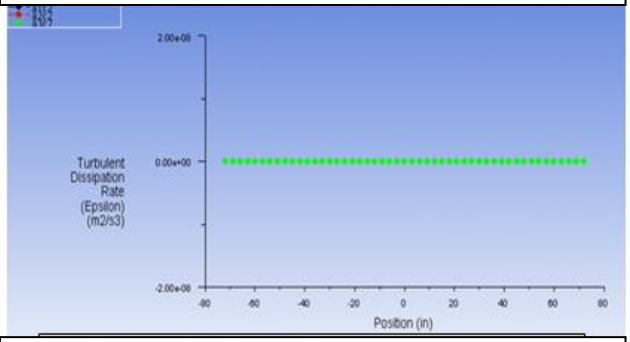

Turbulent Dissipation Rate along y-lines in C2 (x-y) plane at x=3' (Green), x=6'(Red) and x=9'(Black)

Figure 61: Case 2 - Turbulent Dissipation Rate Line Plots at Time T1 = 3:45 AM

Next, we present results at time T2 = 9:20 AM. The key to interpreting the results in the various planes (A1-A3, B1-B3, C1-C3) and along the various lines in the planes inside the room is the same as described before for Figures 54-61 at T1 = 3:45 AM. At T2 = 9:20 AM, the outside temperature is higher as shown in the ASHRAE temperature curve (Figure 7). The air inside the room is therefore warmer than at T1 = 3:45 AM. Figure 62 shows the temperature contours inside the room in A1-A3, B1-B3, and C1-C3 planes. At time T2 = 9:20 AM, we can observe the effects of the cold air coming from the inlet vent in almost every plane considered. We note from A1 plane that the cold air significantly affects the area near the exterior wall, however its effect diminishes as we move through the A2 and A3 planes towards the back of the room. As a result the air is much colder near the hot exterior wall due to the vent placement, and the rear of the room is slightly warmer. Figure 63 shows the velocity contours in different planes of the room at time T2 = 9:20 AM. We notice the high air velocity from the inlet and outlet vents in the B2 plane near the ceiling as expected, however this fast moving air doesn't spread very far into the room, which agrees with our observation from Figure 62 that there is a lack of cold air distribution in the room.

Figure 64 shows the line plots of temperature distributions inside the room, which are somewhat higher those at time T1 = 3:45 AM as expected. These temperature line plots show that the adiabatic temperature boundary condition is satisfied on the five interior walls, and that the highest temperature occurs at the exterior wall. These temperature line plots also show the effects of the radiation slab in the cooler air near the ceiling. The temperature line plots in the C2 plane show that the temperature is fairly constant in the rear of the room, however it suddenly decreases as the area near the vent is approached. It begins to rise again rapidly as the hot exterior wall is approached.

Figures 65-67 show the line plots of velocity in various planes inside the room, which are fairly similar to those in Figures 57-59 at time T1 = 3:45 AM. Figure 66 shows a rapid increase in velocity near the ceiling related to the restricted area due to the presence of the radiation slab. Figure 67 shows that the z-component of velocity matches the form that would be expected with the velocity becoming negative indicating that this region is affected by the inlet vent. Figure 68 shows the line plots of turbulent kinetic energy in various planes inside the room. The turbulent kinetic energy (k) is quite high in the middle of the room as expected, and is nearly zero near the walls. Figure 69 shows the line plots of the turbulent dissipation rate in various planes inside the room. The intensity of both k and ε is increased slightly as expected since the temperature increases at time T2 = 9:20 AM.

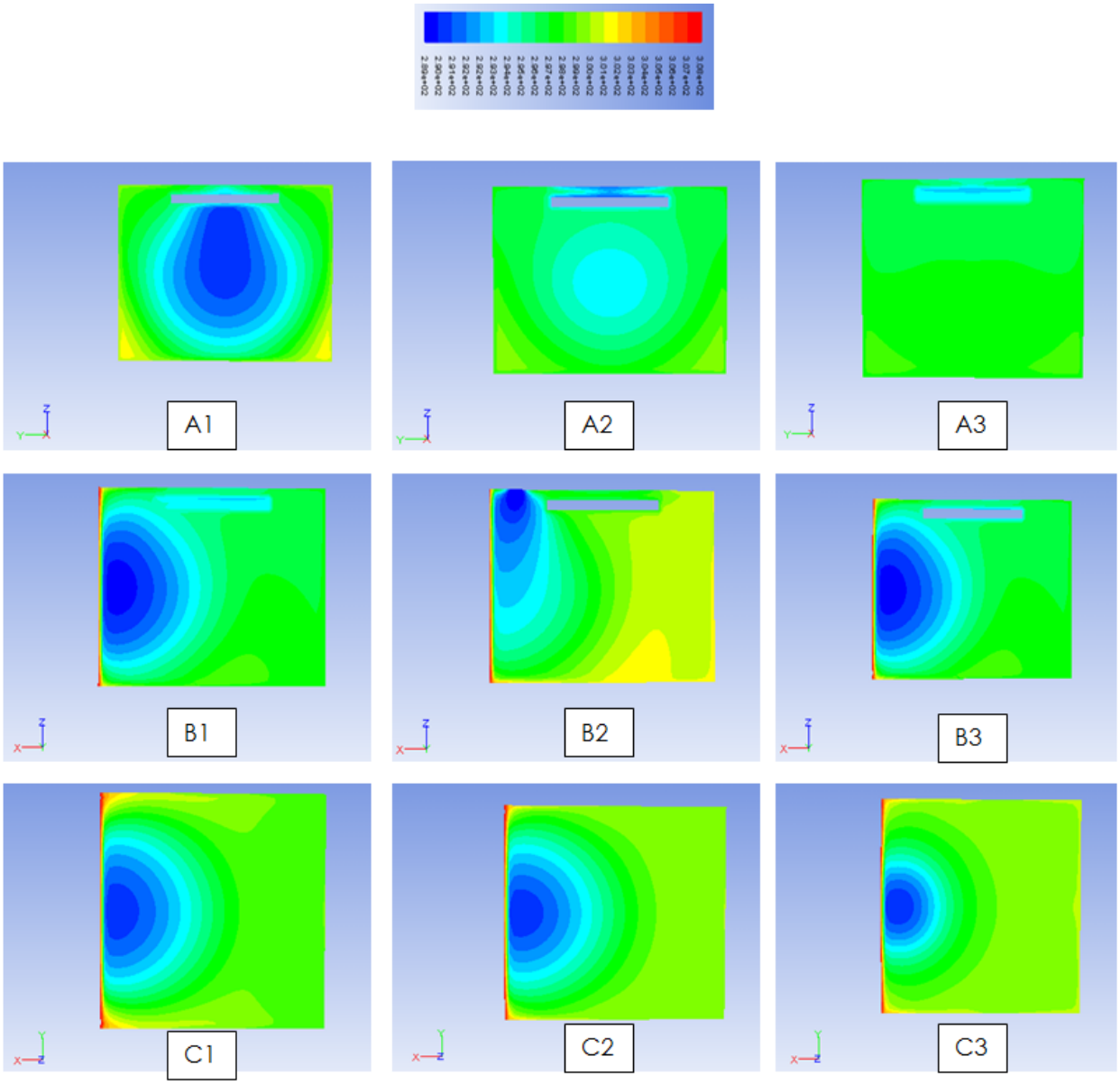

Figure 62: Case 2 - Temperature Contours in Different Planes of Figure 19 at Time T2 = 9:20 AM

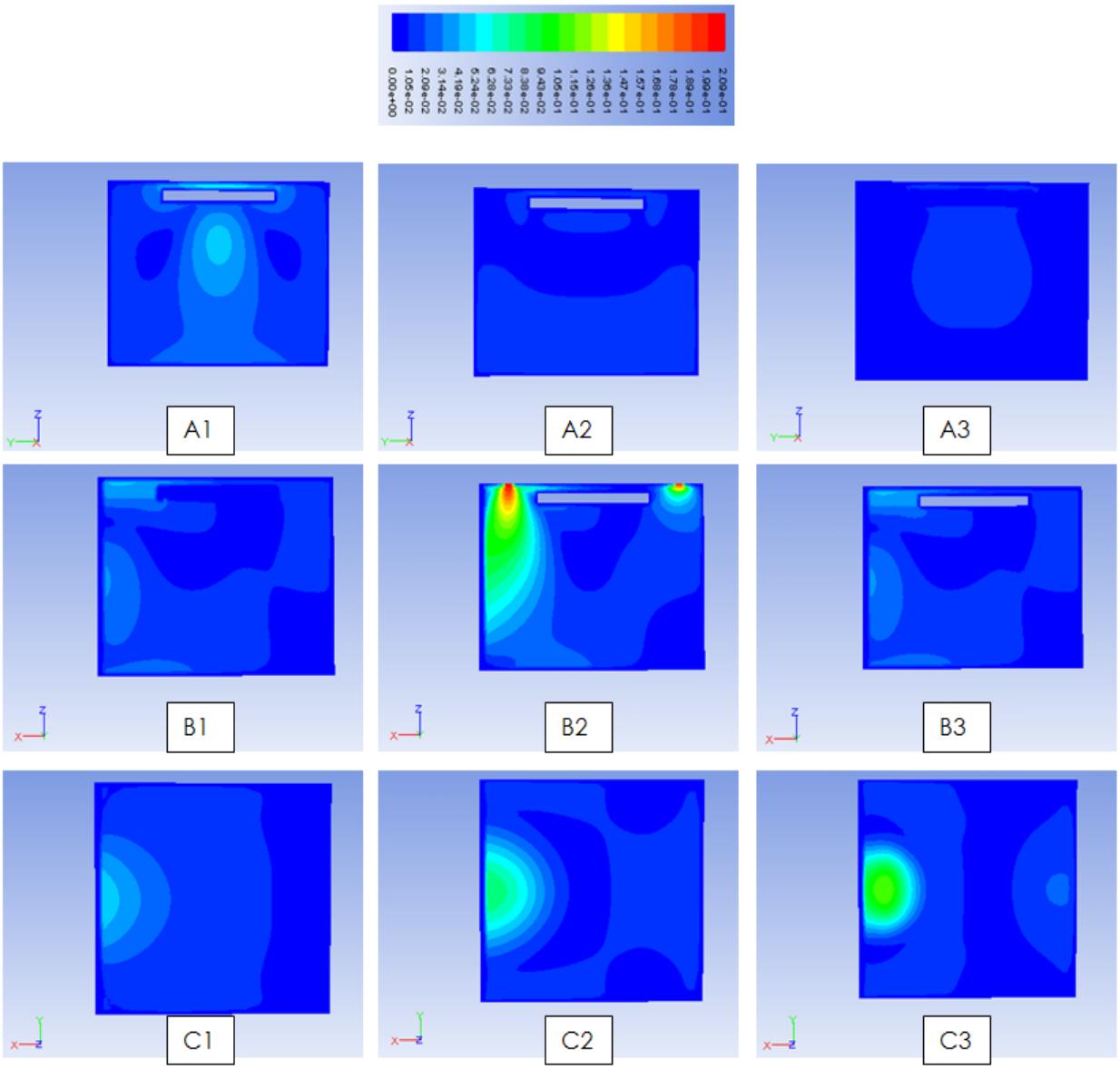

Figure 63: Case 2 - Velocity Contours in Different Planes of Figure 19 at Time T2 = 9:20 AM

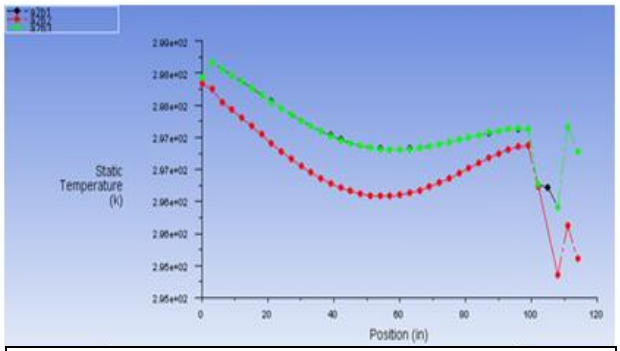

Temperature along z-lines in A2 (y-z) plane at y=3' (Green), y=6'(Red) and y=9'(Black)

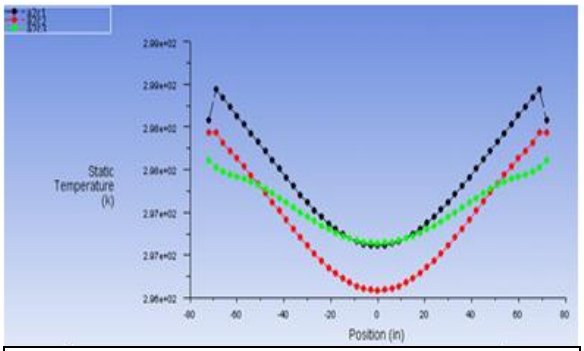

Temperature along y-lines in A2 (y-z) plane at z=2'4.5" (Black), z=4'9"(Red) and z=7'1.5"(Green)

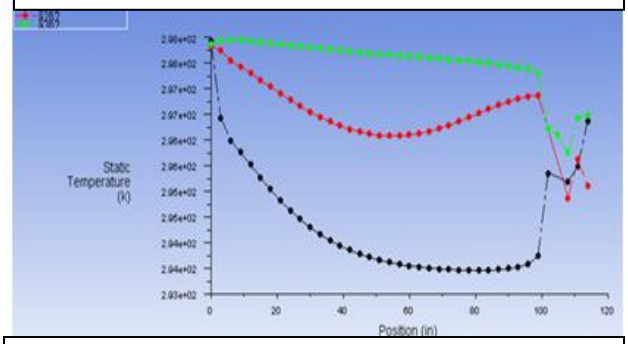

Temperature along z-lines in B2 (x-z) plane at x=3' (Green), x=6'(Red) and x=9'(Black)

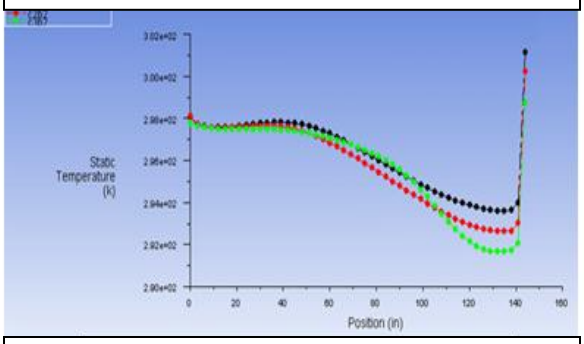

Temperature along x-lines in B2 (x-z) plane at z=2'4.5" (Black), z=4'9"(Red) and z=7'1.5"(Green)

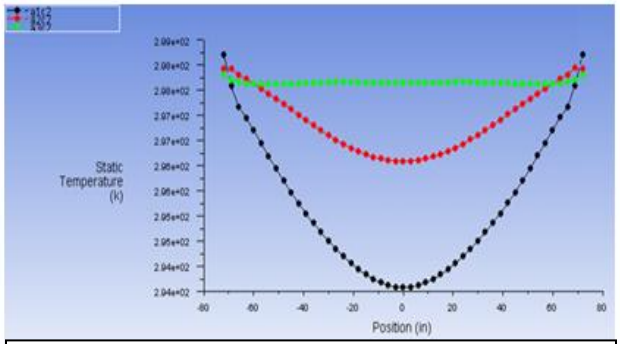

Temperature along x-lines in C2 (x-y) plane at y=3' (Green), y=6'(Red) and y=9'(Black)

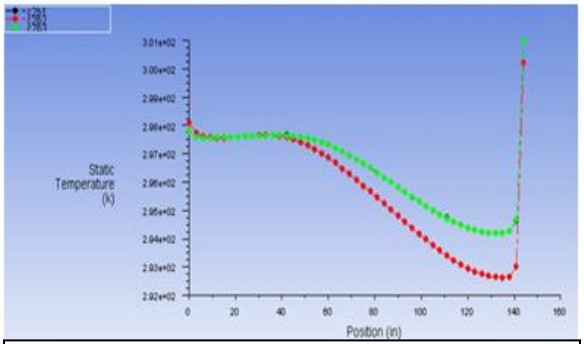

Temperature along y-lines in C2 (x-y) plane at x=3' (Green), x=6'(Red) and x=9'(Black)

Figure 64: Case 2 – Temperature Line Plots at Time T2 = 9:20 AM

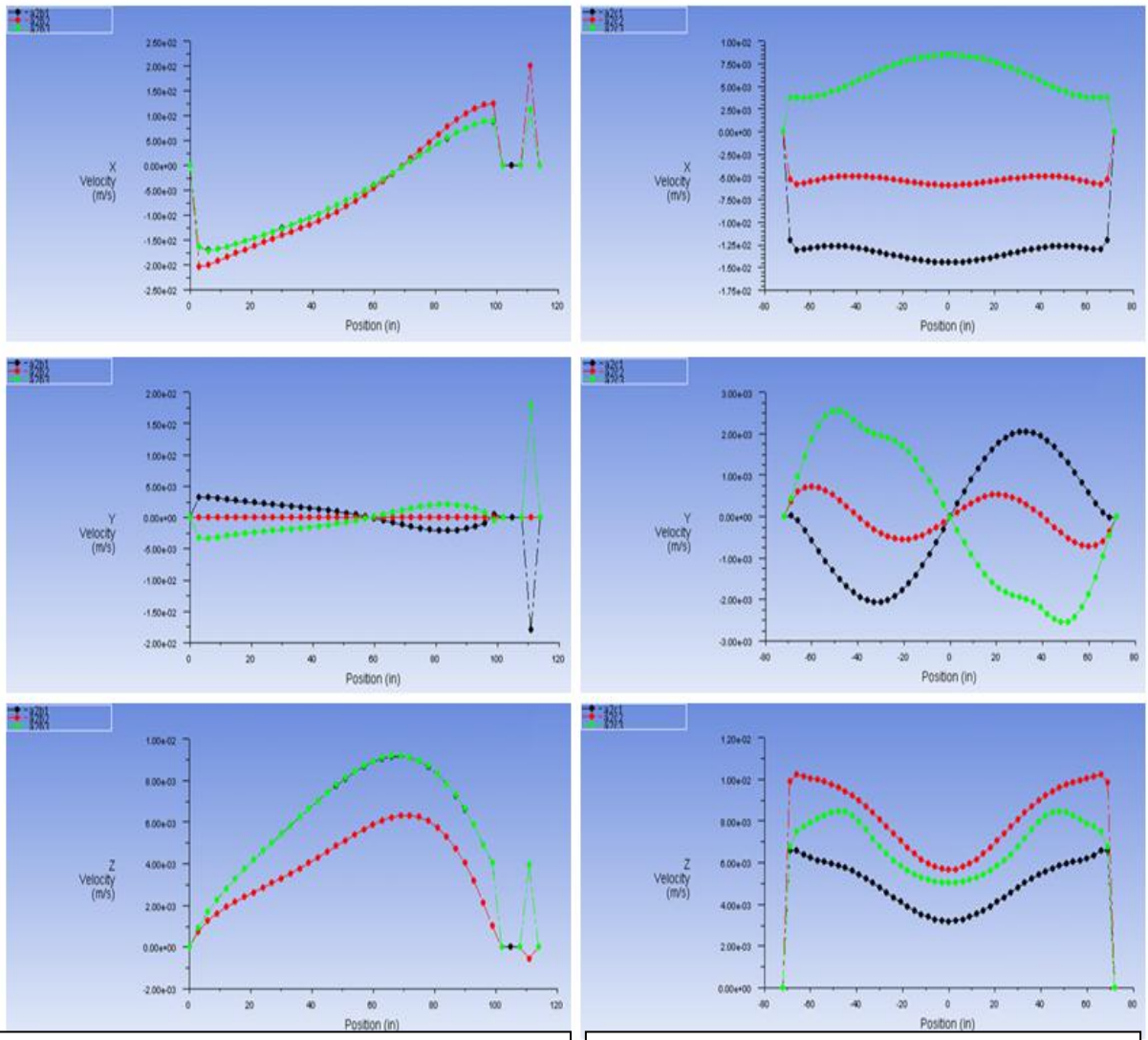

X, Y and Z Velocity Components along z-lines in A2 (y-z) plane at y=3'(Green), y=6'(Red), and y=9'(Black)

X, Y and Z Velocity Components along y-lines in A2 (y-z) plane at z=2'4.5" (Black), z=4'9" (Red), and z=7'1.5" (Green)

Figure 65: Case 2 - Velocity Components in the A2 Plane at Time T2 = 9:20 AM

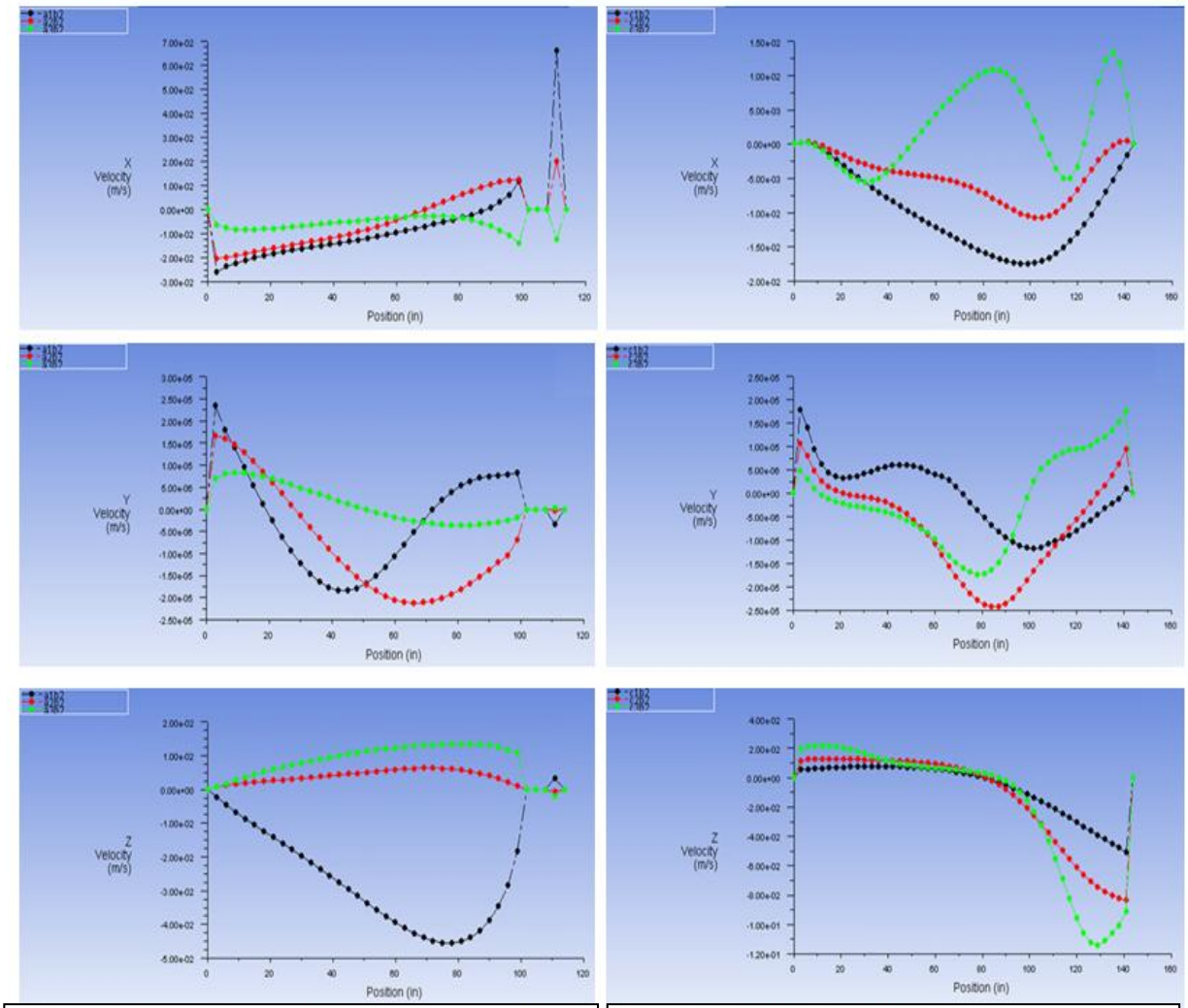

X, Y and Z Velocity Components along z-lines in B2(x-z) plane at x=3'(Green), x=6'(Red), and x=9'(Black)	X, Y and Z Velocity Components along x-lines in B2 (x-z) plane at z=2'4.5" (Black), z=4'9" (Red), and z=7'1.5"(Green)

Figure 66: Case 2 - Velocity Components in the B2 Plane at Time T2 = 9:20 AM

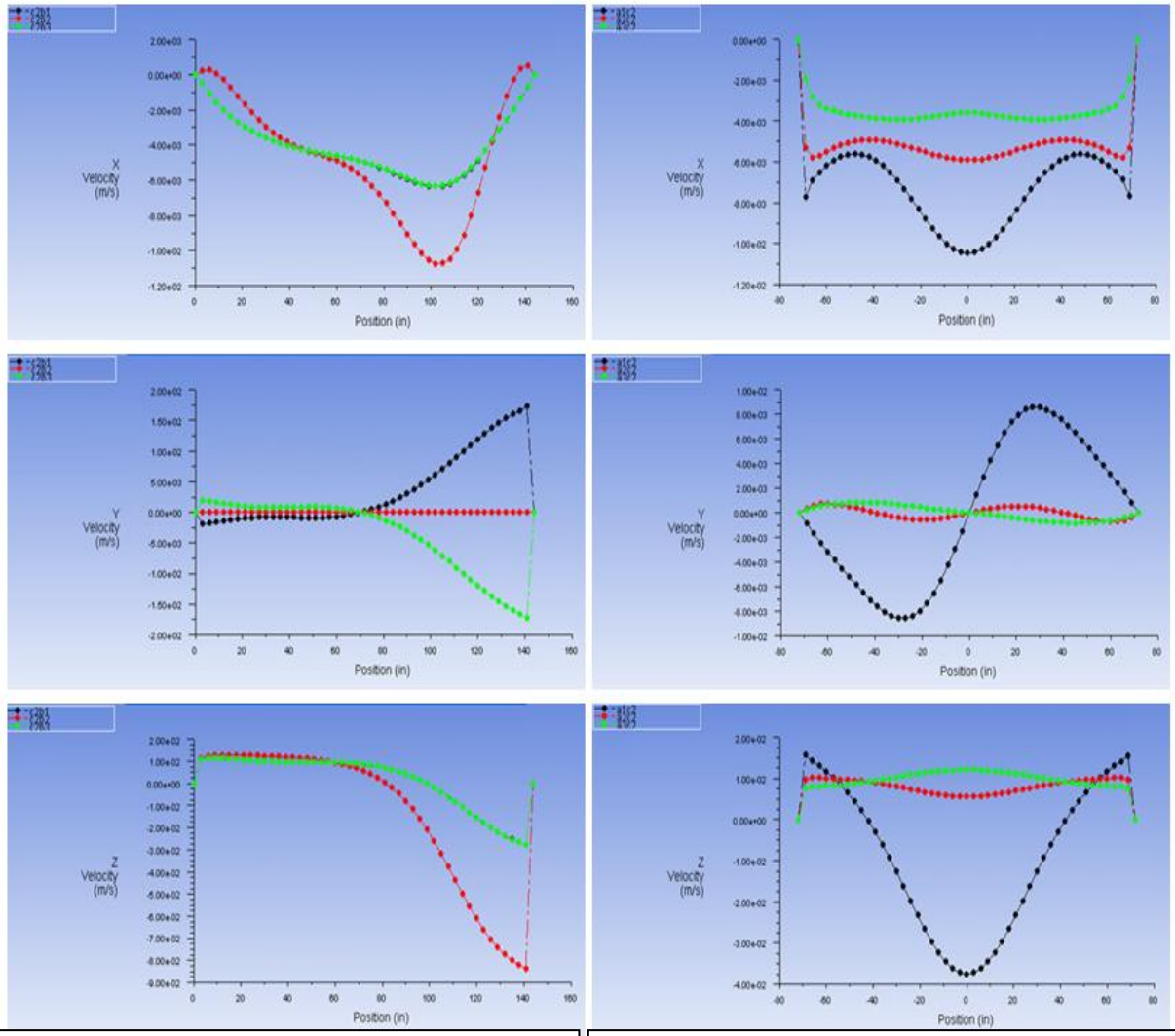

X, Y and Z Velocity Components along x-lines in C2 (x-y) plane at y=3' (Green), y=6' (Red), and y=9' (Black)	X, Y and Z Velocity Components along y-lines in C2 (x-y) plane at x=3' (Green), x=6' (Red), and x=9' (Black)

Figure 67: Case 2 - Velocity Components in the C2 Plane at Time T2 = 9:20 AM

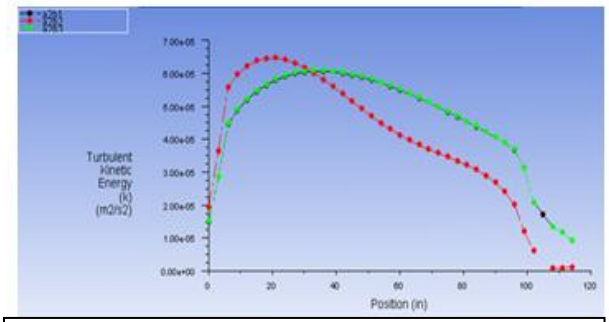

Turbulent Kinetic Energy along z-lines in A2 (y-z) plane at y=3' (Green), y=6'(Red) and y=9'(Black)

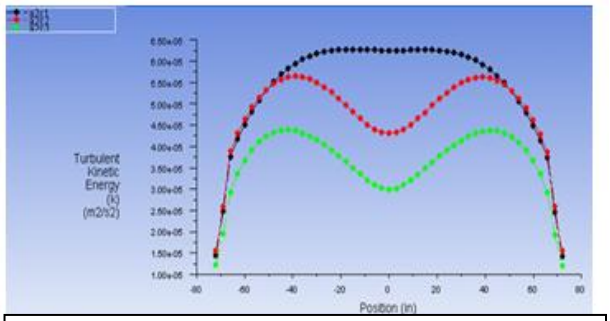

Turbulent Kinetic Energy along y-lines in A2 (y-z) plane at z=2'4.5" (Black), z=4'9"(Red) and z=7'1.5"(Green)

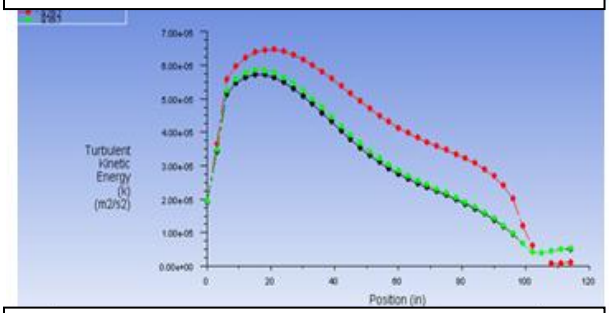

Turbulent Kinetic Energy along z-lines in B2 (x-z) plane at x=3' (Green), x=6'(Red) and x=9'(Black)

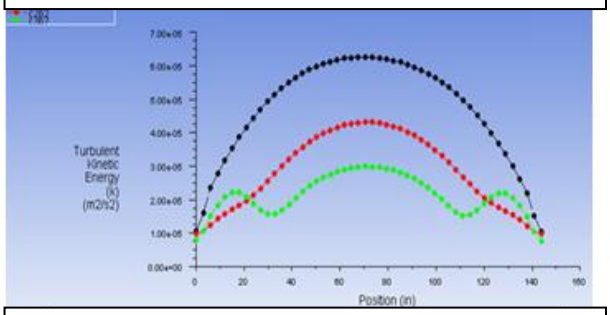

Turbulent Kinetic Energy along x-lines in B2 (x-z) plane at z=2'4.5" (Black), z=4'9"(Red) and z=7'1.5"(Green)

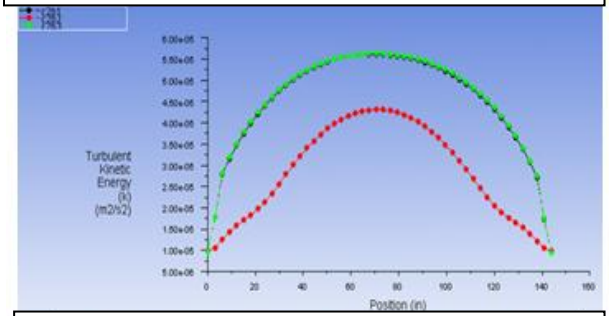

Turbulent Kinetic Energy along x-lines in C2 (x-y) plane at y=3' (Green), y=6'(Red) and y=9'(Black)

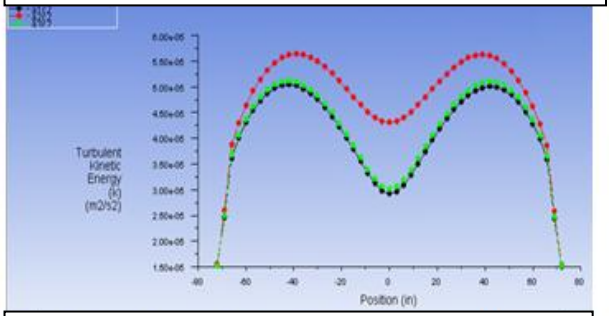

Turbulent Kinetic Energy along y-lines in C2 (x-y) plane at x=3' (Green), x=6'(Red) and x=9'(Black)

Figure 68: Case 2 - Turbulent Kinetic Energy Line Plots at Time T2 = 9:20 AM

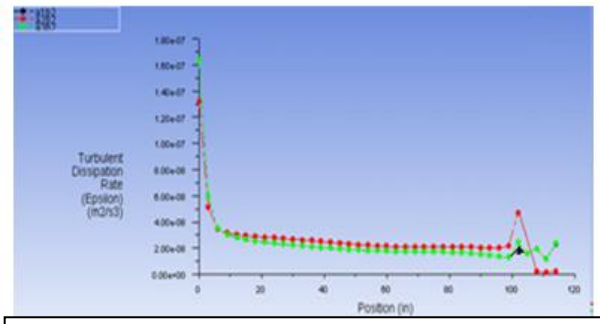

Turbulent Dissipation Rate along z-lines in A2 (y-z) plane at y=3' (Green), y=6'(Red) and y=9'(Black)

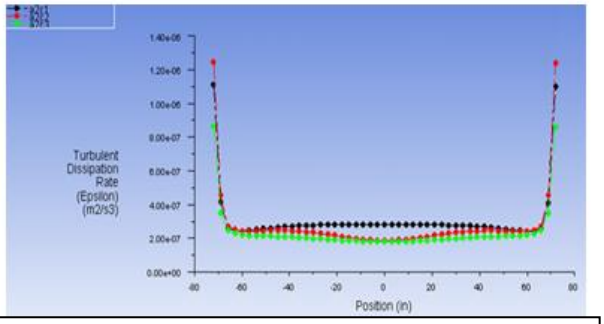

Turbulent Dissipation Rate along y-lines in A2 (y-z) plane at z=2'4.5" (Black), z=4'9"(Red) and z=7'1.5"(Green)

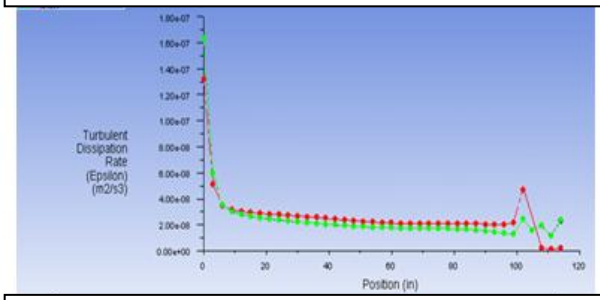

Turbulent Dissipation Rate along z-lines in B2 (x-z) plane at x=3' (Green), x=6'(Red) and x=9'(Black)

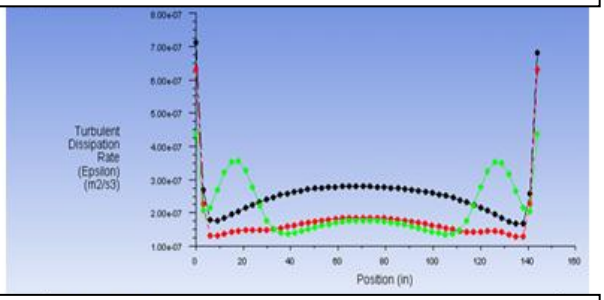

Turbulent Dissipation Rate along x-lines in B2 (x-z) plane at z=2'4.5" (Black), z=4'9"(Red) and z=7'1.5"(Green)

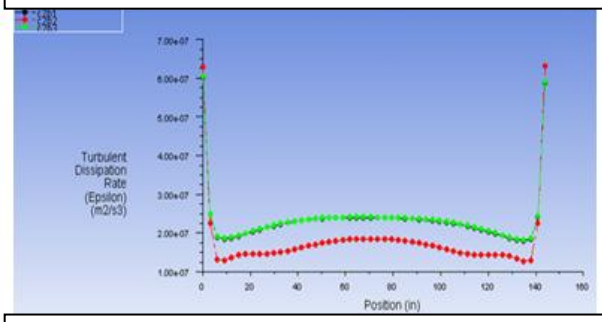

Turbulent Dissipation Rate along x-lines in C2 (x-y) plane at y=3' (Green), y=6'(Red) and y=9'(Black)

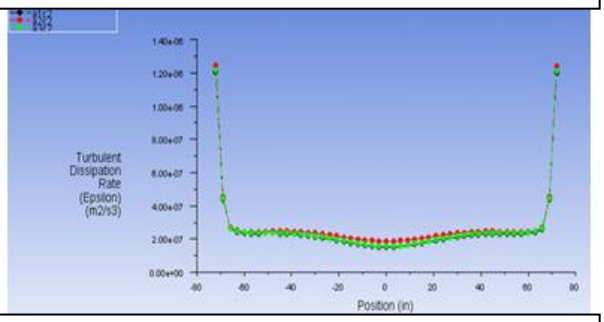

Turbulent Dissipation Rate along y-lines in C2 (x-y) plane at x=3' (Green), x=6'(Red) and x=9'(Black)

Figure 69: Case 2 - Turbulent Dissipation Rate Line Plots at Time T2 = 9:20 AM

Next, we present results at time T3 = 2:53 PM. The key to interpreting the results in the various planes (A1-A3, B1-B3, and C1-C3) and along the various lines in these planes inside the room is the same as described before for Figures 54-61 at time T1=3:45 AM. At T3 = 2:53 PM, the outside temperature is just past its peak as shown in the ASHRAE curve (Figure 7). Figure 70 shows the temperature contours inside the room in the planes (A1-A3, B1-B3, and C1-C3). These contours clearly show the cooling effects of the radiation slab. The temperature in the room is nearly constant, indicating the return of temperature stability to the system. Figure 71 shows the velocity magnitude contours in the different planes of the room as described in Figure 19. These contours show increased velocity along the floor and the ceiling of the room due to the circulation of air caused by the rising warm air. Figure 72 shows the line plots of the temperature distributions inside the room along various lines in planes A1-A3, B1-B3, and C1-C3 shown in Figure 19. These line plots show that the solutions satisfies the adiabatic wall conditions in the room except for the exterior wall where a constant temperature boundary condition is imposed corresponding to the external temperature at time T3. In addition, Figure 72 shows the cooling effects of the radiation slab on the air near the ceiling.

Figures 73-75 show the line plots of the velocity components in the room. These plots show that the velocity components go to zero at the walls. These line plots are a quantitative description of the contour plots shown in Figure 71. Figures 73 and 74 show an increased velocity above the radiation slab due to the restricted space. Figure 76 shows the turbulent kinetic energy line plots along the various cross-sectional lines inside the room; they indicate the relative turbulence intensity in various parts of the room. As expected, the turbulent intensity is greater in the middle of the room than near the walls. Figure 77 shows

line plots of the turbulent dissipation rate (ε) along various cross-sectional lines inside the room. In contrast to k, the value of epsilon peaks near the walls because of large dissipation of turbulence, and is fairly constant across the room in all direction except near the walls.

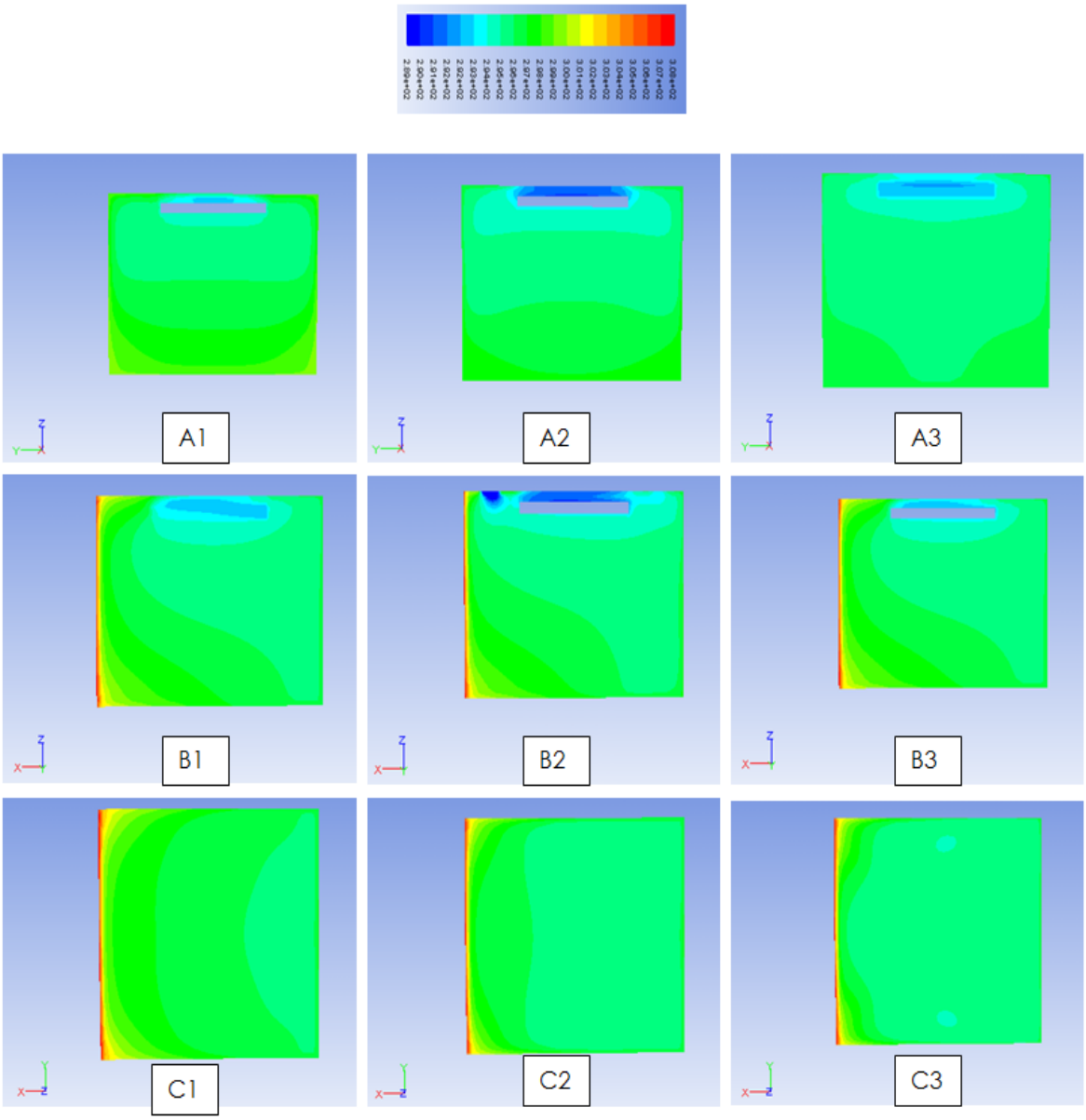

Figure 70: Case 2 - Temperature Contours in Different Planes of Figure 19 at Time T3 = 2:53 PM

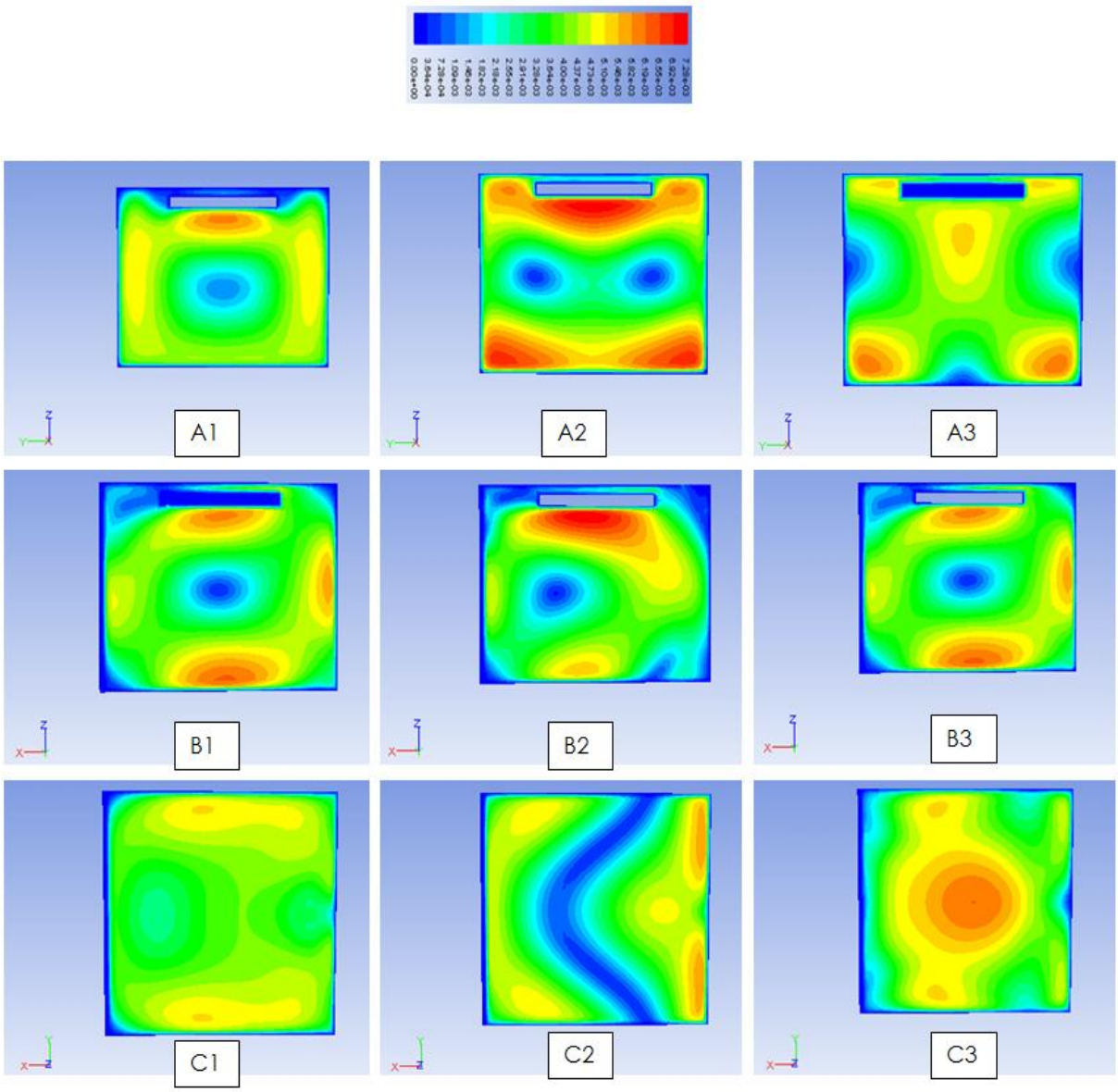

Figure 71: Case 2 - Velocity Contours in Different Planes of Figure 19 at Time T3 = 2:53 PM

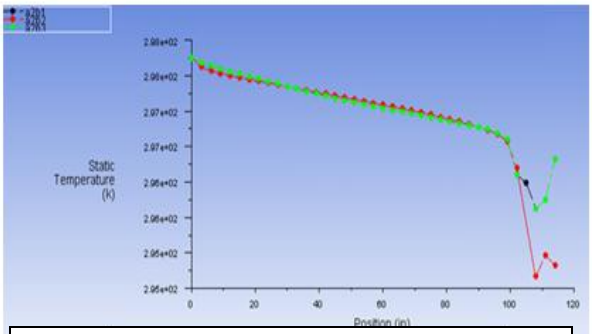

Temperature along z-lines in A2 (y-z) plane at y=3' (Green), y=6'(Red) and y=9'(Black)

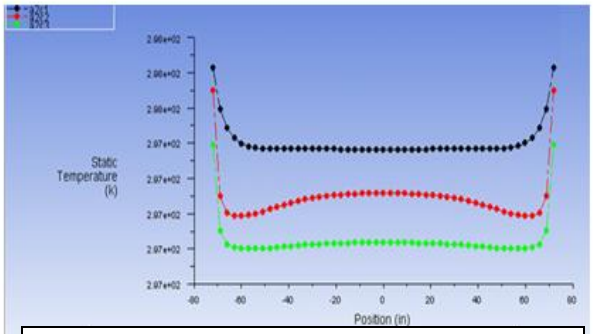

Temperature along y-lines in A2 (y-z) plane at z=2'4.5" (Black), z=4'9"(Red) and z=7'1.5"(Green)

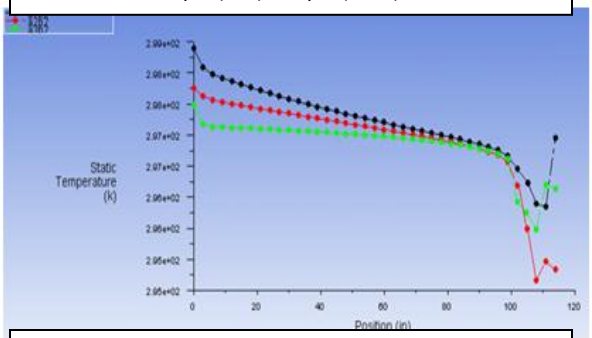

Temperature along z-lines in B2 (x-z) plane at x=3' (Green), x=6'(Red) and x=9'(Black)

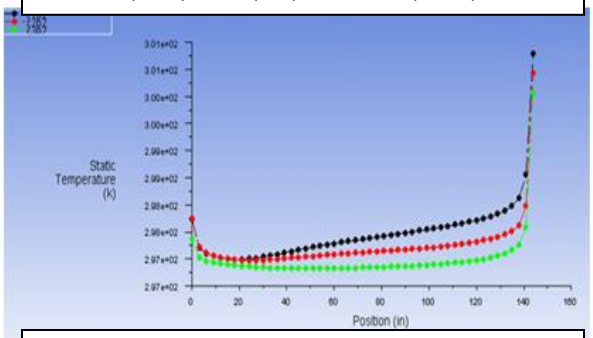

Temperature along x-lines in B2 (x-z) plane at z=2'4.5" (Black), z=4'9"(Red) and z=7'1.5"(Green)

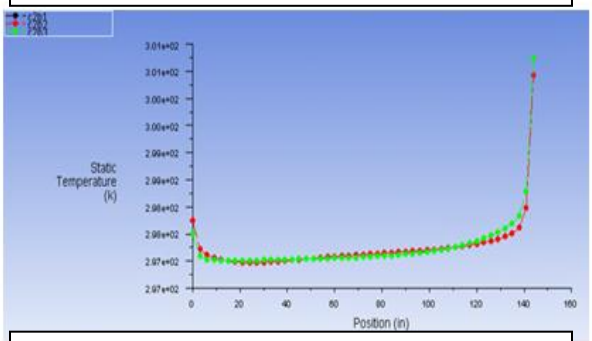

Temperature along x-lines in C2 (x-y) plane at y=3' (Green), y=6'(Red) and y=9'(Black)

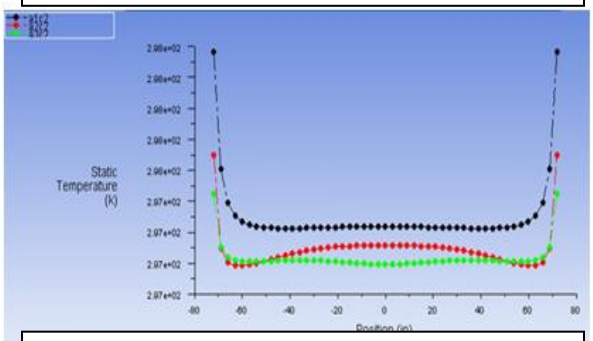

Temperature along y-lines in C2 (x-y) plane at x=3' (Green), x=6'(Red) and x=9'(Black)

Figure 72: Case 2 - Temperature Line Plots at Time T3 = 2:53 PM

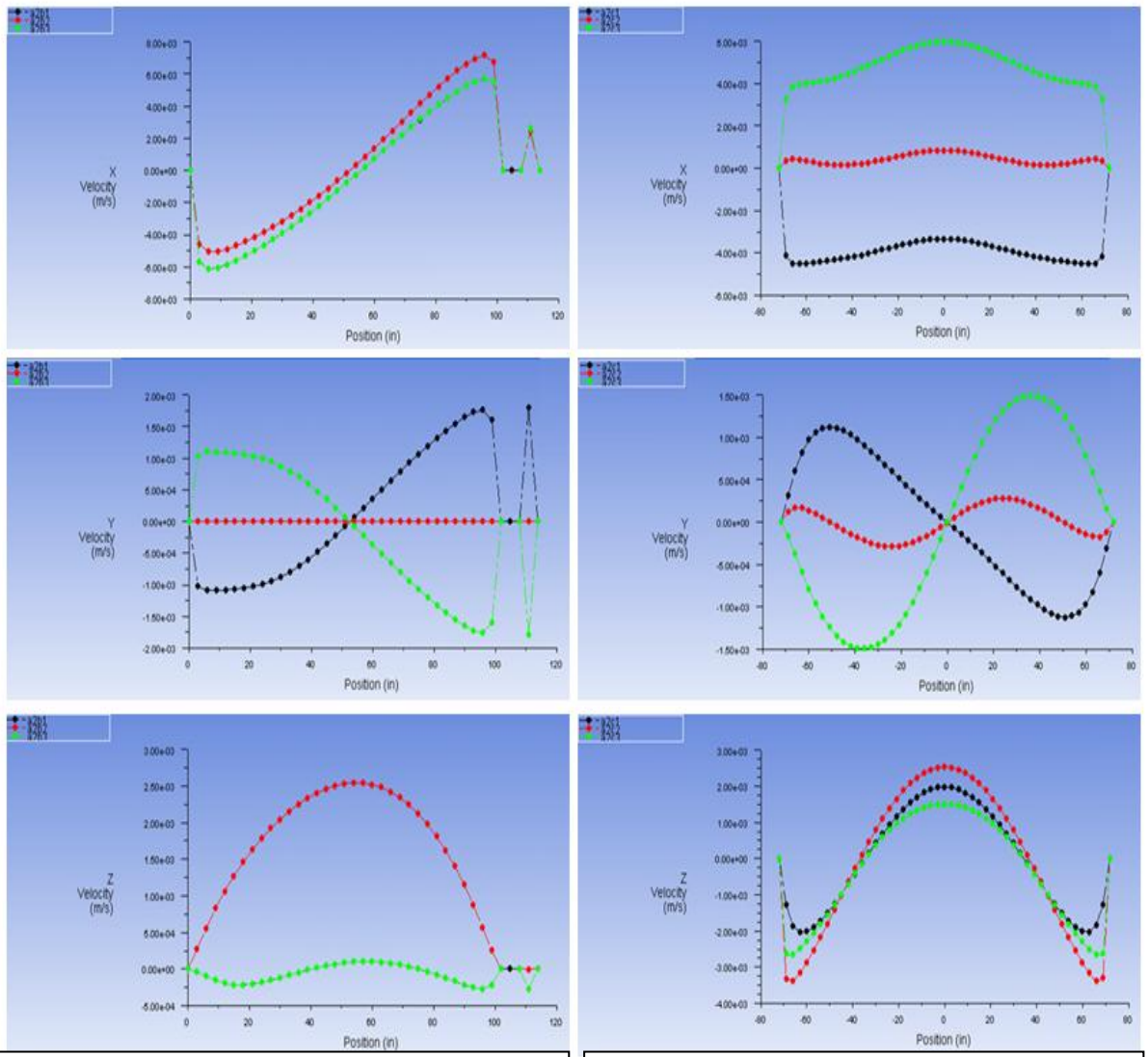

X, Y and Z Velocity Components along z-lines in A2 (y-z) plane at y=3'(Green), y=6'(Red), and y=9'(Black)

X, Y and Z Velocity Components along y-lines in A2 (y-z) plane at z=2'4.5" (Black), z=4'9" (Red), and z=7'1.5" (Green)

Figure 73: Case 2 - Velocity Components in the A2 Plane at Time T3 = 2:53 PM

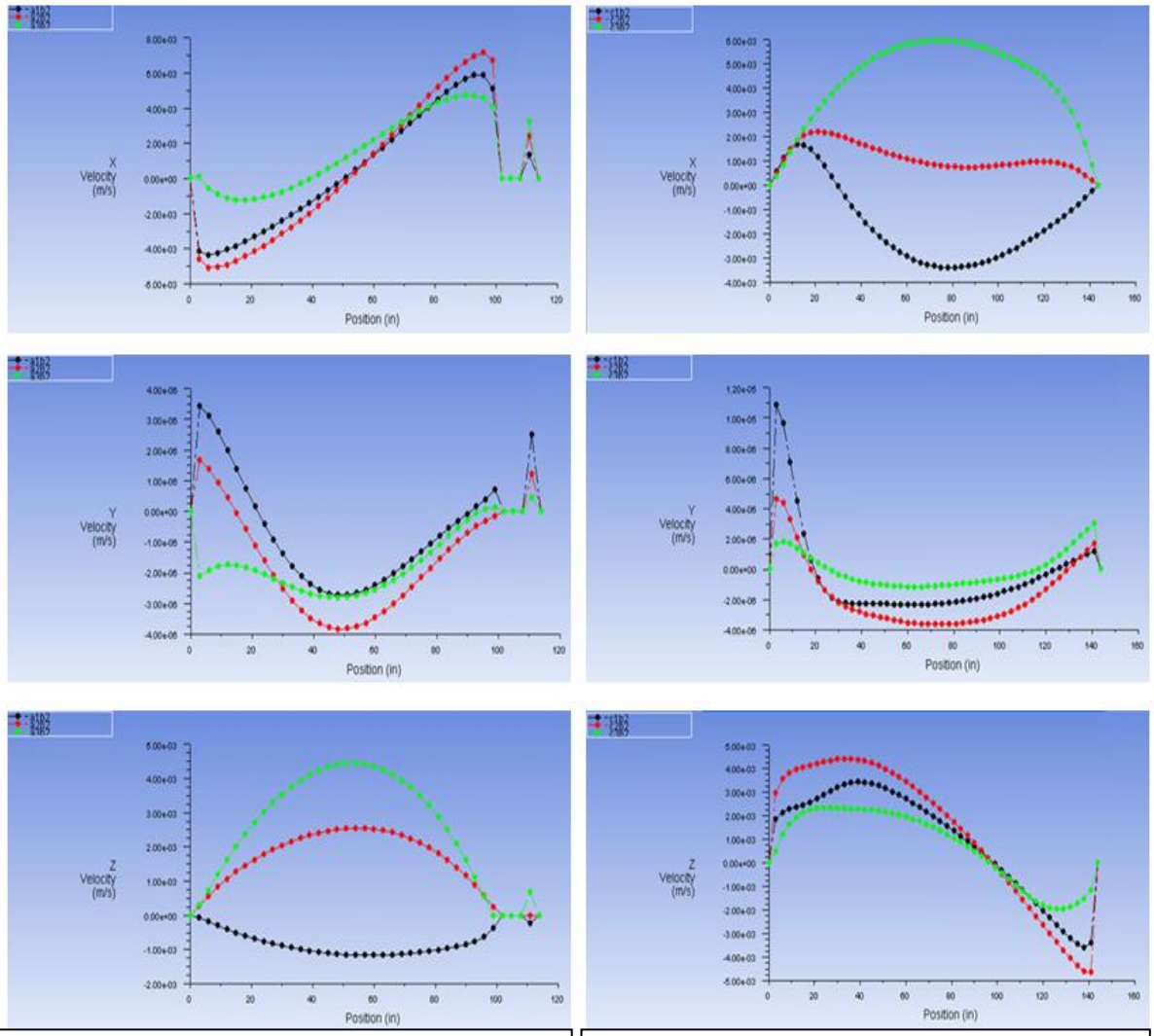

X, Y and Z Velocity Components along z-lines in B2(x-z) plane at x=3'(Green), x=6'(Red), and x=9'(Black)	X, Y and Z Velocity Components along x-lines in B2 (x-z) plane at z=2'4.5" (Black), z=4'9" (Red), and z=7'1.5"(Green)

Figure 74: Case 2 - Velocity Components in the B2 Plane at Time T3 = 2:53 PM

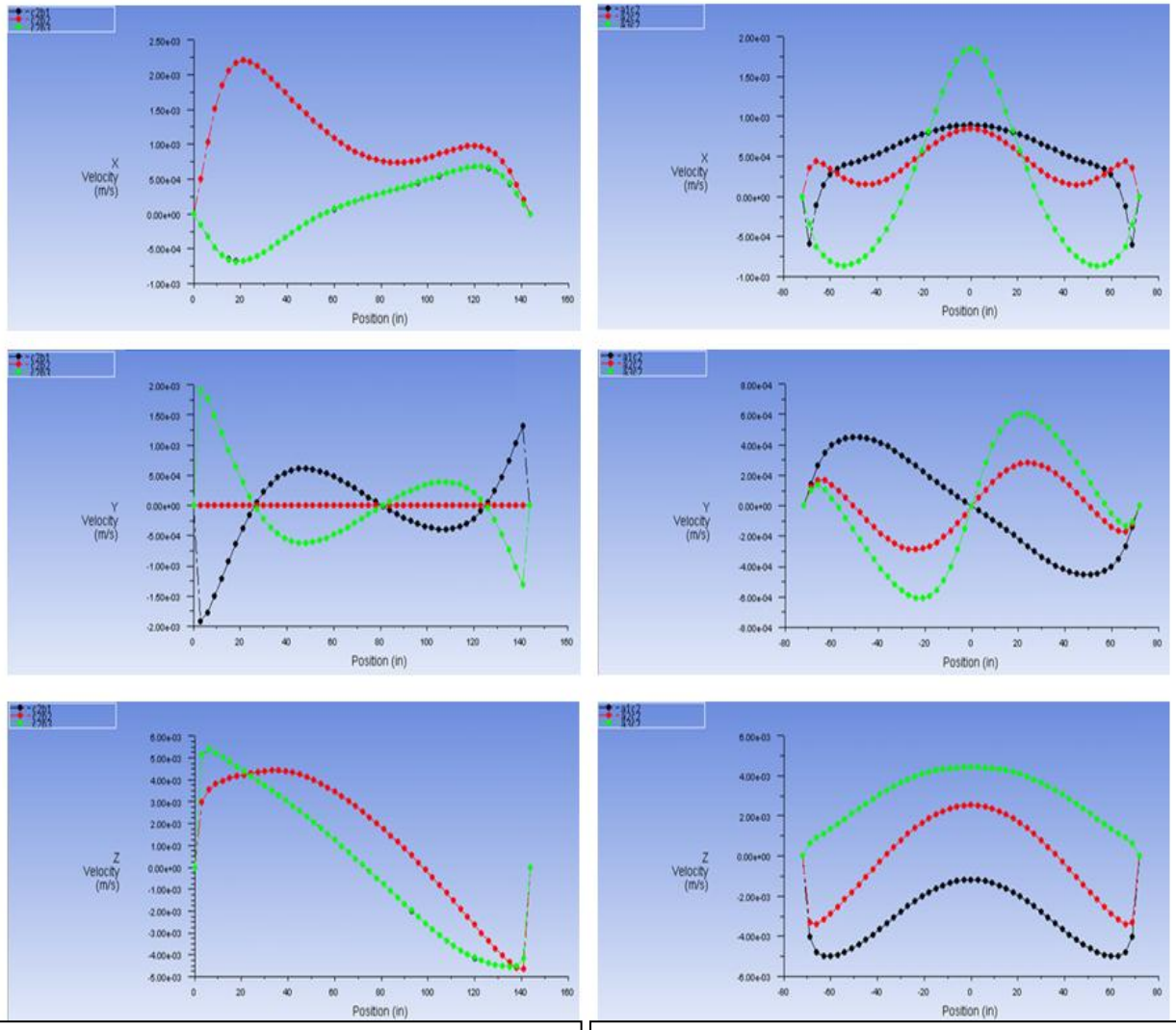

X, Y and Z Velocity Components along x-lines in C2 (x-y) plane at y=3' (Green), y=6' (Red), and y=9' (Black)	X, Y and Z Velocity Components along y-lines in C2 (x-y) plane at x=3' (Green), x=6' (Red), and x=9' (Black)

Figure 75: Case 2 - Velocity Components in the C2 Plane at Time T3 = 2:53 PM

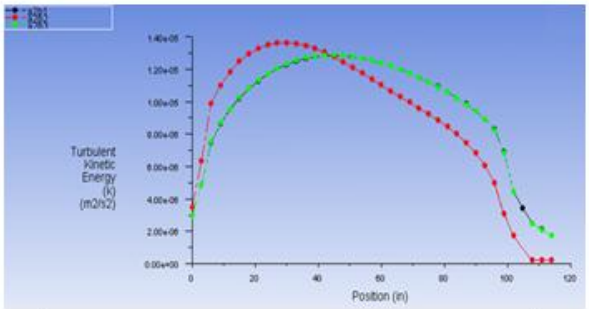

Turbulent Kinetic Energy along z-lines in A2 (y-z) plane at y=3' (Green), y=6'(Red) and y=9'(Black)

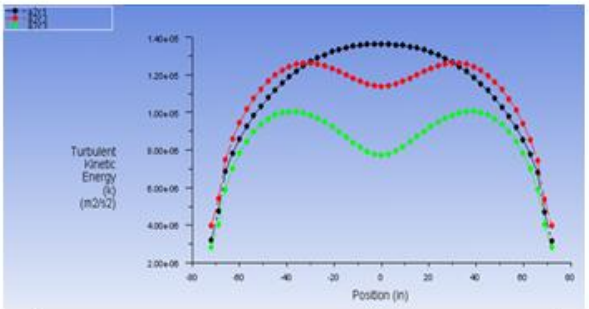

Turbulent Kinetic Energy along y-lines in A2 (y-z) plane at z=2'4.5" (Black), z=4'9"(Red) and z=7'1.5"(Green)

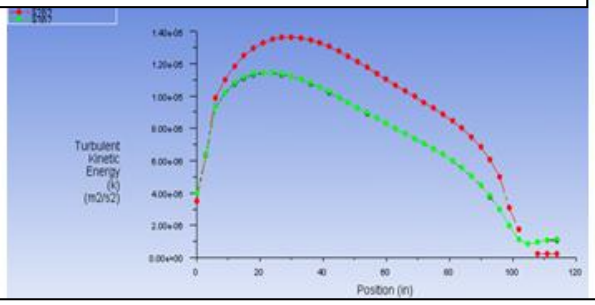

Turbulent Kinetic Energy along z-lines in B2 (x-z) plane at x=3' (Green), x=6'(Red) and x=9'(Black)

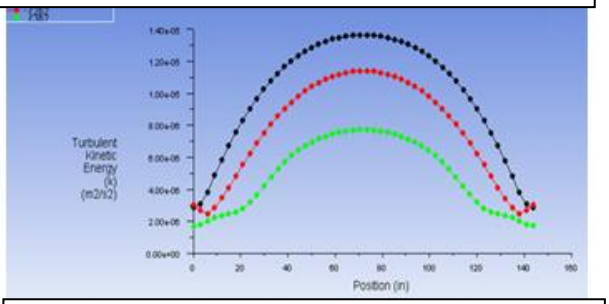

Turbulent Kinetic Energy along x-lines in B2 (x-z) plane at z=2'4.5" (Black), z=4'9"(Red) and z=7'1.5"(Green)

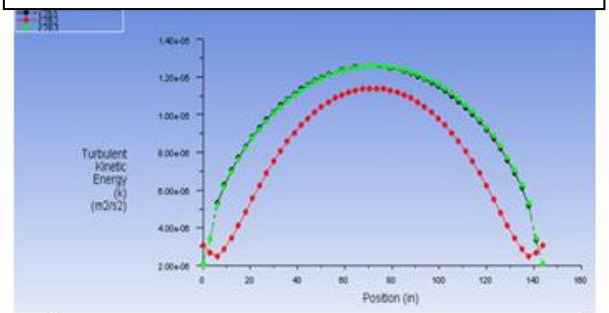

Turbulent Kinetic Energy along x-lines in C2 (x-y) plane at y=3' (Green), y=6'(Red) and y=9'(Black)

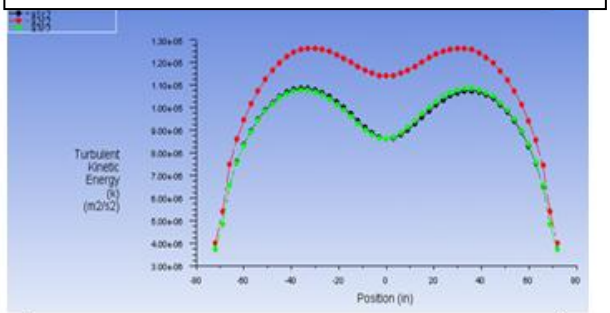

Turbulent Kinetic Energy along y-lines in C2 (x-y) plane at x=3' (Green), x=6'(Red) and x=9'(Black)

Figure 76: Case 2 - Turbulent Kinetic Energy Line Plots at Time T3 = 2:53 PM

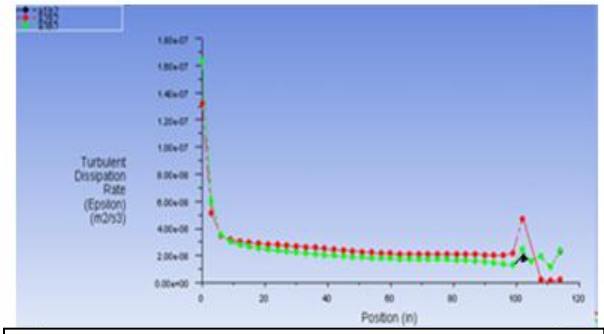

Turbulent Dissipation Rate along z-lines in A2 (y-z) plane at y=3' (Green), y=6'(Red) and y=9'(Black)

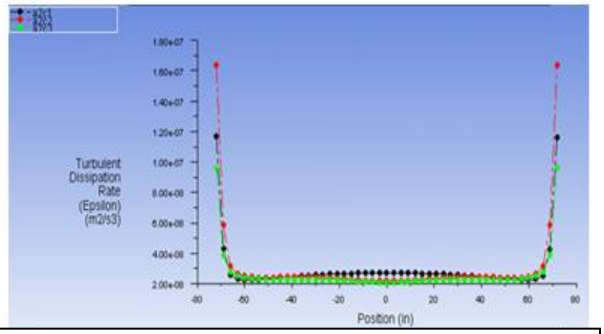

Turbulent Dissipation Rate along y-lines in A2 (y-z) plane at z=2'4.5" (Black), z=4'9"(Red) and z=7'1.5"(Green)

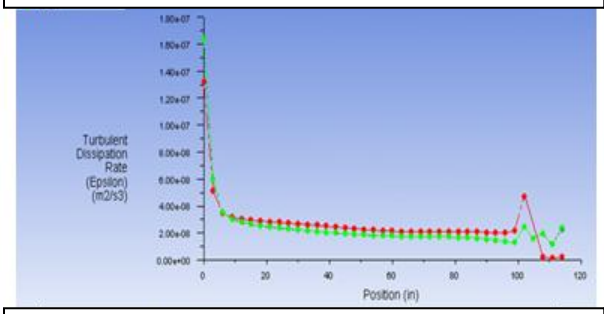

Turbulent Dissipation Rate along z-lines in B2 (x-z) plane at x=3' (Green), x=6'(Red) and x=9'(Black)

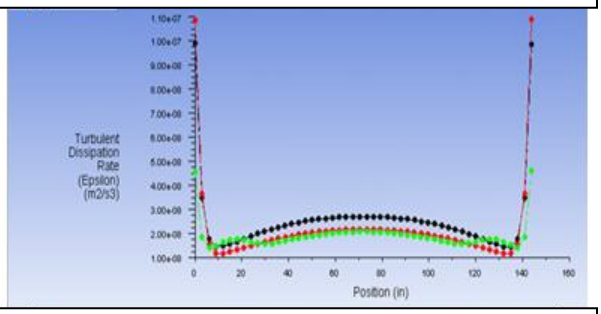

Turbulent Dissipation Rate along x-lines in B2 (x-z) plane at z=2'4.5" (Black), z=4'9"(Red) and z=7'1.5"(Green)

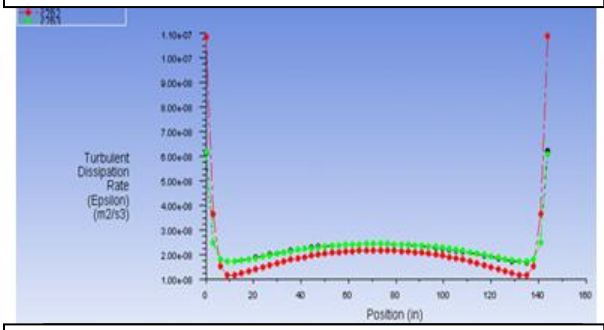

Turbulent Dissipation Rate along x-lines in C2 (x-y) plane at y=3' (Green), y=6'(Red) and y=9'(Black)

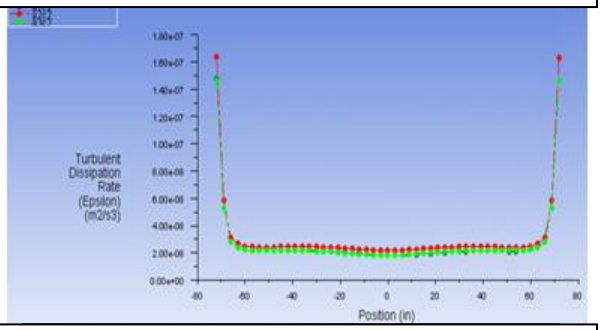

Turbulent Dissipation Rate along y-lines in C2 (x-y) plane at x=3' (Green), x=6'(Red) and x=9'(Black)

Figure 77: Case 2 - Turbulent Dissipation Rate Line Plots at Time T3 = 2:53 PM

The final data set for Case 2 is obtained at T4 = 8:27 PM. This time corresponds to another low temperature inside the room shown by the ASHRAE curve (Figure 7). Figure 78 shows the contours of temperature distributions in the different planes (A1-A3, B1-B3, and C1-C3). The lack of heat from the hot external wall results in a nearly constant room temperature. Figure 79 shows the velocity contours in different planes of the room described in Figure 19. These velocities are all very low because the low constant temperature doesn't require any cooling from the ventilation system. Figure 80 shows the various line plots of temperature distribution inside the room along various lines in planes A1-A3, B1-B3, and C1-C3 shown in Figure 19. These plots show that the solution satisfies the adiabatic wall conditions in the room except for the exterior wall where a constant temperature boundary condition is imposed corresponding to the external temperature at time T4 = 8:27 PM. These plots also show the cooling effects of the radiation slab near the ceiling. These line plots are a quantitative representation of Figure 78.

Figures 81-83 show various velocity components inside the room. These line plots show that the no slip condition is correctly imposed at the walls; all the velocity components go to zero at the walls. Figure 84 shows the turbulent kinetic energy line plots along various cross-sectional lines inside the room, they indicate the relative turbulence intensity in various parts of the room. The values of k are relatively small because of the very low flow velocities. As expected, the turbulent intensity is greater in the middle of the room than near the walls. Figure 85 shows line plots of the turbulent dissipation rate along various cross-sectional lines inside the room. In contrast to k, the value of epsilon is constant across the room in all directions and is extremely small except near the walls.

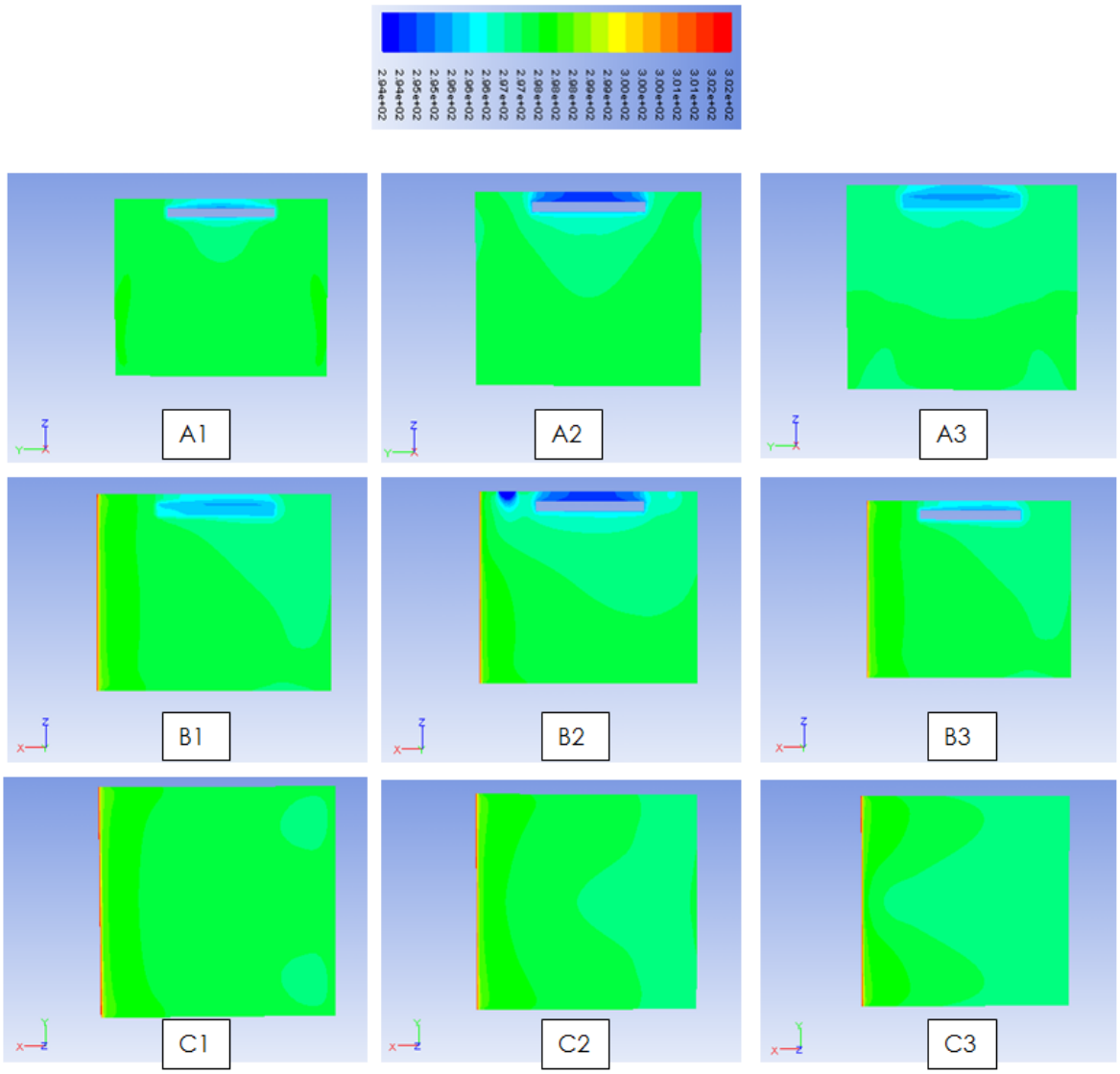

Figure 78: Case 2 - Temperature Contours in Different Planes of Figure 19 at Time T4 = 8:27 PM

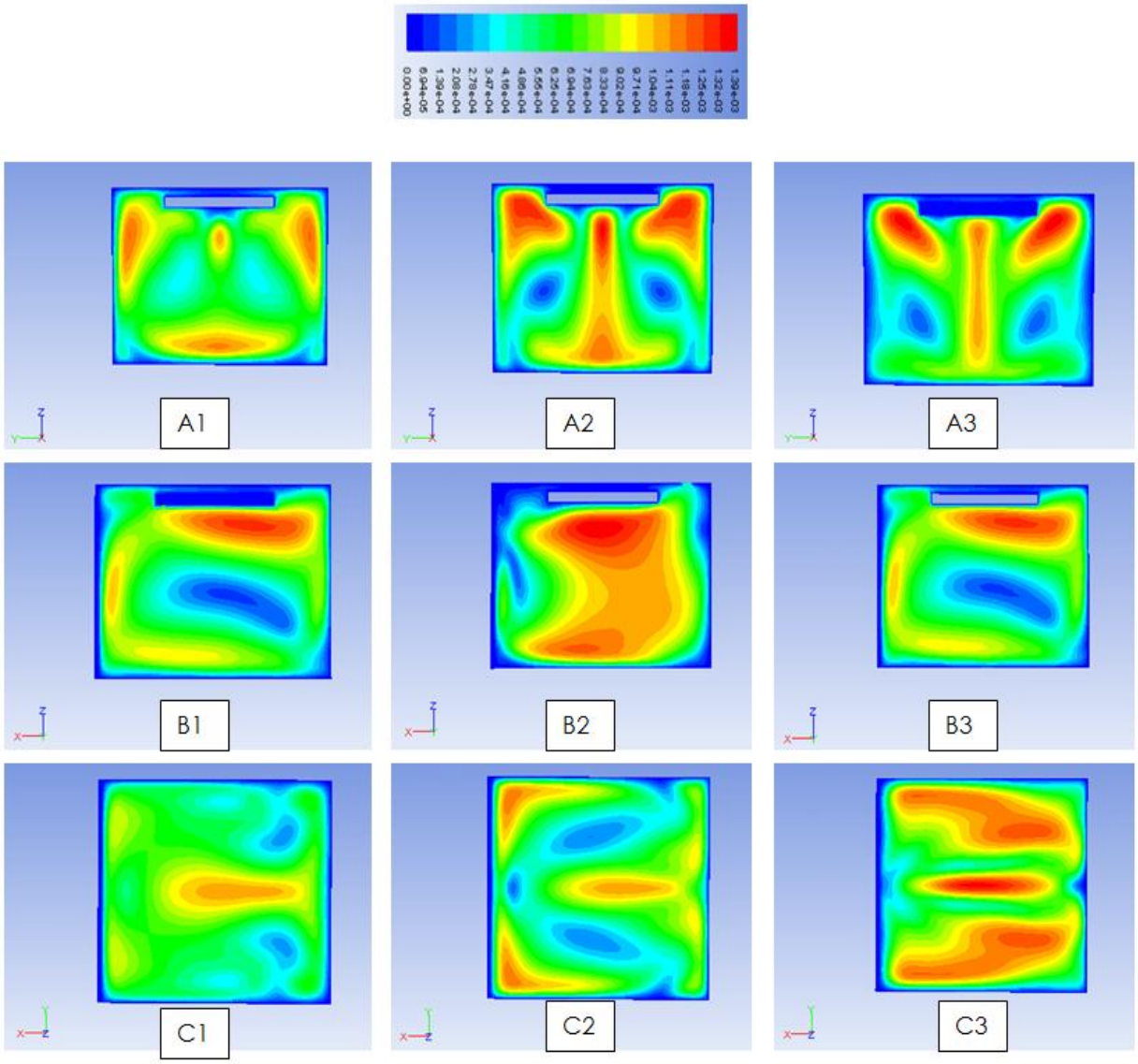

Figure 79: Case 2 - Velocity Contours in Different Planes of Figure 19 at Time T4 = 8:27 PM

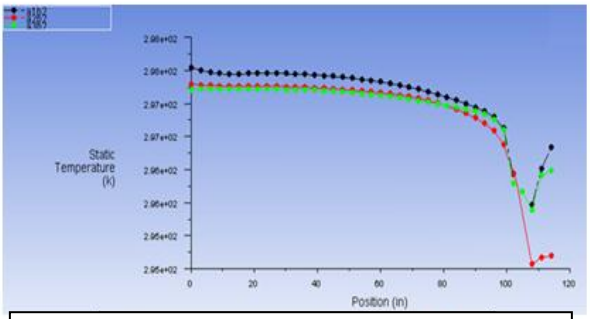

Temperature along z-lines in A2 (y-z) plane at y=3' (Green), y=6'(Red) and y=9'(Black)

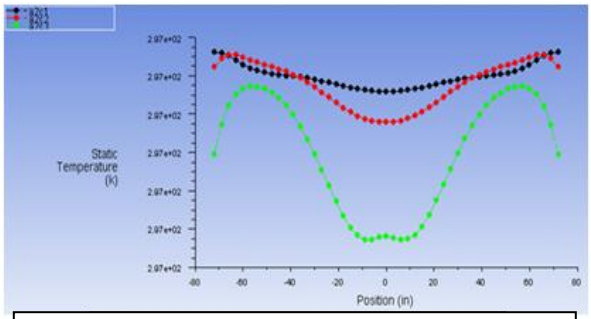

Temperature along y-lines in A2 (y-z) plane at z=2'4.5" (Black), z=4'9"(Red) and z=7'1.5"(Green)

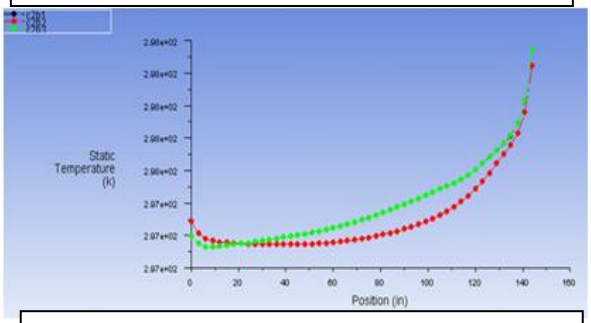

Temperature along z-lines in B2 (x-z) plane at x=3' (Green), x=6'(Red) and x=9'(Black)

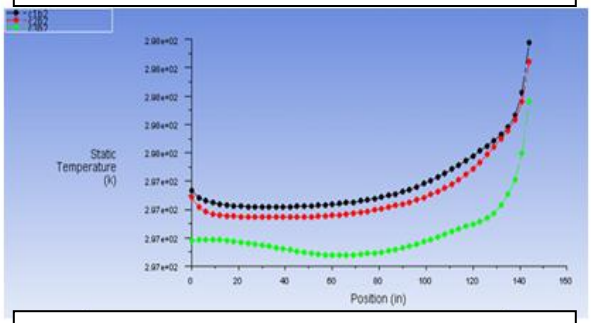

Temperature along x-lines in B2 (x-z) plane at z=2'4.5" (Black), z=4'9"(Red) and z=7'1.5"(Green)

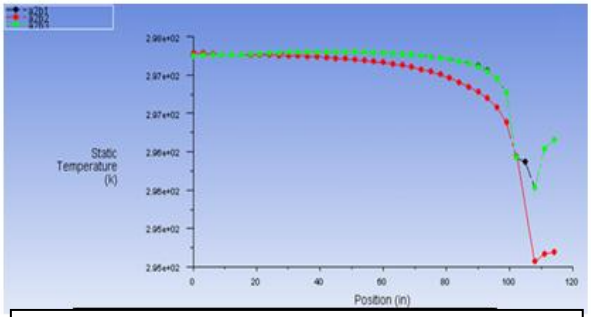

Temperature along x-lines in C2 (x-y) plane at y=3' (Green), y=6'(Red) and y=9'(Black)

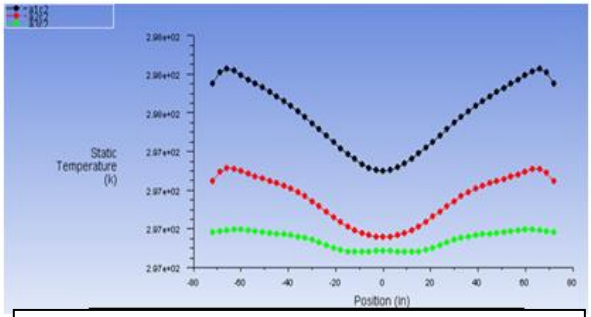

Temperature along y-lines in C2 (x-y) plane at x=3' (Green), x=6'(Red) and x=9'(Black)

Figure 80: Case 2 – Temperature Line Plots at Time T4 = 8:27 PM

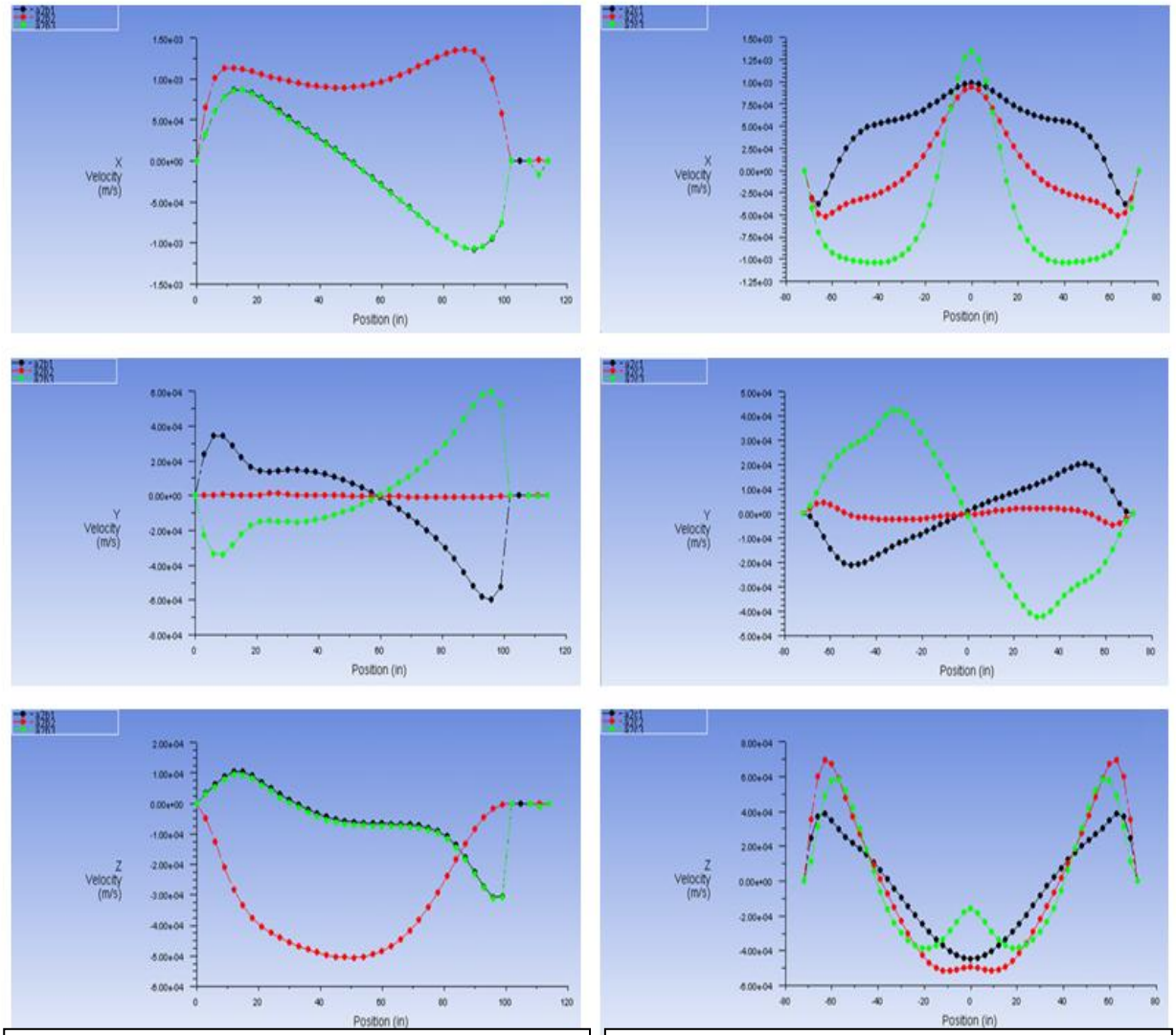

X, Y and Z Velocity Components along z-lines in A2 (y-z) plane at y=3'(Green), y=6'(Red), and y=9'(Black)

X, Y and Z Velocity Components along y-lines in A2 (y-z) plane at z=2'4.5" (Black), z=4'9" (Red), and z=7'1.5" (Green)

Figure 81: Case 2 - Velocity Components in the A2 Plane at Time T4 = 8:27 PM

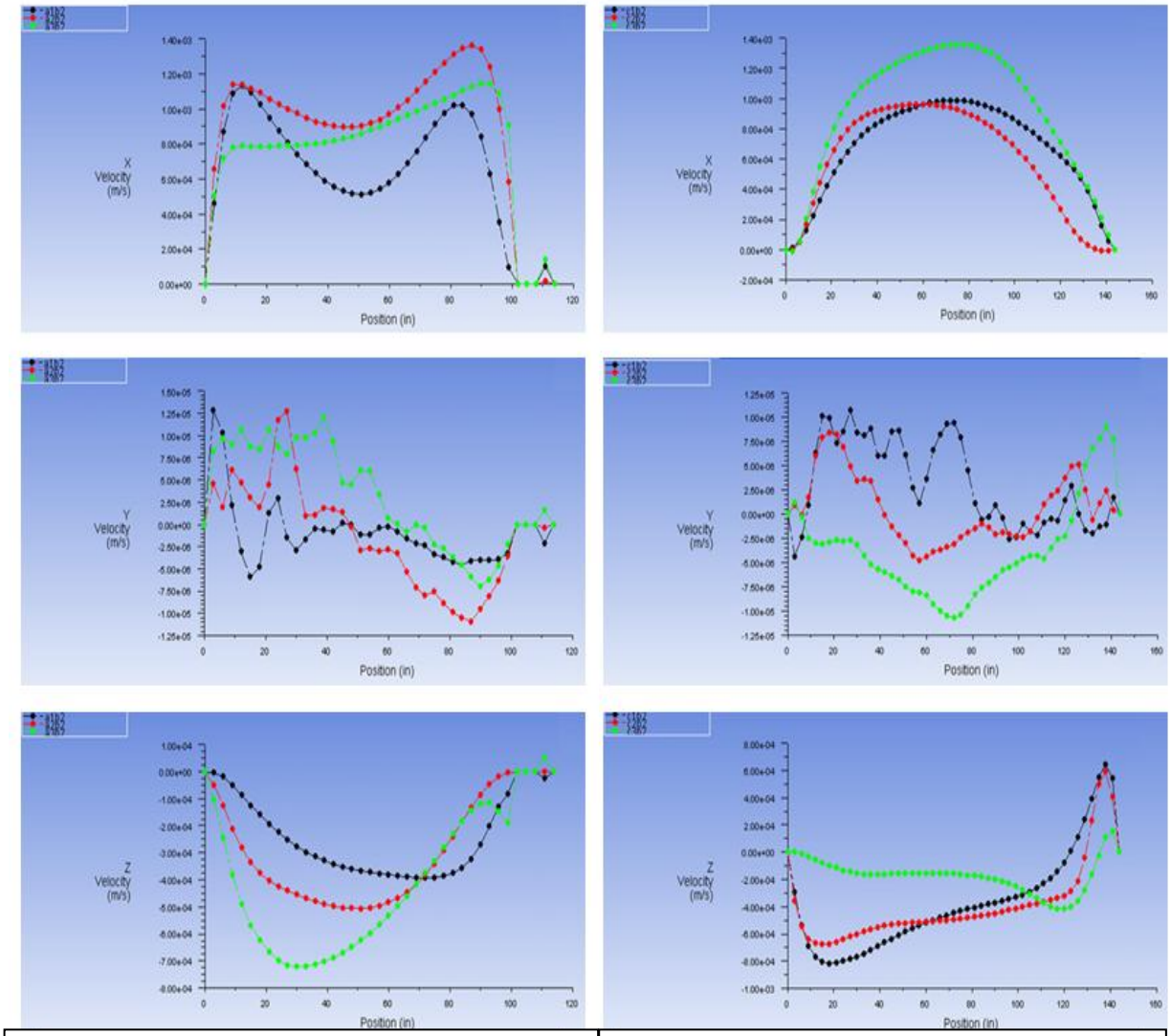

X, Y and Z Velocity Components along z-lines in B2(x-z) plane at x=3'(Green), x=6'(Red), and x=9'(Black)	X, Y and Z Velocity Components along x-lines in B2 (x-z) plane at z=2'4.5" (Black), z=4'9" (Red), and z=7'1.5"(Green)

Figure 82: Case 2 - Velocity Components in the B2 Plane at Time T4 = 8:27 PM

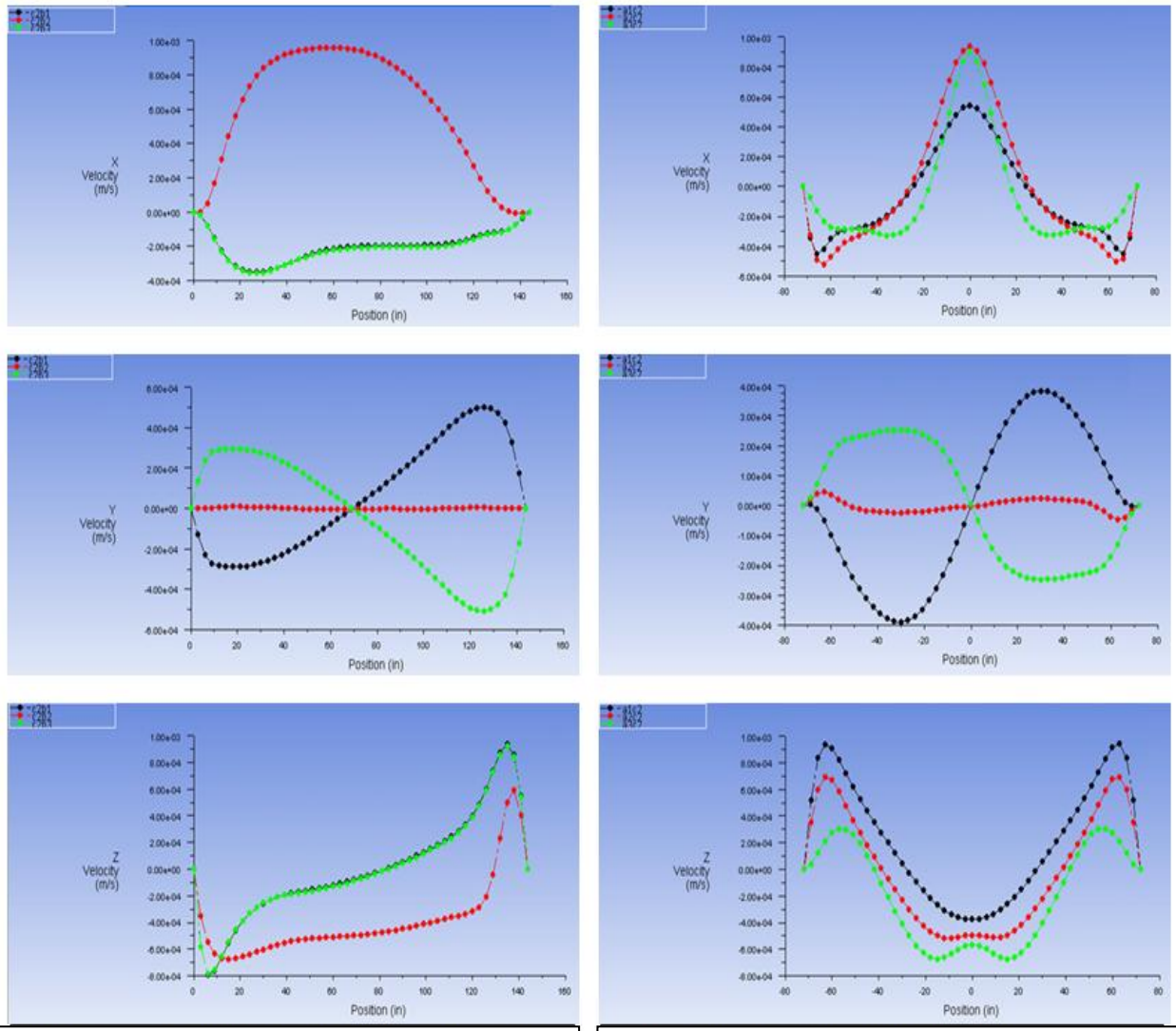

X, Y and Z Velocity Components along x-lines in C2 (x-y) plane at y=3' (Green), y=6' (Red), and y=9' (Black)

X, Y and Z Velocity Components along y-lines in C2 (x-y) plane at x=3' (Green), x=6' (Red), and x=9' (Black)

Figure 83: Case 2 - Velocity Components in the C2 Plane at Time T4 = 8:27 PM

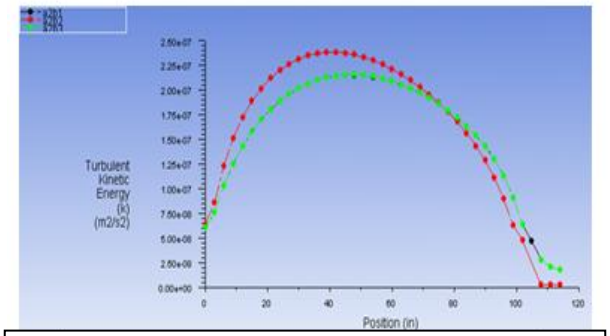

Turbulent Kinetic Energy along z-lines in A2 (y-z) plane at y=3' (Green), y=6'(Red) and y=9'(Black)

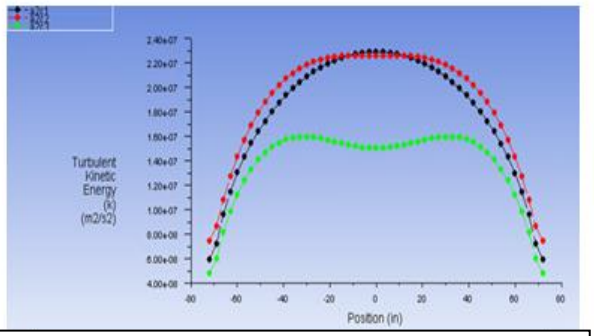

Turbulent Kinetic Energy along y-lines in A2 (y-z) plane at z=2'4.5" (Black), z=4'9"(Red) and z=7'1.5"(Green)

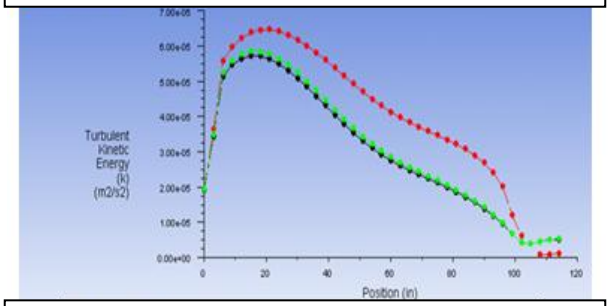

Turbulent Kinetic Energy along z-lines in B2 (x-z) plane at x=3' (Green), x=6'(Red) and x=9'(Black)

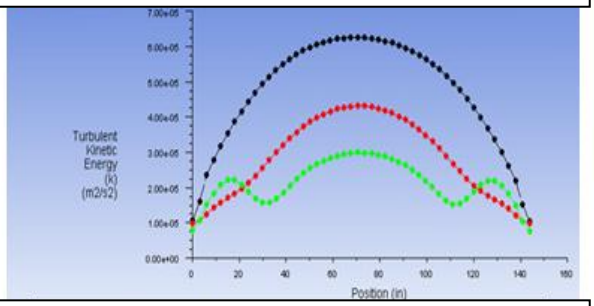

Turbulent Kinetic Energy along x-lines in B2 (x-z) plane at z=2'4.5" (Black), z=4'9"(Red) and z=7'1.5"(Green)

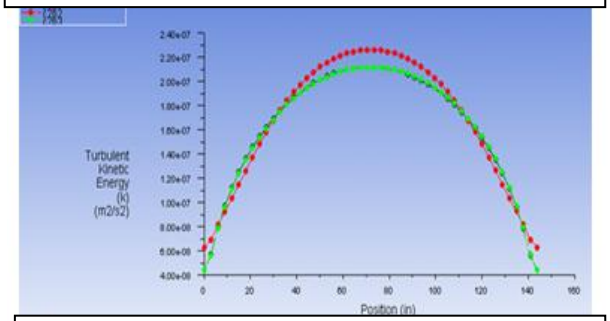

Turbulent Kinetic Energy along x-lines in C2 (x-y) plane at y=3' (Green), y=6'(Red) and y=9'(Black)

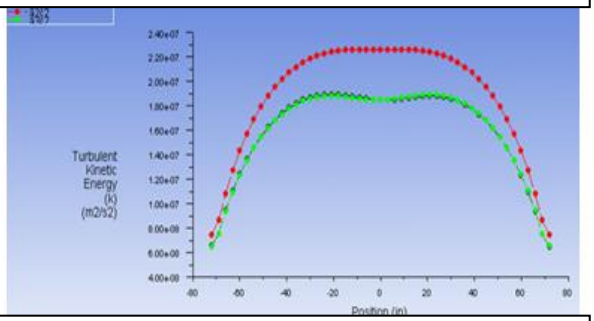

Turbulent Kinetic Energy along y-lines in C2 (x-y) plane at x=3' (Green), x=6'(Red) and x=9'(Black)

Figure 84: Case 2 - Turbulent Kinetic Energy Line Plots at Time T4 = 8:27 PM

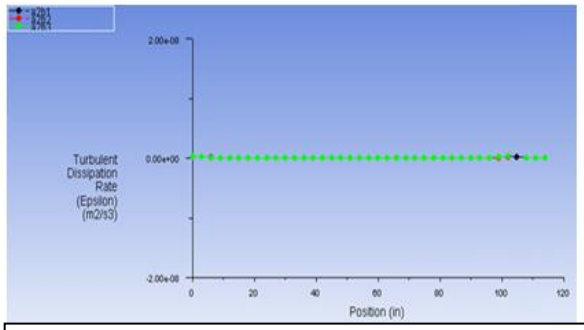

Turbulent Dissipation Rate along z-lines in A2 (y-z) plane at y=3' (Green), y=6'(Red) and y=9'(Black)

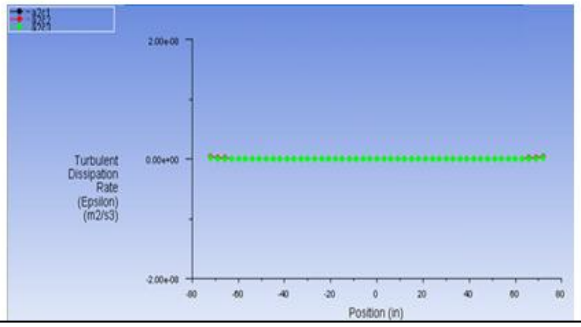

Turbulent Dissipation Rate along y-lines in A2 (y-z) plane at z=2'4.5" (Black), z=4'9"(Red) and z=7'1.5"(Green)

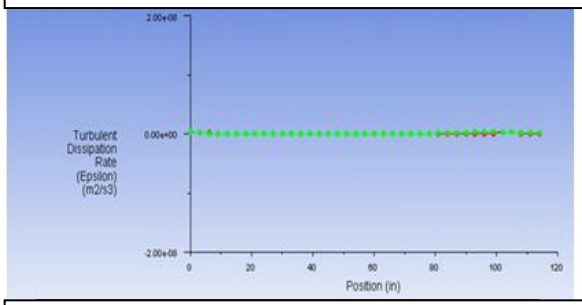

Turbulent Dissipation Rate along z-lines in B2 (x-z) plane at x=3' (Green), x=6'(Red) and x=9'(Black)

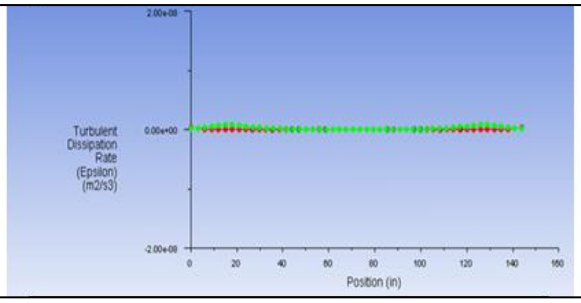

Turbulent Dissipation Rate along x-lines in B2 (x-z) plane at z=2'4.5" (Black), z=4'9"(Red) and z=7'1.5"(Green)

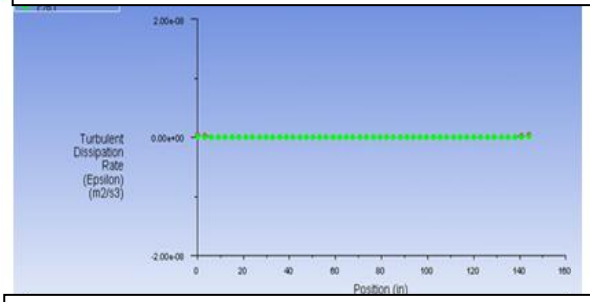

Turbulent Dissipation Rate along x-lines in C2 (x-y) plane at y=3' (Green), y=6'(Red) and y=9'(Black)

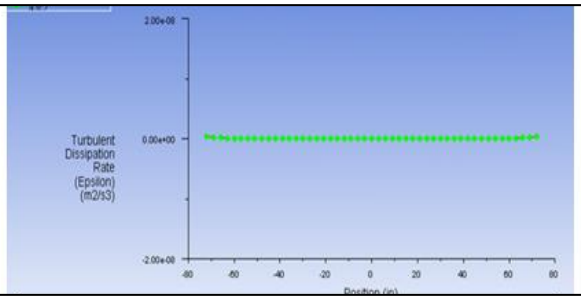

Turbulent Dissipation Rate along y-lines in C2 (x-y) plane at x=3' (Green), x=6'(Red) and x=9'(Black)

Figure 85: Case 2 - Turbulent Dissipation Rate Line Plots at Time T4 = 8:27 PM

5.4.4 Case 3: Distributed Ventilation System

The calculations for Case 3 were performed using the Boussinesq approximation for density, the k-ε realizable turbulence model, and a first order upwind scheme in FLUENT. Computations were performed for two 24-hour time cycles. A time step of 10 seconds was employed in each iteration. 8640 time steps are required for a complete 24-hour cycle. The details of the geometry, mesh, boundary conditions, and mass flow rate into the room for this case are described in sections 5.2 and 5.3 of this chapter. A total of 140030 iterations were required to complete the two 24-hour cycles for Case 3. The solutions obtained during the second 24-hour cycle are free of transient effects due to the initial conditions. Figure 86 shows the convergence history of various flow variables and governing equations. In particular, it represents the change in the residuals during the iterative process.

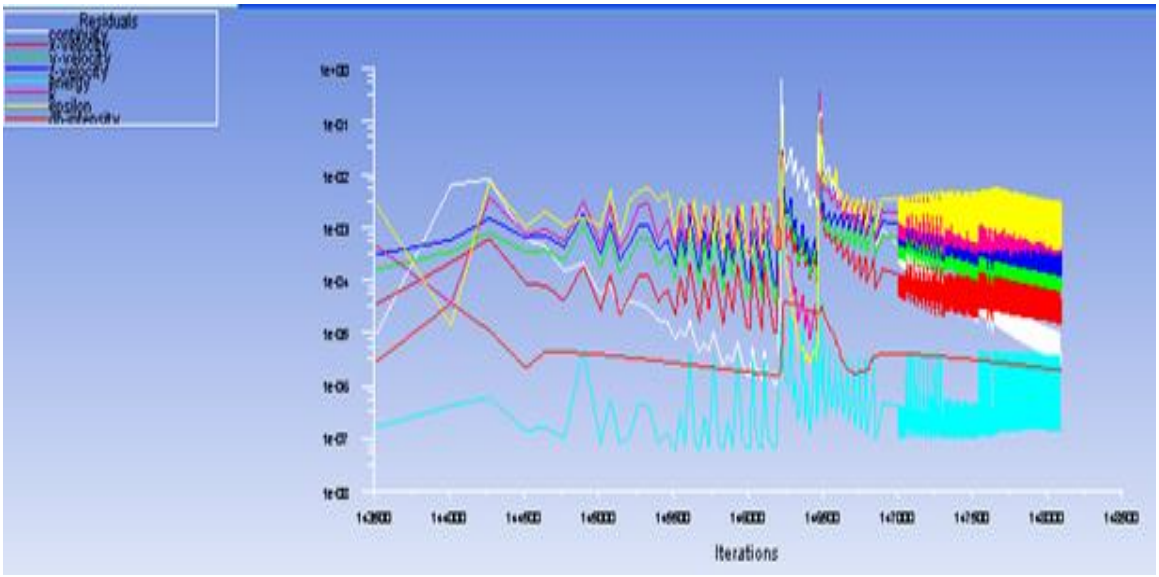

Figure 86: Case 3 - Residual History of Various Flow Variables and Governing Equations During the Iterative Process

Figure 87 shows the contours of temperature distributions in the different planes at T1 = 3:45 AM. T1 corresponds to a low temperature on the ASHRAE curve (Figure 7). As a result, the vents are not required to circulate the air inside the room, and the temperature remains nearly constant. These contours also show that the temperature is slightly cooler near the rear of the room. Figure 88 depicts the velocity contours in different planes of the room as described in Figure 19. These velocities are all very low because the vents have not been active at time T1, and have not been active for a long period of time before time T1 because of the existing cooler temperature. This figure does show that there is some circulation in the room. Also, the velocity is highest in the middle of the front and rear walls.

Figure 89 shows the line plots of temperature distributions inside the room along various lines in planes A1-A3, B1-B3, and C1-C3 as shown in Figure 19. These plots show that the solution satisfies the adiabatic wall conditions in the room except at the exterior wall where a constant temperature boundary condition is imposed corresponding to the external temperature at time T1. This figure a quantitative description of what is shown in the contour plots of Figure 87. These line plots also show that there is very little variation in the temperature inside the room; it varies between 296 and 297 K except for the external wall.

Figures 88-90 show the line plots of various velocity components inside the room. These plots show, as expected, that the no slip condition is correctly imposed at the walls; all velocity components go to zero as they approach the walls. All of these velocities are relatively small in magnitude, which is a quantitative description of the contour plots shown in Figure 88. Figure 91 shows the turbulent kinetic energy line plots along various cross-sectional lines inside the room, which is indicative of the relative turbulence intensity in

various parts of the room. As expected, the turbulent intensity is greater in the middle of the room than near the walls. Figure 92 shows the line plots of the turbulent dissipation rate along various cross-sectional lines inside the room. In contrast to k, the values of epsilon peak near the walls because of the large dissipation of turbulence. The value of epsilon is fairly constant across the room in all directions, except near the walls.

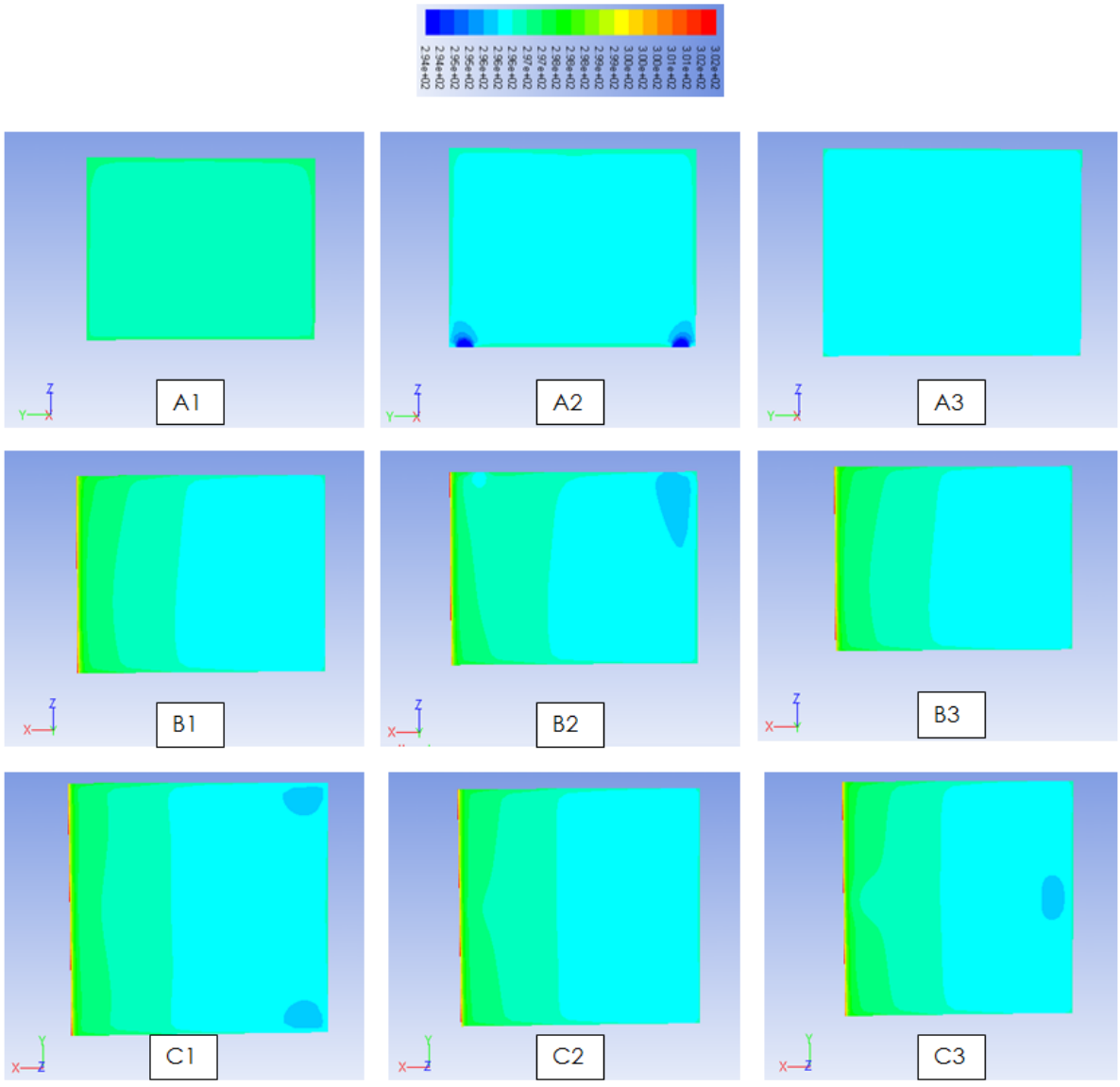

Figure 87: Case 3 - Temperature Contours in Different Planes of Figure 19 at Time T1 = 3:45 AM

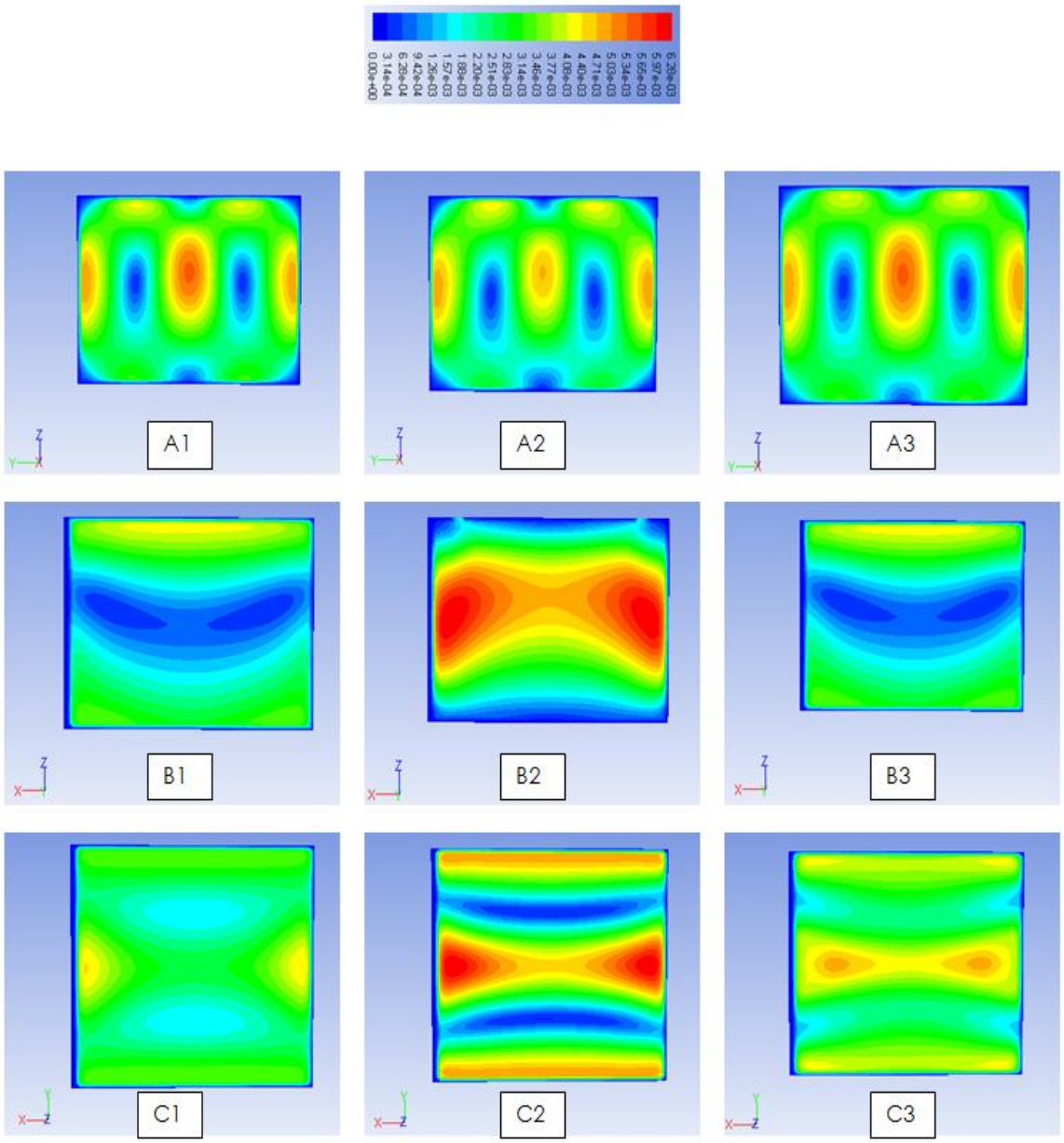

Figure 88: Case 3 - Velocity Contours in Different Planes of Figure 19 at Time T1 = 3:45 AM

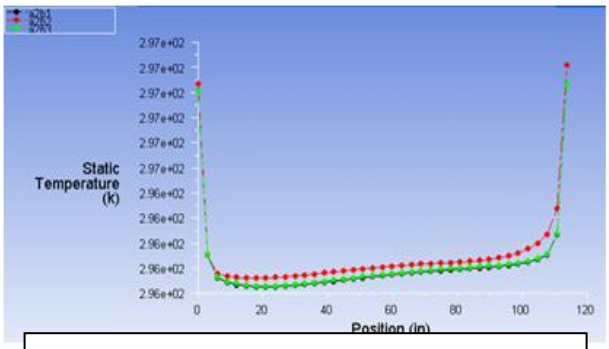

Temperature along z-lines in A2 (y-z) plane at y=3' (Green), y=6'(Red) and y=9'(Black)

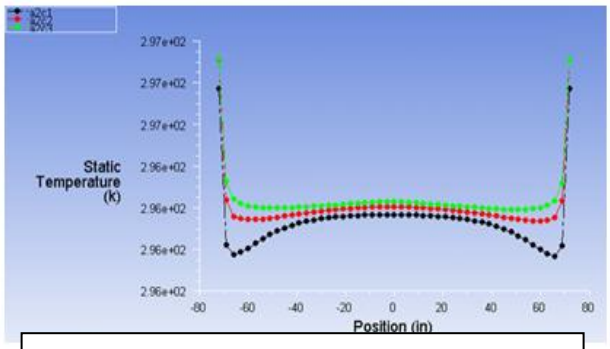

Temperature along y-lines in A2 (y-z) plane at z=2'4.5" (Black), z=4'9"(Red) and z=7'1.5"(Green)

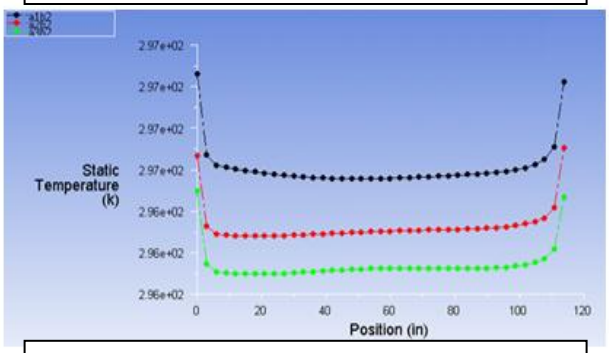

Temperature along z-lines in B2 (x-z) plane at x=3' (Green), x=6'(Red) and x=9'(Black)

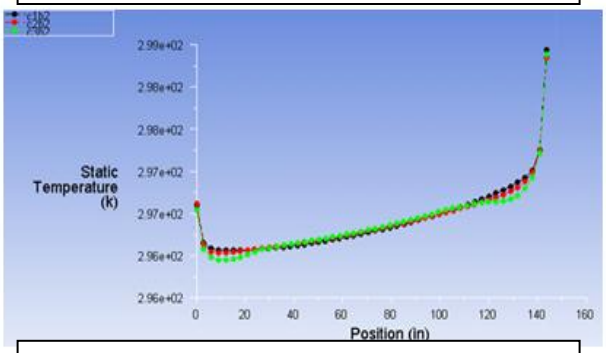

Temperature along x-lines in B2 (x-z) plane at z=2'4.5" (Black), z=4'9"(Red) and z=7'1.5"(Green)

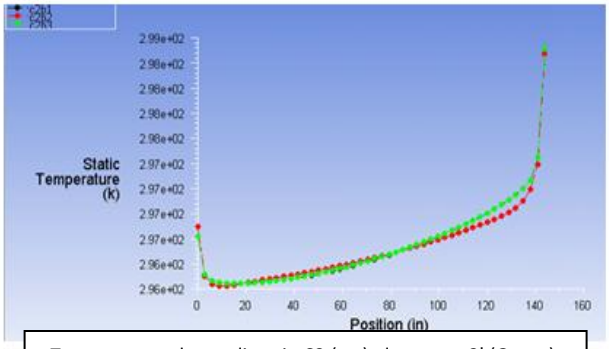

Temperature along x-lines in C2 (x-y) plane at y=3' (Green), y=6'(Red) and y=9'(Black)

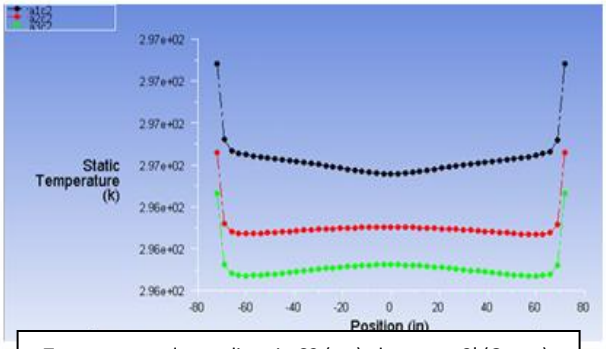

Temperature along y-lines in C2 (x-y) plane at x=3' (Green), x=6'(Red) and x=9'(Black)

Figure 89: Case 3 - Temperature Line Plots at Time T1 = 3:45 AM

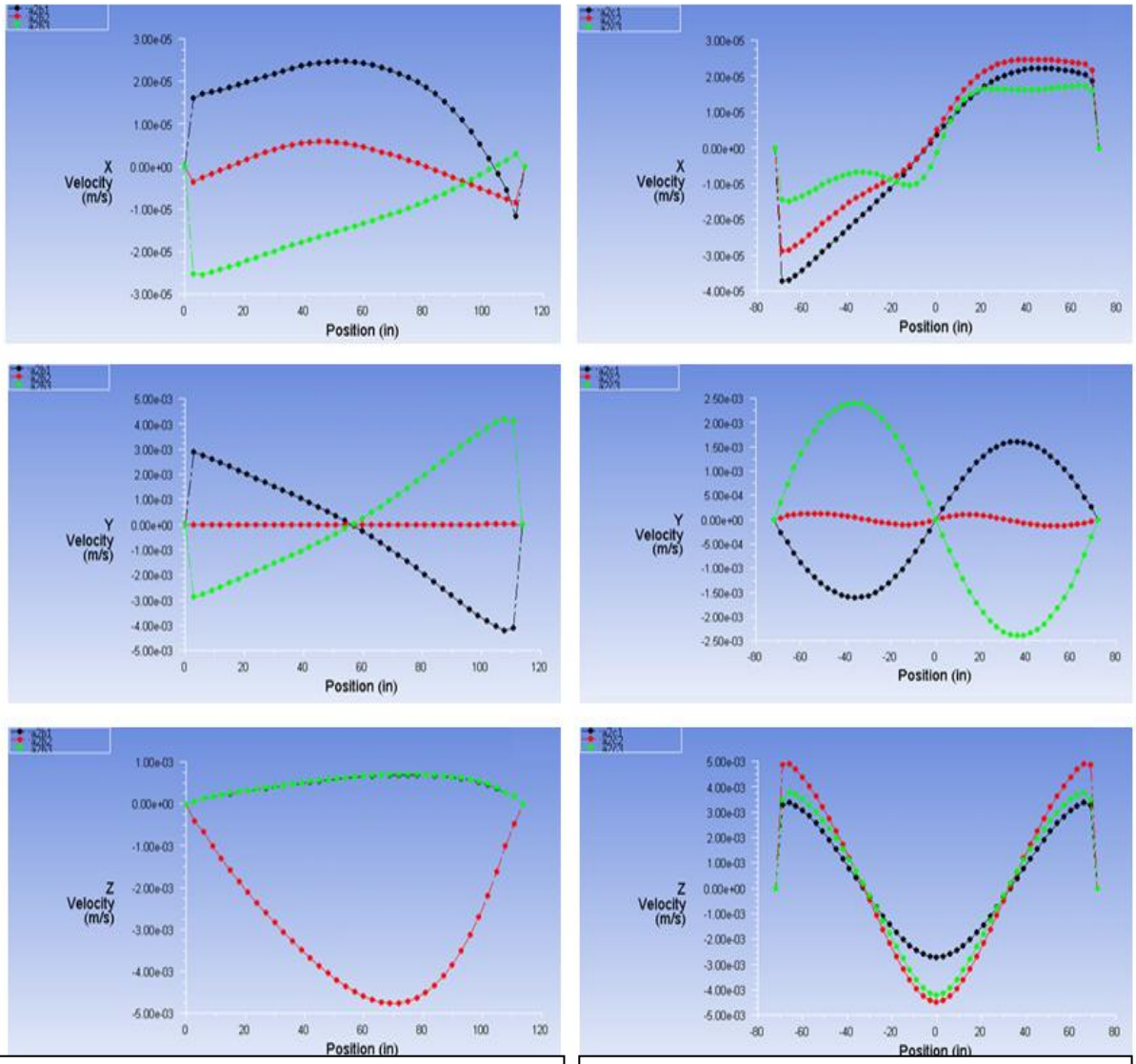

X, Y and Z Velocity Components along z-lines in A2 (y-z) plane at y=3'(Green), y=6'(Red), and y=9'(Black)

X, Y and Z Velocity Components along y-lines in A2 (y-z) plane at z=2'4.5" (Black), z=4'9" (Red), and z=7'1.5" (Green)

Figure 90: Case 3 - Velocity Components in the A2 Plane at Time T1 = 3:45 AM

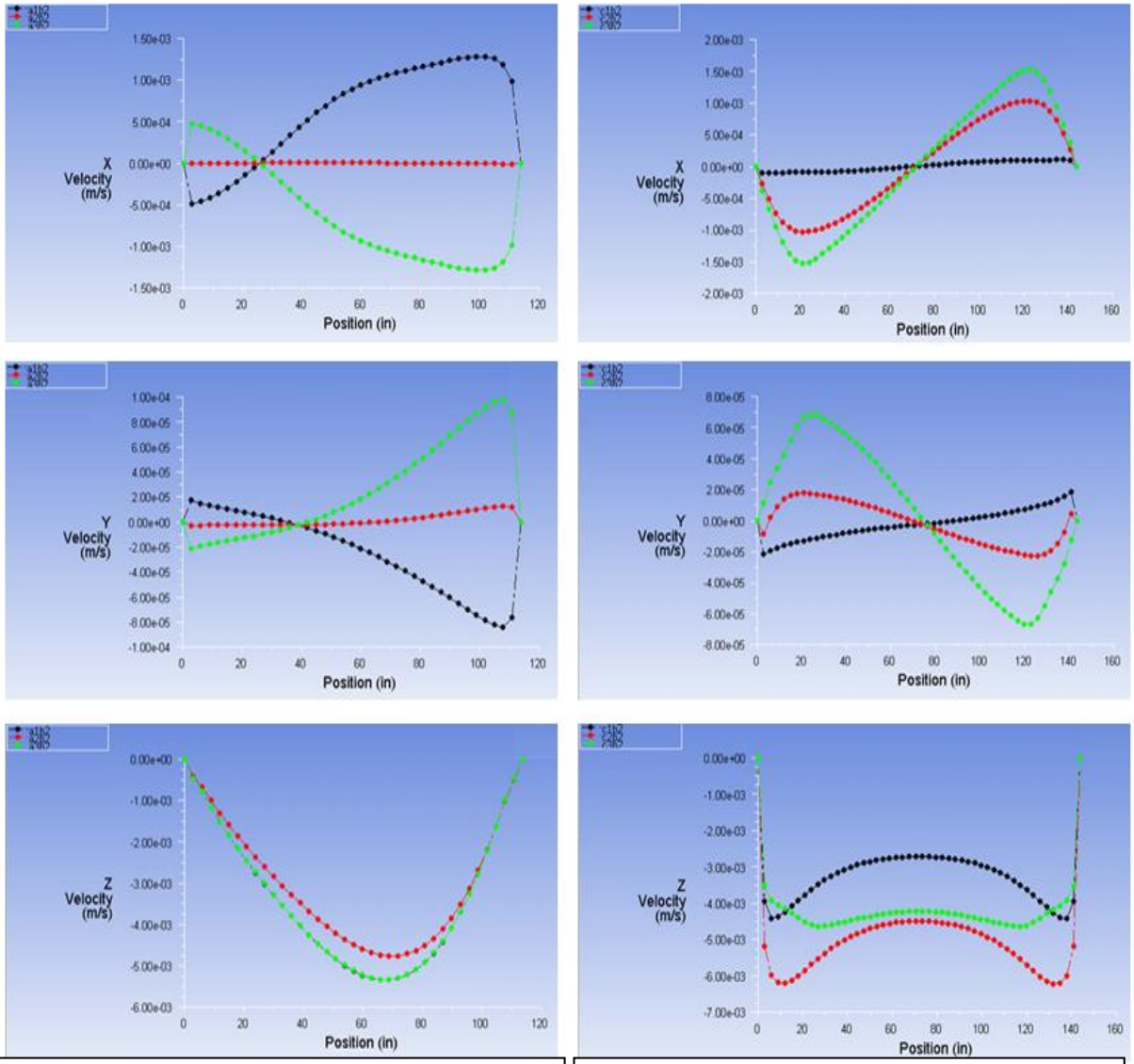

X, Y and Z Velocity Components along z-lines in B2(x-z) plane at x=3'(Green), x=6'(Red), and x=9'(Black)	X, Y and Z Velocity Components along x-lines in B2 (x-z) plane at z=2'4.5" (Black), z=4'9" (Red), and z=7'1.5"(Green)

Figure 91: Case 3 - Velocity Contours on the B2 Plane Time T1 = 3:45 AM

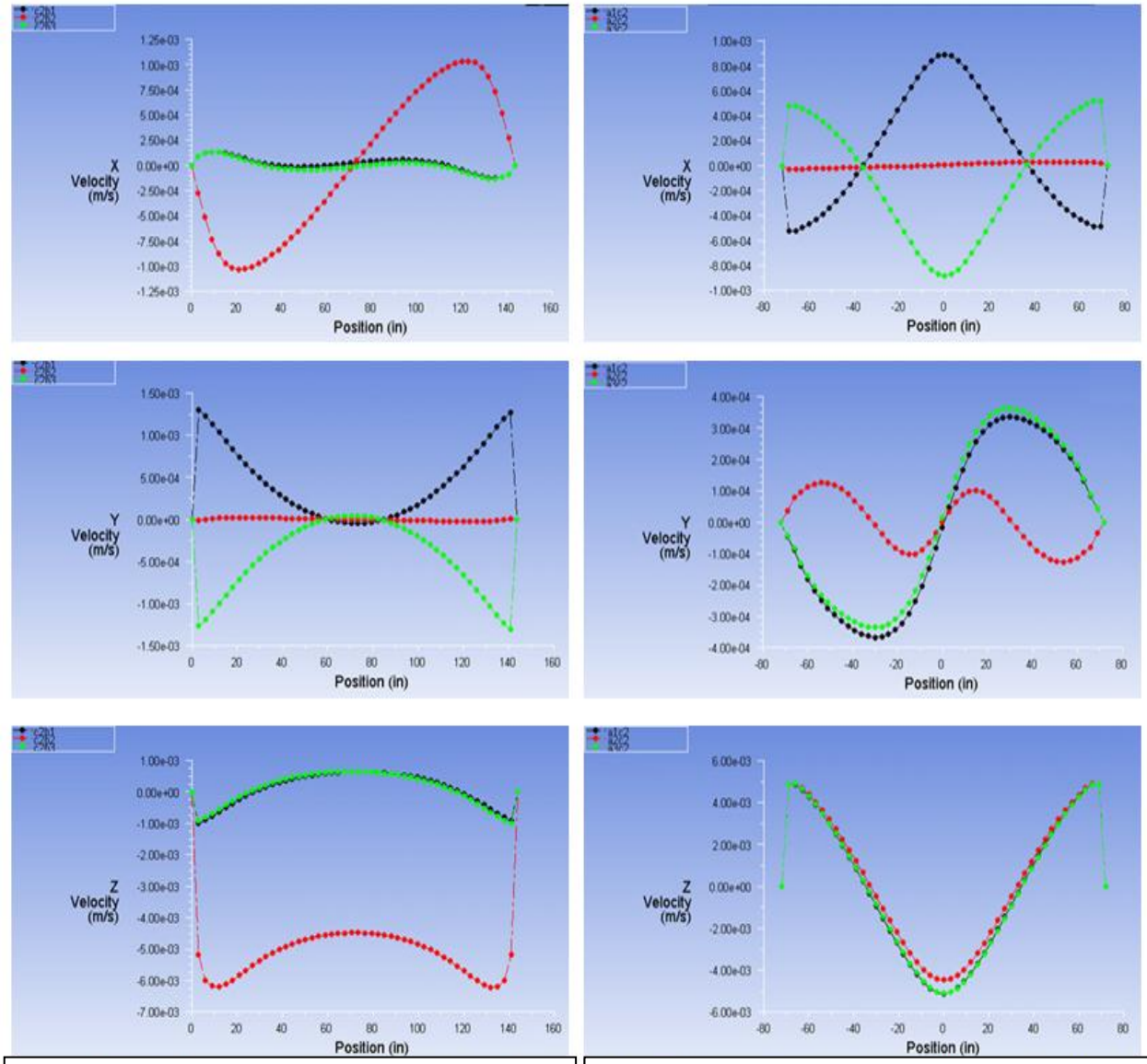

X, Y and Z Velocity Components along x-lines in C2 (x-y) plane at y=3' (Green), y=6' (Red), and y=9' (Black)

X, Y and Z Velocity Components along y-lines in C2 (x-y) plane at x=3' (Green), x=6' (Red), and x=9' (Black)

Figure 92: Case 3 - Velocity Contours on the C2 Plane Time T1 = 3:45 AM

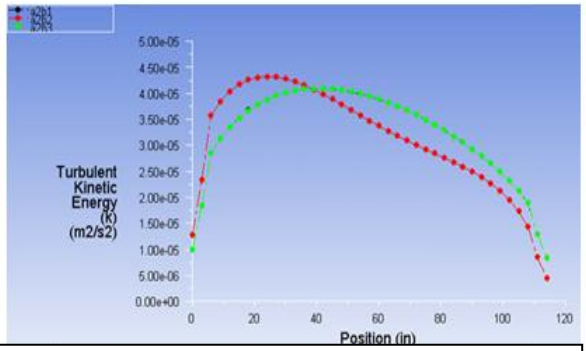

Turbulent Kinetic Energy along z-lines in A2 (y-z) plane at y=3' (Green), y=6'(Red) and y=9'(Black)

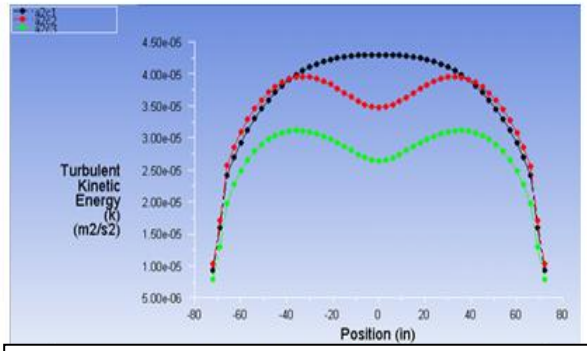

Turbulent Kinetic Energy along y-lines in A2 (y-z) plane at z=2'4.5" (Black), z=4'9"(Red) and z=7'1.5"(Green)

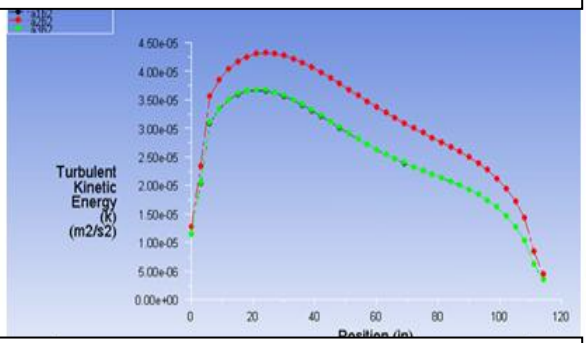

Turbulent Kinetic Energy along z-lines in B2 (x-z) plane at x=3' (Green), x=6'(Red) and x=9'(Black)

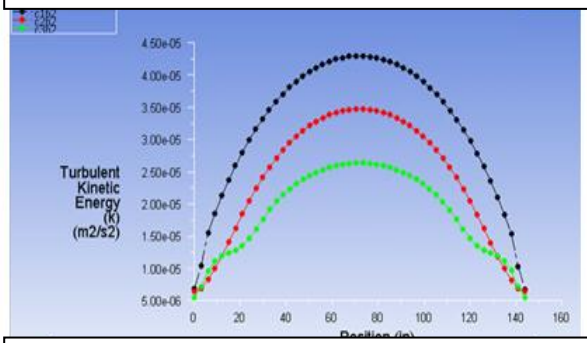

Turbulent Kinetic Energy along x-lines in B2 (x-z) plane at z=2'4.5" (Black), z=4'9"(Red) and z=7'1.5"(Green)

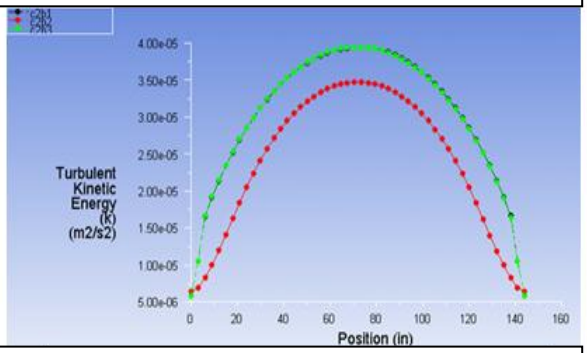

Turbulent Kinetic Energy along x-lines in C2 (x-y) plane at y=3' (Green), y=6'(Red) and y=9'(Black)

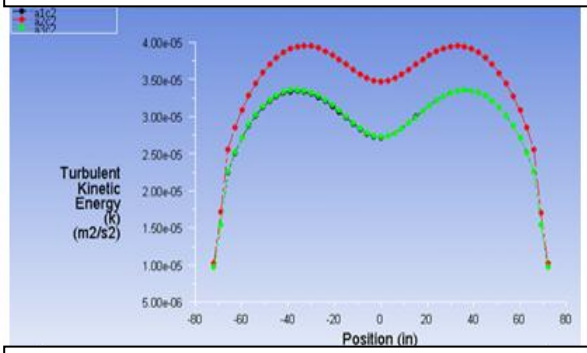

Turbulent Kinetic Energy along y-lines in C2 (x-y) plane at x=3' (Green), x=6'(Red) and x=9'(Black)

Figure 93: Case 3 - Turbulent Kinetic Energy Line Plots at Time T1 = 3:45 AM

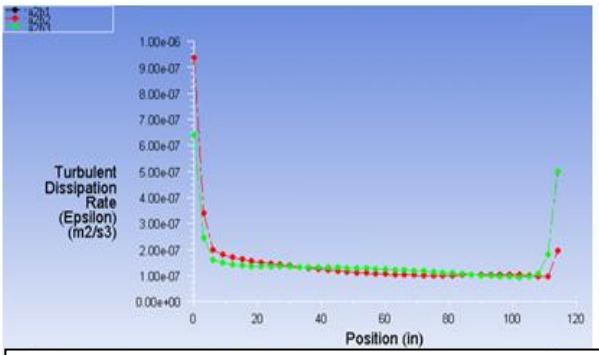

Turbulent Dissipation Rate along z-lines in A2 (y-z) plane at y=3' (Green), y=6'(Red) and y=9'(Black)

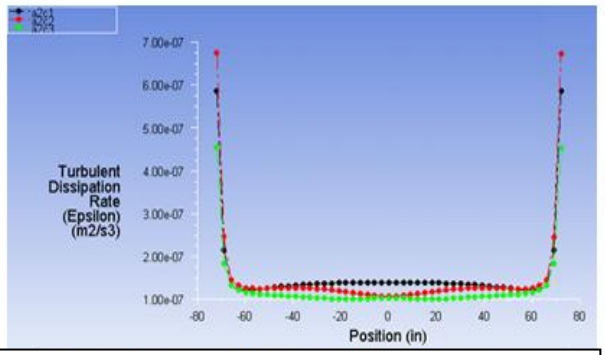

Turbulent Dissipation Rate along y-lines in A2 (y-z) plane at z=2'4.5" (Black), z=4'9"(Red) and z=7'1.5"(Green)

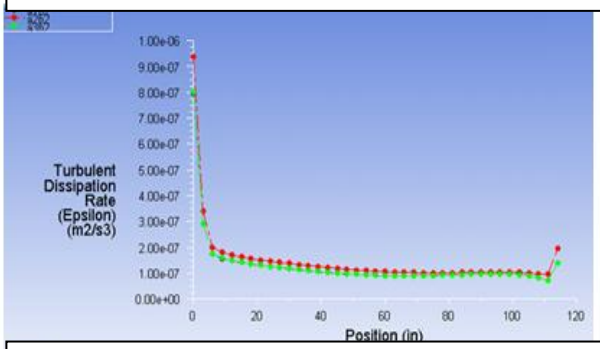

Turbulent Dissipation Rate along z-lines in B2 (x-z) plane at x=3' (Green), x=6'(Red) and x=9'(Black)

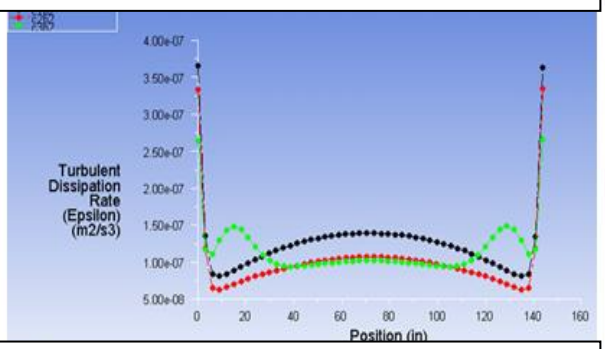

Turbulent Dissipation Rate along x-lines in B2 (x-z) plane at z=2'4.5" (Black), z=4'9"(Red) and z=7'1.5"(Green)

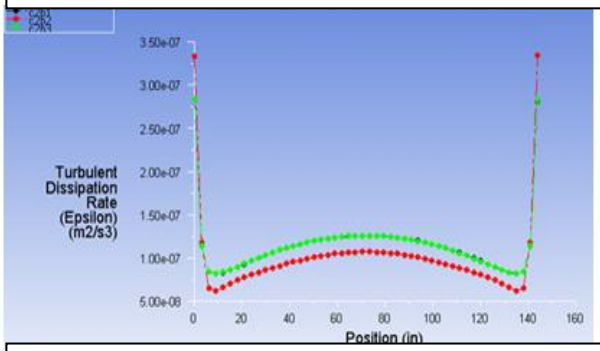

Turbulent Dissipation Rate along x-lines in C2 (x-y) plane at y=3' (Green), y=6'(Red) and y=9'(Black)

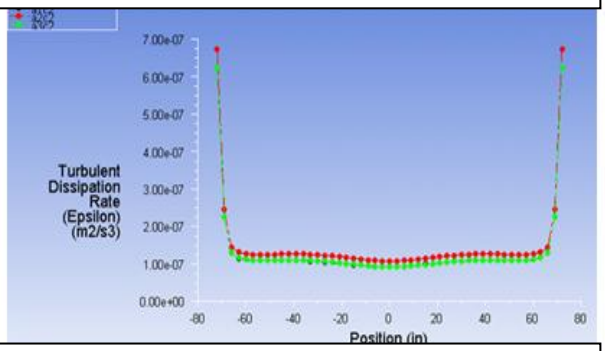

Turbulent Dissipation Rate along y-lines in C2 (x-y) plane at x=3' (Green), x=6'(Red) and x=9'(Black)

Figure 94: Case 3 - Turbulent Dissipation Rate Line Plots at Time T1 = 3:45 AM

Next, we present results at time T2 = 9:20 AM. The key to interpreting the results in the various planes (A1-A3, B1-B3, C1-C3) and along the various lines in the planes inside the room is the same as described before for Figures 87-94 at T1 = 3:45 AM. At T2 = 9:20 AM, the outside temperature is higher as shown in the ASHRAE temperature curve (Figure 7). The air inside the room is therefore warmer than at T1 = 3:45 AM. Figure 95 shows the temperature contours inside the room in A1-A3, B1-B3, and C1-C3 planes. At time T2 = 9:20 AM, we can observe the effects of the cold air collecting near the outlet vent in the rear of the ceiling, and the six vents in the floor. Figure 96 shows the velocity contours in different planes of the room at time T2 = 9:20 AM. We notice that the air velocity is very low within the room because the vents haven't been required. This is evidence that the DV system is very efficient. Although the exterior wall is increasing in temperature, the vents are not required to supply as much cold air to keep the room within a comfortable range of temperatures.

Figure 97 shows the line plots of temperature distributions inside the room, which are somewhat higher those at time T1 = 3:45 AM as expected. These temperature line plots show that the adiabatic temperature boundary condition is satisfied on the five interior walls, and that the highest temperature occurs at the exterior wall. The temperature plots in planes A1-A3, and B1-B3 show that the cold air is nearly constant in the vertical direction indicating that the air is evenly distributed, and the heat from the exterior wall is slowly propagating towards the rear of the room. Figures 98-100 show the line plots of velocity in various planes inside the room, which are fairly similar to those in Figures 90-92 at time T1 = 3:45 AM. Figure 101 shows the line plots of turbulent kinetic energy in various planes inside the room. The turbulent kinetic energy (k) is quite high near the side walls as expected

due to increased air velocity above the inlet vents, and is nearly zero elsewhere. Figure 102 shows the line plots of the turbulent dissipation rate in various planes inside the room. The intensity of both k and ε is as expected since the temperature increases at time T2 = 9:20 AM.

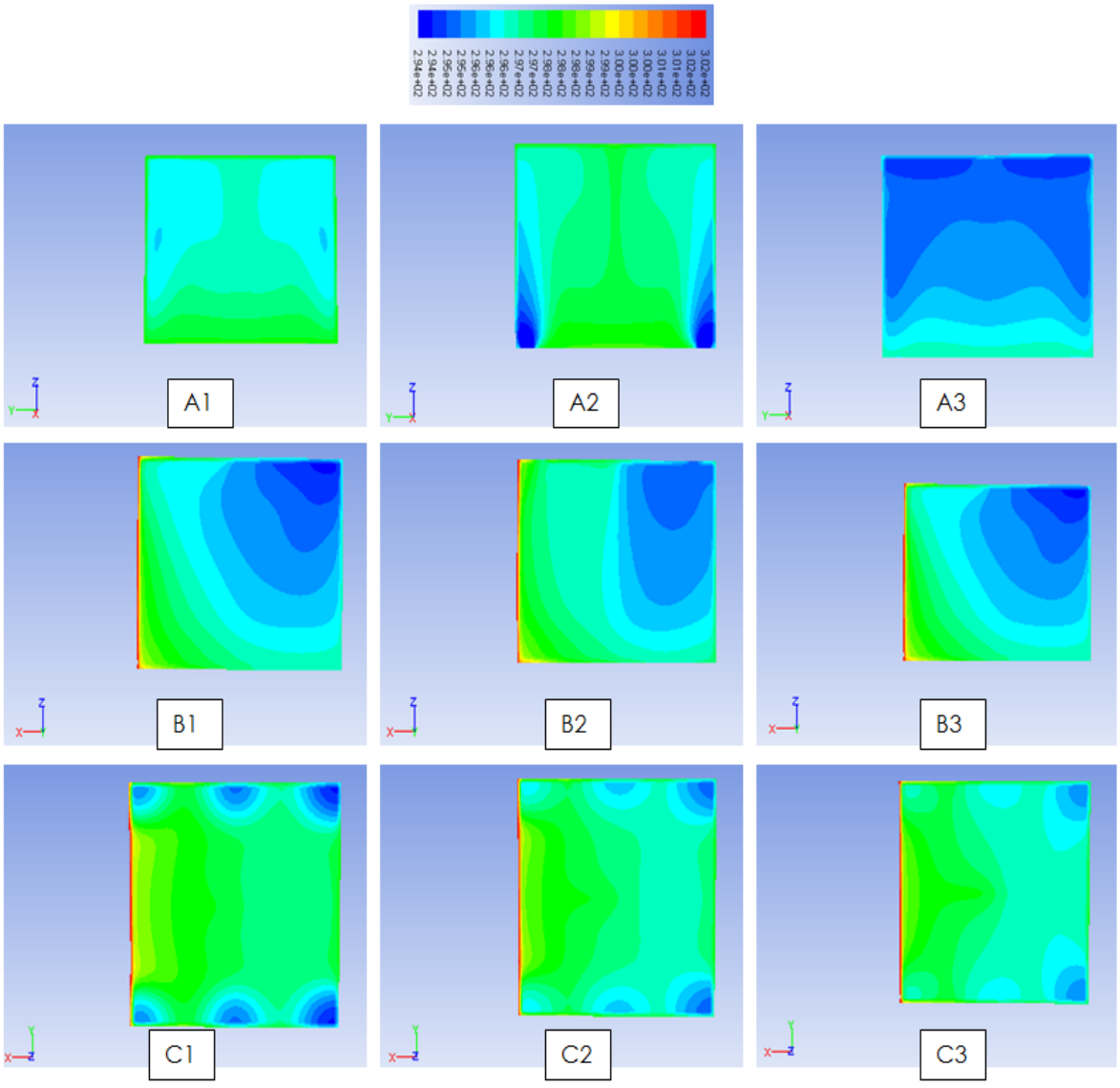

Figure 95: Case 3 - Temperature Contours in Different Planes of Figure 19 at Time T2 = 9:20 AM

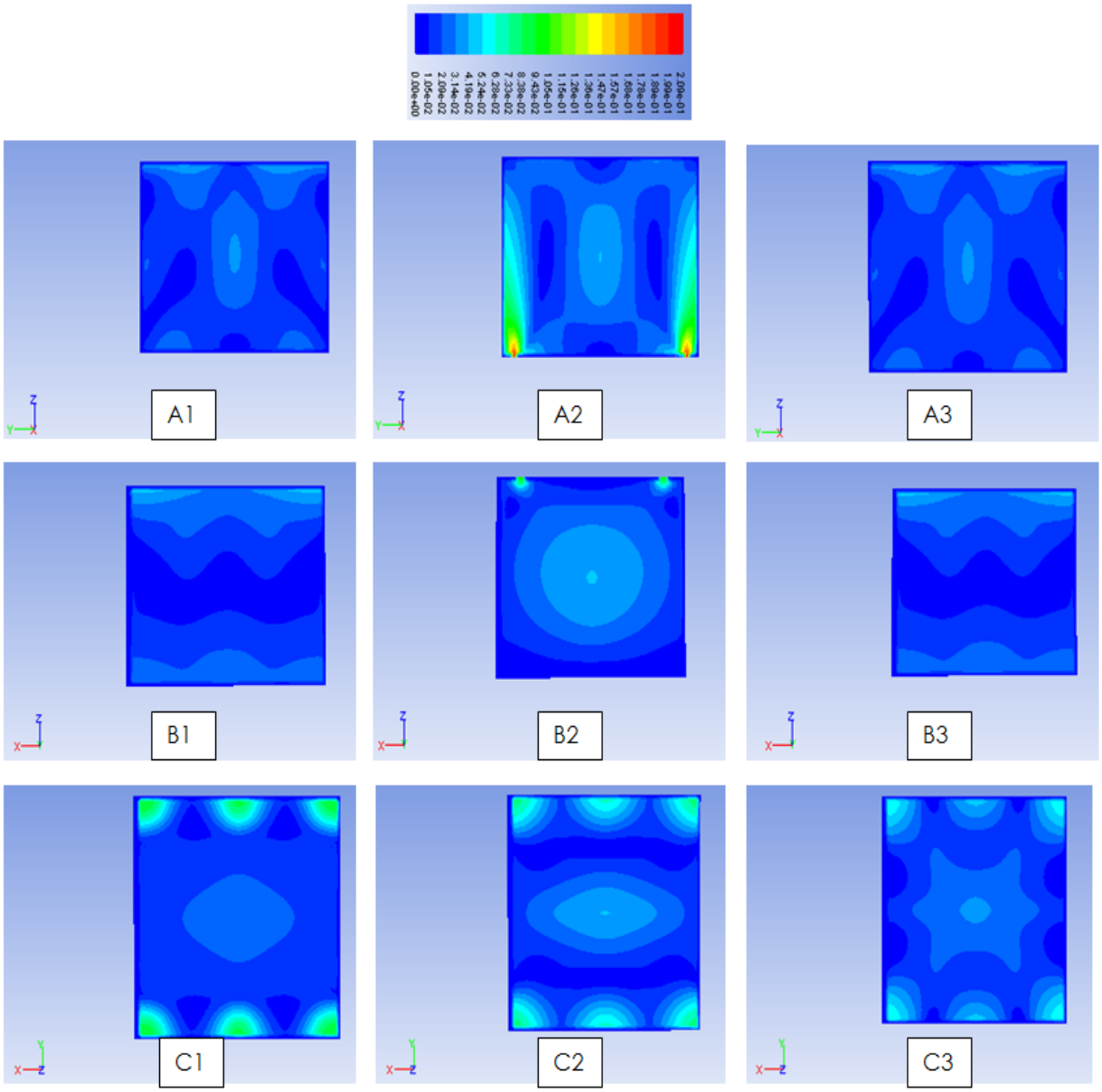

Figure 96: Case 3 - Velocity Contours in Different Planes of Figure 19 at Time T2 = 9:20 AM

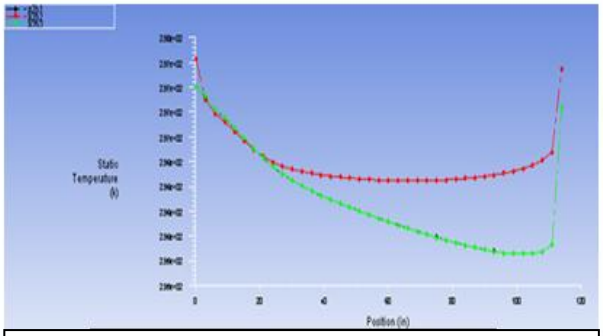

Temperature along z-lines in A2 (y-z) plane at y=3' (Green), y=6'(Red) and y=9'(Black)

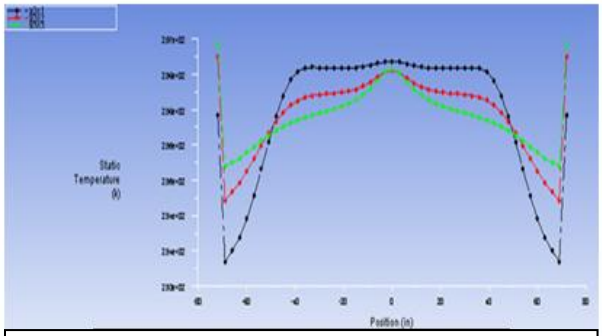

Temperature along y-lines in A2 (y-z) plane at z=2'4.5" (Black), z=4'9"(Red) and z=7'1.5"(Green)

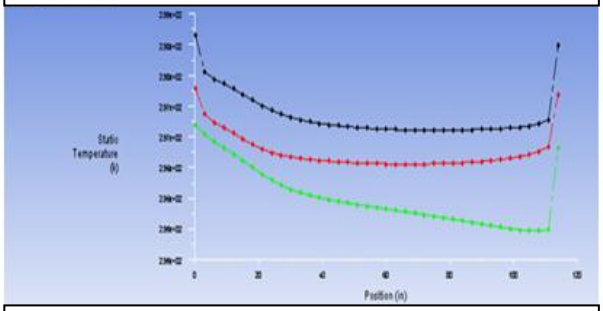

Temperature along z-lines in B2 (x-z) plane at x=3' (Green), x=6'(Red) and x=9'(Black)

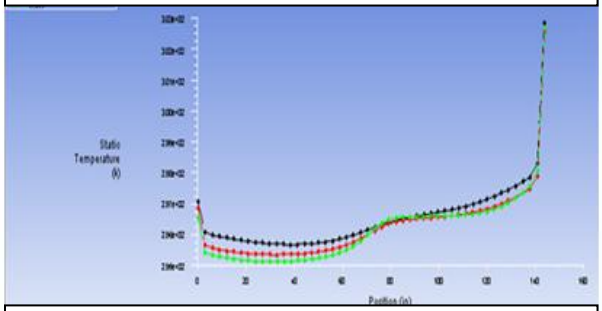

Temperature along x-lines in B2 (x-z) plane at z=2'4.5" (Black), z=4'9"(Red) and z=7'1.5"(Green)

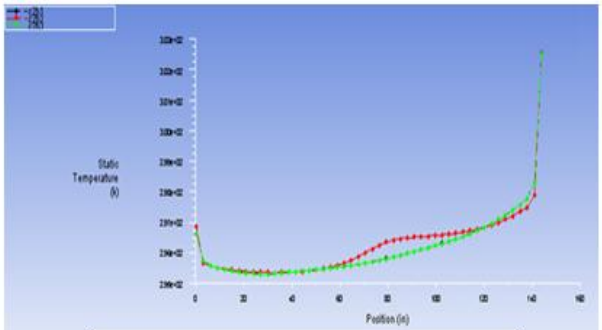

Temperature along x-lines in C2 (x-y) plane at y=3' (Green), y=6'(Red) and y=9'(Black)

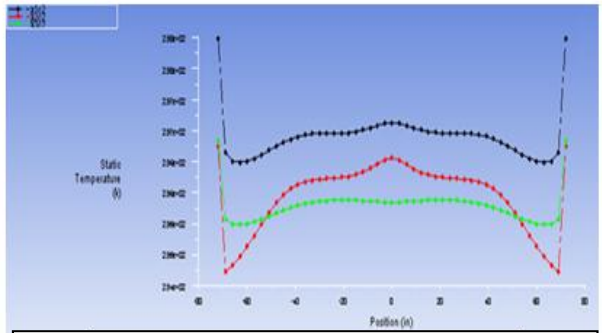

Temperature along y-lines in C2 (x-y) plane at x=3' (Green), x=6'(Red) and x=9'(Black)

Figure 97: Case 3 - Temperature Line Plots at Time T2 = 9:20 AM

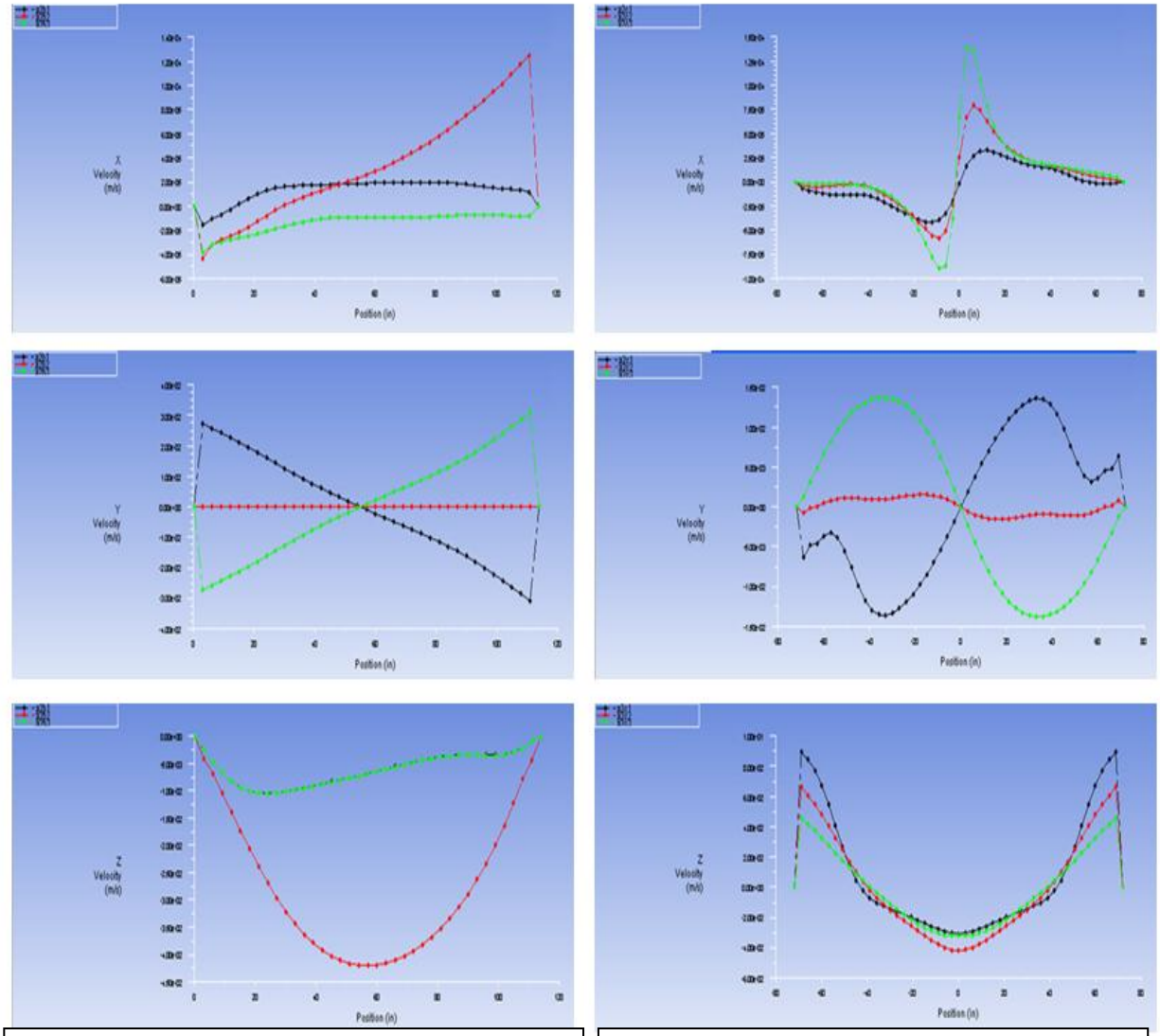

X, Y and Z Velocity Components along z-lines in A2 (y-z) plane at y=3'(Green), y=6'(Red), and y=9'(Black)

X, Y and Z Velocity Components along y-lines in A2 (y-z) plane at z=2'4.5" (Black), z=4'9" (Red), and z=7'1.5" (Green)

Figure 98: Case 3 - Velocity Components in the A2 Plane at Time T2 = 9:20 AM

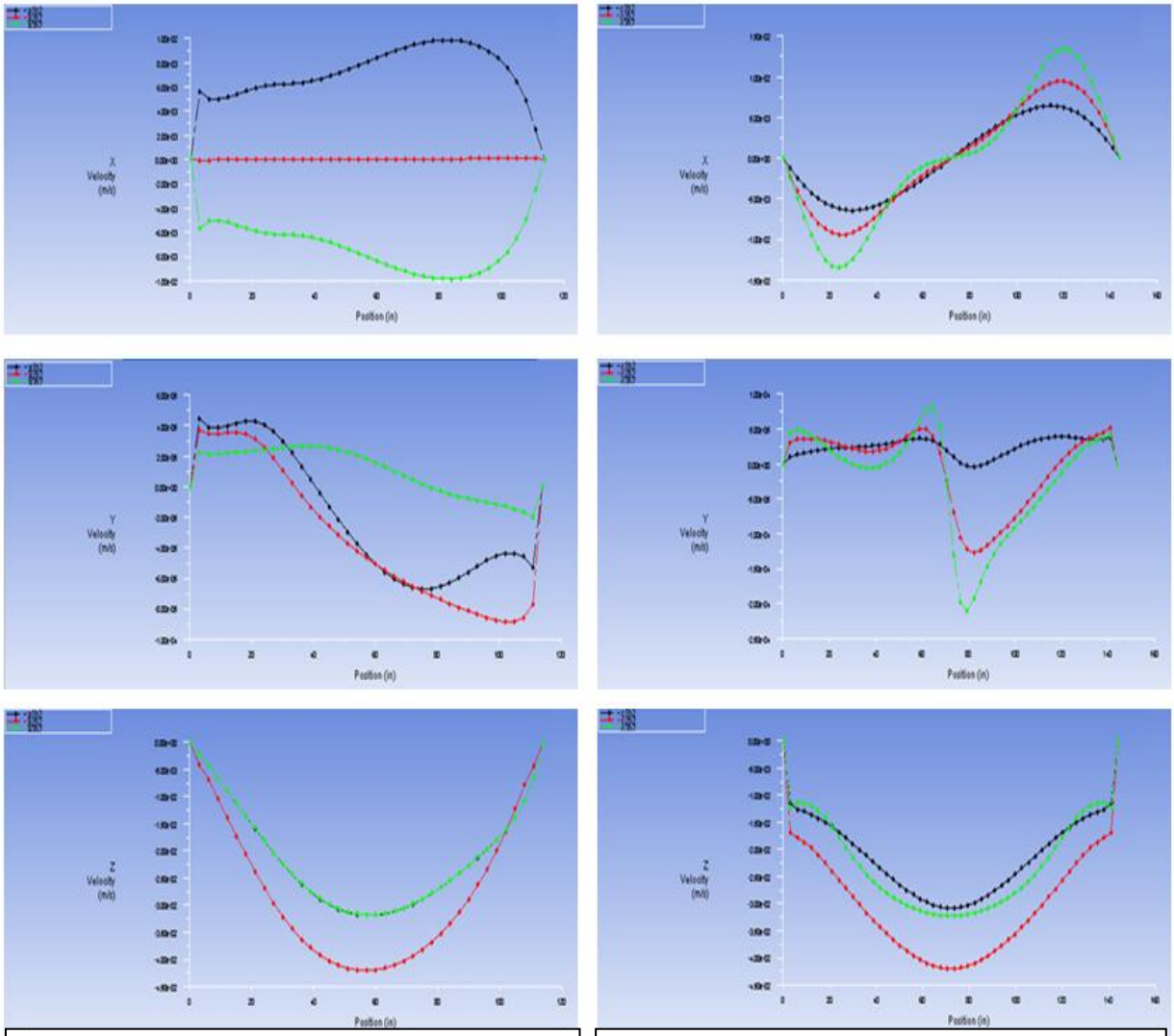

X, Y and Z Velocity Components along z-lines in B2(x-z) plane at x=3'(Green), x=6'(Red), and x=9'(Black)

X, Y and Z Velocity Components along x-lines in B2 (x-z) plane at z=2'4.5" (Black), z=4'9" (Red), and z=7'1.5"(Green)

Figure 99: Case 3 - Velocity Components in the B2 Plane at Time T2 = 9:20 AM

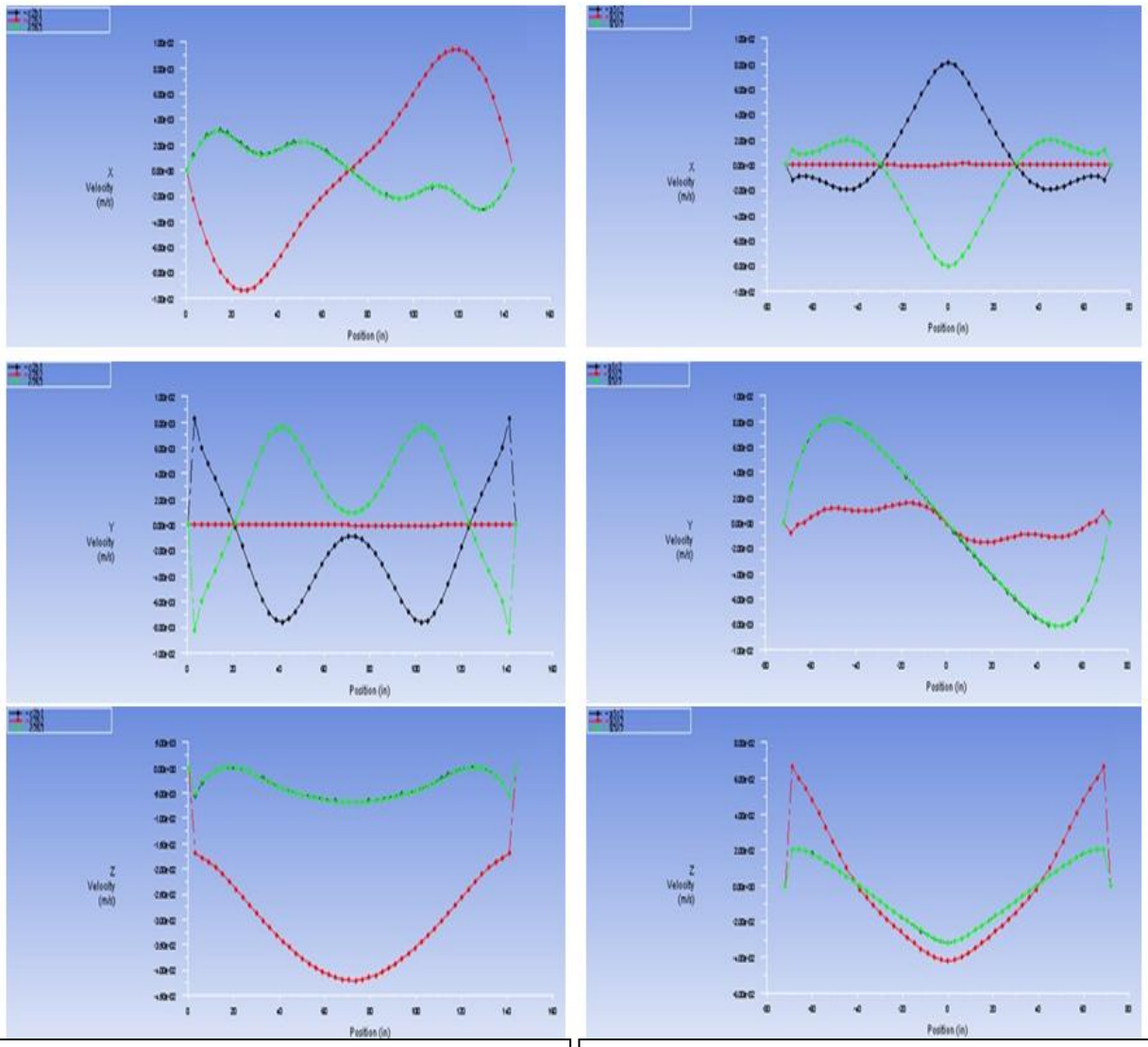

X, Y and Z Velocity Components along x-lines in C2 (x-y) plane at y=3' (Green), y=6' (Red), and y=9' (Black)	X, Y and Z Velocity Components along y-lines in C2 (x-y) plane at x=3' (Green), x=6' (Red), and x=9' (Black)

Figure 100: Case 3 - Velocity Components in the C2 Plane at Time T2 = 9:20 AM

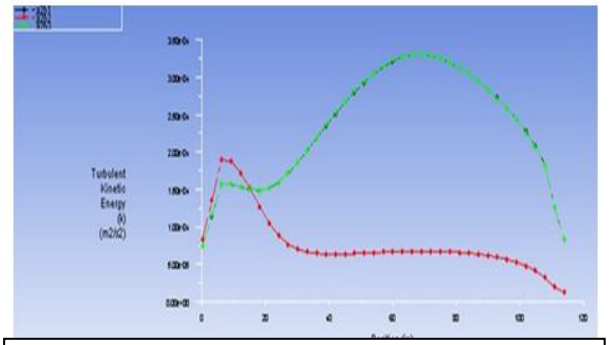

Turbulent Kinetic Energy along z-lines in A2 (y-z) plane at y=3' (Green), y=6'(Red) and y=9'(Black)

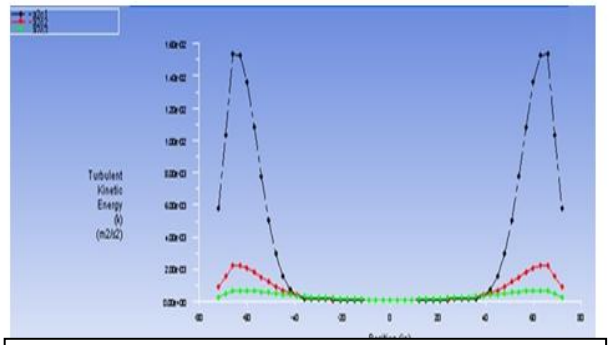

Turbulent Kinetic Energy along y-lines in A2 (y-z) plane at z=2'4.5" (Black), z=4'9"(Red) and z=7'1.5"(Green)

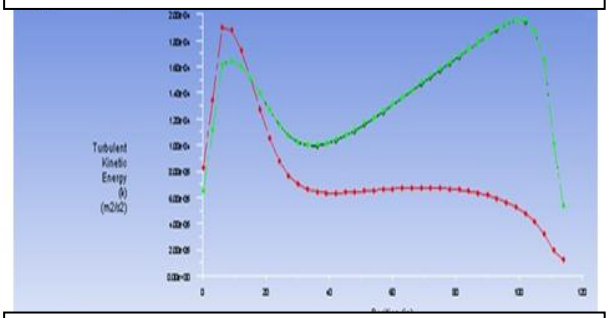

Turbulent Kinetic Energy along z-lines in B2 (x-z) plane at x=3' (Green), x=6'(Red) and x=9'(Black)

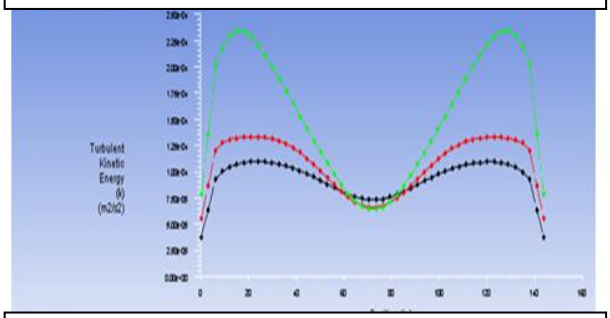

Turbulent Kinetic Energy along x-lines in B2 (x-z) plane at z=2'4.5" (Black), z=4'9"(Red) and z=7'1.5"(Green)

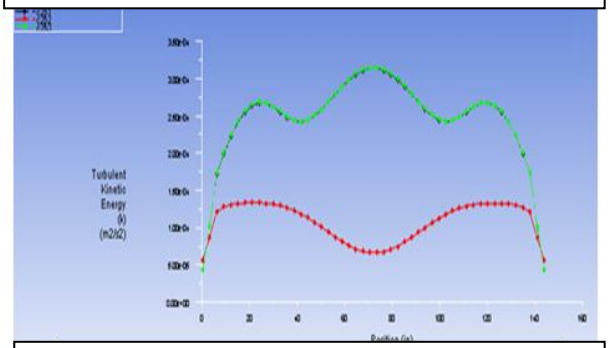

Turbulent Kinetic Energy along x-lines in C2 (x-y) plane at y=3' (Green), y=6'(Red) and y=9'(Black)

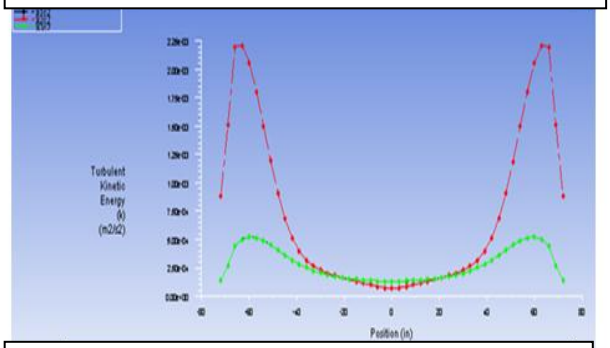

Turbulent Kinetic Energy along y-lines in C2 (x-y) plane at x=3' (Green), x=6'(Red) and x=9'(Black)

Figure 101: Case 3 - Turbulent Kinetic Energy Line Plots at Time T2 = 9:20 AM

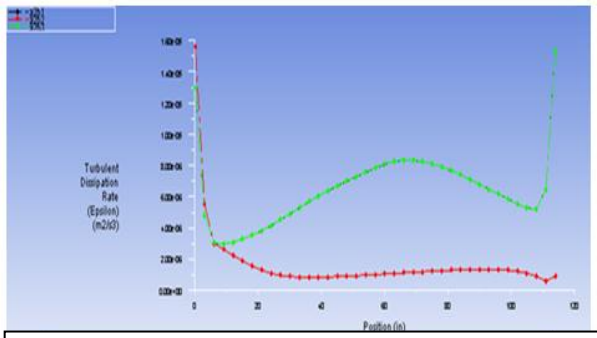

Turbulent Dissipation Rate along z-lines in A2 (y-z) plane at y=3' (Green), y=6'(Red) and y=9'(Black)

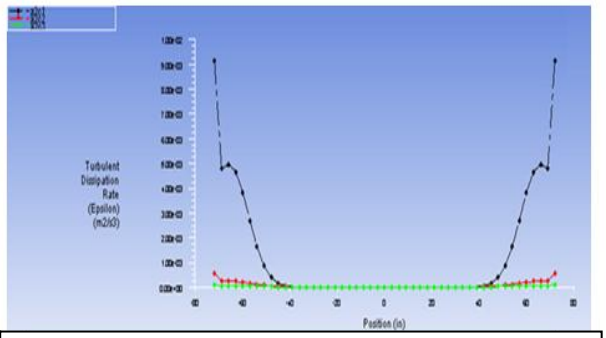

Turbulent Dissipation Rate along y-lines in A2 (y-z) plane at z=2'4.5" (Black), z=4'9"(Red) and z=7'1.5"(Green)

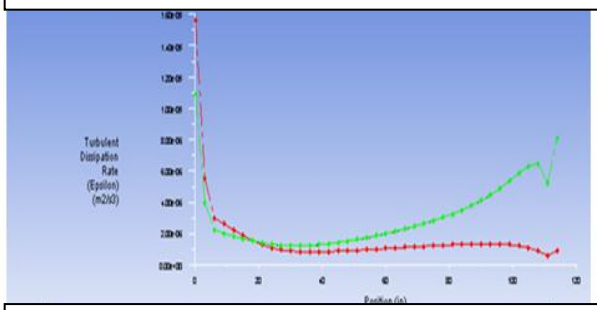

Turbulent Dissipation Rate along z-lines in B2 (x-z) plane at x=3' (Green), x=6'(Red) and x=9'(Black)

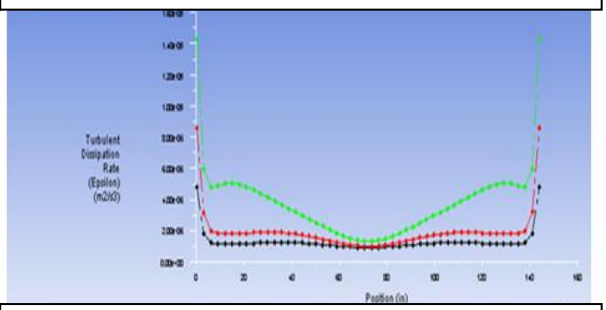

Turbulent Dissipation Rate along x-lines in B2 (x-z) plane at z=2'4.5" (Black), z=4'9"(Red) and z=7'1.5"(Green)

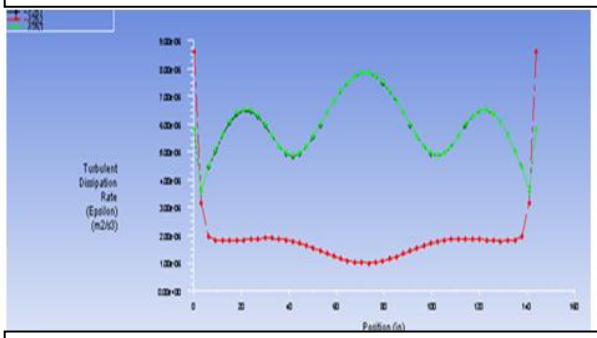

Turbulent Dissipation Rate along x-lines in C2 (x-y) plane at y=3' (Green), y=6'(Red) and y=9'(Black)

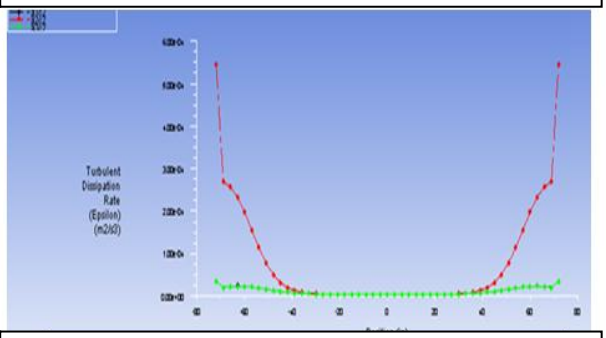

Turbulent Dissipation Rate along y-lines in C2 (x-y) plane at x=3' (Green), x=6'(Red) and x=9'(Black)

Figure 102: Case 3 - Turbulent Dissipation Rate Line Plots at Time T2 = 9:20 AM

Next, we present results at time T3 = 2:53 PM. The key to interpreting the results in the various planes (A1-A3, B1-B3, and C1-C3) and along the various lines in these planes inside the room is the same as described before for Figures 87-94 at time T1=3:45 AM. At T3 = 2:53 PM, the outside temperature is just past its peak as shown in the ASHRAE curve (Figure 7). The temperature in the room is very similar to the temperature distribution at time T2 = 9:20 AM, indicating a relatively stable temperature throughout the day, even with a change in temperature due to the different times of day. Figure 103 shows the temperature contours inside the room in planes (A1-A3, B1-B3, and C1-C3). The temperature in the room is nearly constant, indicating the temperature stability of the system.

Figure 104 shows the velocity magnitude contours in the different planes of the room as described in Figure 19. These contours show increased velocity middle of the room due to the circulation of air caused by the rising warm air. Figure 105 shows the line plots of the temperature distributions inside the room along various lines in planes A1-A3, B1-B3, and C1-C3 shown in Figure 19. These line plots show that the solutions satisfies the adiabatic wall conditions in the room except for the exterior wall where a constant temperature boundary condition is imposed corresponding to the external temperature at time T3.

Figures 106-108 show the line plots of the velocity components in the room. These plots show that the velocity components go to zero at the walls. These line plots are a quantitative description of the contour plots shown in Figure 104. Figure 109 shows the turbulent kinetic energy line plots along the various cross-sectional lines inside the room; they indicate of the relative turbulence intensity in various parts of the room. As expected,

the turbulent intensity is greater in the middle of the room than near the walls. Figure 110 shows line plots of the turbulent dissipation rate (ε) along various cross-sectional lines inside the room. In contrast to previous turbulent dissipation rate plots, the value of epsilon peaks near the walls as well as in the middle of the room.

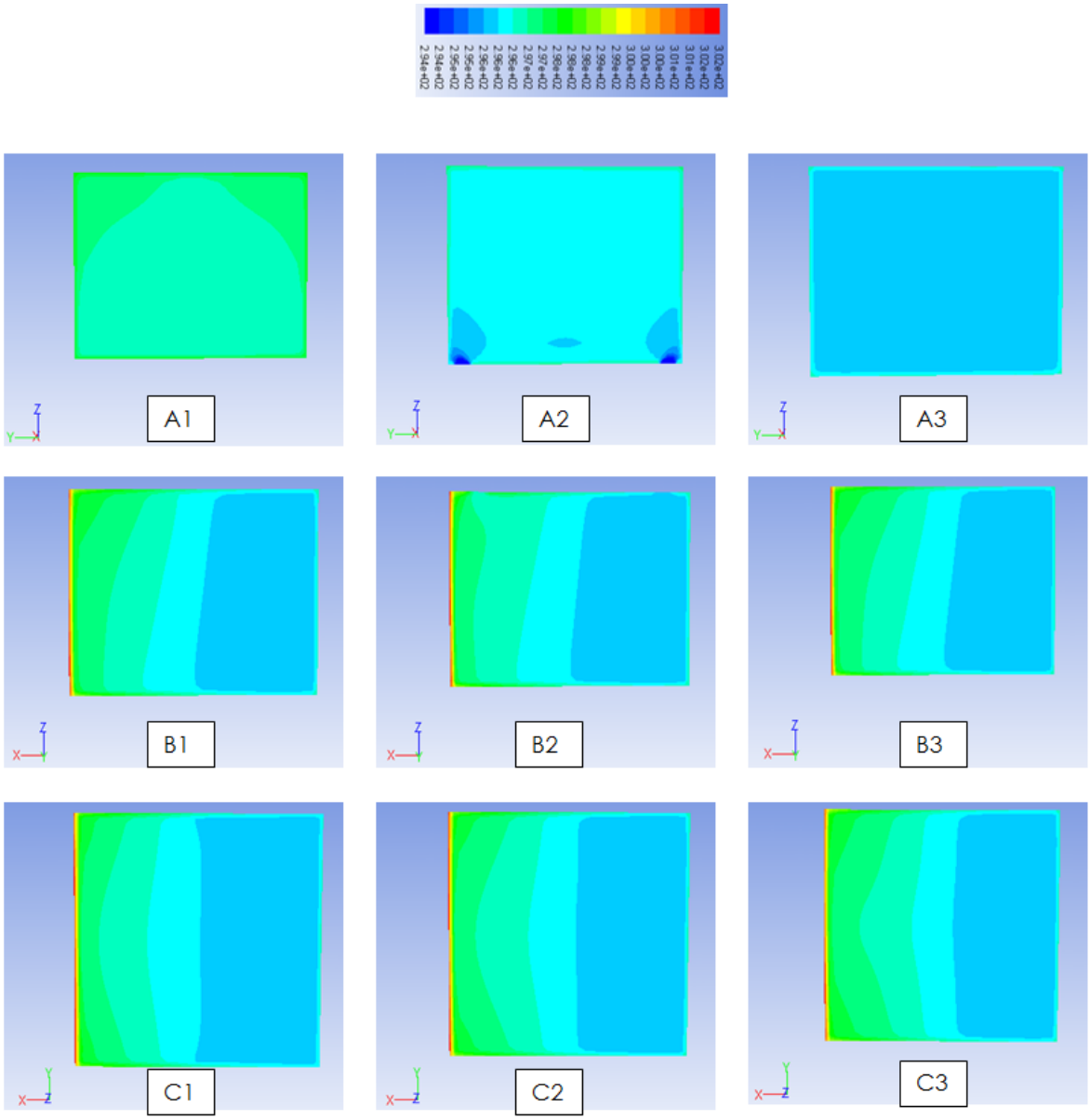

Figure 103: Case 3 - Temperature Contours in Different Planes of Figure 19 at Time T3 = 2:53 PM

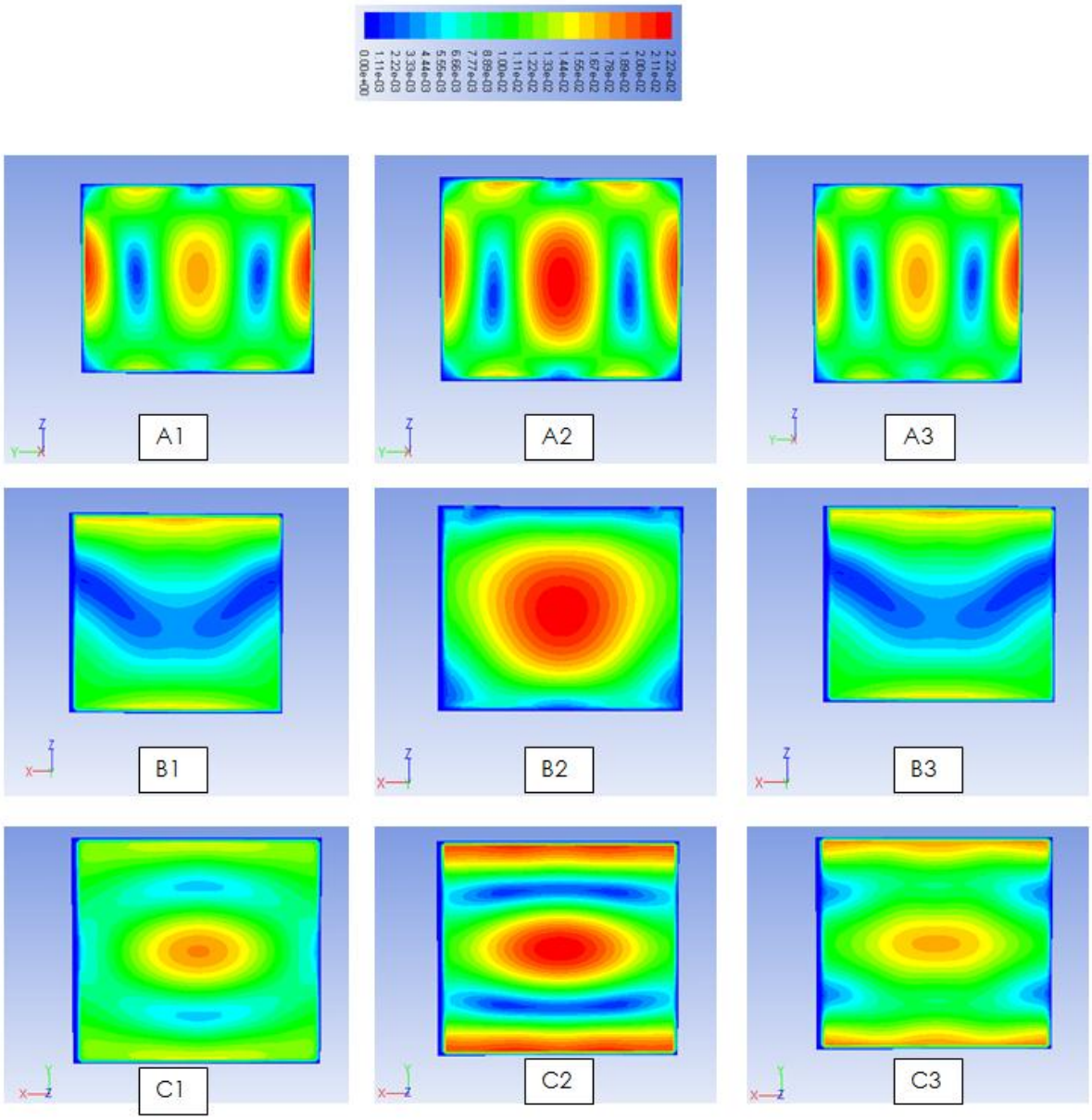

Figure 104: Case 3 - Velocity Contours in Different Planes of Figure 19 at Time T3 = 2:53 PM

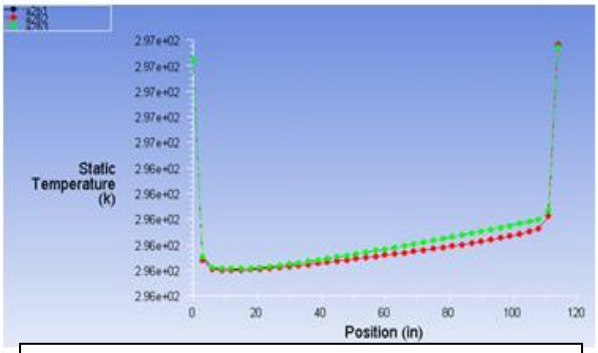

Temperature along z-lines in A2 (y-z) plane at y=3' (Green), y=6'(Red) and y=9'(Black)

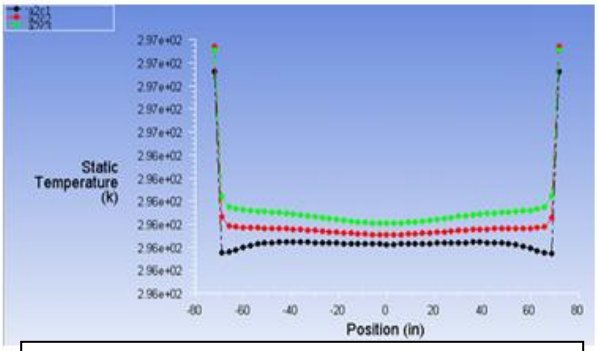

Temperature along y-lines in A2 (y-z) plane at z=2'4.5" (Black), z=4'9"(Red) and z=7'1.5"(Green)

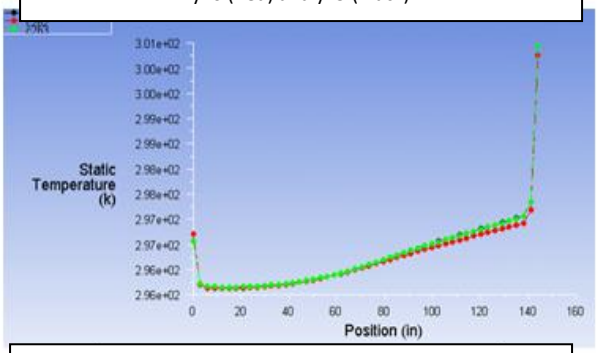

Temperature along z-lines in B2 (x-z) plane at x=3' (Green), x=6'(Red) and x=9'(Black)

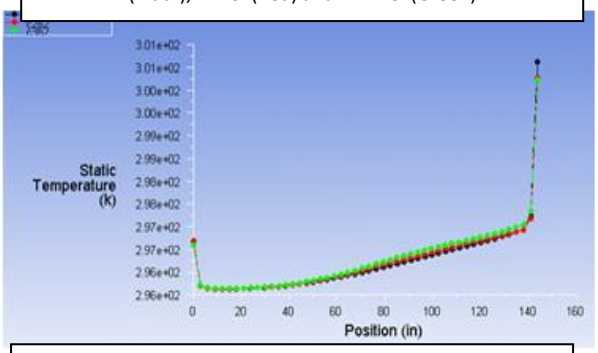

Temperature along x-lines in B2 (x-z) plane at z=2'4.5" (Black), z=4'9"(Red) and z=7'1.5"(Green)

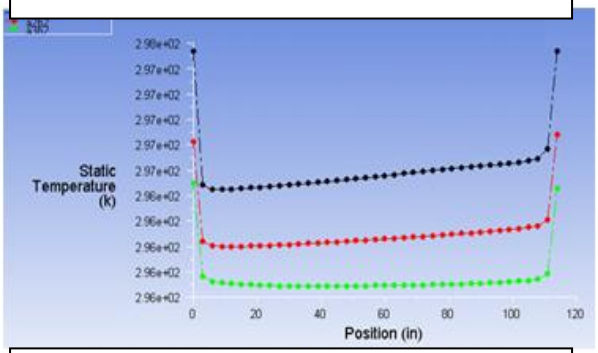

Temperature along x-lines in C2 (x-y) plane at y=3' (Green), y=6'(Red) and y=9'(Black)

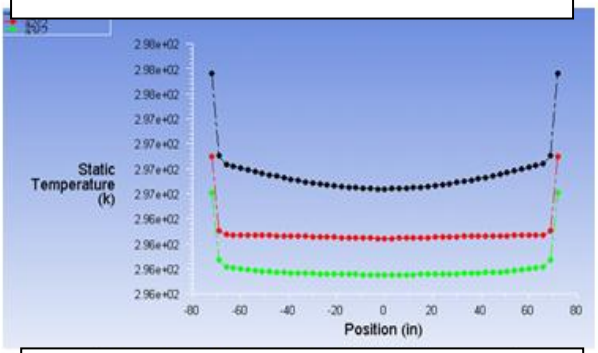

Temperature along y-lines in C2 (x-y) plane at x=3' (Green), x=6'(Red) and x=9'(Black)

Figure 105: Case 3 - Temperature Line Plots at Time T3 = 2:53 PM

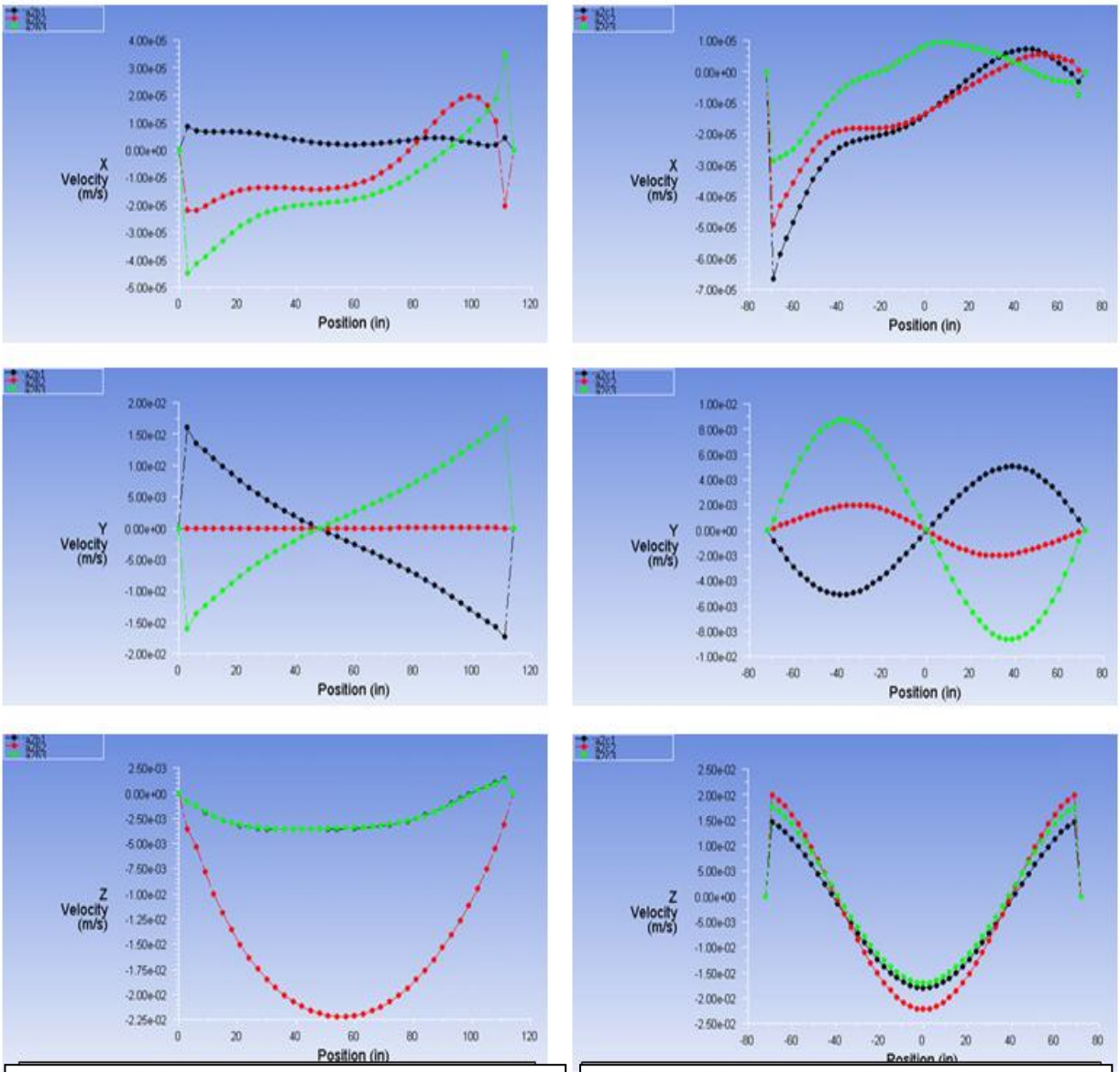

X, Y and Z Velocity Components along z-lines in A2 (y-z) plane at y=3'(Green), y=6'(Red), and y=9'(Black)

X, Y and Z Velocity Components along y-lines in A2 (y-z) plane at z=2'4.5" (Black), z=4'9" (Red), and z=7'1.5" (Green)

Figure 106: Case 3 - Velocity Components in the A2 Plane at Time T3 = 2:53 PM

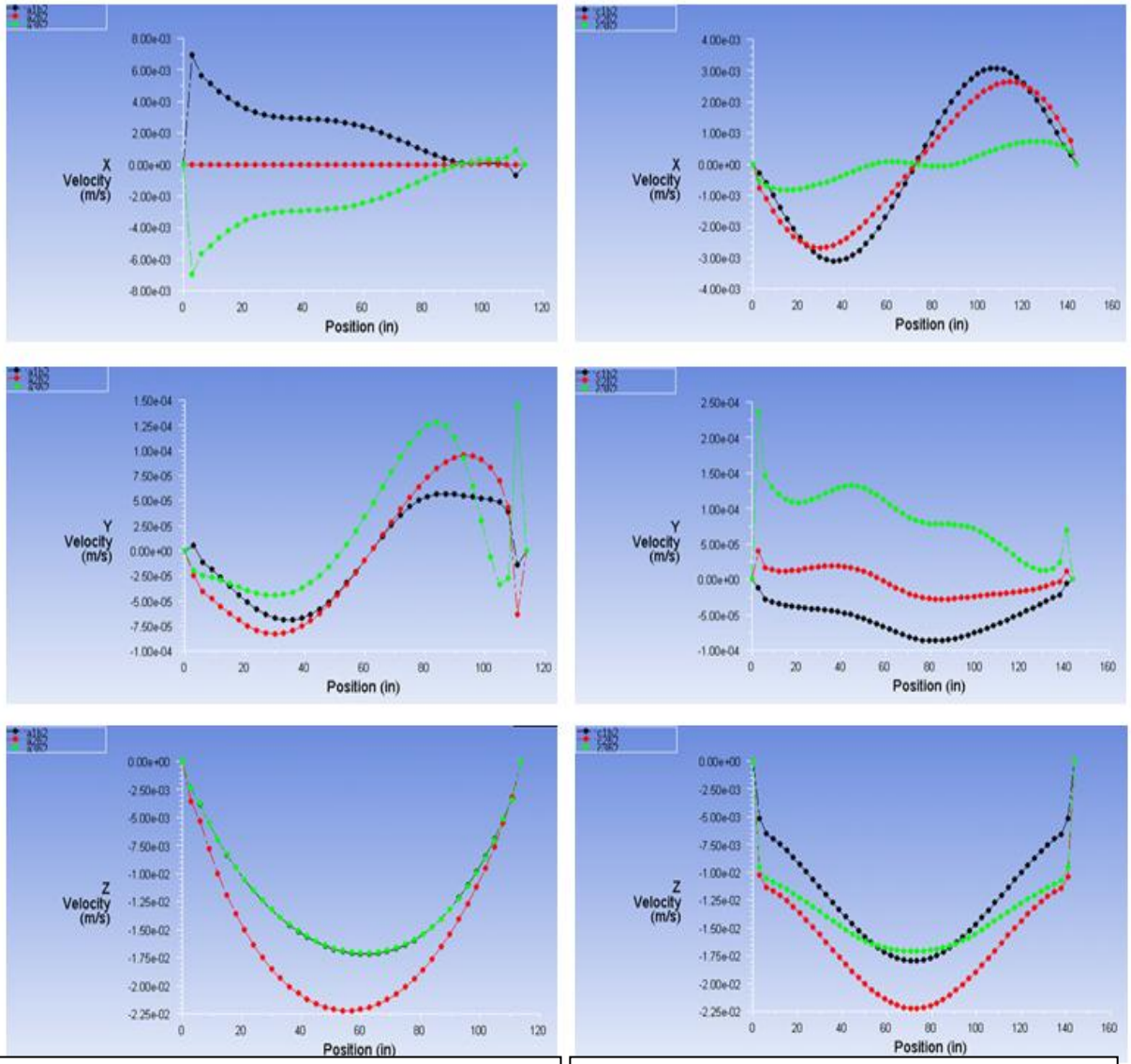

X, Y and Z Velocity Components along z-lines in B2(x-z) plane at x=3'(Green), x=6'(Red), and x=9'(Black)	X, Y and Z Velocity Components along x-lines in B2 (x-z) plane at z=2'4.5" (Black), z=4'9" (Red), and z=7'1.5"(Green)

Figure 107: Case 3 - Velocity Components in the B2 Plane at Time T3 = 2:53 PM

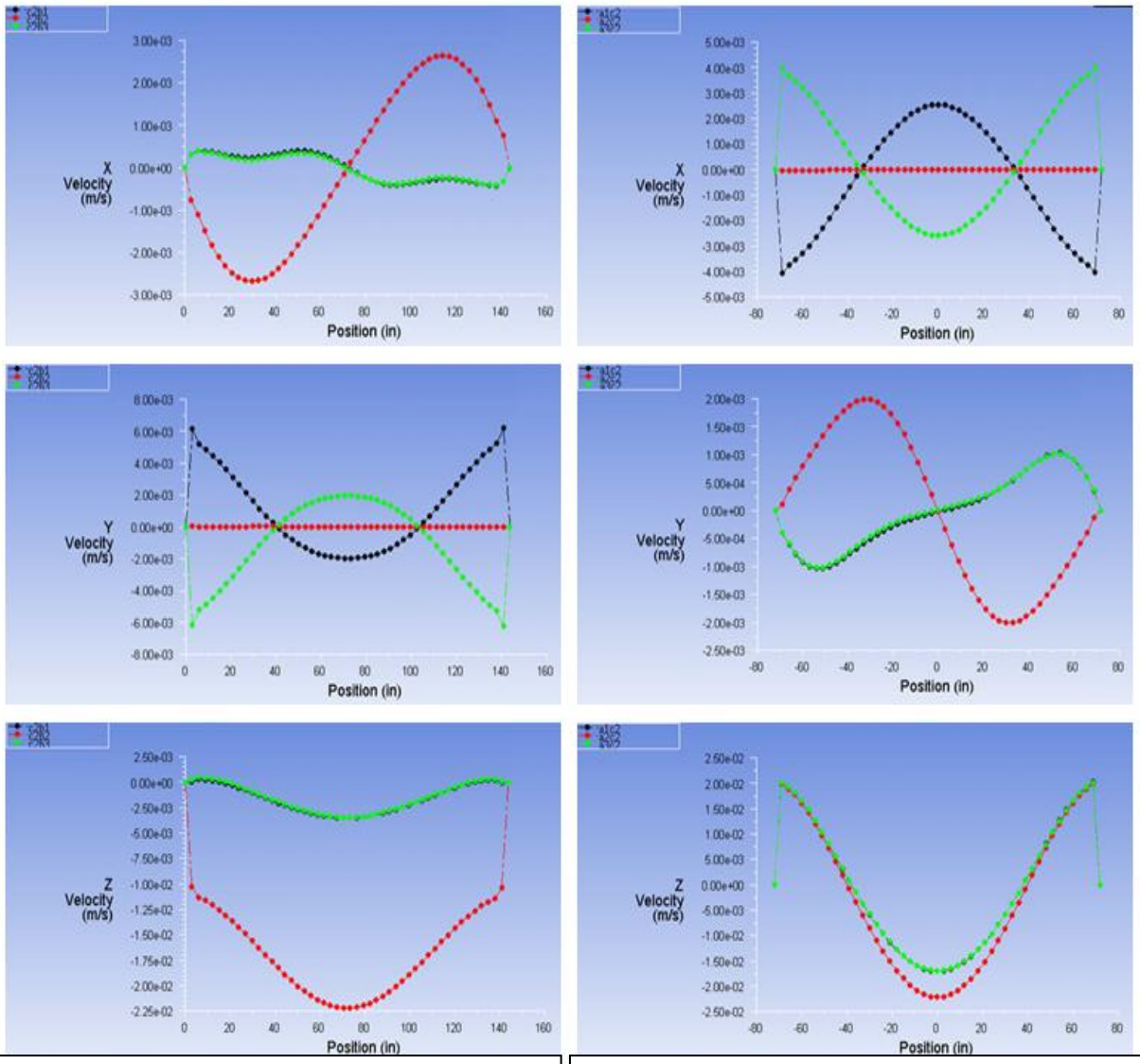

X, Y and Z Velocity Components along x-lines in C2 (x-y) plane at y=3' (Green), y=6' (Red), and y=9' (Black)	X, Y and Z Velocity Components along y-lines in C2 (x-y) plane at x=3' (Green), x=6' (Red), and x=9' (Black)

Figure 108: Case 3 - Velocity Components in the C2 Plane at Time T3 = 2:53 PM

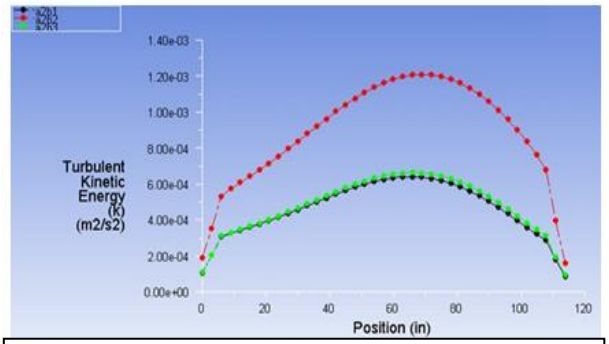

Turbulent Kinetic Energy along z-lines in A2 (y-z) plane at y=3' (Green), y=6'(Red) and y=9'(Black)

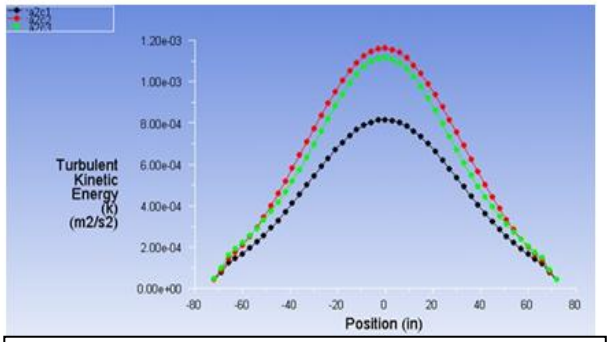

Turbulent Kinetic Energy along y-lines in A2 (y-z) plane at z=2'4.5" (Black), z=4'9"(Red) and z=7'1.5"(Green)

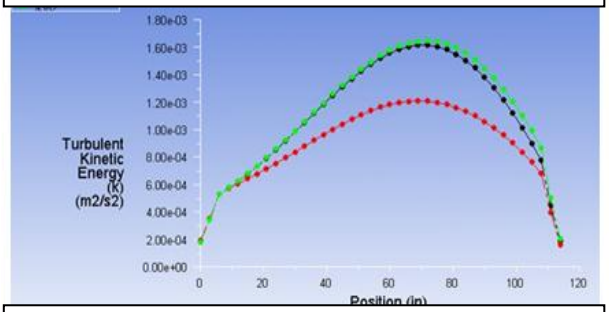

Turbulent Kinetic Energy along z-lines in B2 (x-z) plane at x=3' (Green), x=6'(Red) and x=9'(Black)

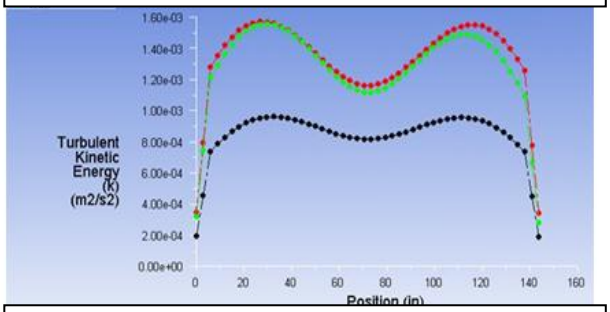

Turbulent Kinetic Energy along x-lines in B2 (x-z) plane at z=2'4.5" (Black), z=4'9"(Red) and z=7'1.5"(Green)

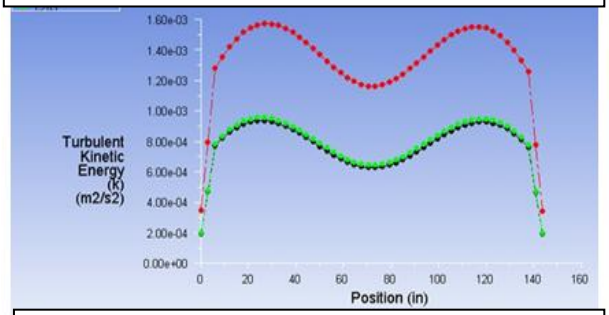

Turbulent Kinetic Energy along x-lines in C2 (x-y) plane at y=3' (Green), y=6'(Red) and y=9'(Black)

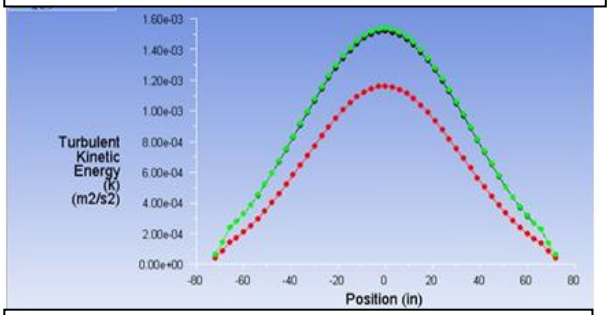

Turbulent Kinetic Energy along y-lines in C2 (x-y) plane at x=3' (Green), x=6'(Red) and x=9'(Black)

Figure 109: Case 3 - Turbulent Kinetic Energy Line Plots at Time T3 = 2:53 PM

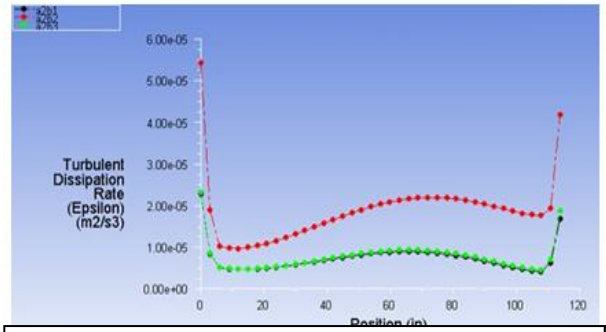

Turbulent Dissipation Rate along z-lines in A2 (y-z) plane at y=3' (Green), y=6'(Red) and y=9'(Black)

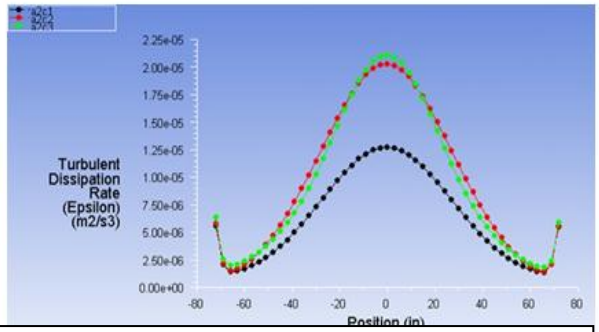

Turbulent Dissipation Rate along y-lines in A2 (y-z) plane at z=2'4.5" (Black), z=4'9"(Red) and z=7'1.5"(Green)

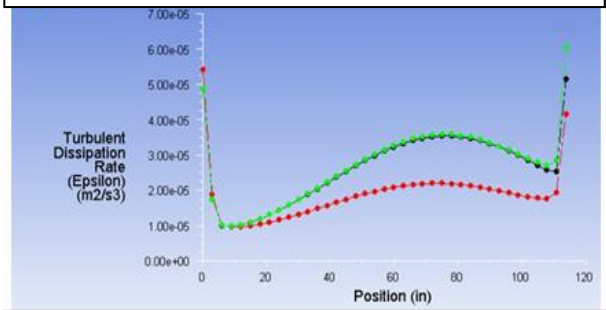

Turbulent Dissipation Rate along z-lines in B2 (x-z) plane at x=3' (Green), x=6'(Red) and x=9'(Black)

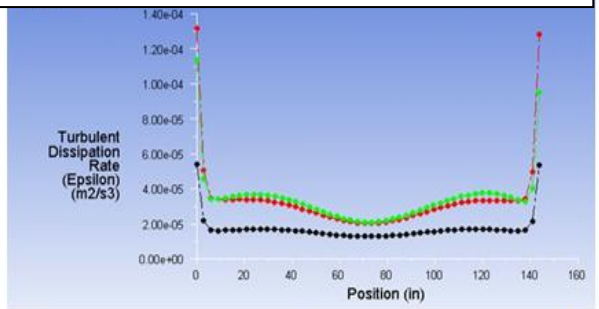

Turbulent Dissipation Rate along x-lines in B2 (x-z) plane at z=2'4.5" (Black), z=4'9"(Red) and z=7'1.5"(Green)

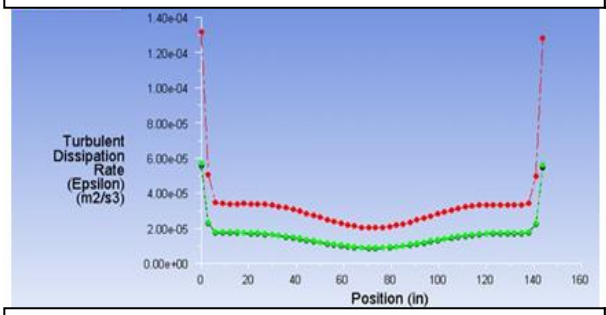

Turbulent Dissipation Rate along x-lines in C2 (x-y) plane at y=3' (Green), y=6'(Red) and y=9'(Black)

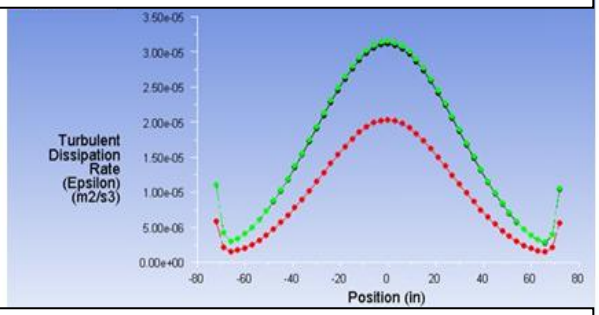

Turbulent Dissipation Rate along y-lines in C2 (x-y) plane at x=3' (Green), x=6'(Red) and x=9'(Black)

Figure 110: Case 3 - Turbulent Dissipation Rate Line Plots at Time T3 = 2:53 PM

The final data set for Case 3 is obtained at T4 = 8:27 PM. This time corresponds to another low temperature inside the room shown by the ASHRAE curve (Figure 7). Figure 111 shows the contours of temperature distributions in the different planes (A1-A3, B1-B3, and C1-C3). The lack of heat from the hot external wall results in a nearly constant room temperature. Figure 112 shows the velocity contours in different planes of the room described in Figure 19. These velocities are all very low because the low constant temperature doesn't require much cooling from the ventilation system. Figure 113 shows the various line plots of temperature distribution inside the room along various lines in planes A1-A3, B1-B3, and C1-C3 shown in Figure 19. These plots show that the solution satisfies the adiabatic wall conditions in the room except for the exterior wall where a constant temperature boundary condition is imposed corresponding to the external temperature at time T4 = 8:27 PM. These line plots are a quantitative representation of Figure 111.

Figures 114-116 show various velocity components inside the room. These line plots show that the no slip condition is correctly imposed at the walls; all the velocity components go to zero near the walls. Figure 117 shows the turbulent kinetic energy line plots along various cross-sectional lines inside the room, they indicate the relative turbulence intensity in various parts of the room. The values of k are very small because of the very low flow velocities. As expected, the turbulent intensity is greater in the middle of the room than near the walls. Figure 118 shows line plots of the turbulent dissipation rate along various cross-sectional lines inside the room. In contrast to k, the value of epsilon peak near the walls because of the large dissipation of turbulence there. The value of epsilon is fairly constant across the room in all directions except near the wall.

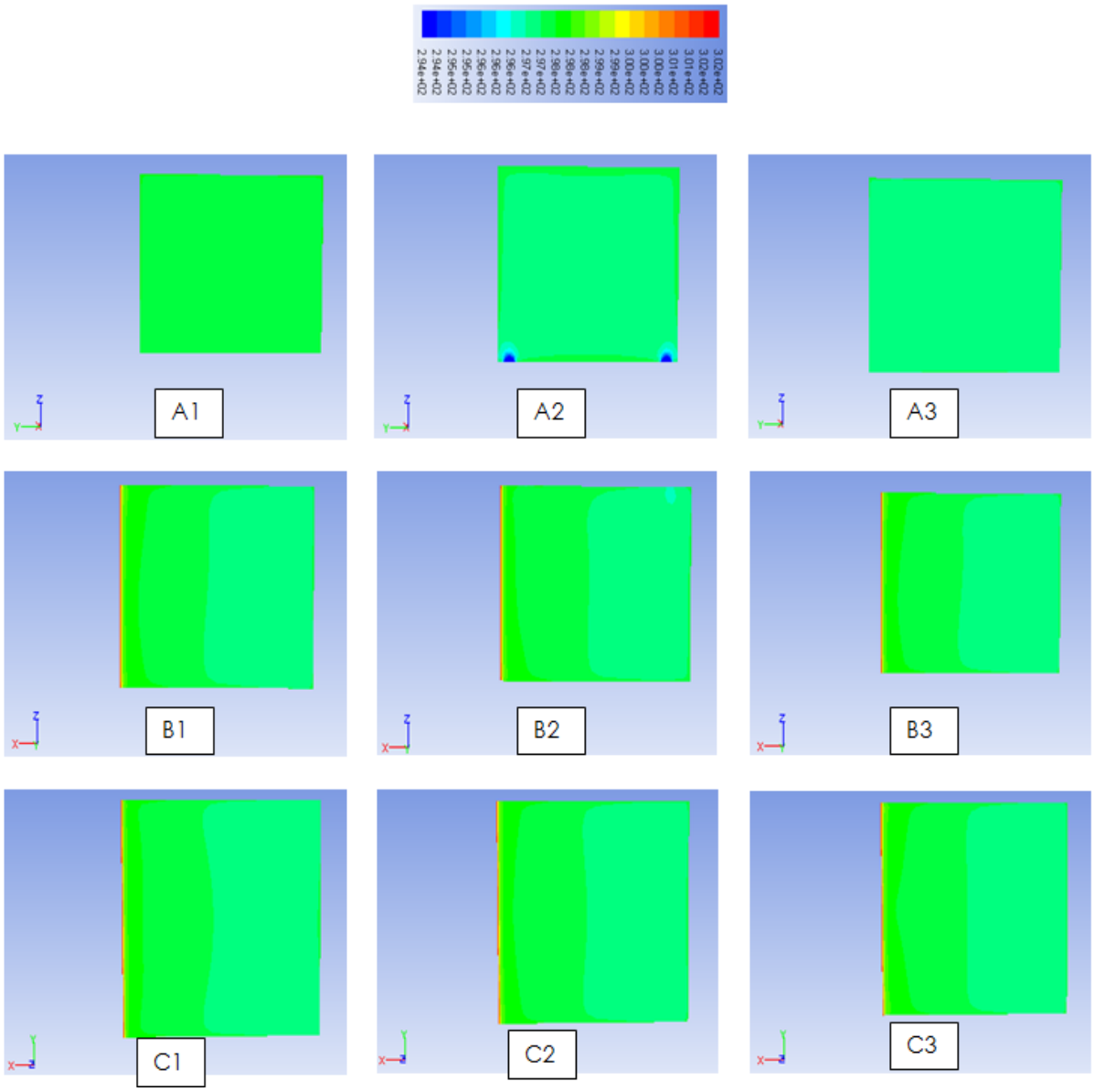

Figure 111: Case 3 - Temperature Contours in Different Planes of Figure 19 at Time T4 = 8:27 PM

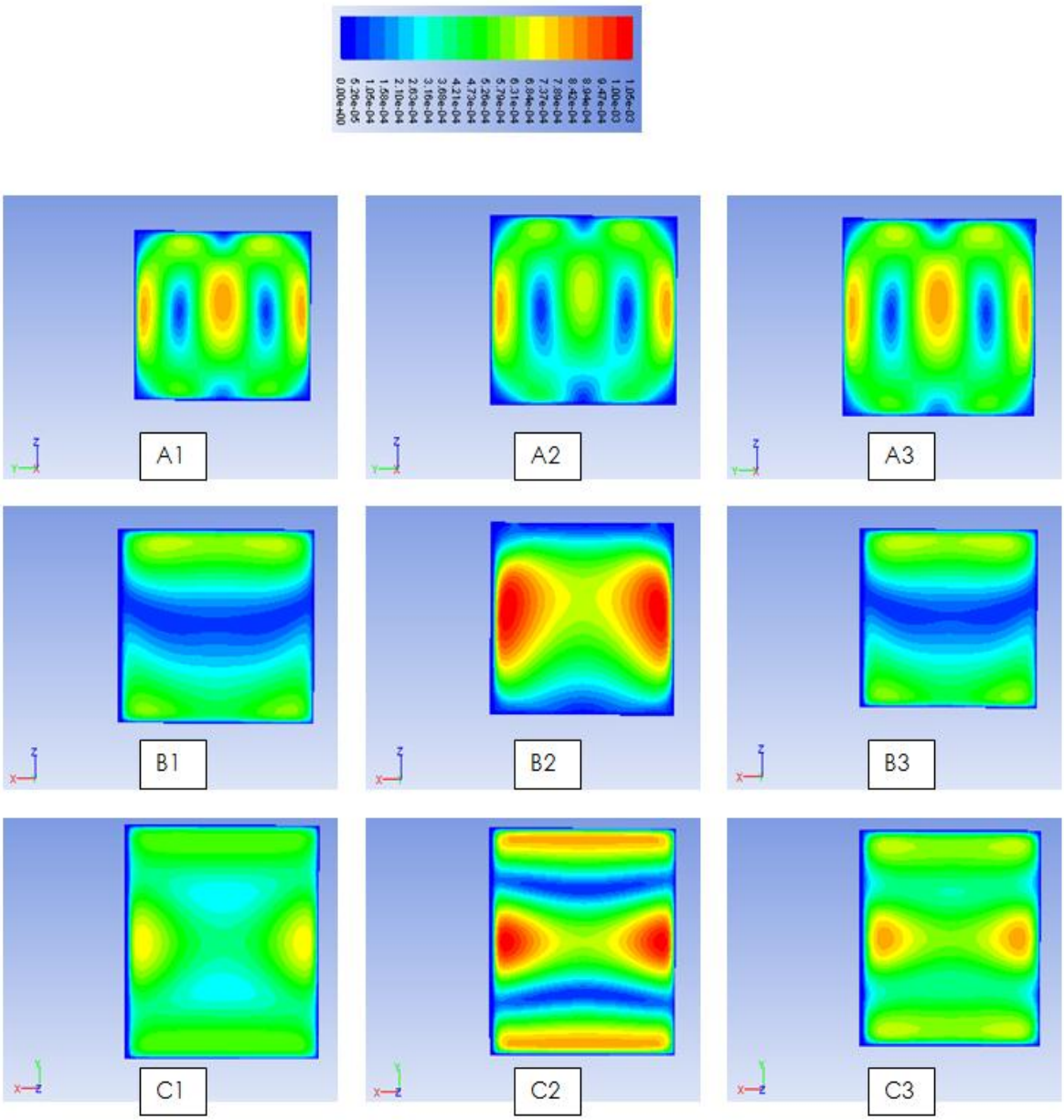

Figure 112: Case 3 - Velocity Contours in Different Planes of Figure 19 at Time T4 = 8:27 PM

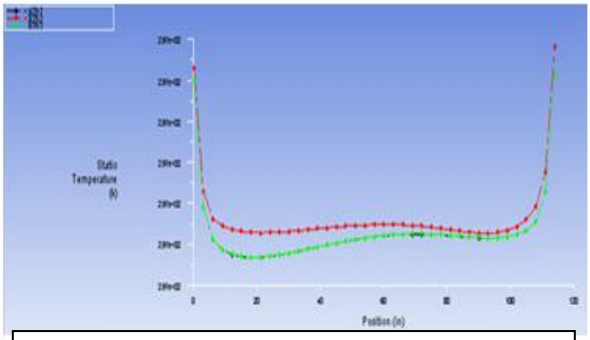

Temperature along z-lines in A2 (y-z) plane at y=3' (Green), y=6'(Red) and y=9'(Black)

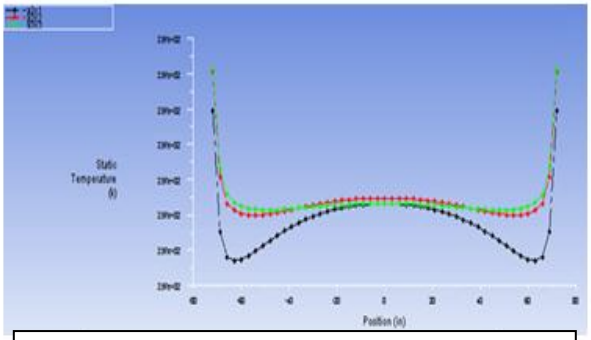

Temperature along y-lines in A2 (y-z) plane at z=2'4.5" (Black), z=4'9"(Red) and z=7'1.5"(Green)

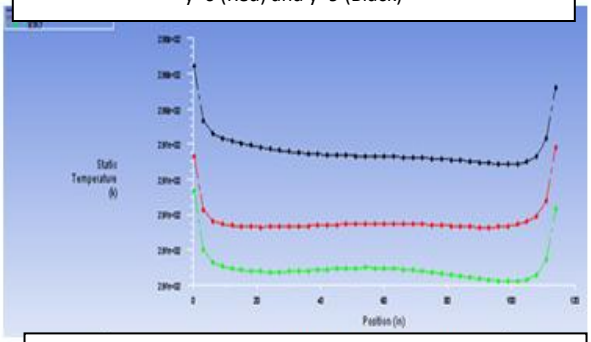

Temperature along z-lines in B2 (x-z) plane at x=3' (Green), x=6'(Red) and x=9'(Black)

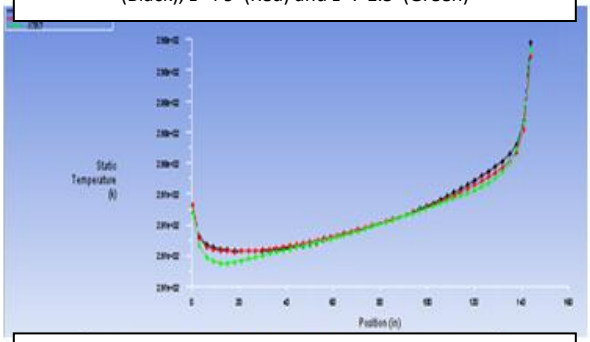

Temperature along x-lines in B2 (x-z) plane at z=2'4.5" (Black), z=4'9"(Red) and z=7'1.5"(Green)

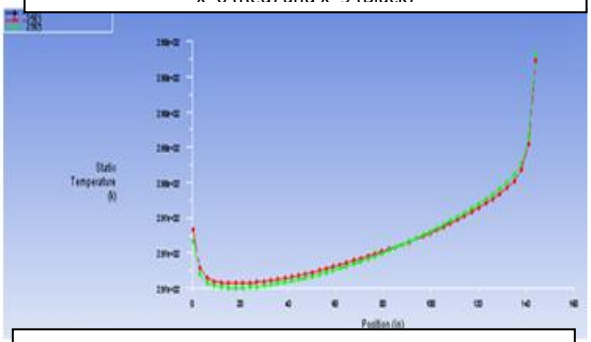

Temperature along x-lines in C2 (x-y) plane at y=3' (Green), y=6'(Red) and y=9'(Black)

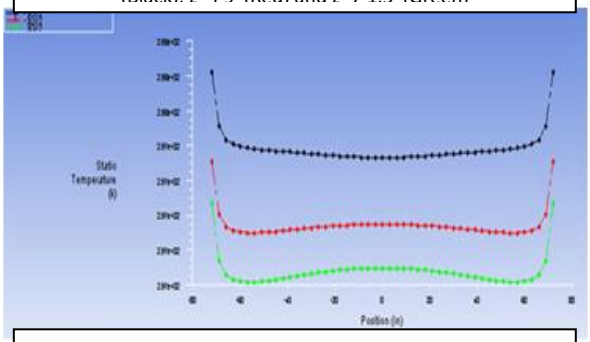

Temperature along y-lines in C2 (x-y) plane at x=3' (Green), x=6'(Red) and x=9'(Black)

Figure 113: Case 3 - Temperature Line Plots at Time T4 = 8:27 PM

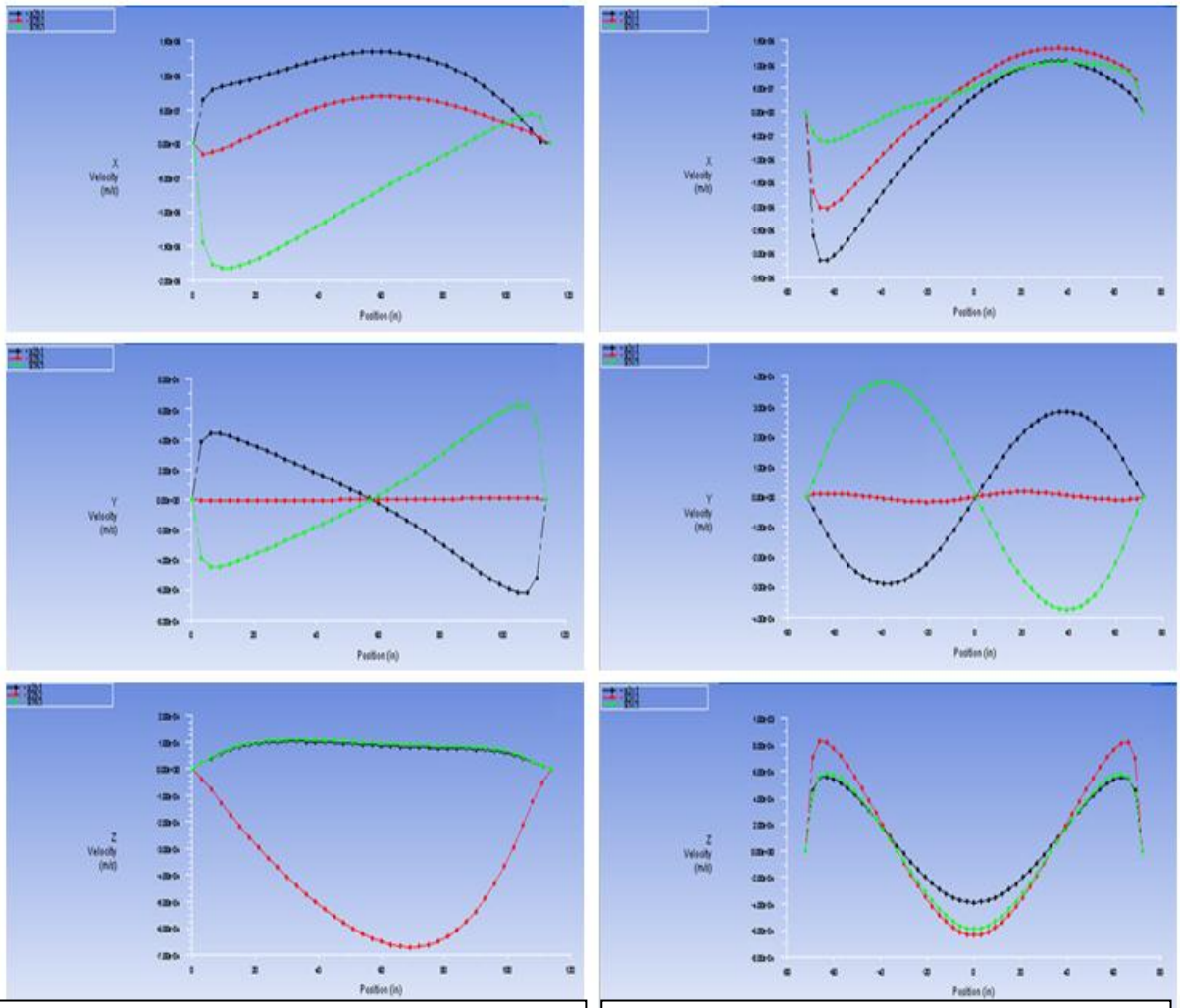

X, Y and Z Velocity Components along z-lines in A2 (y-z) plane at y=3'(Green), y=6'(Red), and y=9'(Black)

X, Y and Z Velocity Components along y-lines in A2 (y-z) plane at z=2'4.5" (Black), z=4'9" (Red), and z=7'1.5" (Green)

Figure 114: Case 3 - Velocity Components in the A2 Plane at Time T4 = 8:27 PM

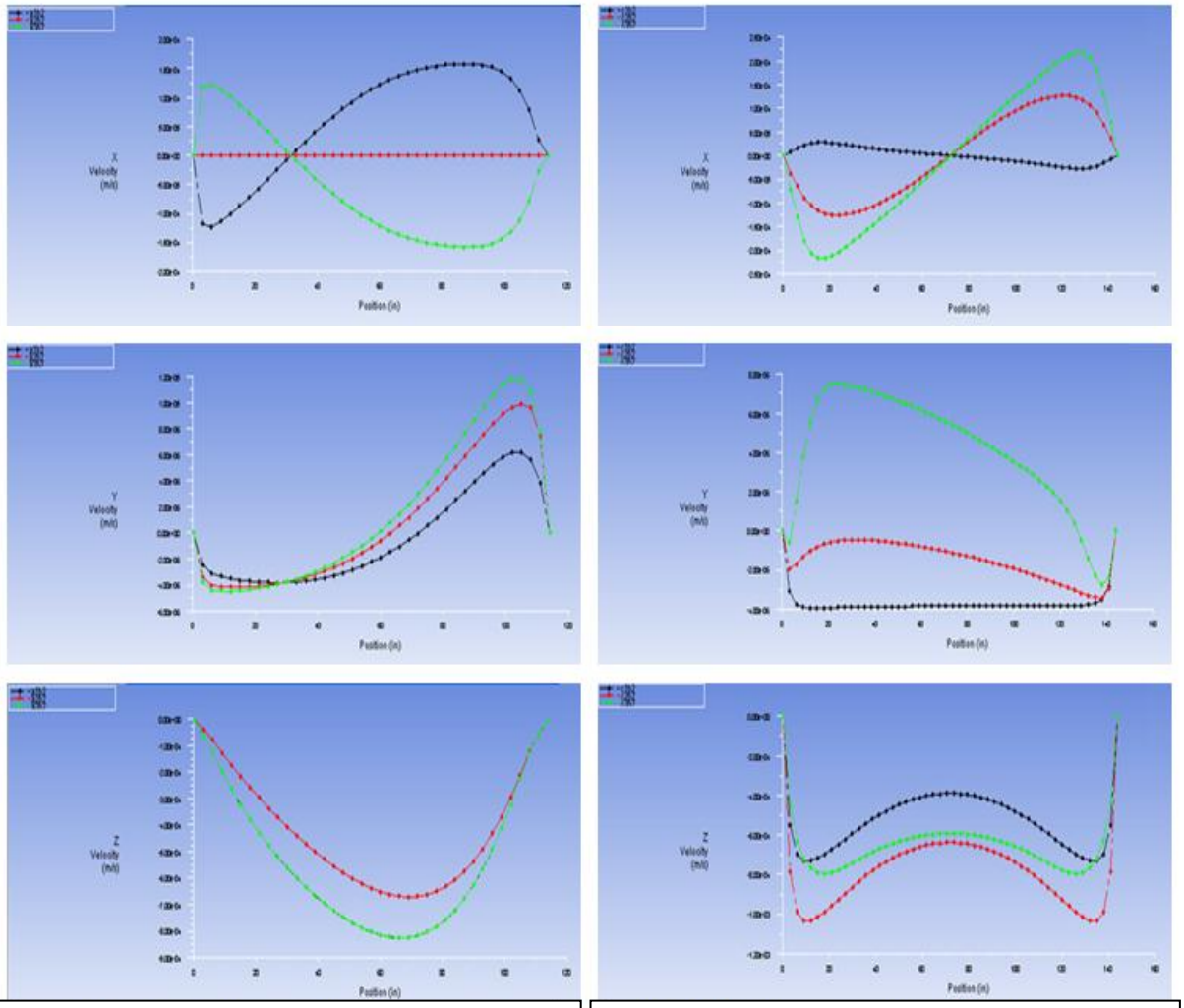

X, Y and Z Velocity Components along z-lines in B2(x-z) plane at x=3'(Green), x=6'(Red), and x=9'(Black)	X, Y and Z Velocity Components along x-lines in B2 (x-z) plane at z=2'4.5" (Black), z=4'9" (Red), and z=7'1.5"(Green)

Figure 115: Case 3 - Velocity Components in the B2 Plane at Time T4 = 8:27 PM

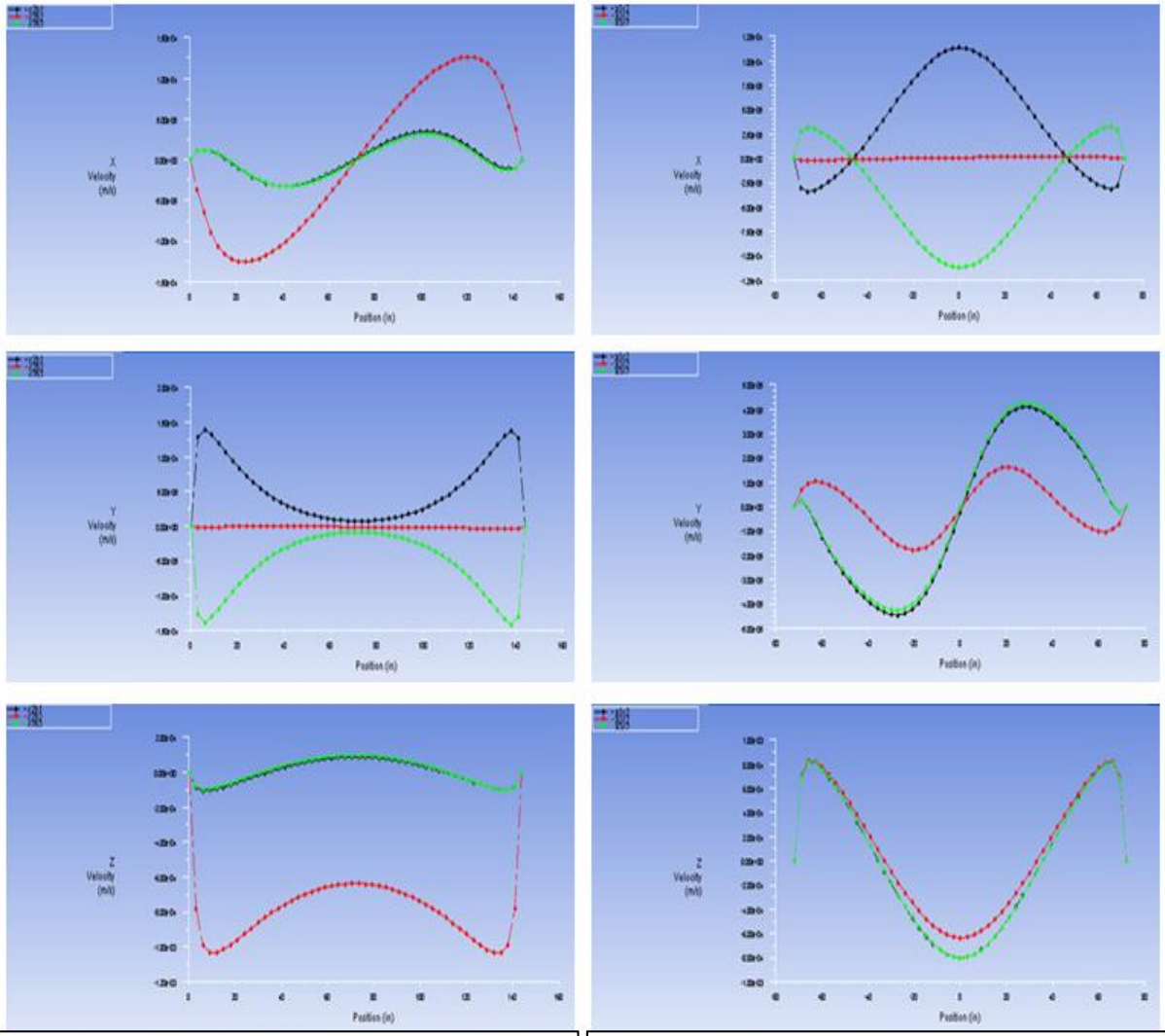

X, Y and Z Velocity Components along x-lines in C2 (x-y) plane at y=3' (Green), y=6' (Red), and y=9' (Black)	X, Y and Z Velocity Components along y-lines in C2 (x-y) plane at x=3' (Green), x=6' (Red), and x=9' (Black)

Figure 116: Case 3 - Velocity Components in the C2 Plane at Time T4 = 8:27 PM

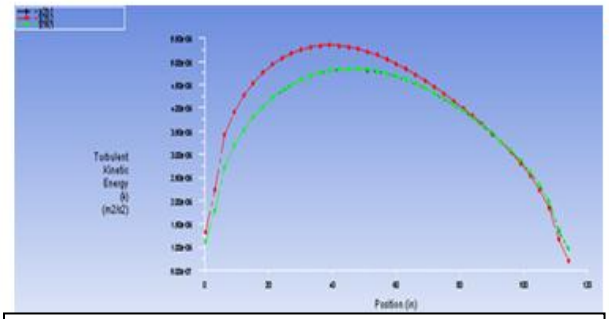

Turbulent Kinetic Energy along z-lines in A2 (y-z) plane at y=3' (Green), y=6'(Red) and y=9'(Black)

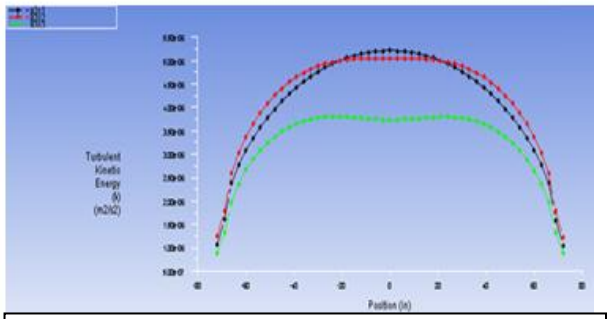

Turbulent Kinetic Energy along y-lines in A2 (y-z) plane at z=2'4.5" (Black), z=4'9"(Red) and z=7'1.5"(Green)

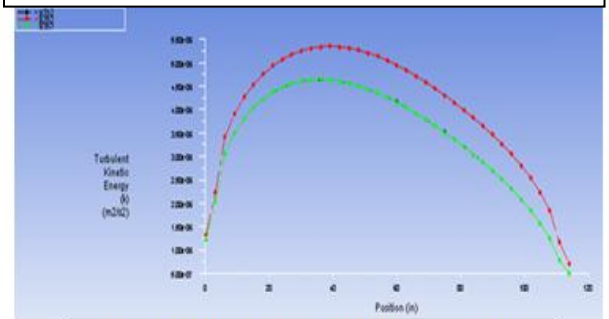

Turbulent Kinetic Energy along z-lines in B2 (x-z) plane at x=3' (Green), x=6'(Red) and x=9'(Black)

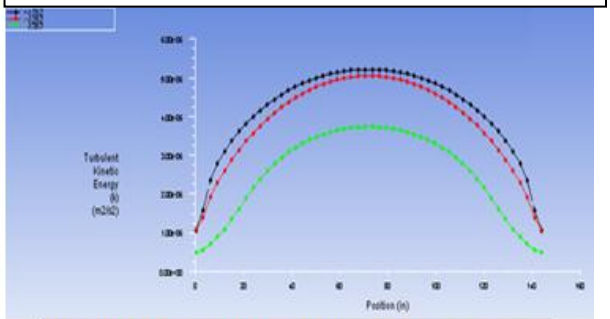

Turbulent Kinetic Energy along x-lines in B2 (x-z) plane at z=2'4.5" (Black), z=4'9"(Red) and z=7'1.5"(Green)

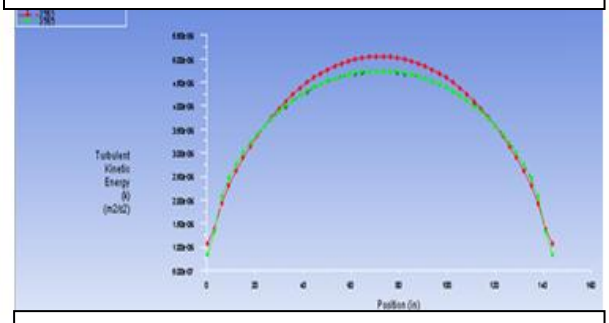

Turbulent Kinetic Energy along x-lines in C2 (x-y) plane at y=3' (Green), y=6'(Red) and y=9'(Black)

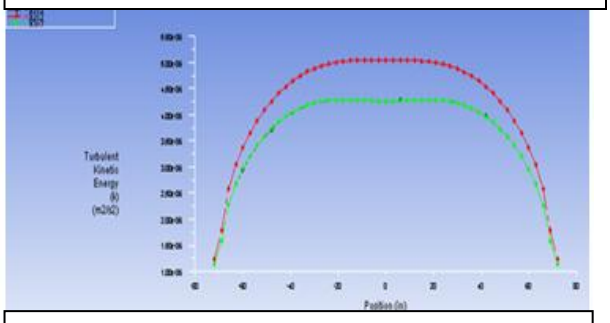

Turbulent Kinetic Energy along y-lines in C2 (x-y) plane at x=3' (Green), x=6'(Red) and x=9'(Black)

Figure 117: Case 3 - Turbulent Kinetic Energy Line Plots at Time T4 = 8:27 PM

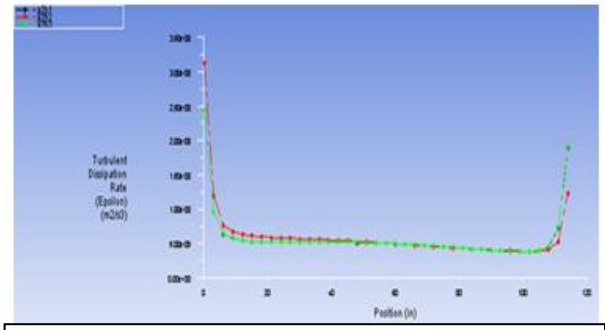

Turbulent Dissipation Rate along z-lines in A2 (y-z) plane at y=3' (Green), y=6'(Red) and y=9'(Black)

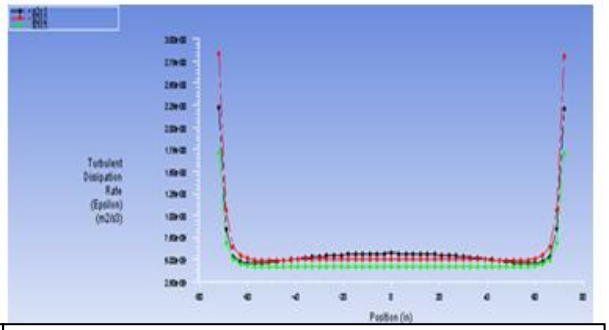

Turbulent Dissipation Rate along y-lines in A2 (y-z) plane at z=2'4.5" (Black), z=4'9"(Red) and z=7'1.5"(Green)

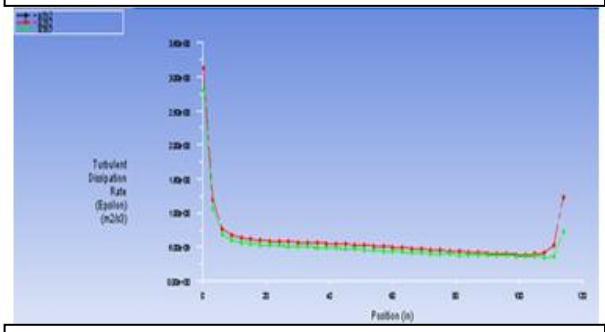

Turbulent Dissipation Rate along z-lines in B2 (x-z) plane at x=3' (Green), x=6'(Red) and x=9'(Black)

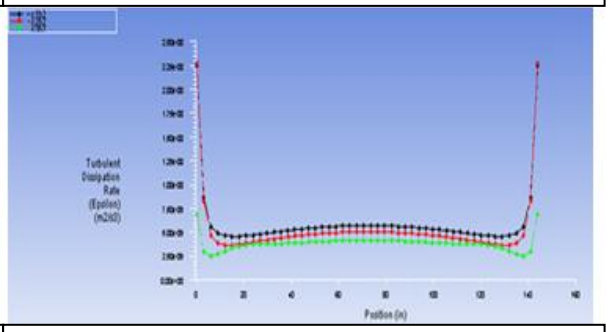

Turbulent Dissipation Rate along x-lines in B2 (x-z) plane at z=2'4.5" (Black), z=4'9"(Red) and z=7'1.5"(Green)

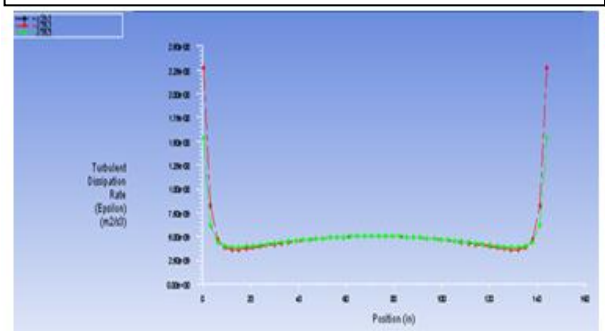

Turbulent Dissipation Rate along x-lines in C2 (x-y) plane at y=3' (Green), y=6'(Red) and y=9'(Black)

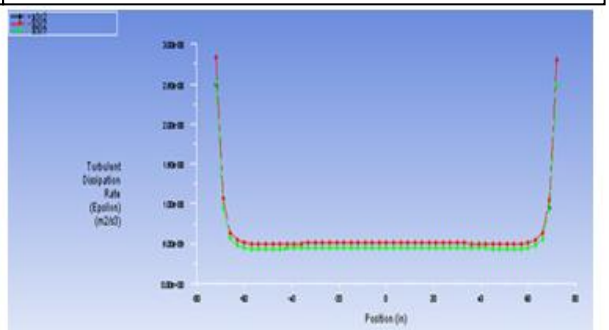

Turbulent Dissipation Rate along y-lines in C2 (x-y) plane at x=3' (Green), x=6'(Red) and x=9'(Black)

Figure 118: Case 3 - Turbulent Dissipation Rate Line Plots at Time T4 = 8:27 PM

5.4.5 Case 4: Distributed Ventilation System with Radiant Cooling

The calculations for Case 4 were performed using the Boussinesq approximation for density, the k-ε realizable turbulence model, and a first order upwind scheme in FLUENT. Computations were performed for two 24-hour time cycles. A time step of 10 seconds was employed in each iteration. Thus, 8640 time steps were required to cover a 24-hour period. The details of the geometry, mesh, boundary conditions, and mass flow rate into the room for this case are described in sections 5.2 and 5.3 of this chapter. A total of 115342 iterations were required to complete the two 24-hour cycles for Case 4. The solutions obtained during the second 24-hour cycle are free of transient effects due to the initial conditions. Figure 119 shows the convergence history of various flow variables and governing equations. In particular, it represents the change in the residuals during the iterative process.

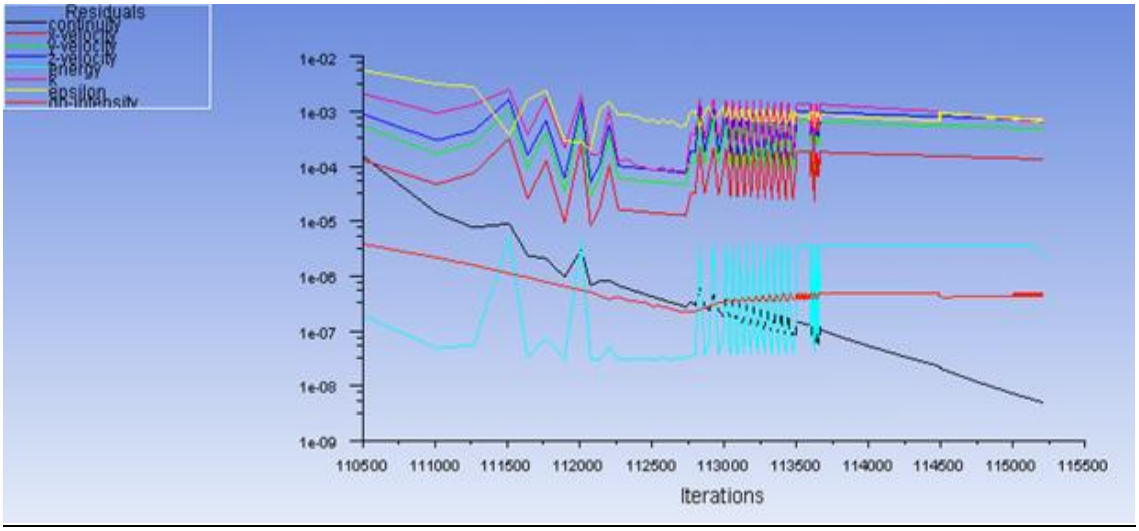

Figure 119: Case 4 - Residual History of Various Flow Variables and Governing Equations During the Iterative Process

Figure 120 shows the contours of temperature distributions in the different planes at T1 = 3:45 AM. T1 corresponds to a low temperature on the ASHRAE curve (Figure 7). As a result, the vents are not required to circulate the air inside the room, and the temperature remains nearly constant except the area above the radiation slab where the air is much cooler. This area has a lower temperature than the rest of the room due to its proximity to the slab. Figure 121 depicts the velocity contours in different planes of the room as described in Figure 19. These velocities are slightly different than those of Case 3 due to the presence of the radiation slab, but are all still very low because the vents have not been active at time T1, and have not been active for a long period of time before time T1 because of the existing cooler temperature. This figure does show that there is some circulation in the room, and that the velocity is highest in the middle of the room. Figure 122 shows the line plots of temperature distributions inside the room along various lines in planes A1-A3, B1-B3, and C1-C3 as shown in Figure 19. These plots show that the solution satisfies the adiabatic wall conditions in the room except at the exterior wall there a constant temperature boundary condition is imposed corresponding to the external temperature at time T1. In addition we note from Figure 122 that the temperature is much cooler near the radiation slab in the ceiling as expected. This is a quantitative description of what is shown in the contour plots of Figure 120. These line plots also show that there is very little variation in the temperature inside the room that isn't near the radiation slab or the exterior wall.

Figures 123-125 show the line plots of various velocity components inside the room. These plots show, as expected, that the no slip condition is correctly imposed at the walls; all velocity components go to zero as they approach the walls. All of these velocities are very small in magnitude, which is a quantitative description of the contour plots shown in Figure

121. Figure 126 shows the turbulent kinetic energy line plots along various cross-sectional lines inside the room, which is indicative of the relative turbulence intensity in various parts of the room. The values of k are very small because of low flow velocities except near the ceiling around the radiation slab where the restricted area leads to slightly elevated turbulence. As expected, the turbulent intensity is generally greater in the middle of the room than near the walls, and near the radiation slab. Figure 127 shows the line plots of the turbulent dissipation rate along various cross-sectional lines inside the room. In contrast to k, the values of epsilon are nearly zero due to the very low air velocity. The value of epsilon is fairly constant across the room in all directions with values on the order of 10^{-12}.

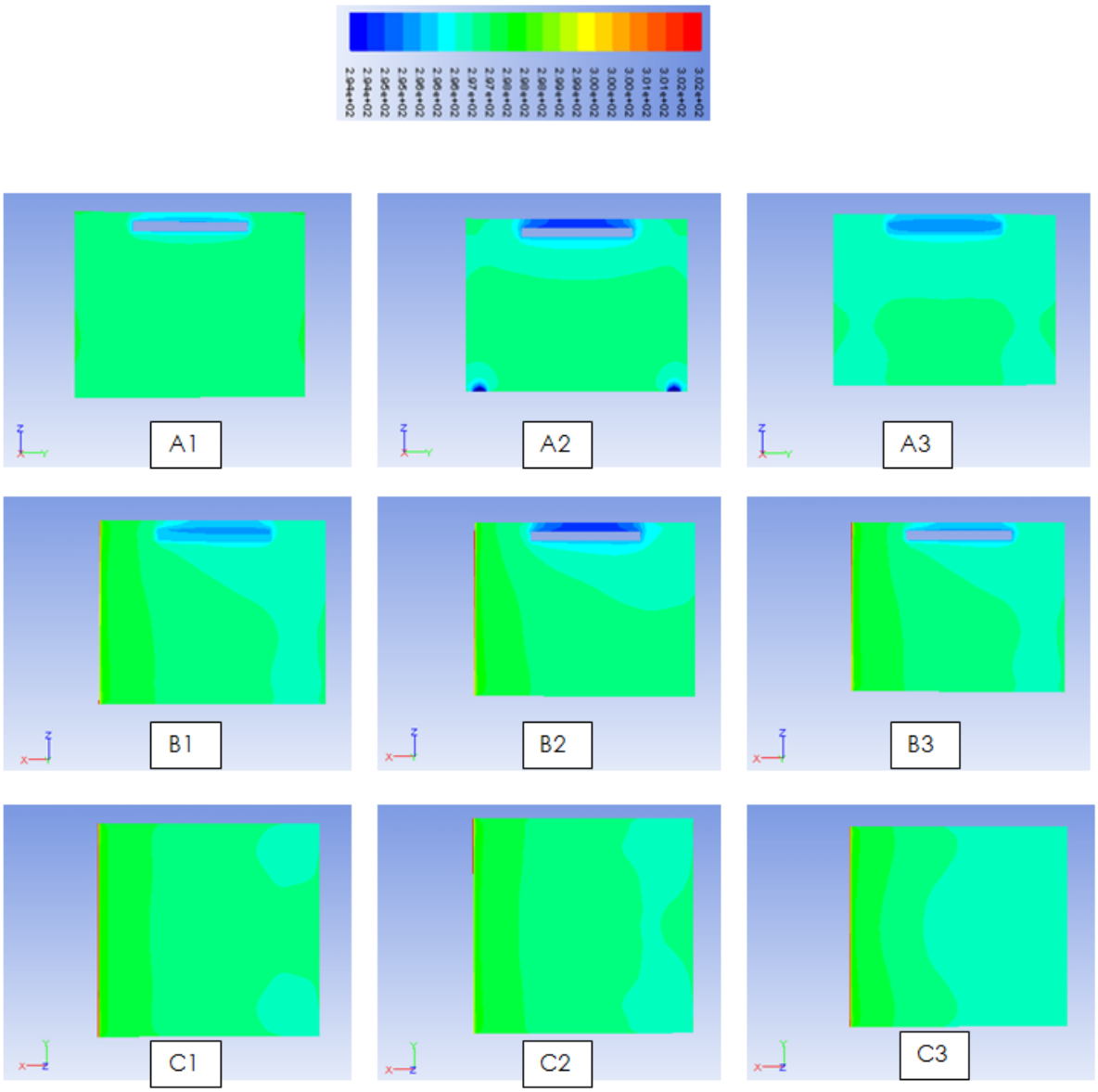

Figure 120: Case 4 - Temperature Contours in Different Planes of Figure 19 at Time T1 = 3:45 AM

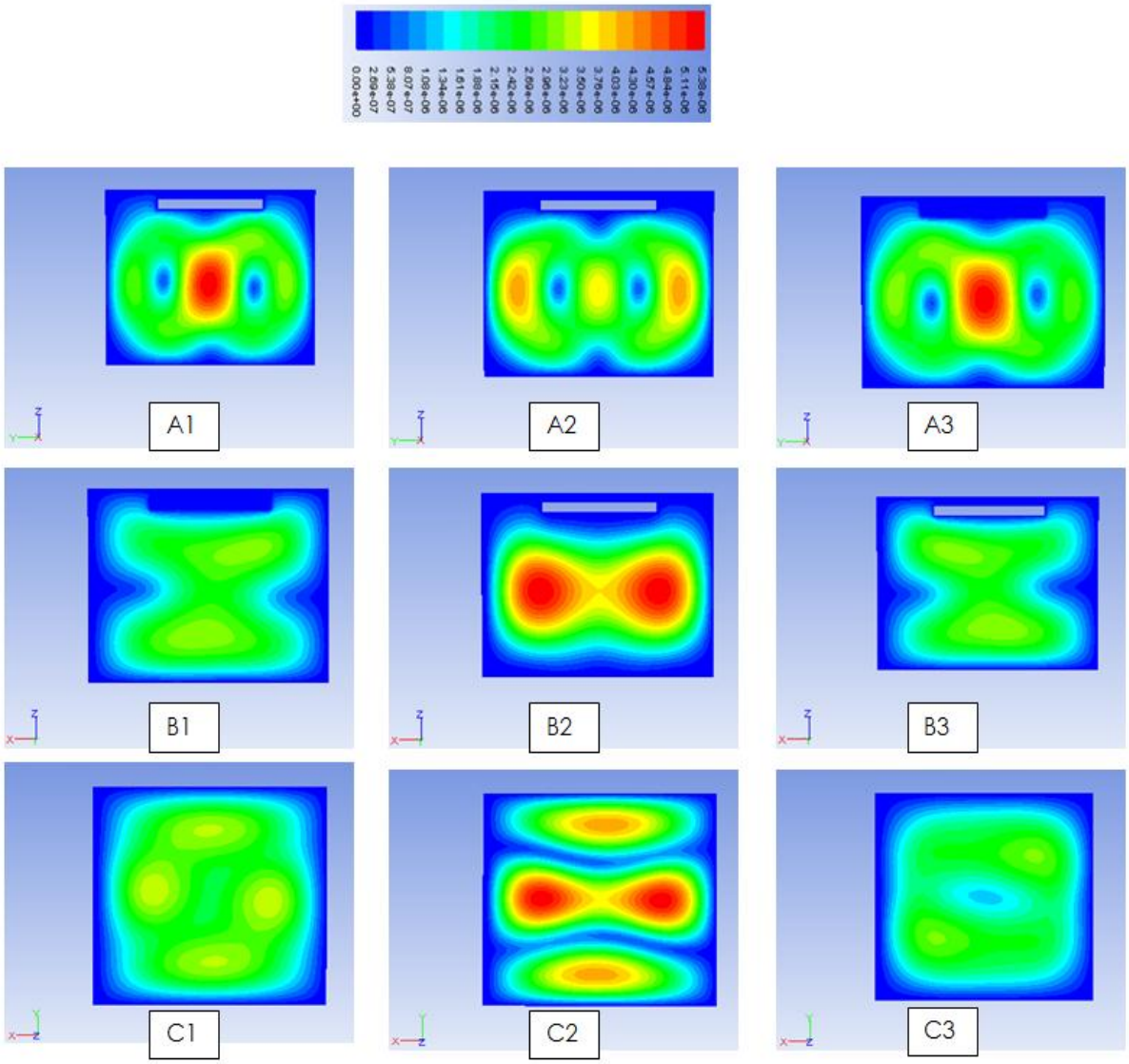

Figure 121: Case 4 - Velocity Contours in Different Planes of Figure 19 at Time T1 = 3:45 AM

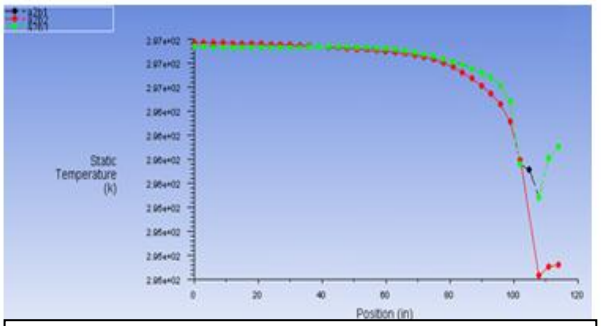

Temperature along z-lines in A2 (y-z) plane at y=3' (Green), y=6'(Red) and y=9'(Black)

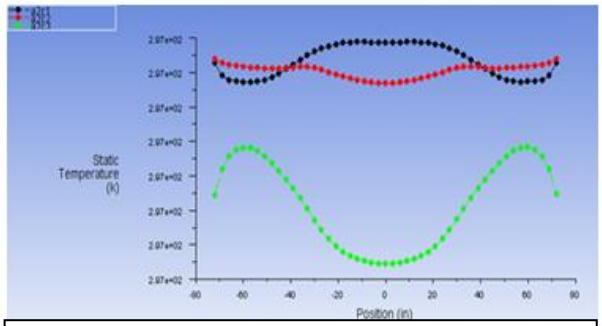

Temperature along y-lines in A2 (y-z) plane at z=2'4.5" (Black), z=4'9"(Red) and z=7'1.5"(Green)

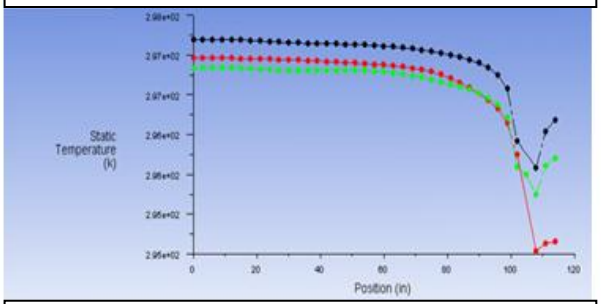

Temperature along z-lines in B2 (x-z) plane at x=3' (Green), x=6'(Red) and x=9'(Black)

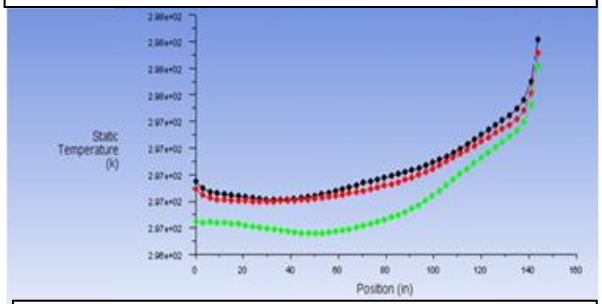

Temperature along x-lines in B2 (x-z) plane at z=2'4.5" (Black), z=4'9"(Red) and z=7'1.5"(Green)

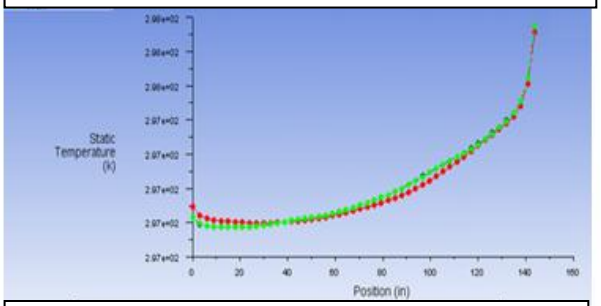

Temperature along x-lines in C2 (x-y) plane at y=3' (Green), y=6'(Red) and y=9'(Black)

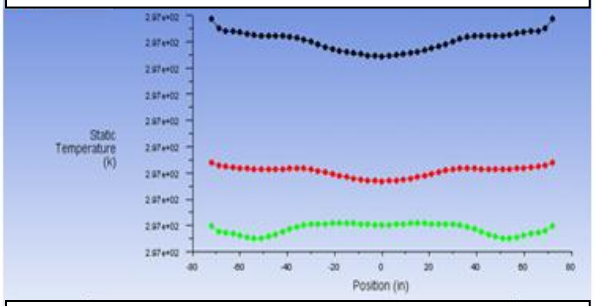

Temperature along y-lines in C2 (x-y) plane at x=3' (Green), x=6'(Red) and x=9'(Black)

Figure 122: Case 4 - Temperature Line Plots at Time T1 = 3:45 AM

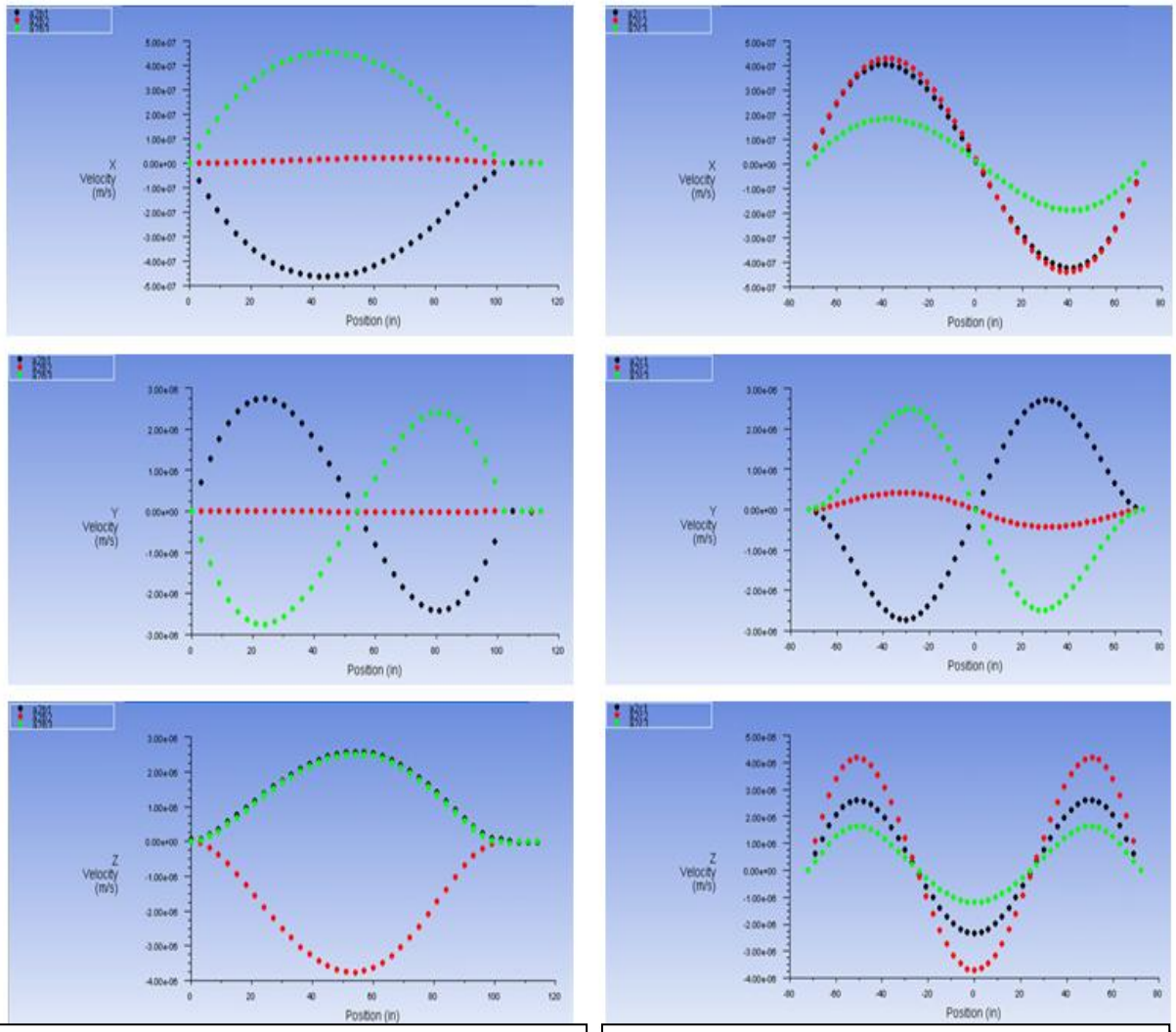

X, Y and Z Velocity Components along z-lines in A2 (y-z) plane at y=3'(Green), y=6'(Red), and y=9'(Black)

X, Y and Z Velocity Components along y-lines in A2 (y-z) plane at z=2'4.5" (Black), z=4'9" (Red), and z=7'1.5" (Green)

Figure 123: Case 4 - Velocity Components in the A2 Plane at Time T1 = 3:45 AM

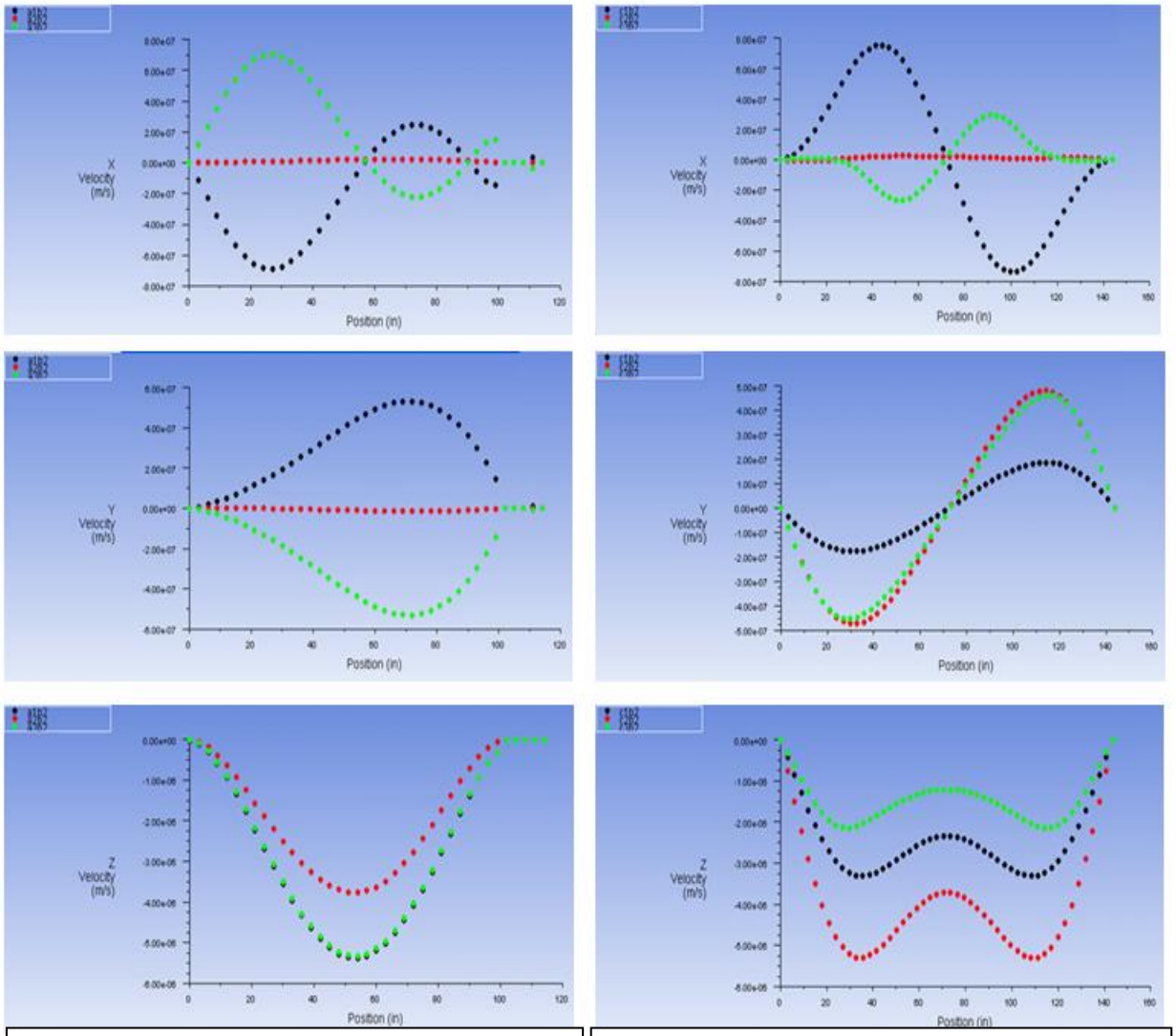

X, Y and Z Velocity Components along z-lines in B2(x-z) plane at x=3'(Green), x=6'(Red), and x=9'(Black)	X, Y and Z Velocity Components along x-lines in B2 (x-z) plane at z=2'4.5" (Black), z=4'9" (Red), and z=7'1.5"(Green)

Figure 124: Case 4 - Velocity Components in the B2 Plane at Time T1 = 3:45 AM

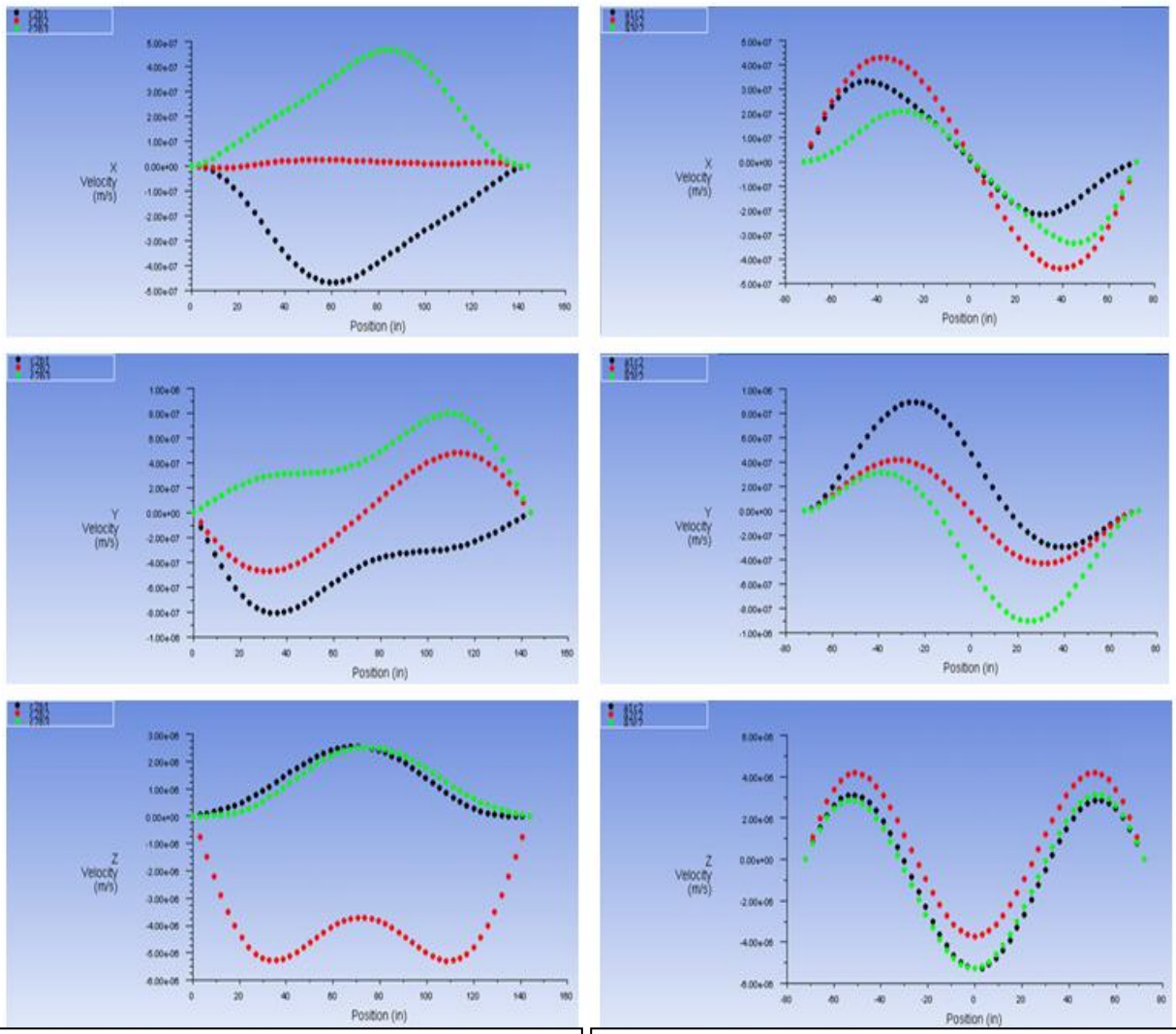

X, Y and Z Velocity Components along x-lines in C2 (x-y) plane at y=3' (Green), y=6' (Red), and y=9' (Black)

X, Y and Z Velocity Components along y-lines in C2 (x-y) plane at x=3' (Green), x=6' (Red), and x=9' (Black)

Figure 125: Case 4 - Velocity Components in the C2 Plane at Time T1 = 3:45 AM

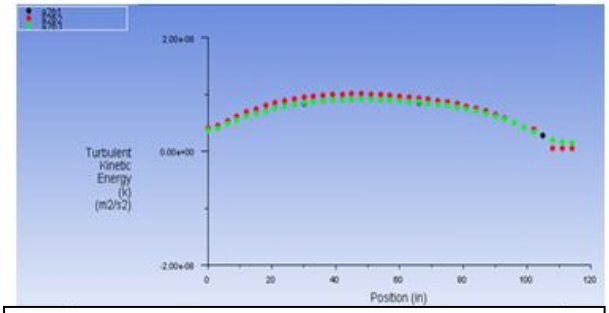

Turbulent Kinetic Energy along z-lines in A2 (y-z) plane at y=3' (Green), y=6'(Red) and y=9'(Black)

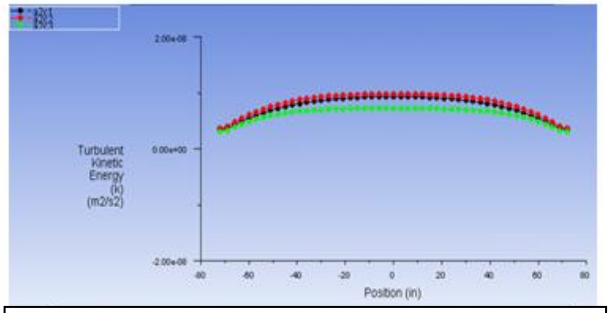

Turbulent Kinetic Energy along y-lines in A2 (y-z) plane at z=2'4.5" (Black), z=4'9"(Red) and z=7'1.5"(Green)

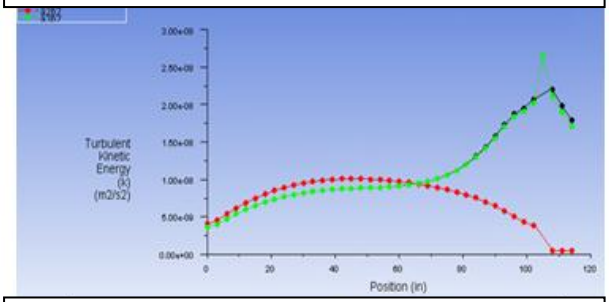

Turbulent Kinetic Energy along z-lines in B2 (x-z) plane at x=3' (Green), x=6'(Red) and x=9'(Black)

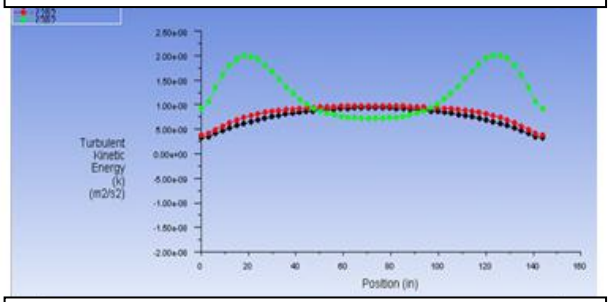

Turbulent Kinetic Energy along x-lines in B2 (x-z) plane at z=2'4.5" (Black), z=4'9"(Red) and z=7'1.5"(Green)

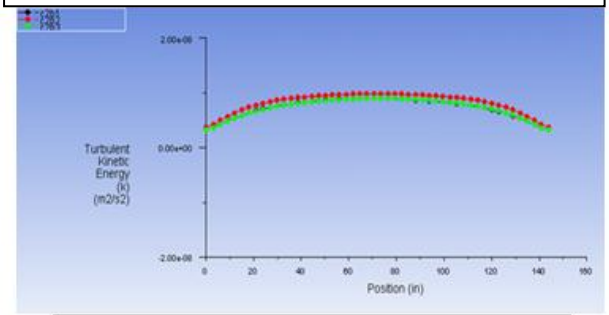

Turbulent Kinetic Energy along x-lines in C2 (x-y) plane at y=3' (Green), y=6'(Red) and y=9'(Black)

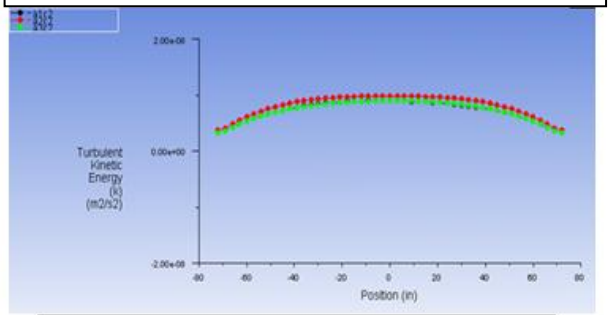

Turbulent Kinetic Energy along y-lines in C2 (x-y) plane at x=3' (Green), x=6'(Red) and x=9'(Black)

Figure 126: Case 4 - Turbulent Kinetic Energy Line Plots at Time T1 = 3:45 AM

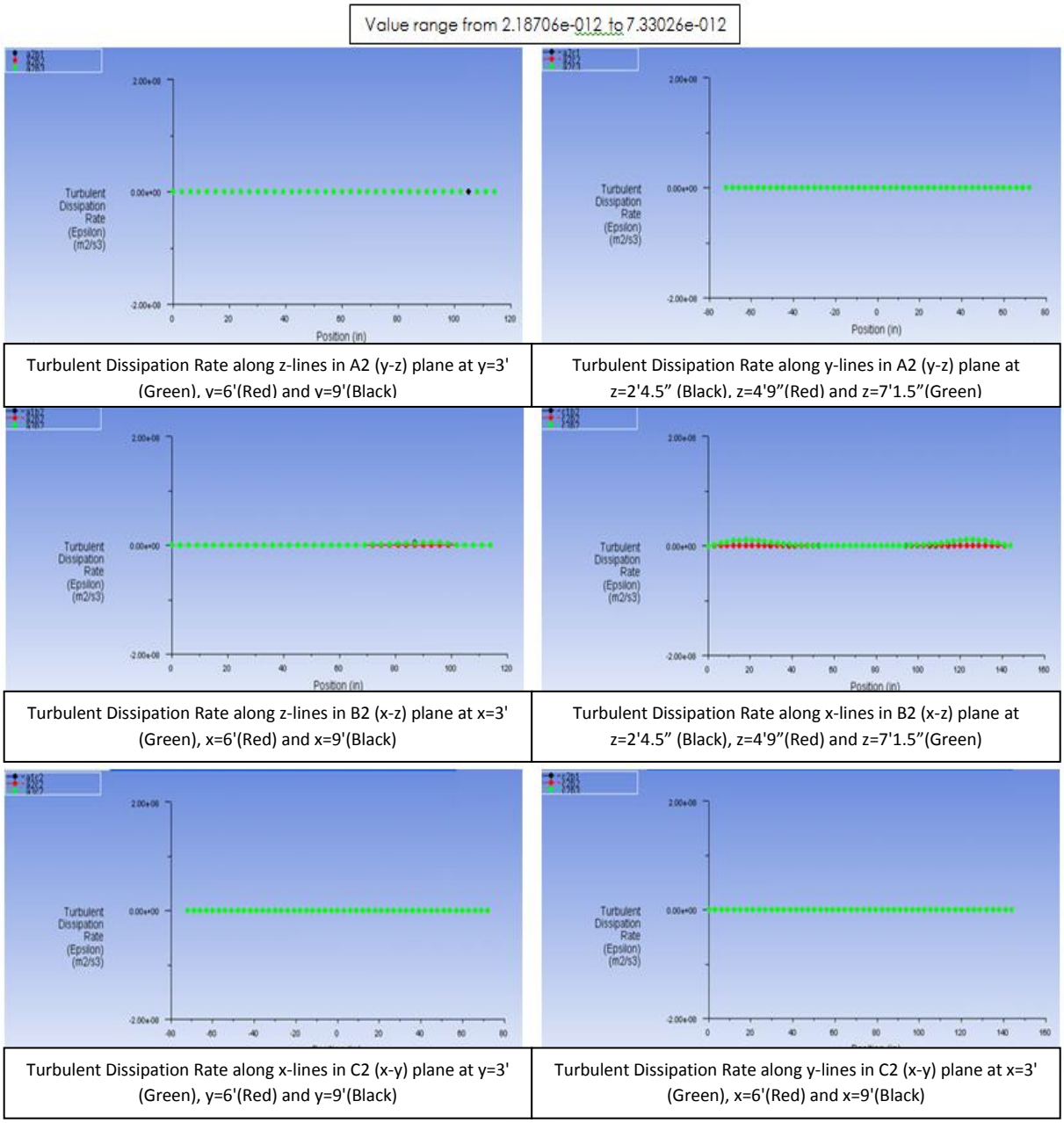

Turbulent Dissipation Rate along z-lines in A2 (y-z) plane at y=3' (Green), v=6'(Red) and v=9'(Black)	Turbulent Dissipation Rate along y-lines in A2 (y-z) plane at z=2'4.5" (Black), z=4'9"(Red) and z=7'1.5"(Green)
Turbulent Dissipation Rate along z-lines in B2 (x-z) plane at x=3' (Green), x=6'(Red) and x=9'(Black)	Turbulent Dissipation Rate along x-lines in B2 (x-z) plane at z=2'4.5" (Black), z=4'9"(Red) and z=7'1.5"(Green)
Turbulent Dissipation Rate along x-lines in C2 (x-y) plane at y=3' (Green), y=6'(Red) and y=9'(Black)	Turbulent Dissipation Rate along y-lines in C2 (x-y) plane at x=3' (Green), x=6'(Red) and x=9'(Black)

Figure 127: Case 4 - Turbulent Dissipation Rate Line Plots at Time T1 = 3:45 AM

Next, we present results at time T2 = 9:20 AM. The key to interpreting the results in the various planes (A1-A3, B1-B3, C1-C3) and along the various lines in the planes inside the room is the same as described before for Figures 120-127 at T1 = 3:45 AM. At T2 = 9:20 AM, the outside temperature is higher as shown in the ASHRAE temperature curve (Figure 7). The air inside the room is therefore warmer than at T1 = 3:45 AM. Figure 128 shows the temperature contours inside the room in A1-A3, B1-B3, and C1-C3 planes. At time T2 = 9:20 AM, we can observe to cold air collecting near the rear of the room. We note from the A3 plane that the cold air significantly affects the area near the rear wall. Figure 129 shows the velocity contours in different planes of the room at time T2 = 9:20 AM. We notice the air velocity is higher than at T1 = 3:45 AM, but still remains relatively small as a result of lack of perturbation from the air vents.

Figure 130 shows the line plots of temperature distributions inside the room, which are somewhat higher those at time T1 = 3:45 AM as expected. These temperature line plots show that the adiabatic temperature boundary condition is satisfied on the five interior walls, and that the highest temperature occurs at the exterior wall. These temperature line plots also show the effects of the radiation slab in the cooler air near the ceiling. The temperature line plots in the C2 plane show that the temperature is fairly constant in the rear of the room, although it rises rapidly as the exterior wall is approached.

Figures 131-133 show the line plots of velocity in various planes inside the room, which more variation than Figures 123-125 at time T1 = 3:45 AM, resulting from the mixing in the room due to buoyancy effects. Figures 131 and 132 show a rapid increase in velocity near the ceiling related to the restricted area due to the presence of the radiation slab. Figure

134 shows the line plots of turbulent kinetic energy in various planes inside the room. The turbulent kinetic energy (k) is quite high in the middle of the room as expected, and is nearly zero near the walls. Figure 135 shows the line plots of the turbulent dissipation rate in various planes inside the room. The intensity of both k and ε is increased slightly as expected since the temperature increases at time T2 = 9:20 AM. The turbulent dissipation spikes near the surface of the radiation slab as well as at the ceiling in Figure 135 as expected.

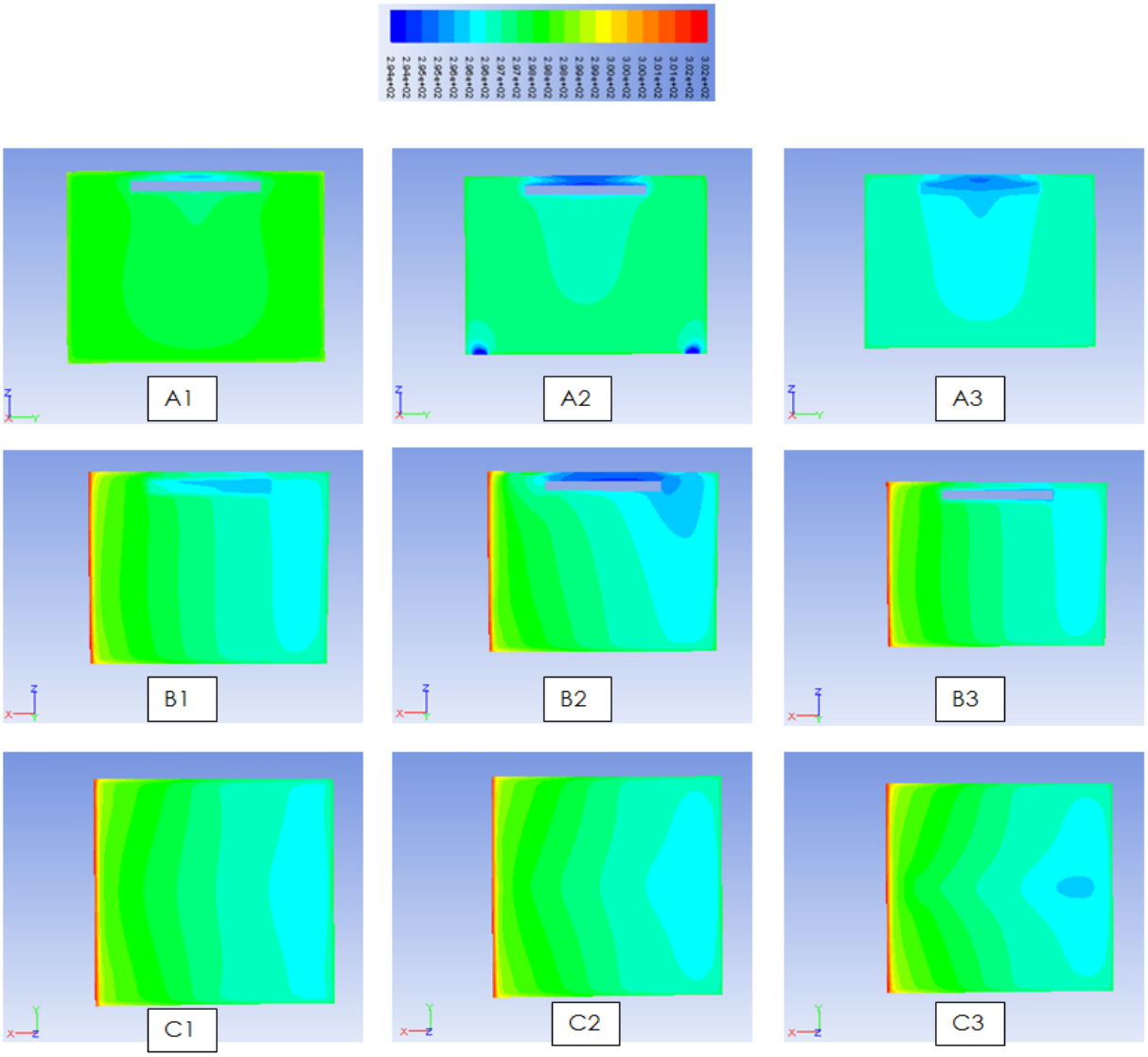

Figure 128: Case 4 - Temperature Contours in Different Planes of Figure 19 at Time T2 = 9:20 AM

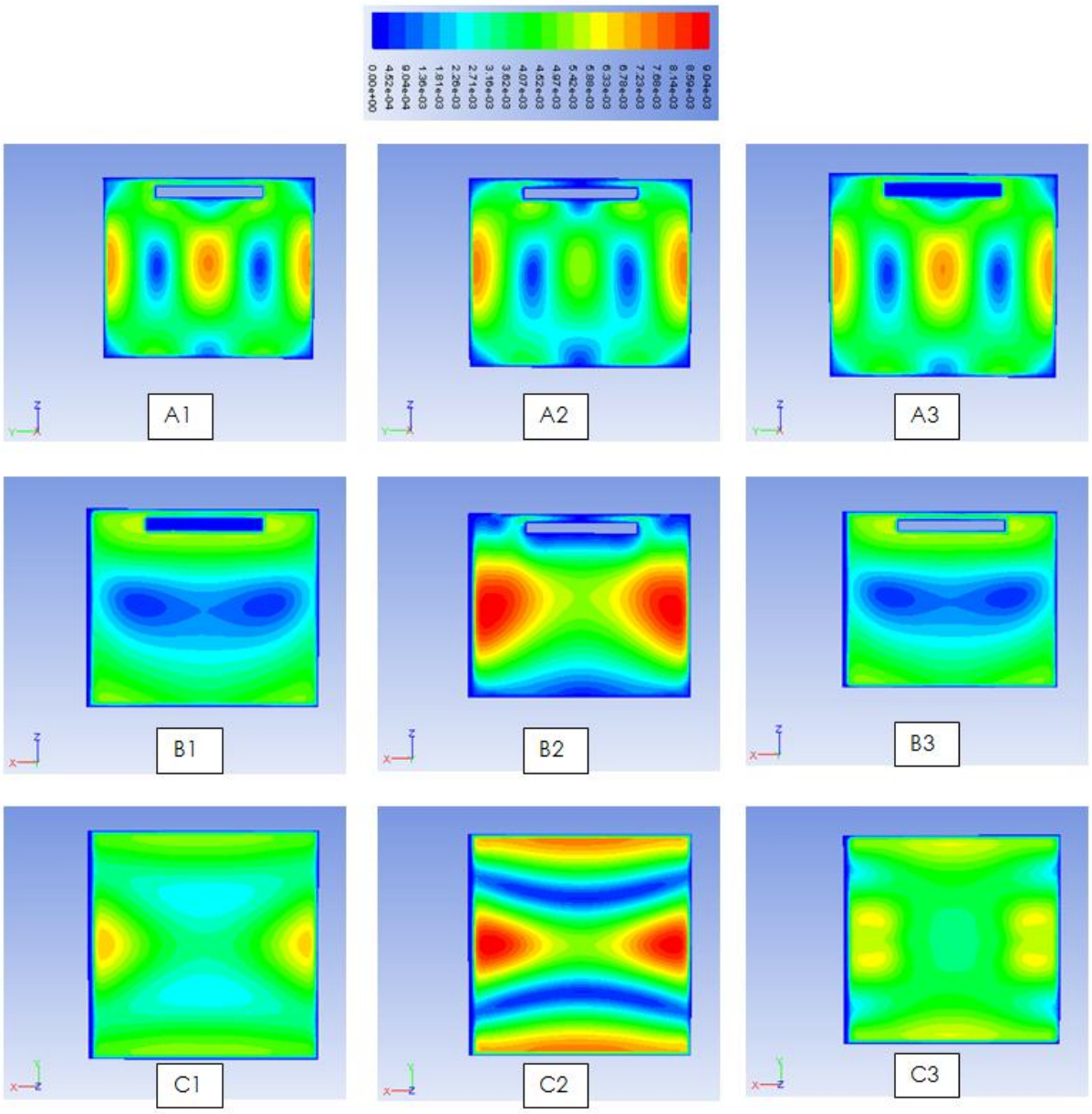

Figure 129: Case 4 - Velocity Contours in Different Planes of Figure 19 at Time T2 = 9:20 AM

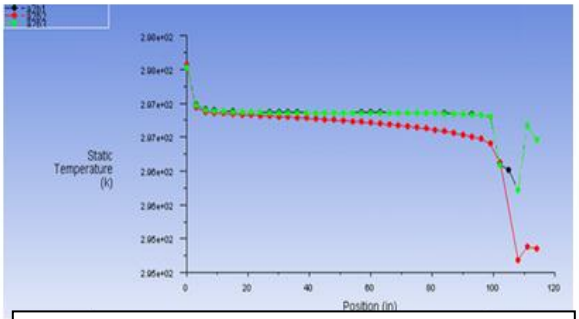

Temperature along z-lines in A2 (y-z) plane at y=3' (Green), y=6'(Red) and y=9'(Black)

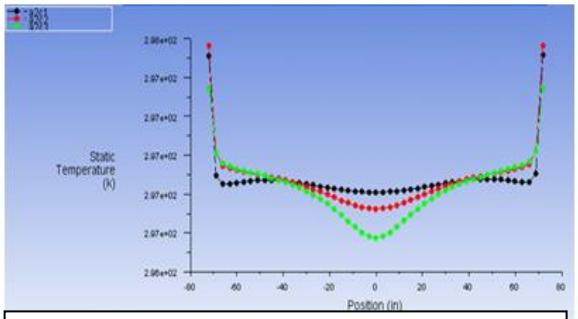

Temperature along y-lines in A2 (y-z) plane at z=2'4.5" (Black), z=4'9"(Red) and z=7'1.5"(Green)

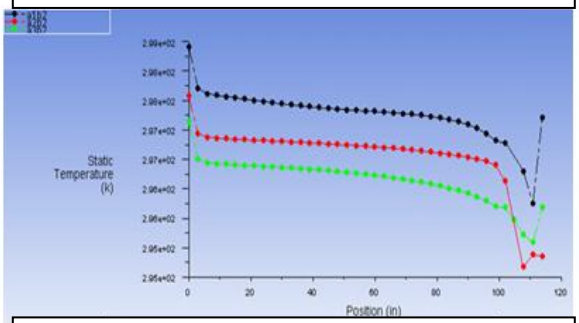

Temperature along z-lines in B2 (x-z) plane at x=3' (Green), x=6'(Red) and x=9'(Black)

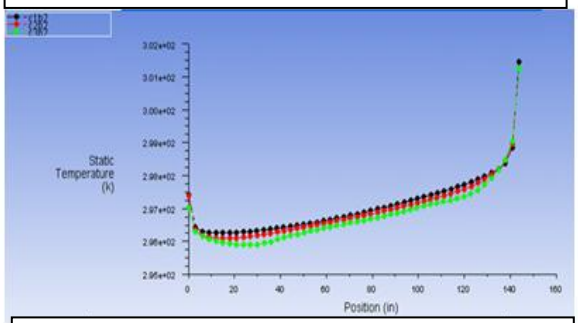

Temperature along x-lines in B2 (x-z) plane at z=2'4.5" (Black), z=4'9"(Red) and z=7'1.5"(Green)

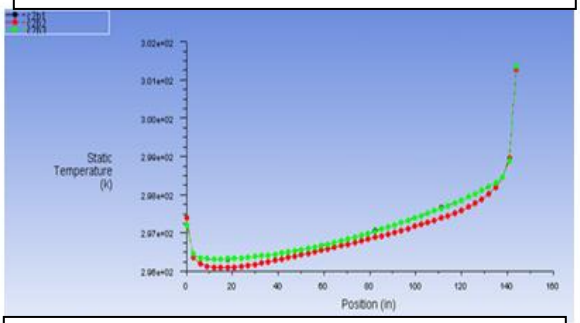

Temperature along x-lines in C2 (x-y) plane at y=3' (Green), y=6'(Red) and y=9'(Black)

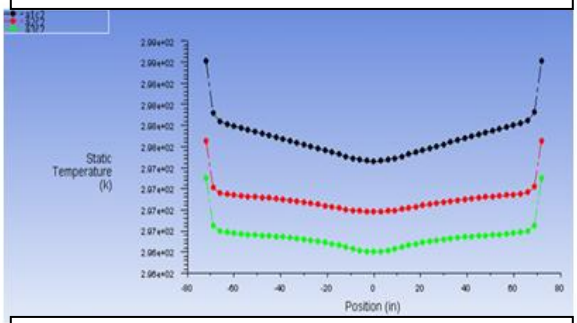

Temperature along y-lines in C2 (x-y) plane at x=3' (Green), x=6'(Red) and x=9'(Black)

Figure 130: Case 4 – Temperature Line Plots at Time T2 = 9:20 AM

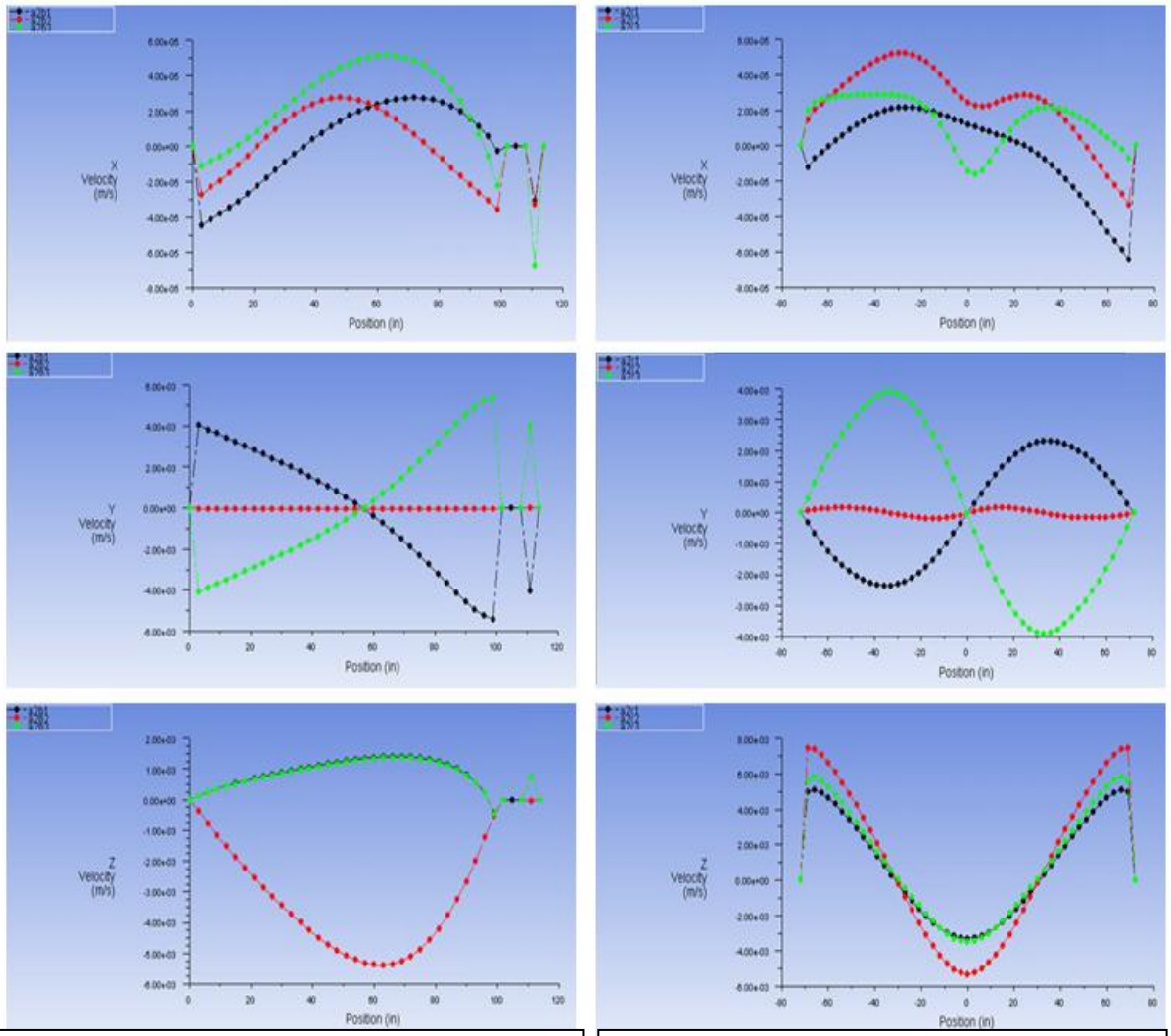

X, Y and Z Velocity Components along z-lines in A2 (y-z) plane at y=3'(Green), y=6'(Red), and y=9'(Black)

X, Y and Z Velocity Components along y-lines in A2 (y-z) plane at z=2'4.5" (Black), z=4'9" (Red), and z=7'1.5" (Green)

Figure 131: Case 4 - Velocity Components in the A2 Plane at Time T2 = 9:20 AM

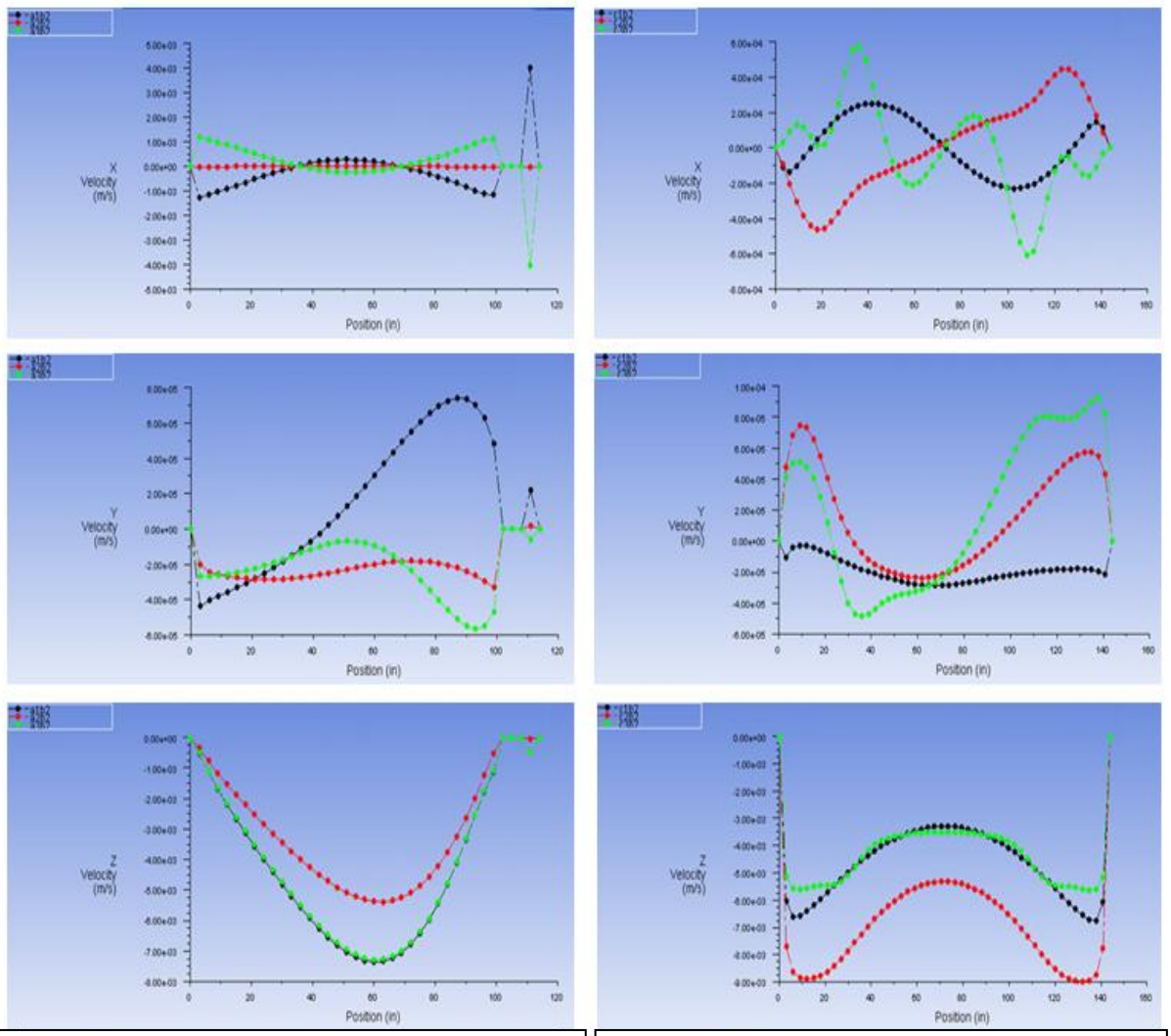

X, Y and Z Velocity Components along z-lines in B2(x-z) plane at x=3'(Green), x=6'(Red), and x=9'(Black)	X, Y and Z Velocity Components along x-lines in B2 (x-z) plane at z=2'4.5" (Black), z=4'9" (Red), and z=7'1.5"(Green)

Figure 132: Case 4 - Velocity Components in the B2 Plane at Time T2 = 9:20 AM

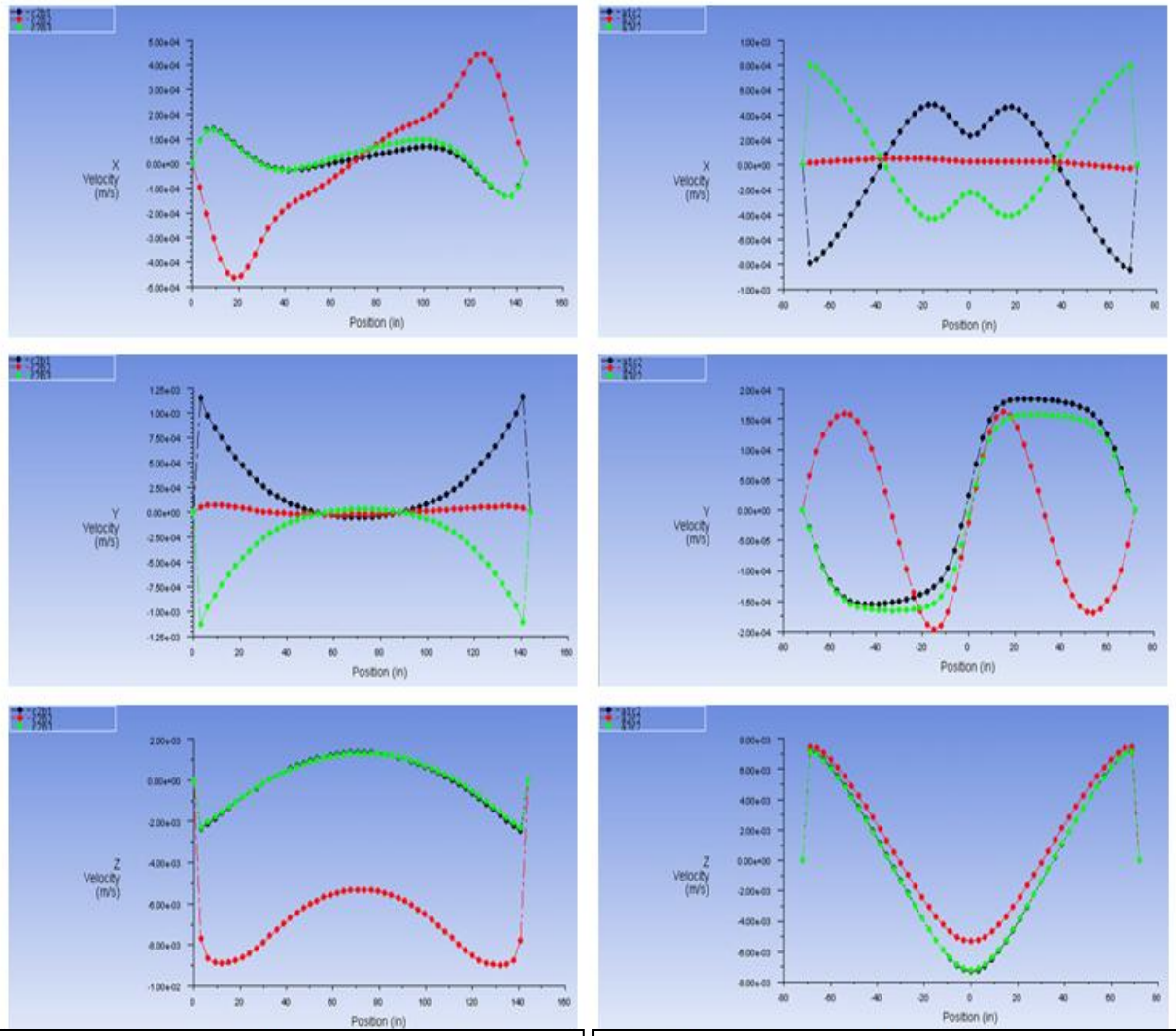

X, Y and Z Velocity Components along x-lines in C2 (x-y) plane at y=3' (Green), y=6' (Red), and y=9' (Black)	X, Y and Z Velocity Components along y-lines in C2 (x-y) plane at x=3' (Green), x=6' (Red), and x=9' (Black)

Figure 133: Case 4 - Velocity Components in the C2 Plane at Time T2 = 9:20 AM

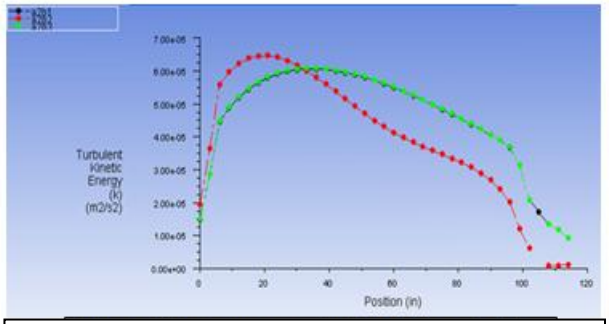

Turbulent Kinetic Energy along z-lines in A2 (y-z) plane at y=3' (Green), y=6'(Red) and y=9'(Black)

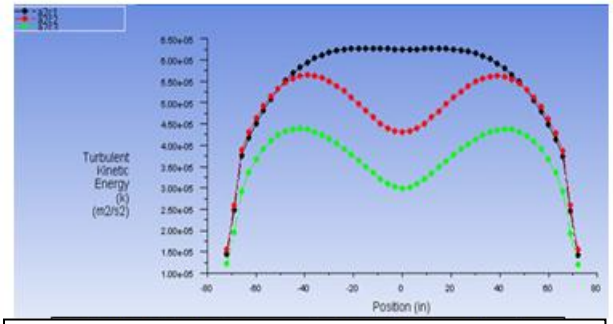

Turbulent Kinetic Energy along y-lines in A2 (y-z) plane at z=2'4.5" (Black), z=4'9"(Red) and z=7'1.5"(Green)

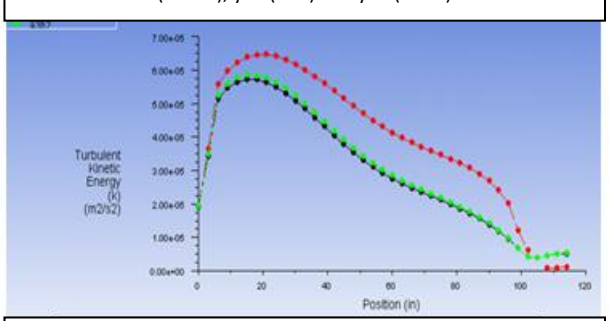

Turbulent Kinetic Energy along z-lines in B2 (x-z) plane at x=3' (Green), x=6'(Red) and x=9'(Black)

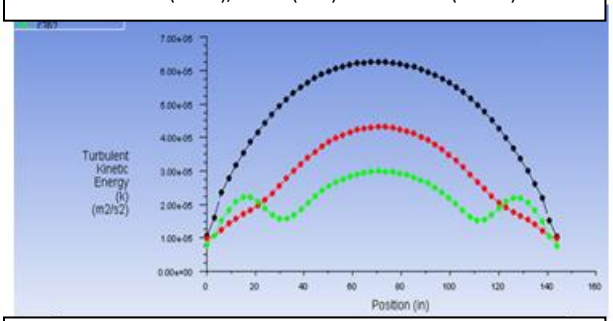

Turbulent Kinetic Energy along x-lines in B2 (x-z) plane at z=2'4.5" (Black), z=4'9"(Red) and z=7'1.5"(Green)

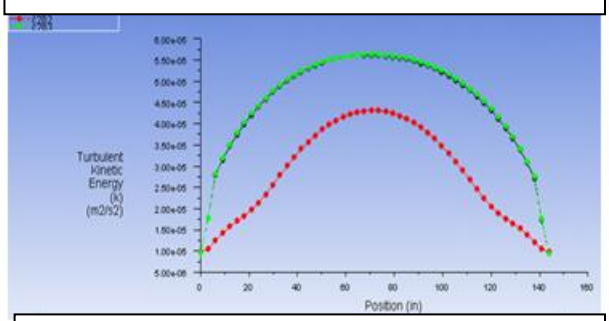

Turbulent Kinetic Energy along x-lines in C2 (x-y) plane at y=3' (Green), y=6'(Red) and y=9'(Black)

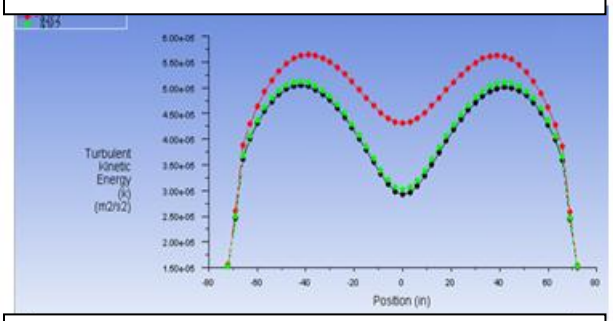

Turbulent Kinetic Energy along y-lines in C2 (x-y) plane at x=3' (Green), x=6'(Red) and x=9'(Black)

Figure 134: Case 4 - Turbulent Kinetic Energy Line Plots at Time T2 = 9:20 AM

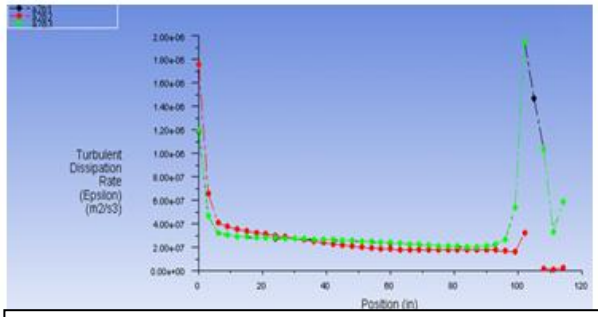

Turbulent Dissipation Rate along z-lines in A2 (y-z) plane at y=3' (Green), y=6'(Red) and y=9'(Black)

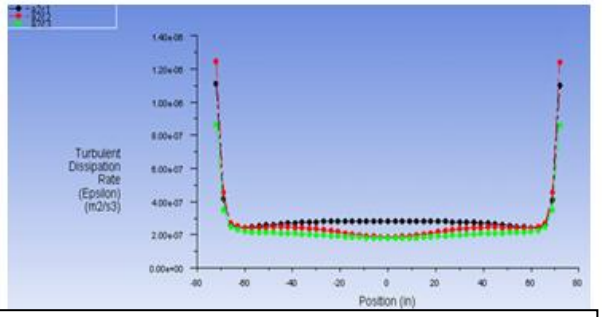

Turbulent Dissipation Rate along y-lines in A2 (y-z) plane at z=2'4.5" (Black), z=4'9"(Red) and z=7'1.5"(Green)

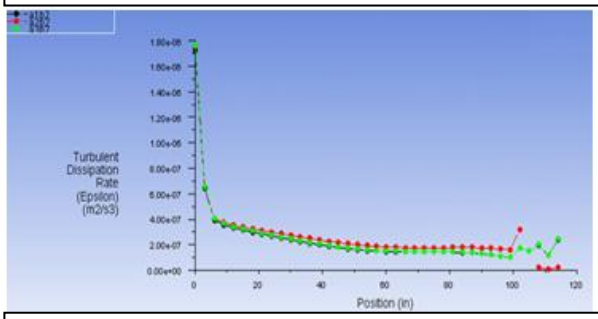

Turbulent Dissipation Rate along z-lines in B2 (x-z) plane at x=3' (Green), x=6'(Red) and x=9'(Black)

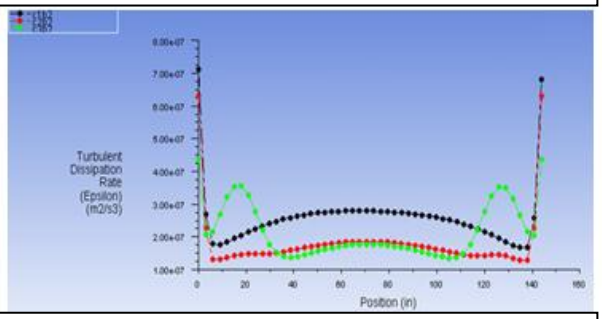

Turbulent Dissipation Rate along x-lines in B2 (x-z) plane at z=2'4.5" (Black), z=4'9"(Red) and z=7'1.5"(Green)

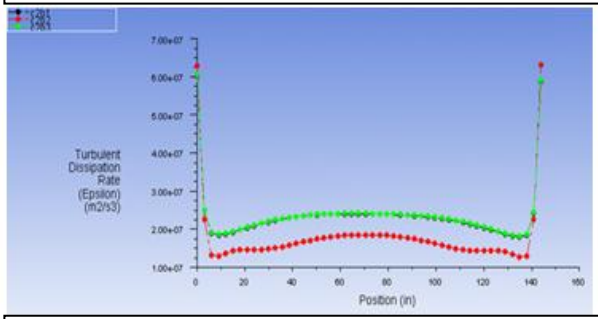

Turbulent Dissipation Rate along x-lines in C2 (x-y) plane at y=3' (Green), y=6'(Red) and y=9'(Black)

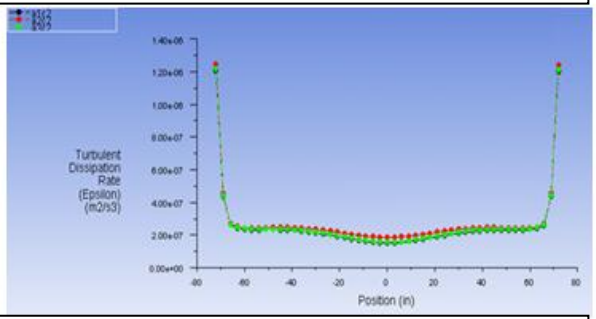

Turbulent Dissipation Rate along y-lines in C2 (x-y) plane at x=3' (Green), x=6'(Red) and x=9'(Black)

Figure 135: Case 4 - Turbulent Dissipation Rate Line Plots at Time T2 = 9:20 AM

Next, we present results at time T3 = 2:53 PM. The key to interpreting the results in the various planes (A1-A3, B1-B3, and C1-C3) and along the various lines in these planes inside the room is the same as described before for Figures 120-127 at time T1=3:45 AM. At T3 = 2:53 PM, the outside temperature is just past its peak as shown in the ASHRAE curve (Figure 7). The air in the room is experiencing the highest temperature load from the exterior wall, yet the majority of the air is within the comfortable temperature band. Figure 136 shows the temperature contours inside the room planes (A1-A3, B1-B3, and C1-C3). These contours clearly show how effective the ventilation system of Case 4 is at preventing the air temperature in the room from rising above comfortable levels. Figure 137 shows the velocity magnitude contours in the different planes of the room as described in Figure 19. These contours show increased velocity along the front and rear walls of the room due to the circulation of air caused by the rising warm air. Figure 138 shows the line plots of the temperature distributions inside the room along various lines in planes A1-A3, B1-B3, and C1-C3 shown in Figure 19. These line plots show that the solutions satisfies the adiabatic wall conditions in the room except for the exterior wall where a constant temperature boundary condition is imposed corresponding to the external temperature at time T3. In addition, Figure 138 shows the cooling effects of the radiation slab on the air near the ceiling.

Figures 139-141 show the line plots of the velocity components in the room. These plots show that the velocity components go to zero at the walls. These line plots are a quantitative description of the contour plots shown in Figure 137. Figures 139 and 140 show an increased velocity above the radiation slab due to the restricted space. Figure 142 shows the turbulent kinetic energy line plots along the various cross-sectional lines inside the room;

they indicate the relative turbulence intensity in various parts of the room. As expected, the turbulent intensity is greater in the middle of the room than near the walls. Figure 143 shows line plots of the turbulent dissipation rate (ε) along various cross-sectional lines inside the room. In contrast to k, the value of epsilon peaks near the walls and at the radiation slab surface because of large dissipation of turbulence, and is fairly constant across the room in all direction except near the walls.

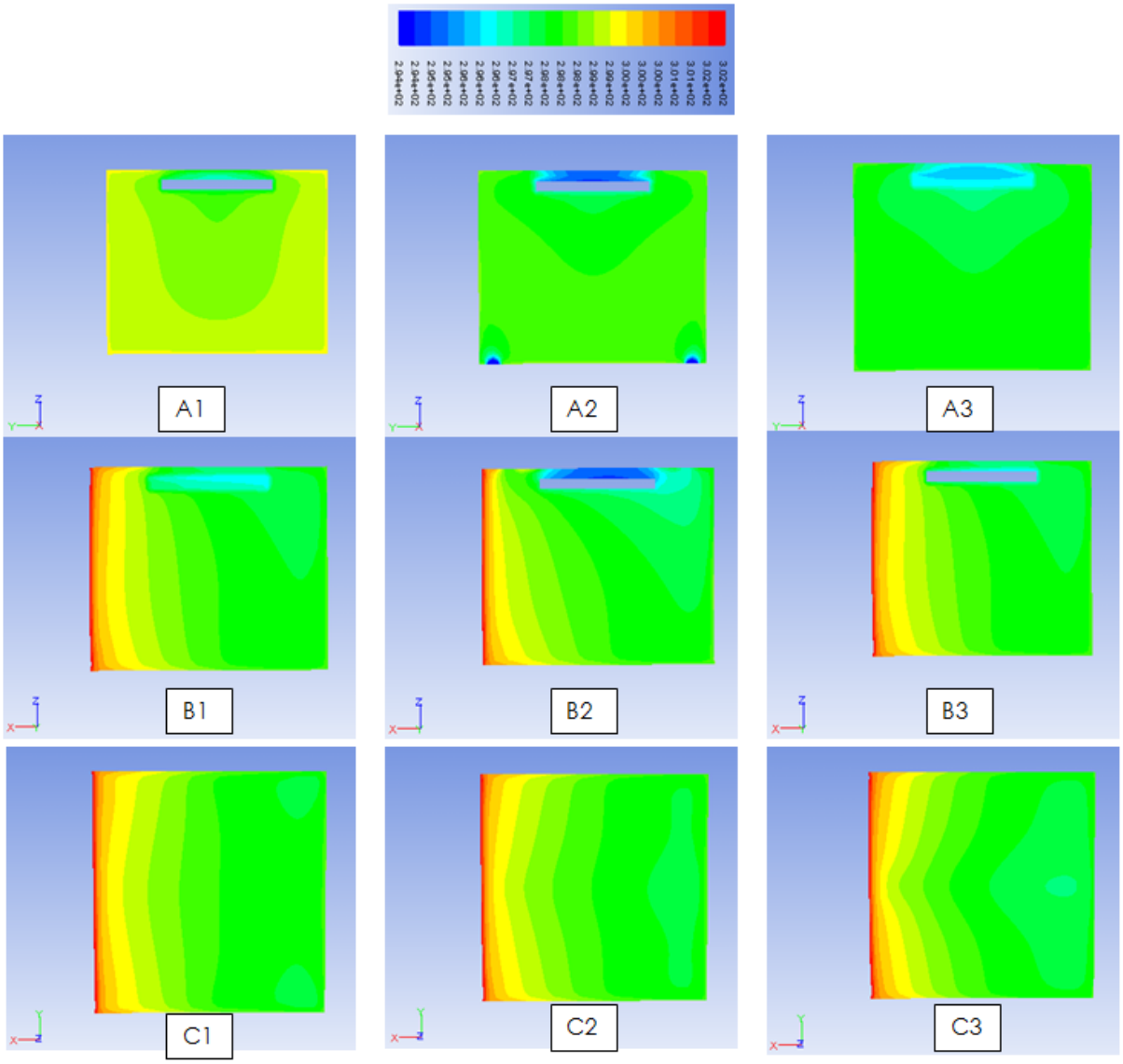

Figure 136: Case 4 - Temperature Contours in Different Planes of Figure 19 at Time T3 = 2:53 PM

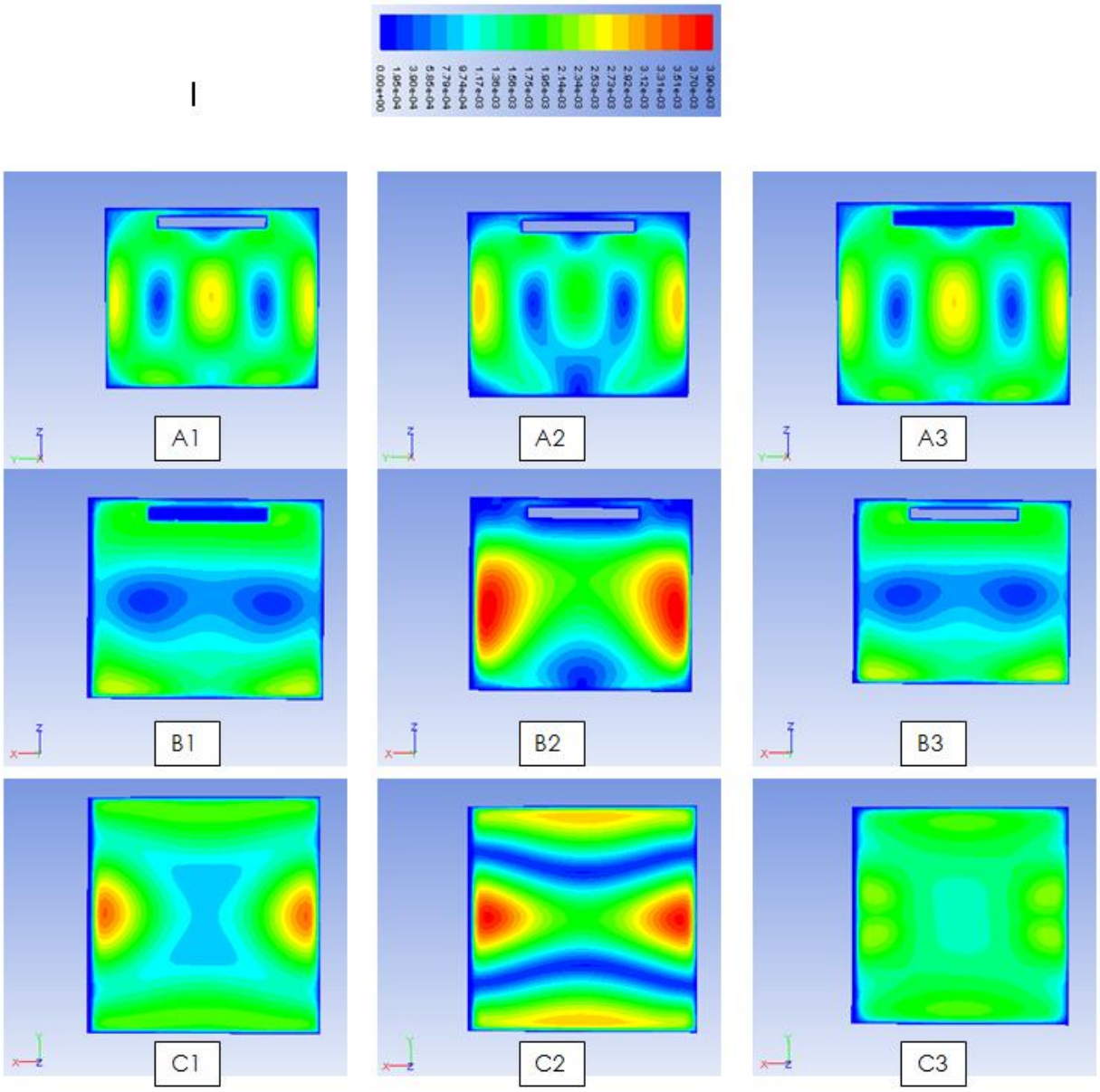

Figure 137: Case 4 - Velocity Contours in Different Planes of Figure 19 at Time T3 = 2:53 PM

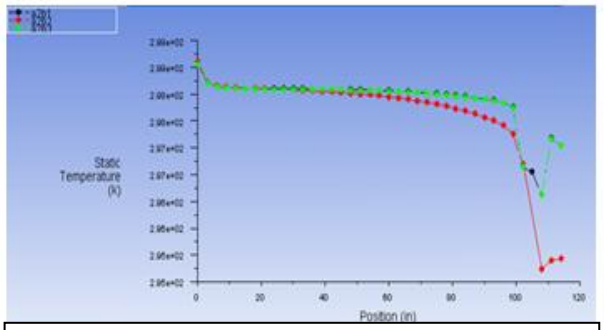

Temperature along z-lines in A2 (y-z) plane at y=3' (Green), y=6'(Red) and y=9'(Black)

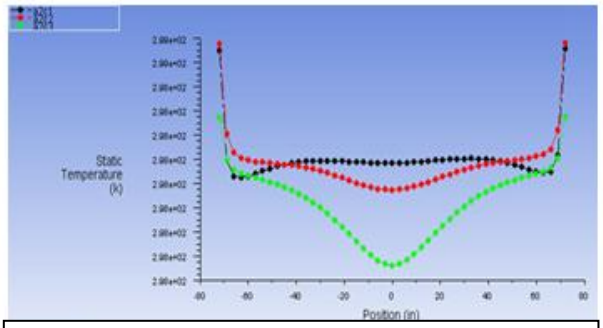

Temperature along y-lines in A2 (y-z) plane at z=2'4.5" (Black), z=4'9"(Red) and z=7'1.5"(Green)

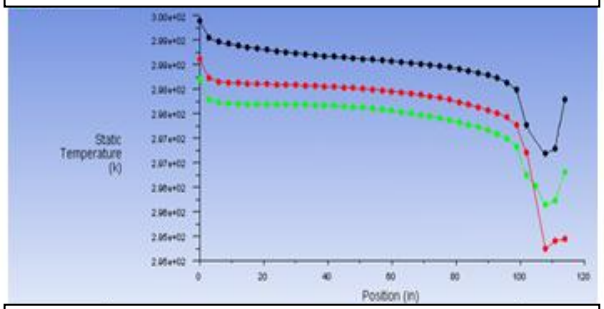

Temperature along z-lines in B2 (x-z) plane at x=3' (Green), x=6'(Red) and x=9'(Black)

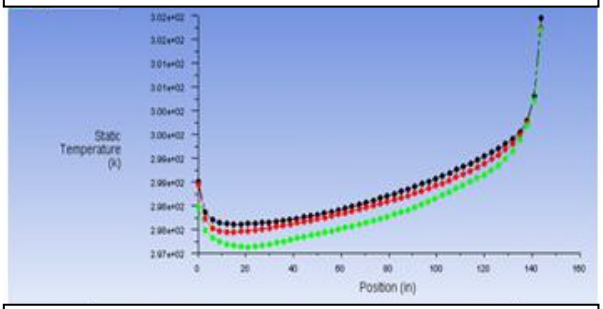

Temperature along x-lines in B2 (x-z) plane at z=2'4.5" (Black), z=4'9"(Red) and z=7'1.5"(Green)

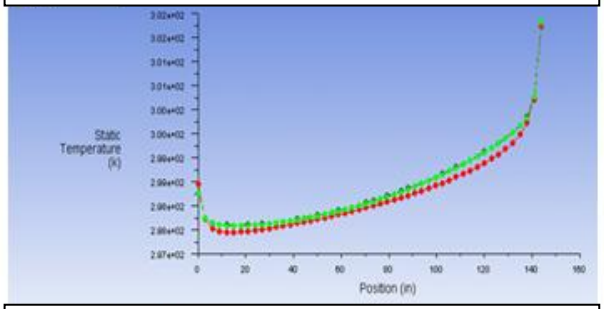

Temperature along x-lines in C2 (x-y) plane at y=3' (Green), y=6'(Red) and y=9'(Black)

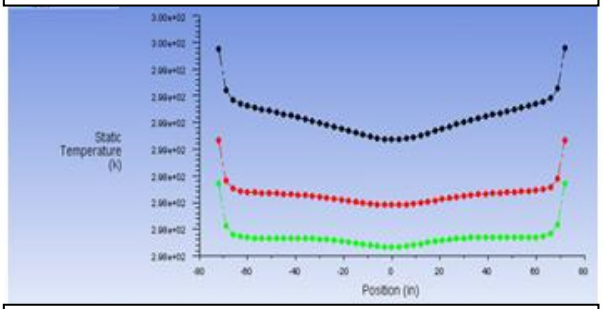

Temperature along y-lines in C2 (x-y) plane at x=3' (Green), x=6'(Red) and x=9'(Black)

Figure 138: Case 4 – Temperature Line Plots at Time T3 = 2:53 PM

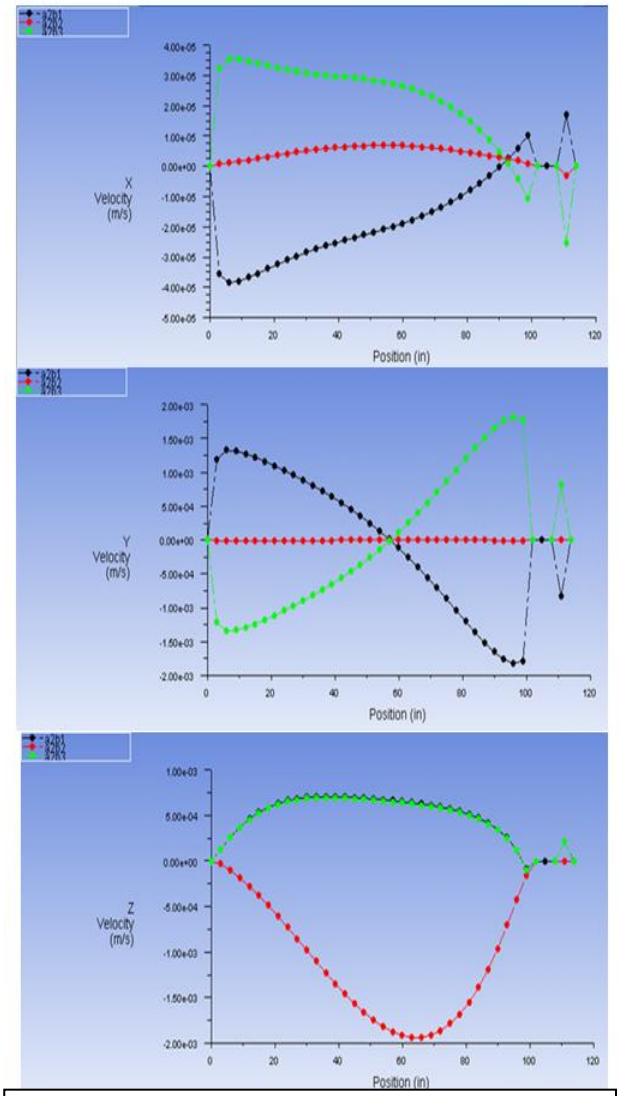

X, Y and Z Velocity Components along z-lines in A2 (y-z) plane at y=3'(Green), y=6'(Red), and y=9'(Black)

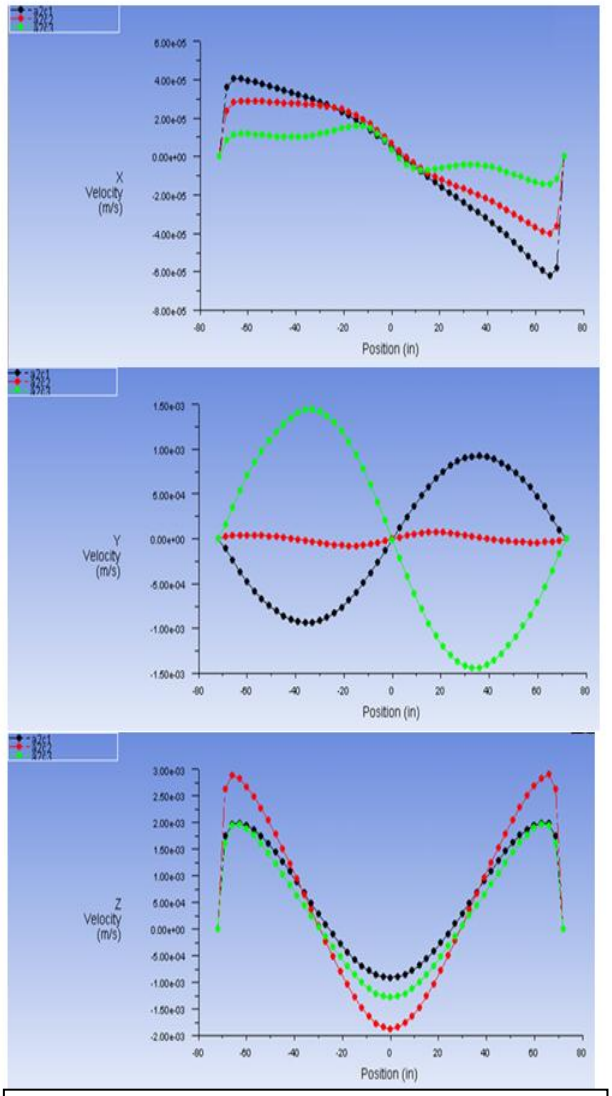

X, Y and Z Velocity Components along y-lines in A2 (y-z) plane at z=2'4.5" (Black), z=4'9" (Red), and z=7'1.5" (Green)

Figure 139: Case 4 - Velocity Components in the A2 Plane at Time T3 = 2:53 PM

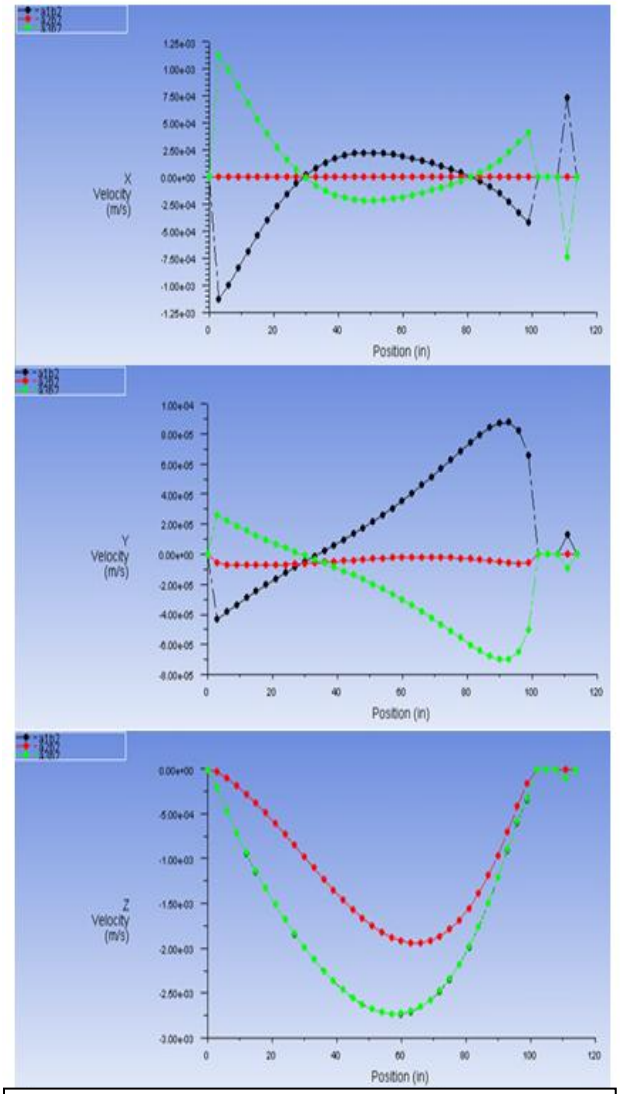

X, Y and Z Velocity Components along z-lines in A2 (y-z) plane at y=3'(Green), y=6'(Red), and y=9'(Black)

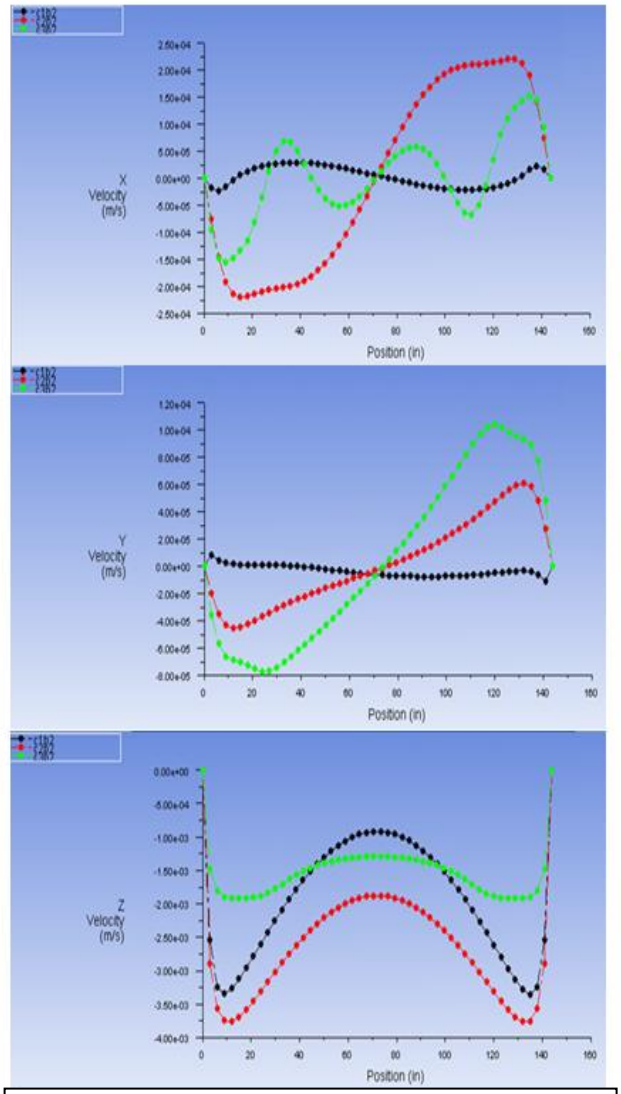

X, Y and Z Velocity Components along y-lines in A2 (y-z) plane at z=2'4.5" (Black), z=4'9" (Red), and z=7'1.5" (Green)

Figure 140: Case 4 - Velocity Components in the B2 Plane at Time T3 = 2:53 PM

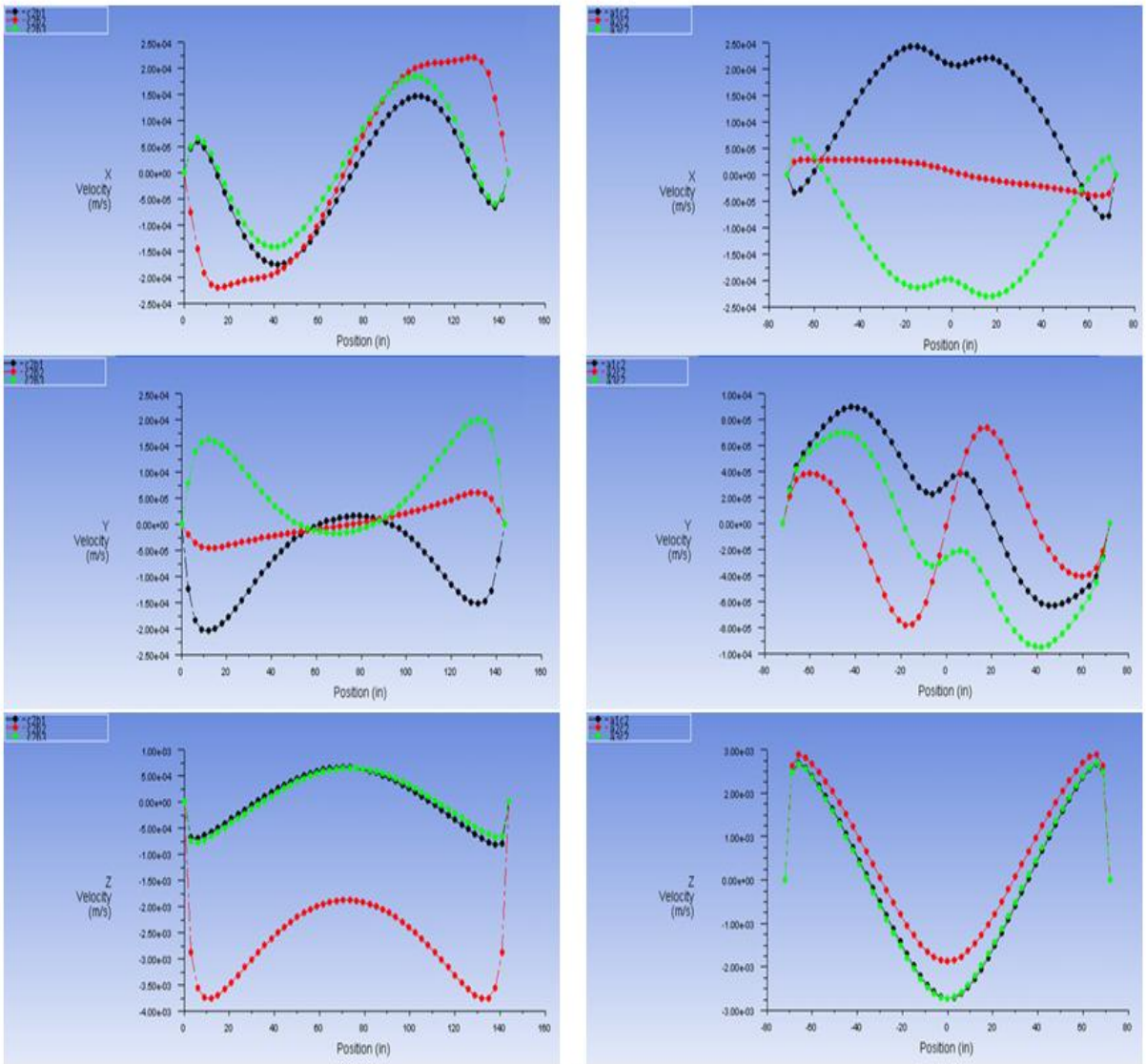

X, Y and Z Velocity Components along x-lines in C2 (x-y) plane at y=3' (Green), y=6' (Red), and y=9' (Black)	X, Y and Z Velocity Components along y-lines in C2 (x-y) plane at x=3' (Green), x=6' (Red), and x=9' (Black)

Figure 141: Case 4 - Velocity Components in the C2 Plane at Time T3 = 2:53 PM

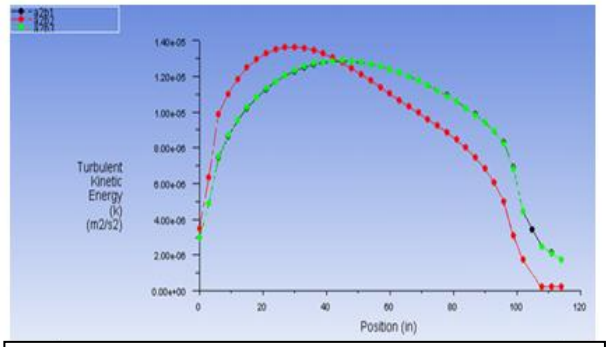

Turbulent Kinetic Energy along z-lines in A2 (y-z) plane at y=3' (Green), y=6'(Red) and y=9'(Black)

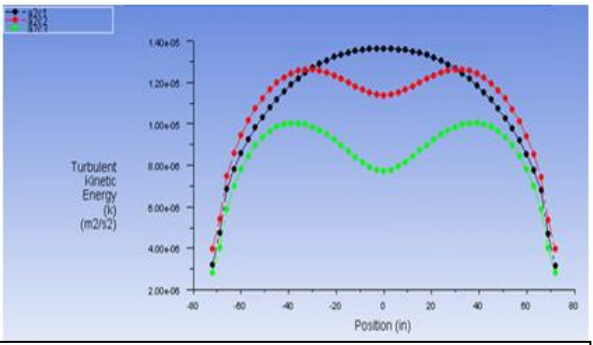

Turbulent Kinetic Energy along y-lines in A2 (y-z) plane at z=2'4.5" (Black), z=4'9"(Red) and z=7'1.5"(Green)

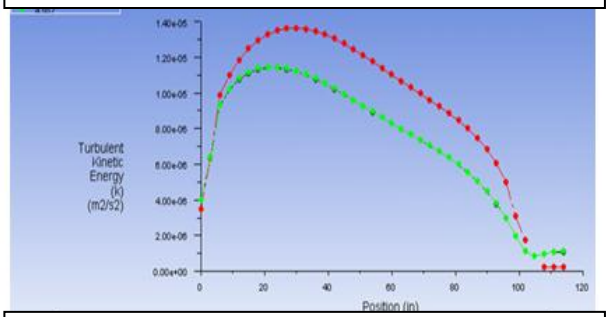

Turbulent Kinetic Energy along z-lines in B2 (x-z) plane at x=3' (Green), x=6'(Red) and x=9'(Black)

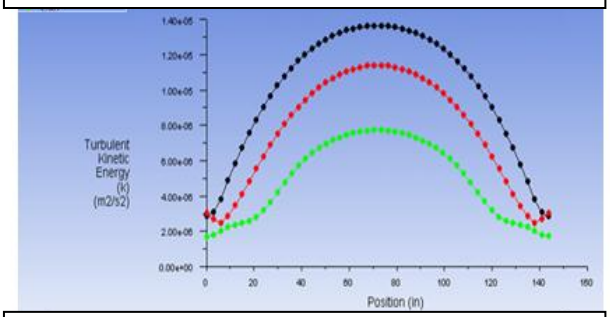

Turbulent Kinetic Energy along x-lines in B2 (x-z) plane at z=2'4.5" (Black), z=4'9"(Red) and z=7'1.5"(Green)

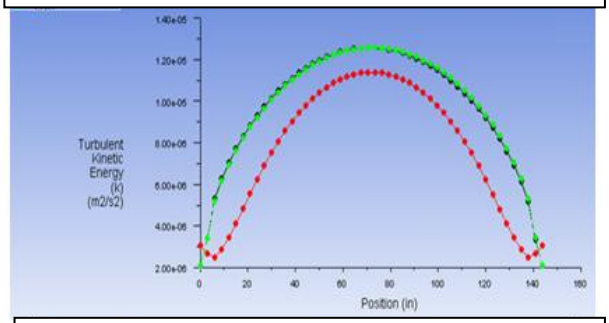

Turbulent Kinetic Energy along x-lines in C2 (x-y) plane at y=3' (Green), y=6'(Red) and y=9'(Black)

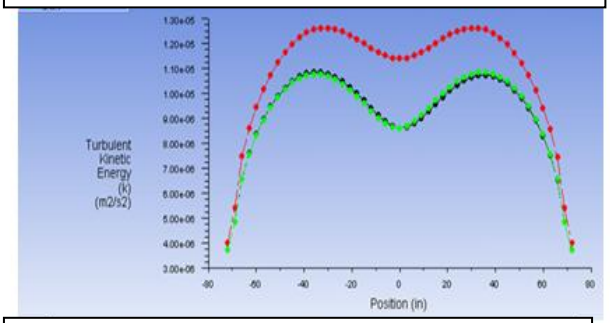

Turbulent Kinetic Energy along y-lines in C2 (x-y) plane at x=3' (Green), x=6'(Red) and x=9'(Black)

Figure 142: Case 4 - Turbulent Kinetic Energy Line Plots at Time T3 = 2:53 PM

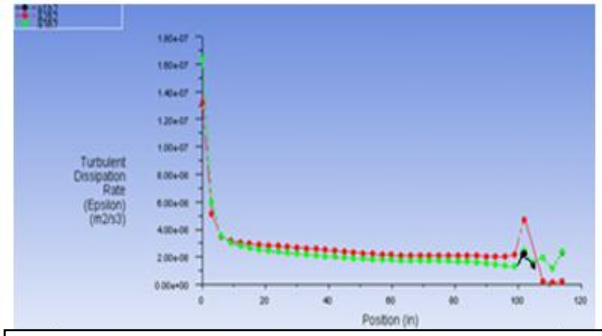

Turbulent Dissipation Rate along z-lines in A2 (y-z) plane at y=3' (Green), y=6'(Red) and y=9'(Black)

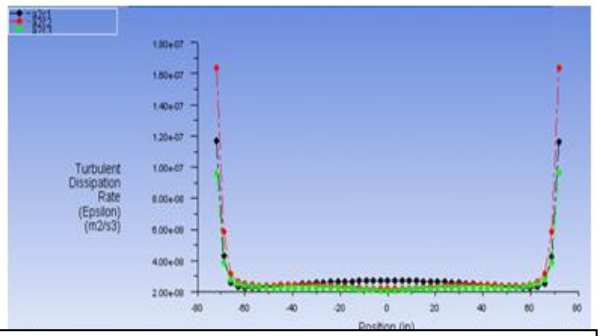

Turbulent Dissipation Rate along y-lines in A2 (y-z) plane at z=2'4.5" (Black), z=4'9"(Red) and z=7'1.5"(Green)

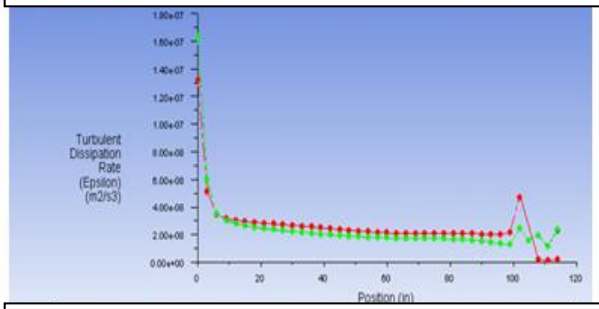

Turbulent Dissipation Rate along z-lines in B2 (x-z) plane at x=3' (Green), x=6'(Red) and x=9'(Black)

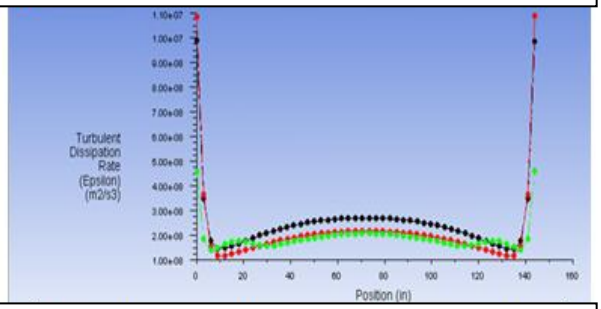

Turbulent Dissipation Rate along x-lines in B2 (x-z) plane at z=2'4.5" (Black), z=4'9"(Red) and z=7'1.5"(Green)

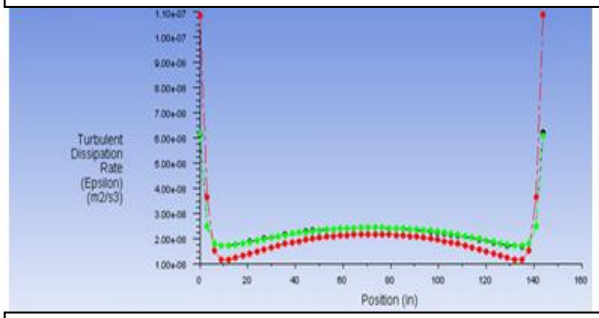

Turbulent Dissipation Rate along x-lines in C2 (x-y) plane at y=3' (Green), y=6'(Red) and y=9'(Black)

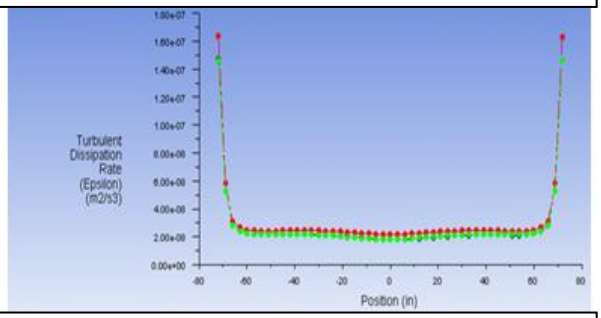

Turbulent Dissipation Rate along y-lines in C2 (x-y) plane at x=3' (Green), x=6'(Red) and x=9'(Black)

Figure 143: Case 4 - Turbulent Dissipation Rate Line Plots at Time T3 = 2:53 PM

The final data set for Case 4 is obtained at T4 = 8:27 PM. This time corresponds to another low temperature inside the room shown by the ASHRAE curve (Figure 7). Figure 144 shows the contours of temperature distributions in different planes (A1-A3, B1-B3, and C1-C3). The lack of heat from the hot external wall results in a nearly constant room temperature. Figure 145 shows the velocity contours in different planes of the room described in Figure 19. These velocities are all very low because the low constant temperature doesn't require much cooling from the ventilation system. Figure 146 shows the various line plots of temperature distribution inside the room along various lines in planes A1-A3, B1-B3, and C1-C3 shown in Figure 19. These plots show that the solution satisfies the adiabatic wall conditions in the room except for the exterior wall where a constant temperature boundary condition is imposed corresponding to the external temperature at time T4 = 8:27PM. These line plots are a quantitative representation of Figure 144.

Figures 147-149 show various velocity components inside the room. These line plots show that the no slip condition is correctly imposed at the walls; all the velocity components go to zero at the walls. Figure 150 shows the turbulent kinetic energy line plots along various cross-sectional lines inside the room; they indicate the relative turbulence intensity in various parts of the room. The values of k are very small because of the very low flow velocities. As expected, the turbulent intensity is greater in the middle of the room than near the walls. Figure 151 shows line plots of the turbulent dissipation rate along various cross-sectional lines inside the room. In contrast to k, the values of epsilon peak near the walls because of the large dissipation of turbulence there. The value of epsilon is fairly constant across the room in all directions and is extremely small near the walls.

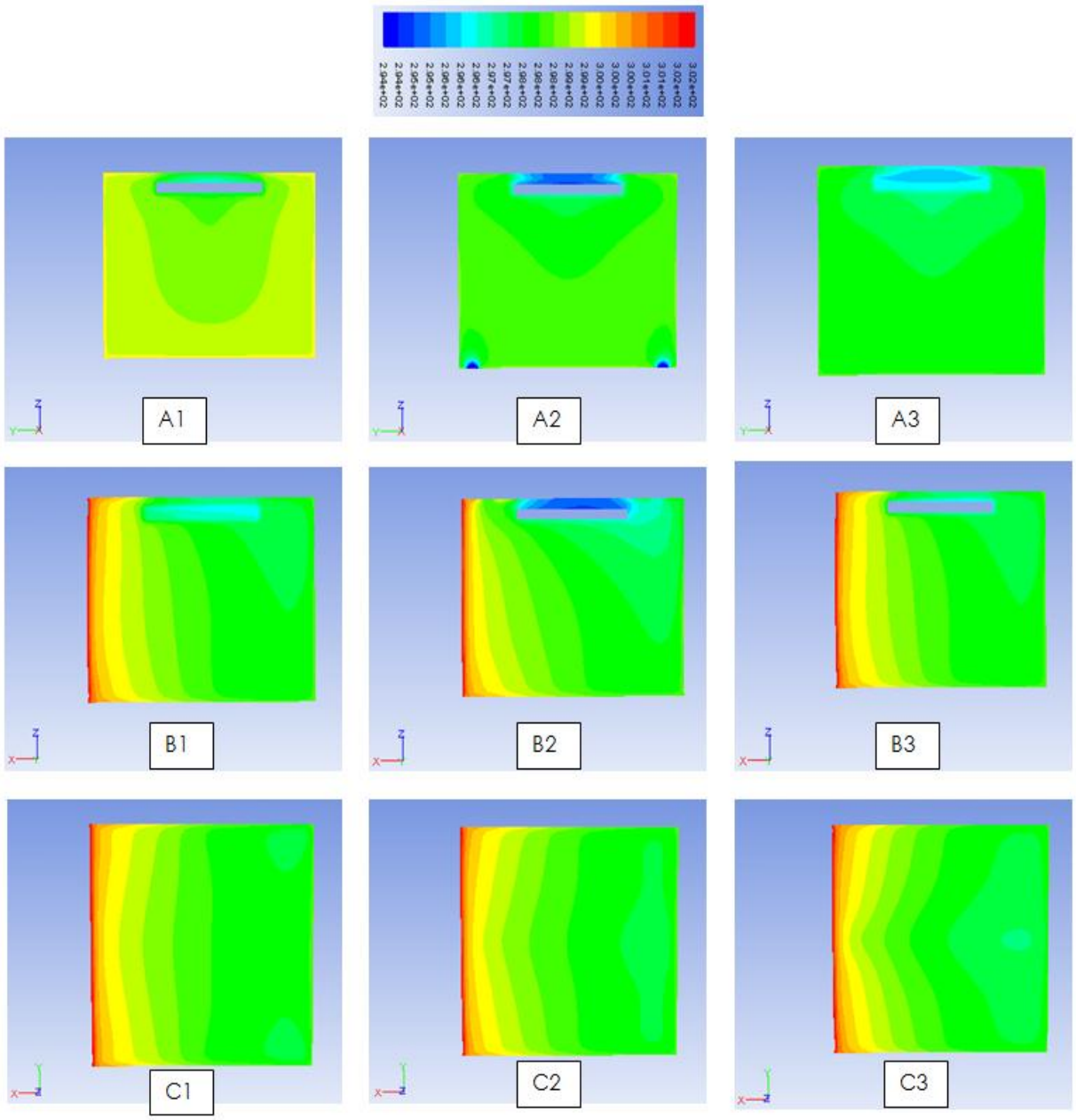

Figure 144: Case 4 - Temperature Contours in Different Planes of Figure 19 at Time T4 = 8:27 PM

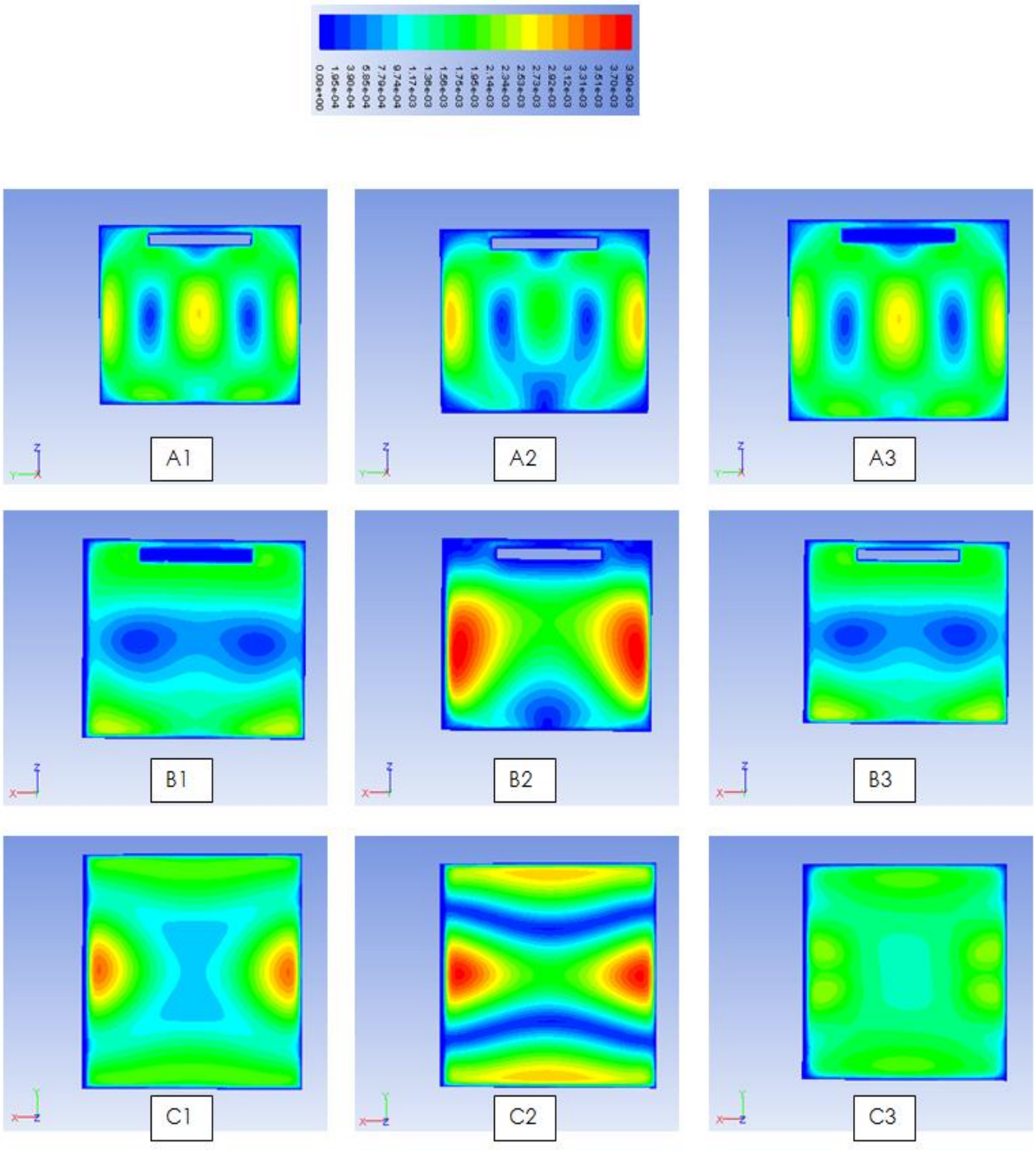

Figure 145: Case 4 - Velocity Contours in Different Planes of Figure 19 at Time T4 = 8:27 PM

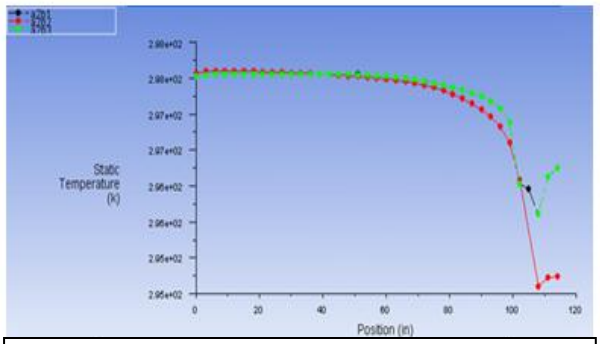

Temperature along z-lines in A2 (y-z) plane at y=3' (Green), y=6'(Red) and y=9'(Black)

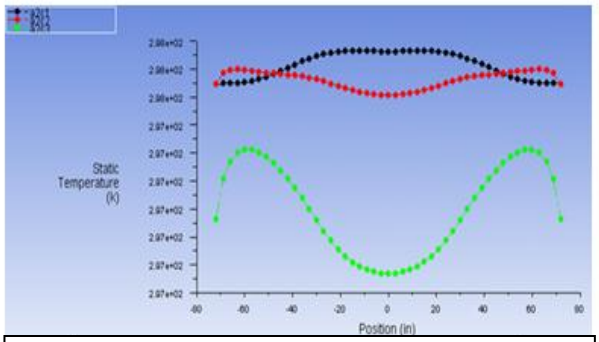

Temperature along y-lines in A2 (y-z) plane at z=2'4.5" (Black), z=4'9"(Red) and z=7'1.5"(Green)

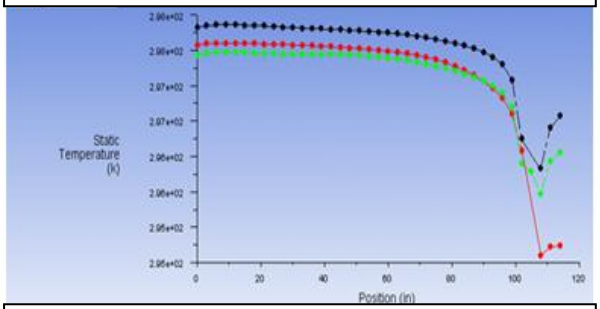

Temperature along z-lines in B2 (x-z) plane at x=3' (Green), x=6'(Red) and x=9'(Black)

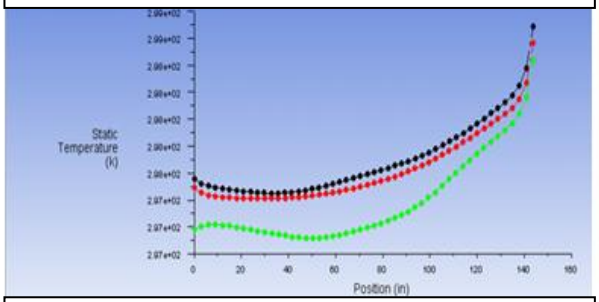

Temperature along x-lines in B2 (x-z) plane at z=2'4.5" (Black), z=4'9"(Red) and z=7'1.5"(Green)

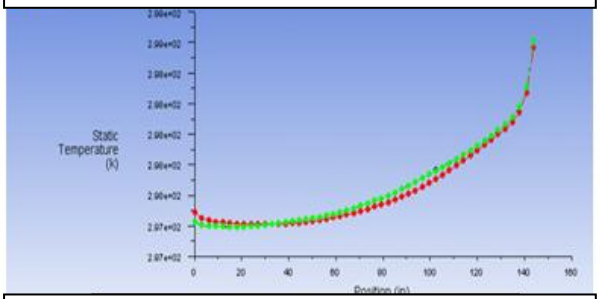

Temperature along x-lines in C2 (x-y) plane at y=3' (Green), y=6'(Red) and y=9'(Black)

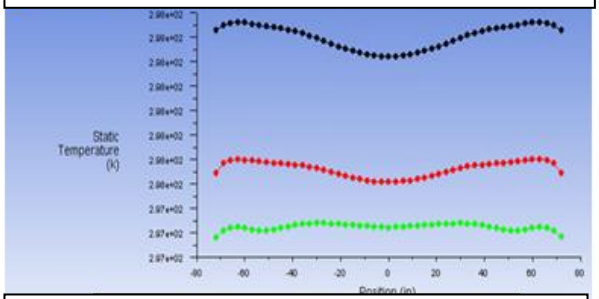

Temperature along y-lines in C2 (x-y) plane at x=3' (Green), x=6'(Red) and x=9'(Black)

Figure 146: Case 4 – Temperature Line Plots at Time T4 = 8:27 PM

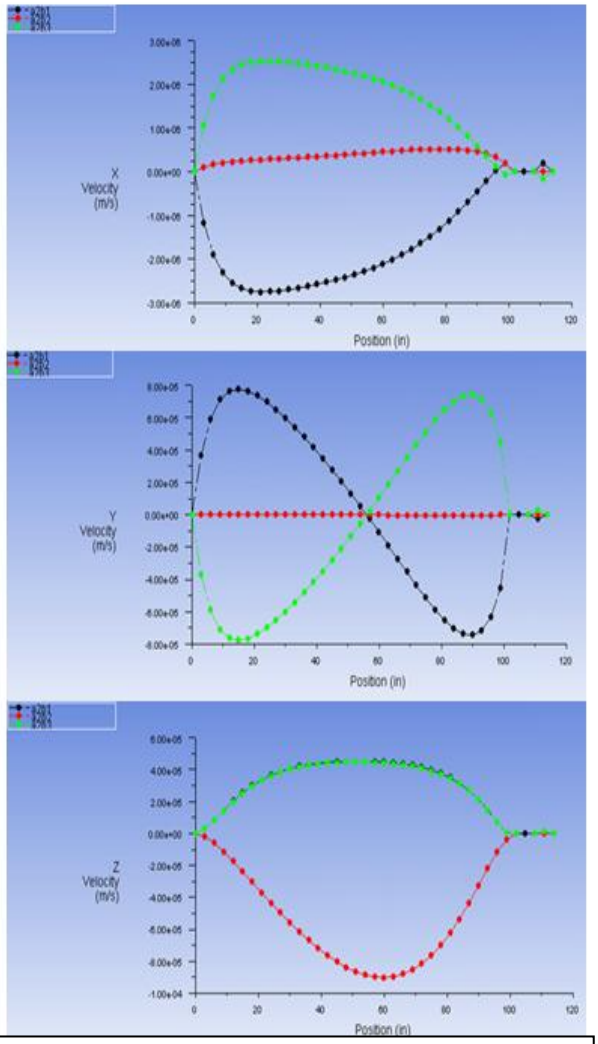

X, Y and Z Velocity Components along z-lines in A2 (y-z) plane at y=3'(Green), y=6'(Red), and y=9'(Black)

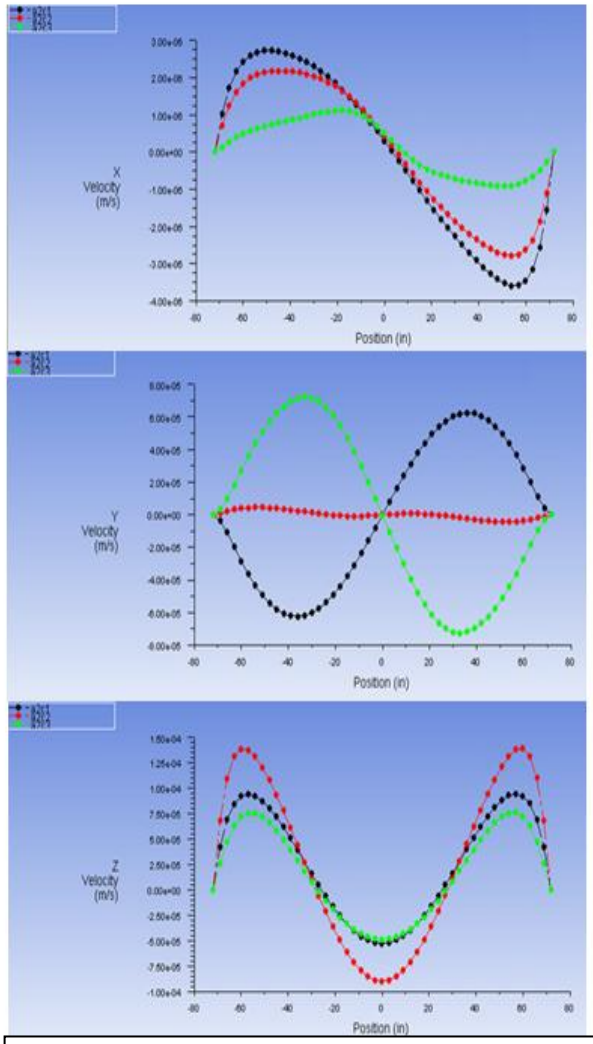

X, Y and Z Velocity Components along y-lines in A2 (y-z) plane at z=2'4.5" (Black), z=4'9" (Red), and z=7'1.5" (Green)

Figure 147: Case 4 - Velocity Plots on the A2 Plane at Time T4 = 8:27 PM

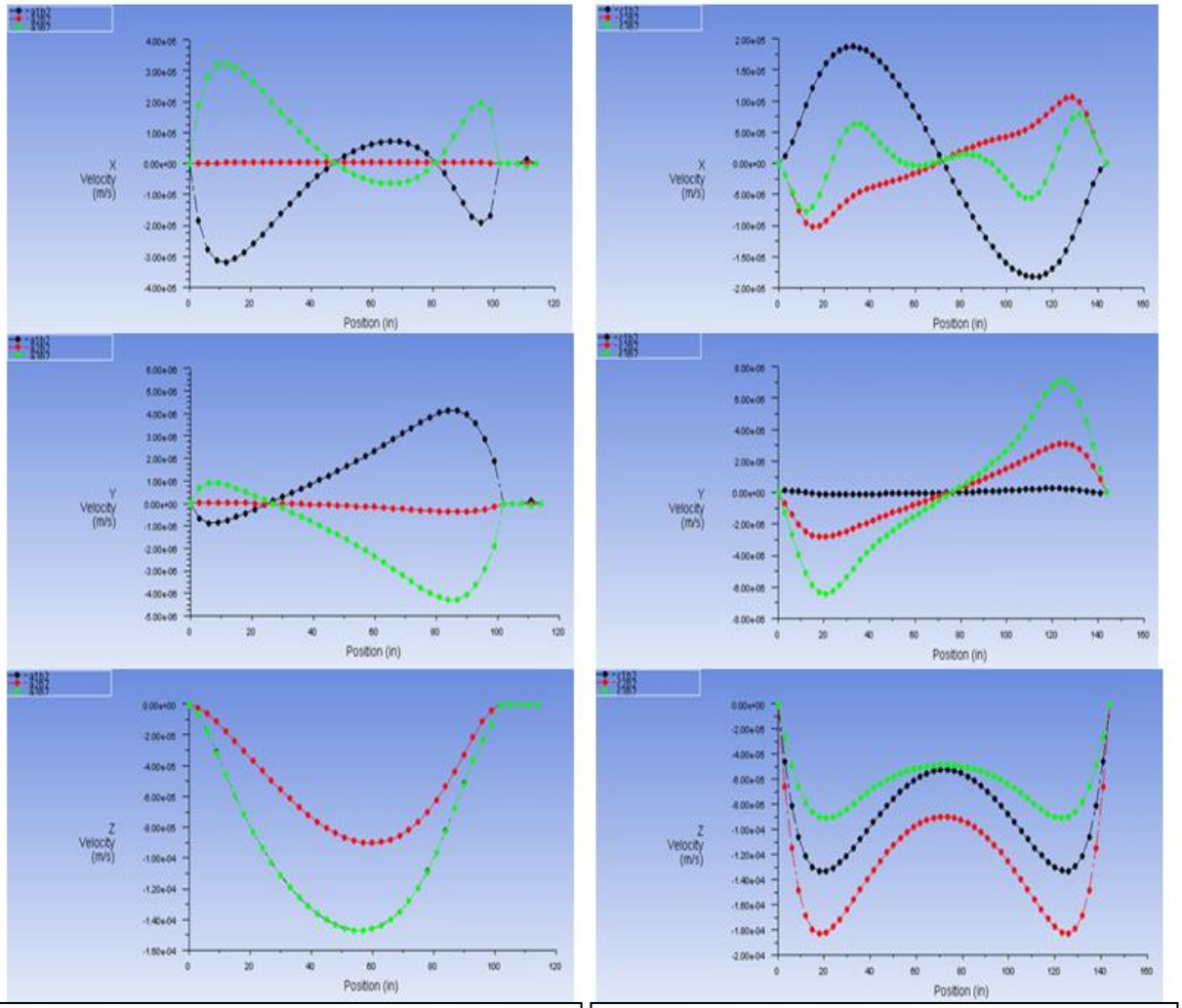

X, Y and Z Velocity Components along z-lines in B2(x-z) plane at x=3'(Green), x=6'(Red), and x=9'(Black)	X, Y and Z Velocity Components along x-lines in B2 (x-z) plane at z=2'4.5" (Black), z=4'9" (Red), and z=7'1.5"(Green)

Figure 148: Case 4 - Velocity Components in the B2 Plane at Time T4 = 8:27 PM

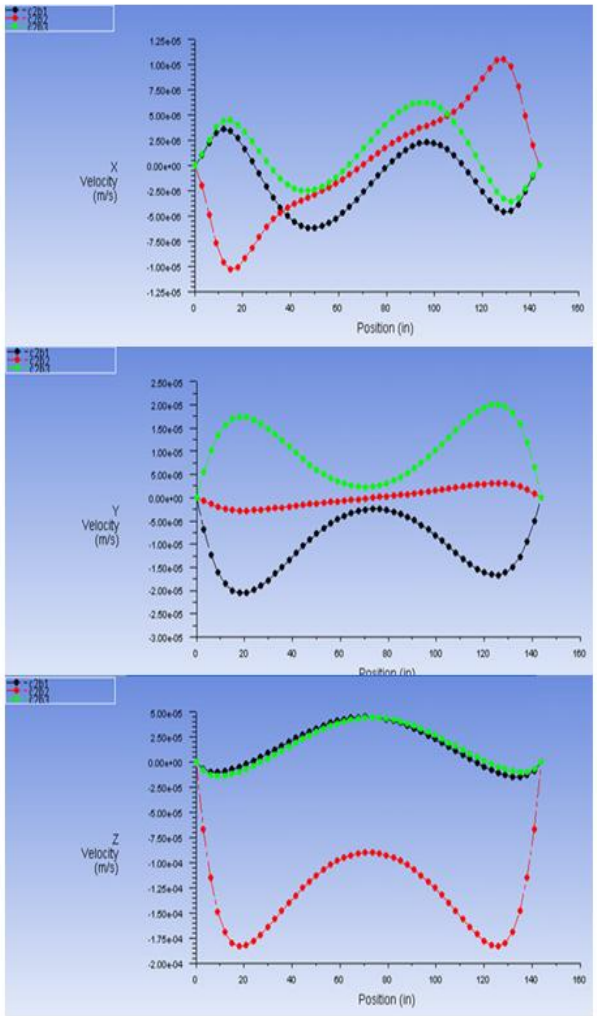

X, Y and Z Velocity Components along x-lines in C2 (x-y) plane at y=3' (Green), y=6' (Red), and y=9' (Black)

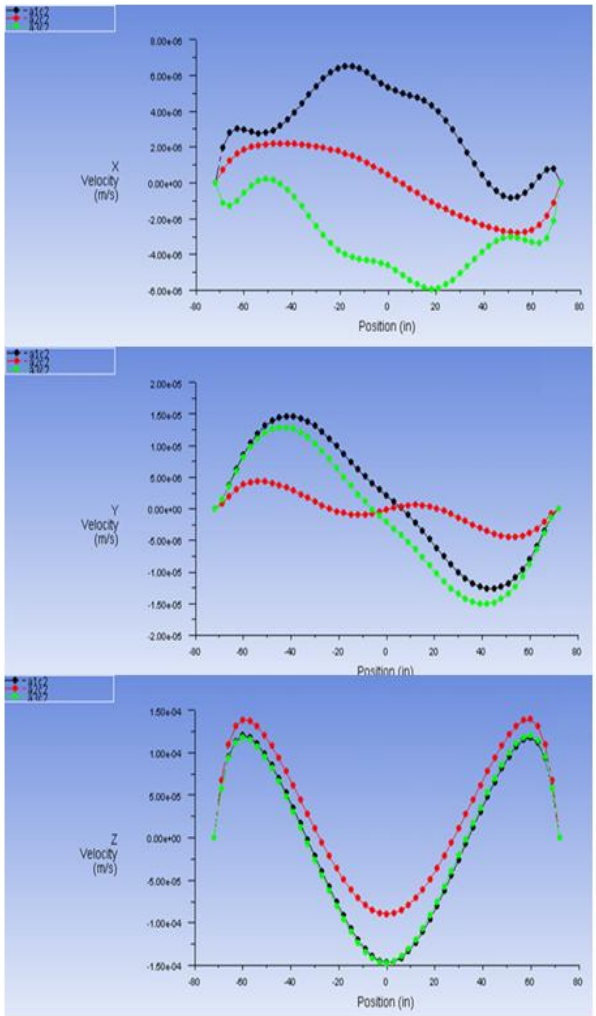

X, Y and Z Velocity Components along y-lines in C2 (x-y) plane at x=3' (Green), x=6' (Red), and x=9' (Black)

Figure 149: Case 4 - Velocity Components in the C2 Plane at Time T4 = 8:27 PM

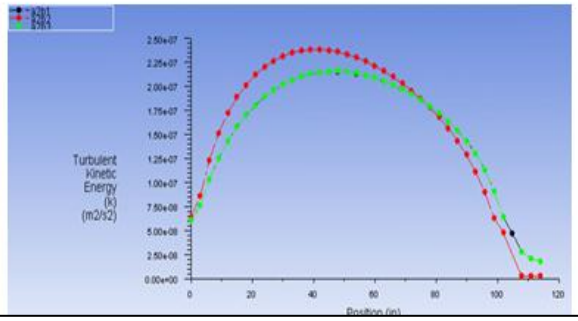

Turbulent Kinetic Energy along z-lines in A2 (y-z) plane at y=3' (Green), y=6'(Red) and y=9'(Black)

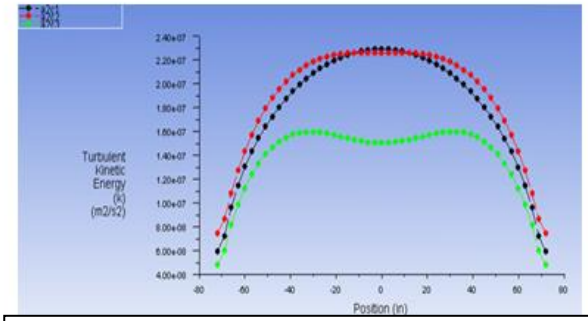

Turbulent Kinetic Energy along y-lines in A2 (y-z) plane at z=2'4.5" (Black), z=4'9"(Red) and z=7'1.5"(Green)

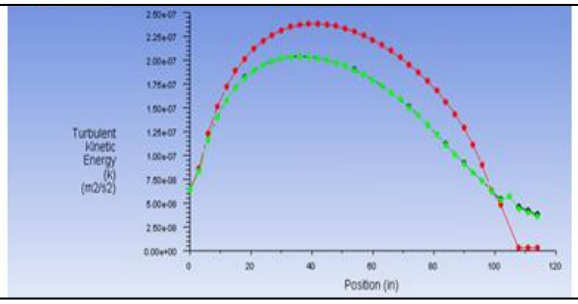

Turbulent Kinetic Energy along z-lines in B2 (x-z) plane at x=3' (Green), x=6'(Red) and x=9'(Black)

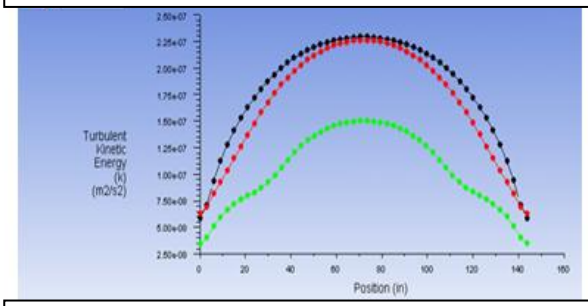

Turbulent Kinetic Energy along x-lines in B2 (x-z) plane at z=2'4.5" (Black), z=4'9"(Red) and z=7'1.5"(Green)

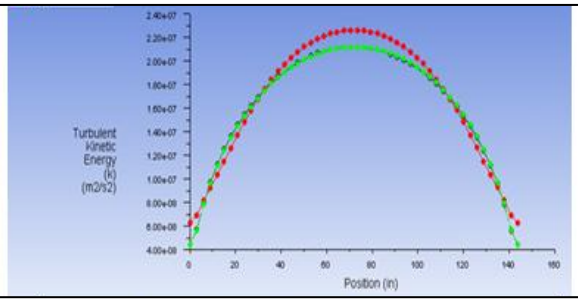

Turbulent Kinetic Energy along x-lines in C2 (x-y) plane at y=3' (Green), y=6'(Red) and y=9'(Black)

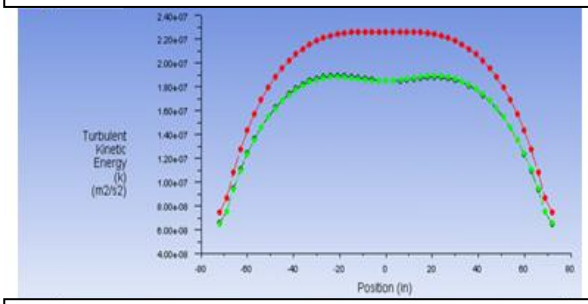

Turbulent Kinetic Energy along y-lines in C2 (x-y) plane at x=3' (Green), x=6'(Red) and x=9'(Black)

Figure 150: Case 4 - Turbulent Kinetic Energy Line Plots at Time T4 = 8:27 PM

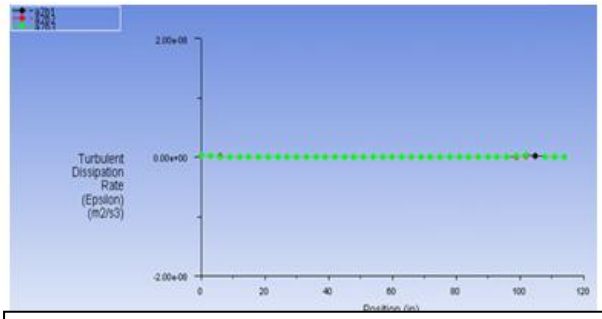

Turbulent Dissipation Rate along z-lines in A2 (y-z) plane at y=3' (Green), y=6'(Red) and y=9'(Black)

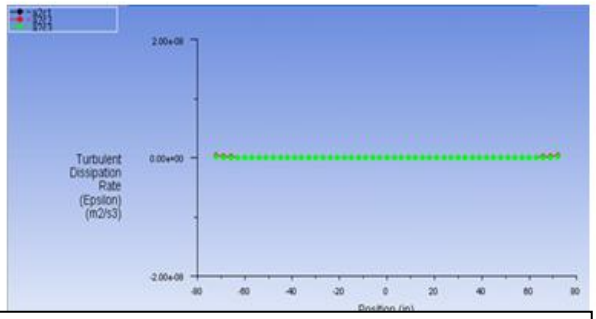

Turbulent Dissipation Rate along y-lines in A2 (y-z) plane at z=2'4.5" (Black), z=4'9"(Red) and z=7'1.5"(Green)

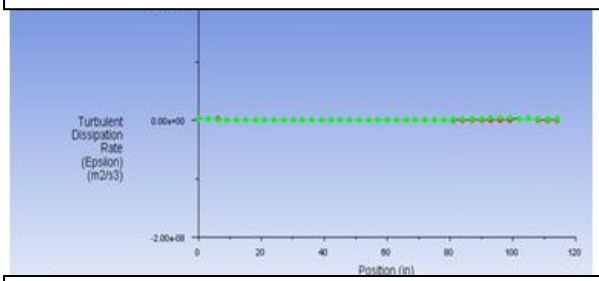

Turbulent Dissipation Rate along z-lines in B2 (x-z) plane at x=3' (Green), x=6'(Red) and x=9'(Black)

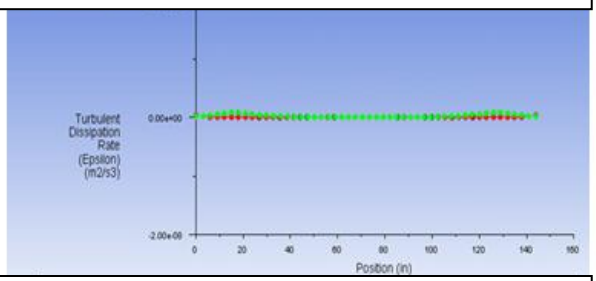

Turbulent Dissipation Rate along x-lines in B2 (x-z) plane at z=2'4.5" (Black), z=4'9"(Red) and z=7'1.5"(Green)

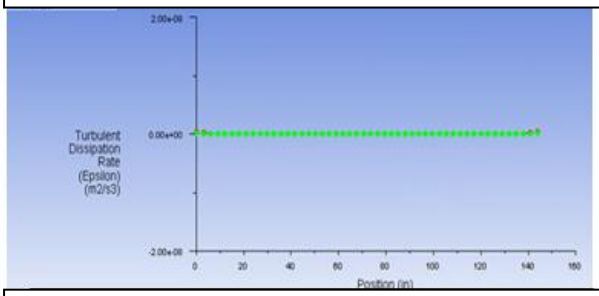

Turbulent Dissipation Rate along x-lines in C2 (x-y) plane at y=3' (Green), y=6'(Red) and y=9'(Black)

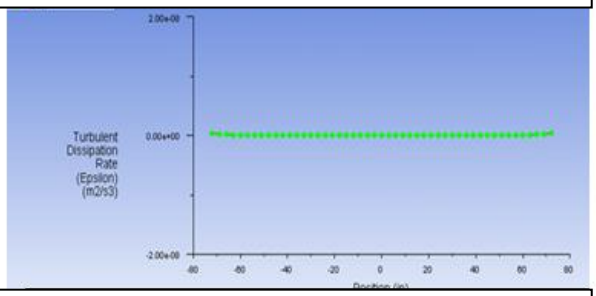

Turbulent Dissipation Rate along y-lines in C2 (x-y) plane at x=3' (Green), x=6'(Red) and x=9'(Black)

Figure 151: Case 4 - Turbulent Dissipation Rate Line Plots at Time T4 = 8:27 PM

5.4.6 3-D Temperature Contours

In order to get a better visualization of the temperature distribution in the entire room, 3-D contours have been generated as shown in Figures 152-167. These figures show these contours for all four ventilation systems at four different time intervals (T1 = 3:45 AM, T2 = 9:20 AM, T3 = 2:53 PM and T4 = 8:27 PM) during a 24 hour day. In each of these figures, the exterior wall is closest to the viewer. From these figures, it can be noticed that as the day progresses, the external wall grows hotter as expected, until time T3 = 2:53PM. By the time T4 = 8:27 PM, the external wall has become substantially cooler which is reflected in the temperature distribution inside the room. These three-dimensional views are also very helpful in comparing the temperatures in various parts of the room for the four ventilation systems at different times during the day. It is clear from Figures 164-167 that the temperature distribution for the DV system with radiation slab is the most uniform and therefore is the most desirable for thermal comfort.

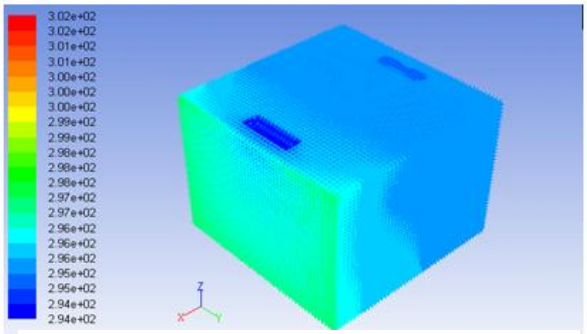

Figure 152: Case 1 – 3-D Temperature Contours at T1

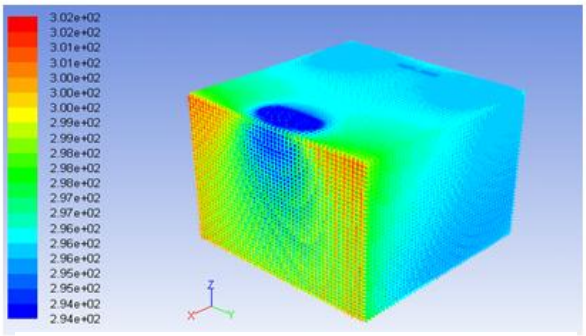

Figure 153: Case 1 – 3-D Temperature Contours at T2

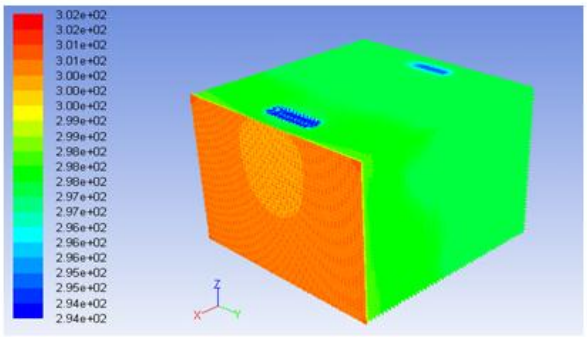

Figure 154: Case 1 – 3-D Temperature Contours at T3

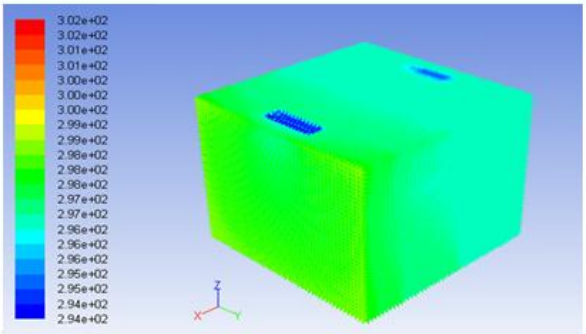

Figure 155: Case 1 – 3-D Temperature Contours at T4

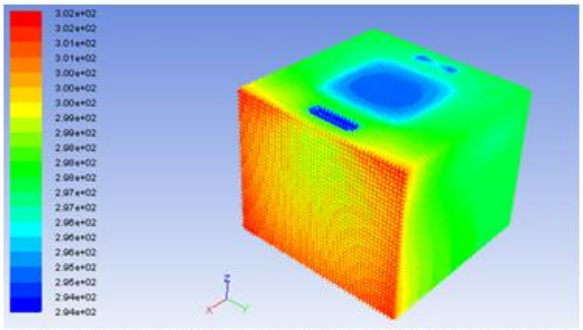

Figure 156: Case 2 – 3-D Temperature Contours at T1

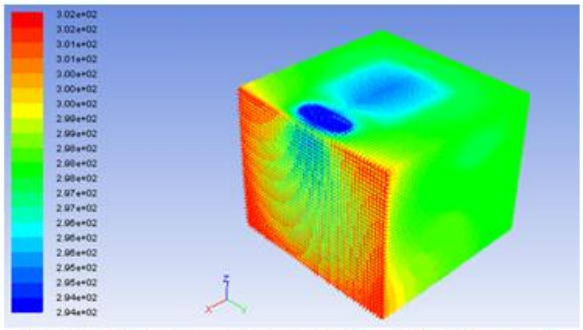

Figure 157: Case 2 – 3-D Temperature Contours at T2

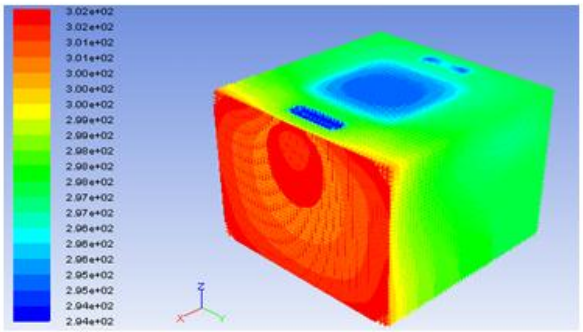

Figure 158: Case 2 – 3-D Temperature Contours at T3

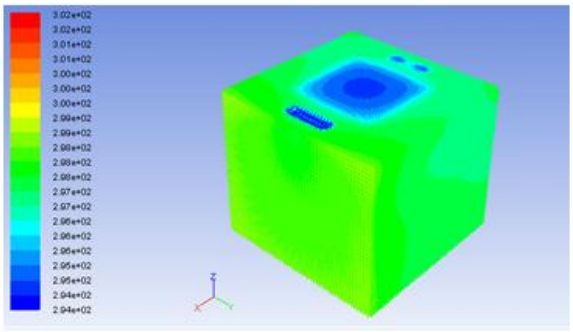

Figure 159: Case 2 – 3-D Temperature Contours at T4

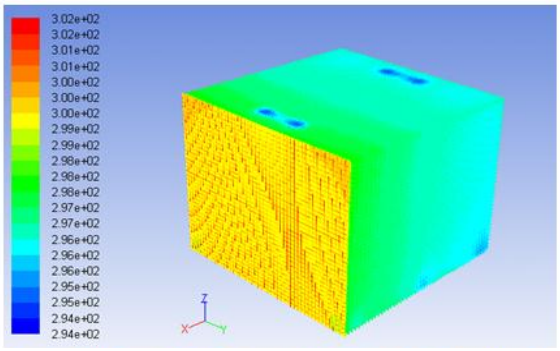

Figure 160: Case 3 – 3-D Temperature Contours at T1

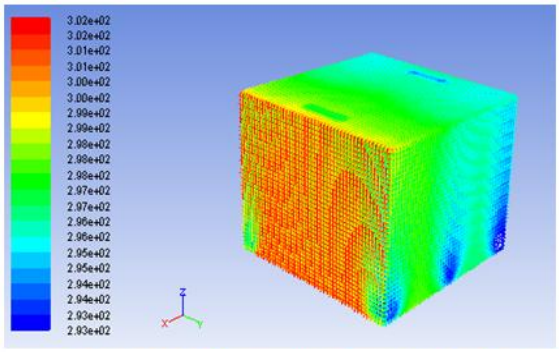

Figure 161: Case 3 – 3-D Temperature Contours at T2

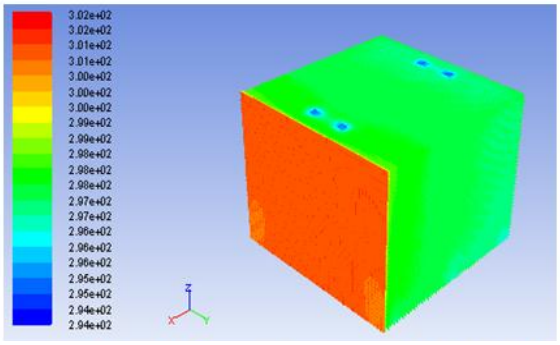

Figure 162: Case 3 – 3-D Temperature Contours at T3

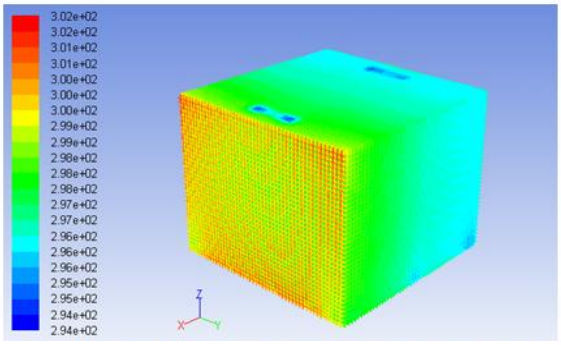

Figure 163: Case 3 – 3-D Temperature Contours at T4

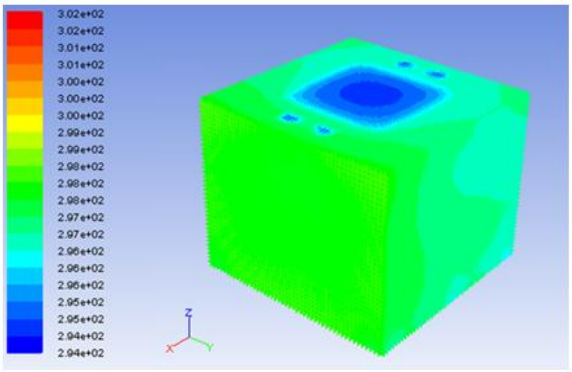

Figure 164: Case 4 – 3-D Temperature Contours at T1

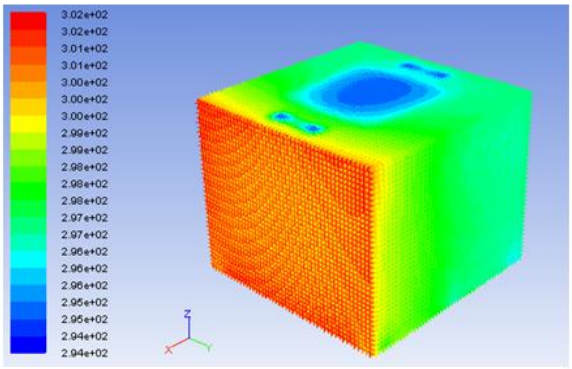

Figure 165: Case 4 – 3-D Temperature Contours at T2

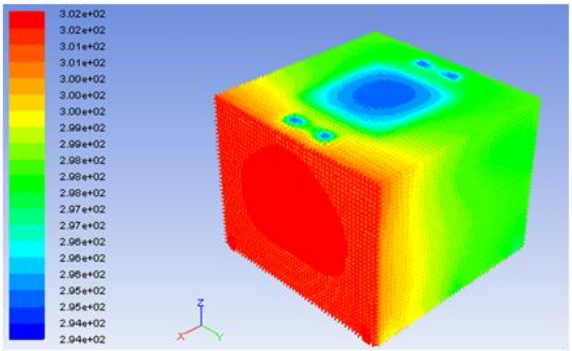

Figure 166: Case 4 – 3-D Temperature Contours at T3

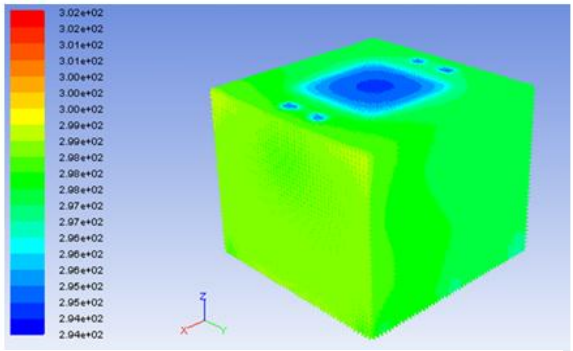

Figure 167: Case 4 – 3-D Temperature Contours at T4

5.4.7 Total Mass Flow and Energy Input

The calculation of total mass flow circulation inside the room during a 24-hour period is an excellent way to determine the relative efficiency of different ventilation systems. Although each ventilation system supplies the same amount of air at the same rate when it is on, its frequency varies with time. Figures 168-171 show the mass flow rate injected into the room at different time steps (each time step = 10 seconds) throughout the day for each ventilation system. By comparing the mass flow injected into the room for the four cases (Figures 168-171), it can be easily noticed that the addition of radiation cooling in both the VAV and DV system requires much less input of mass flow of low temperature air into the room to keep it at the desired comfortable temperature. Case 2 (VAV with radiation slab) and Case 4 (DV with radiation slab) use the air ventilation system only during the hotter parts of the day, whereas Case 1 (VAV) and Case 3 (DV) require the ventilation systems to cycle air all through the day. Figures 172-175 show the variation of average volume temperature and the controller temperature for the four ventilation systems. The controller temperature and the average volume temperature behave in similar fashion; however, in the case of DV, the average volume temperature tends to be higher than the control point temperature, while the reverse is true in the cases for the VAV system. This is most likely caused by the way the flow field develops in these cases. The DV case takes more advantage of the natural buoyancy of the air, effectively pushing the warmer air higher towards the ceiling. Therefore, while the average volume temperature for the DV case may be slightly higher, the air temperature in the larger part of the room is nearly the same as in other cases. It can also be noticed that at some instances of time, the average volume temperature and the controller temperature overshoot the desired upper and lower values of

the temperatures in the room; however the overall performance of the controller is acceptable and is sufficient for the evaluation of the four ventilation systems.

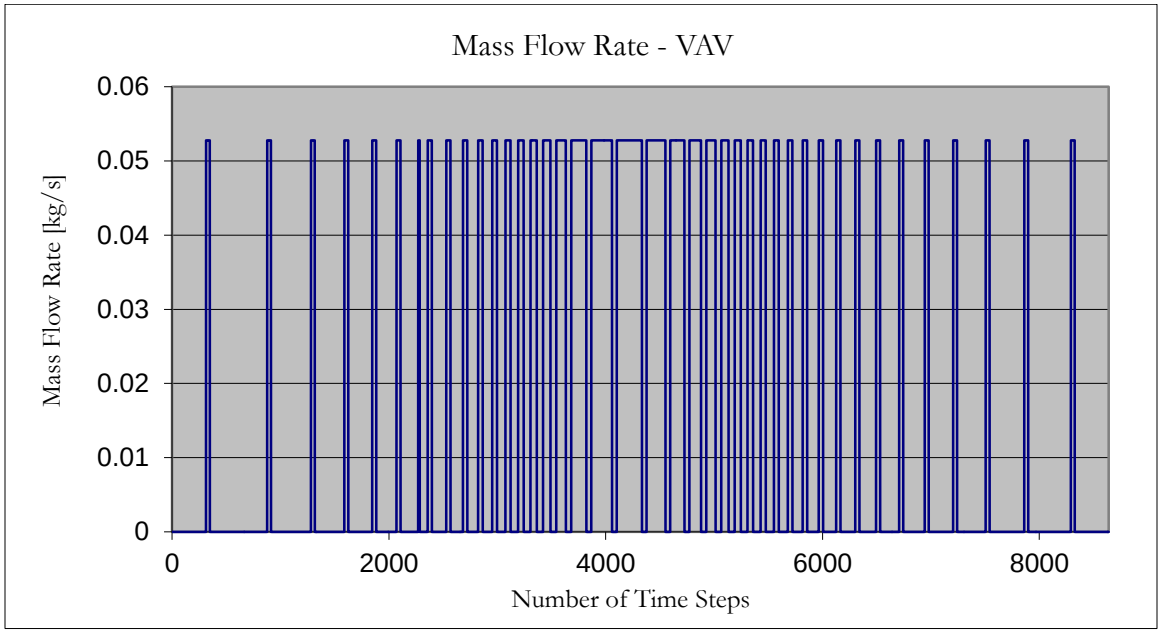

Figure 168: Mass Flow Rate for the VAV System with 10 Second Time Steps

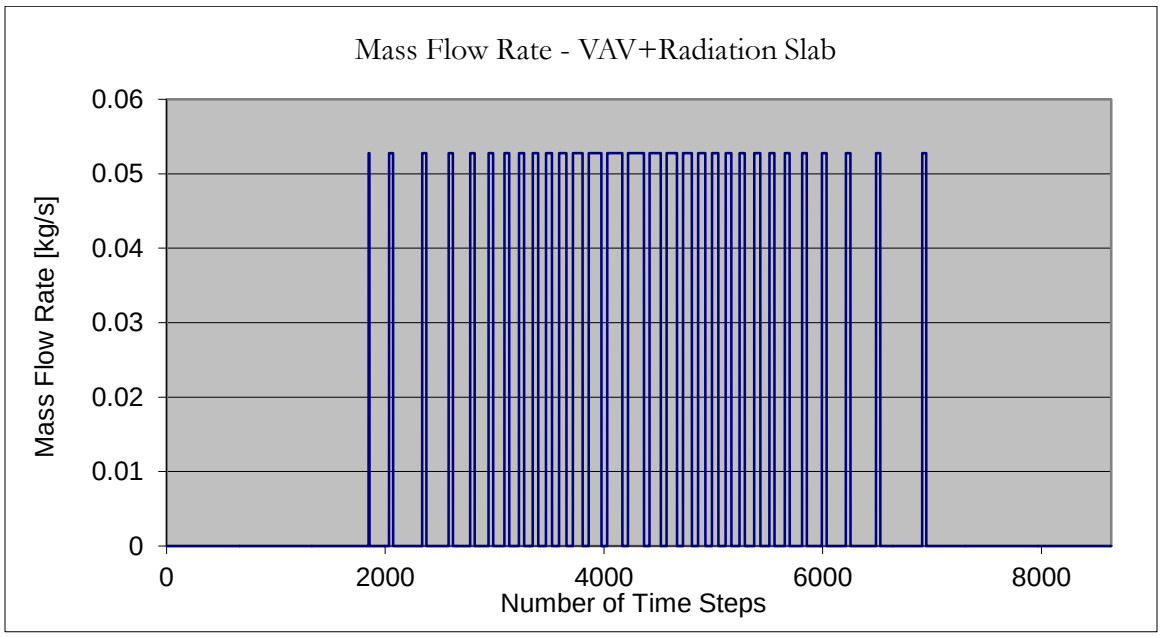

Figure 169: Mass Flow Rate for the VAV System with Radiant Cooling with 10 Second Time Steps

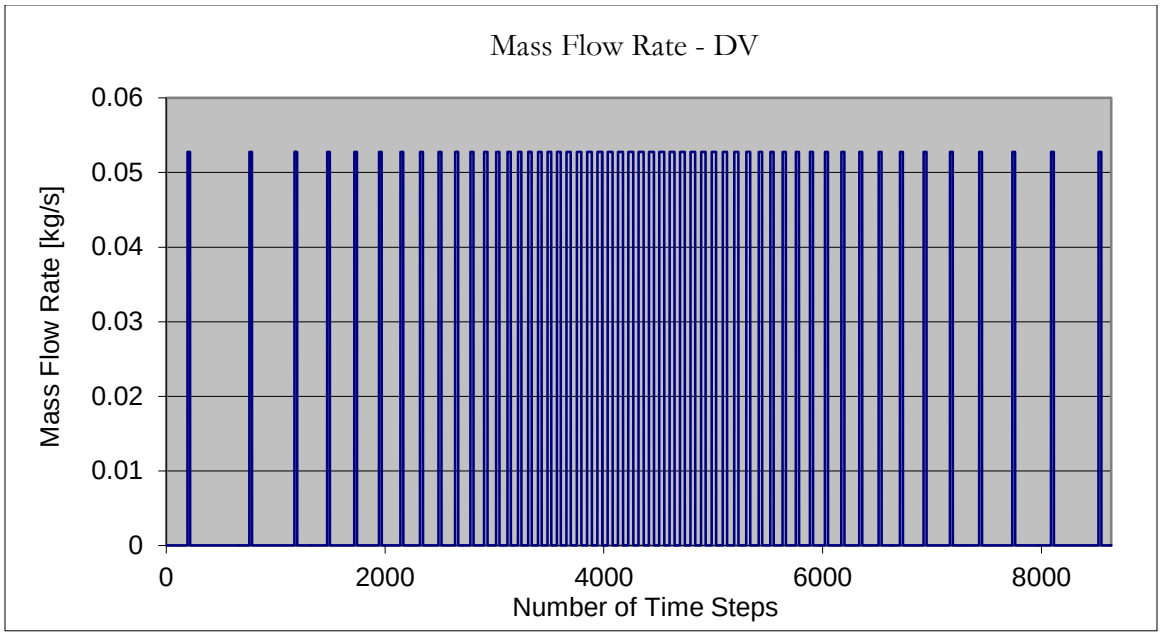

Figure 170: Mass Flow Rate for the DV System with 10 Second Time Steps

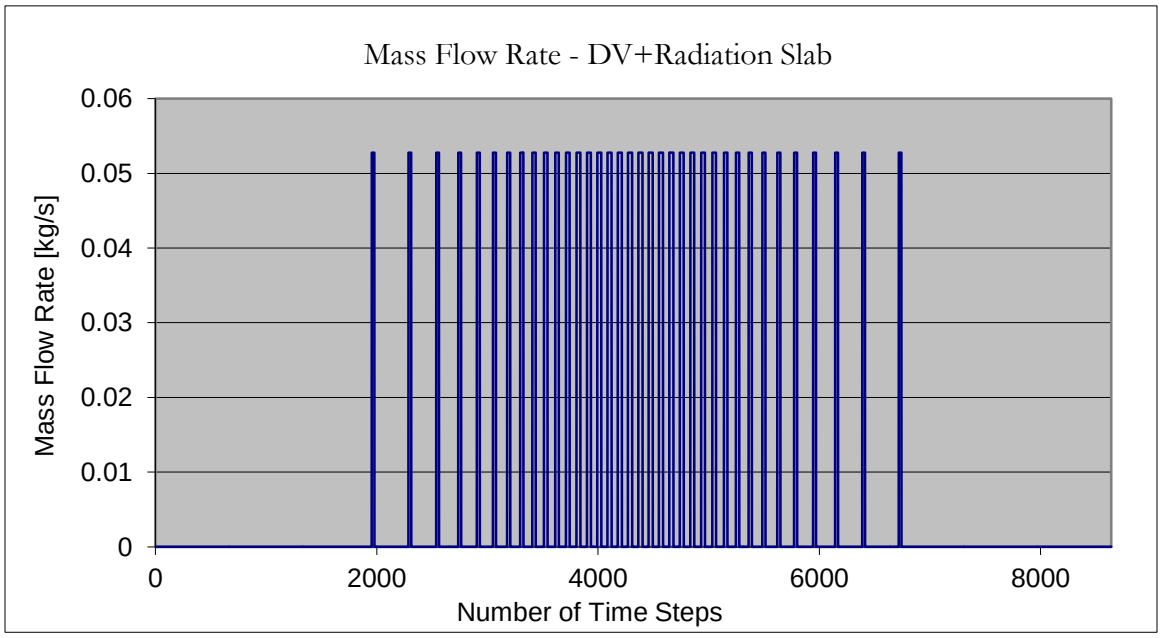

Figure 171: Mass Flow Rate for the DV System with Radiant Cooling with 10 Second Time Steps

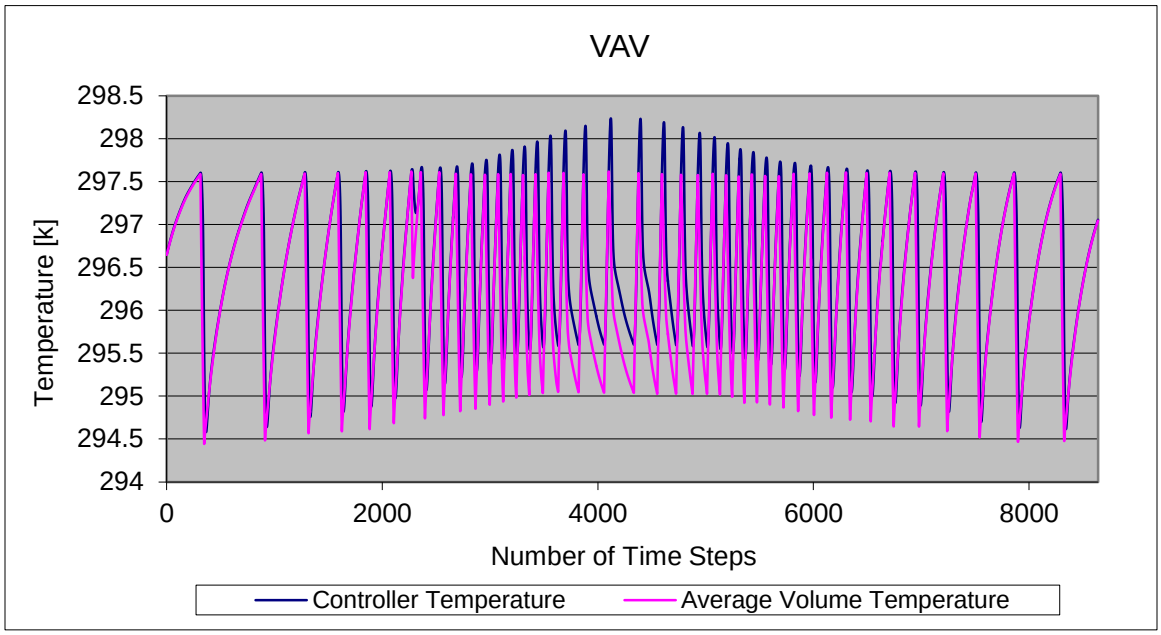

Figure 172: Controller Temperature and Average Room Temperature for the VAV System with 10 Second Time Steps

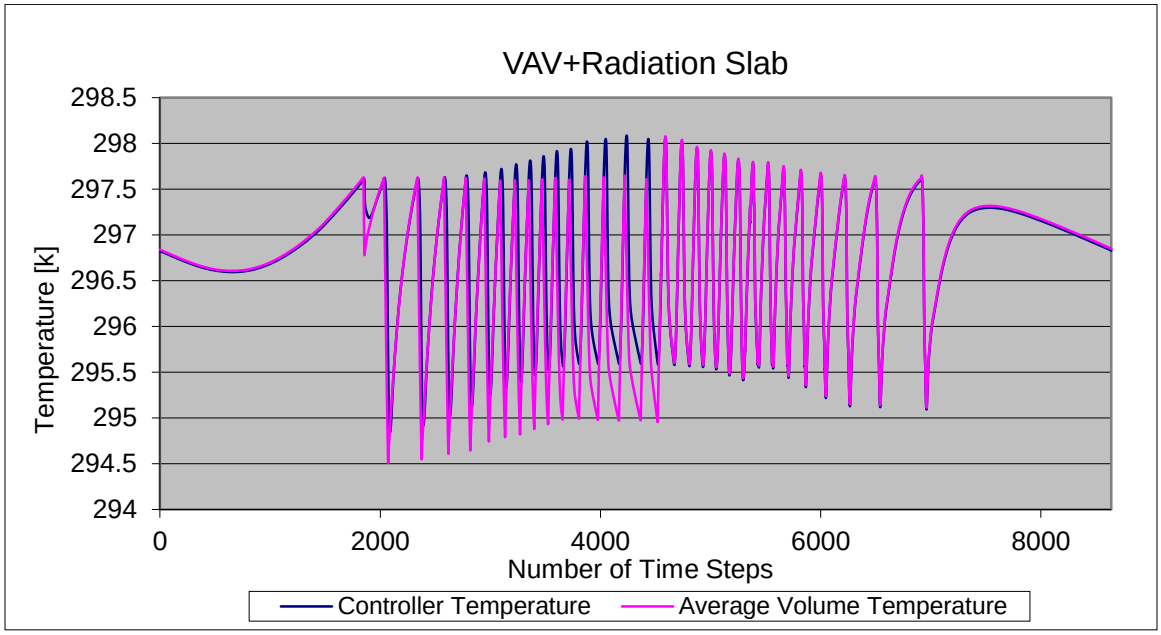

Figure 173: Controller Temperature and Average Room Temperature for the VAV System with Radiant Cooling with 10 Second Time Steps

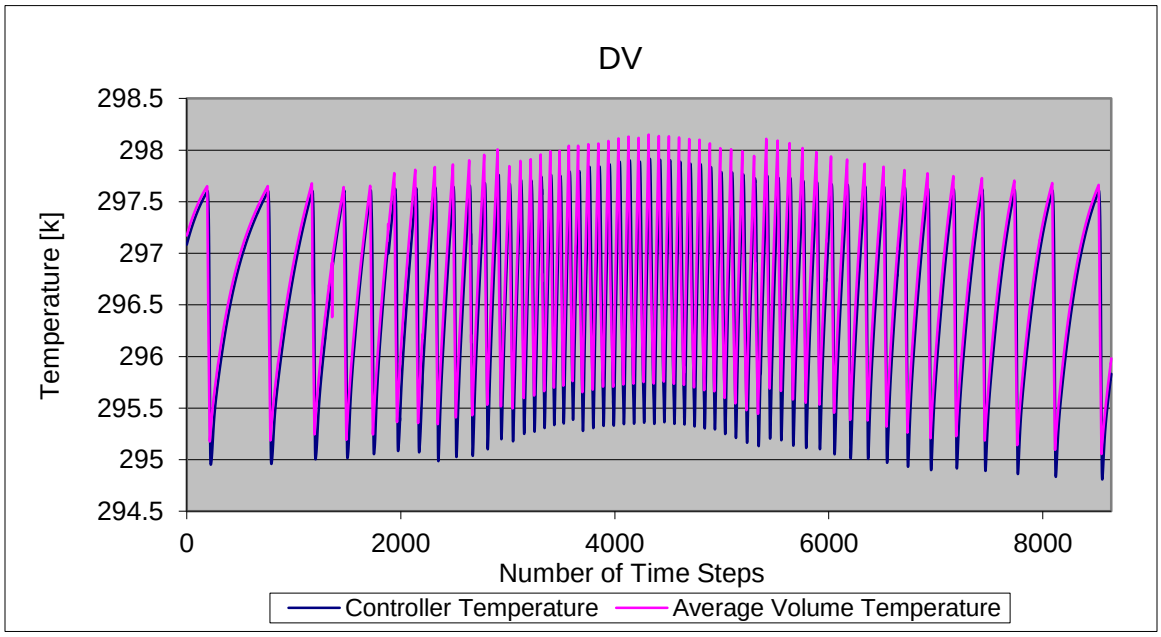

Figure 174: Controller Temperature and Average Room Temperature for the DV System with 10 Second Time Steps

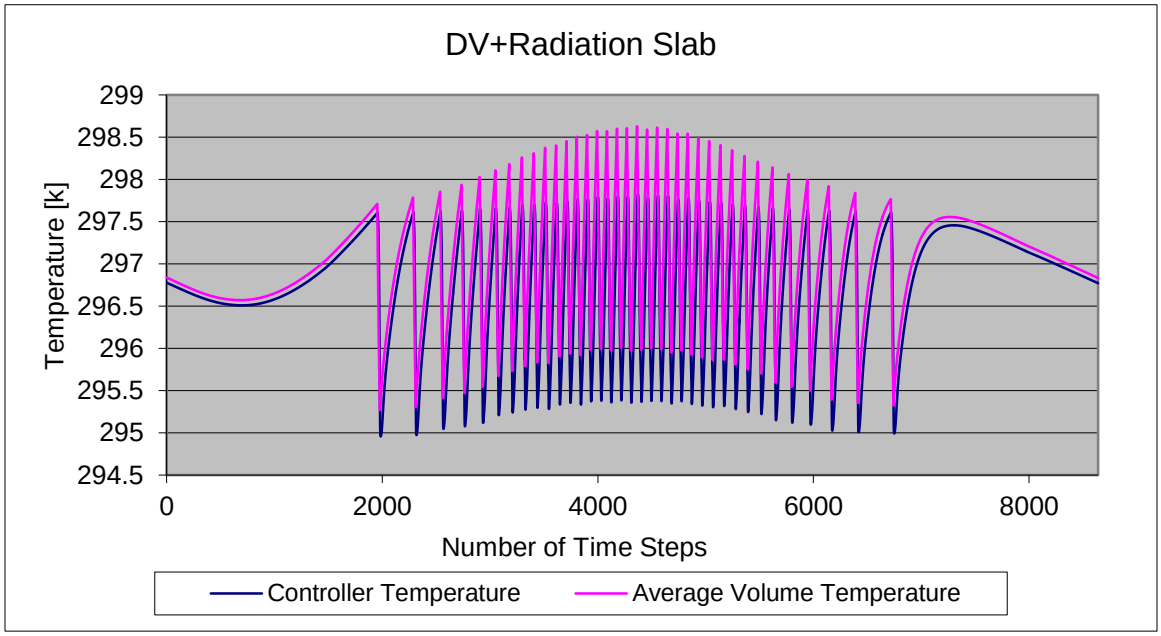

Figure 175: Controller Temperature and Average Room Temperature for the DV System with Radiant Cooling with 10 Second Time Steps

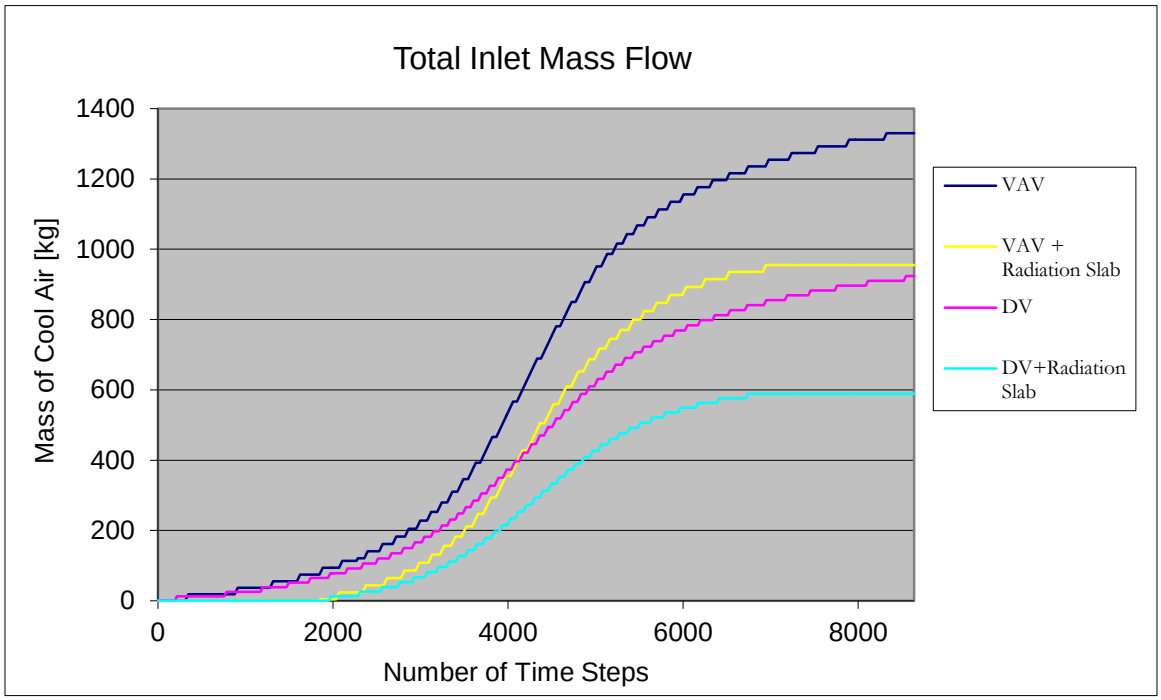

Figure 176: Total Mass of Cold Air Injected into the Room for Cases 1 ,2, 3 and 4 with 10 Second Time Steps

Figure 176 shows the total amount of cold air injected into the room over a 24 hour cycle for the four ventilation systems. This figure shows that in order to keep the model room within the same specified temperature band, the VAV system requires the maximum amount of cold air, followed by the VAV system with radiant cooling , which is followed by the DV system. The DV system with radiant cooling requires the least amount of cold air. By comparing the total mass flows required by the four ventilation systems, it can be observed that by switching from the VAV system to a DV system, cold air requirements can be reduced by 26%. When a radiation slab is added to the VAV system, cold air requirements are reduced by 28%. When a radiation slab is added to the DV system, cold air requirements are reduced by 39%; they reduce by 56% compared to the VAV system.

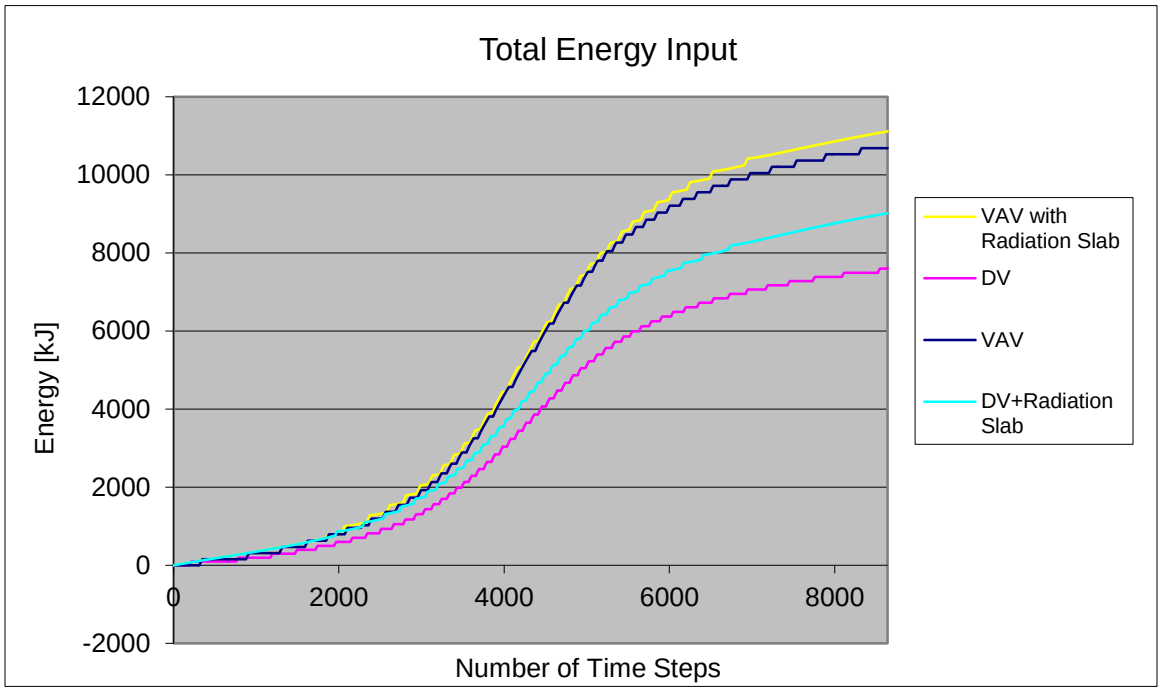

Figure 177: Total Energy Input into Ventilation Systems

The most informative way to compare the efficiency of the four ventilation systems is to compare the amount of energy required to keep the temperature in the room within the specified temperature band. This energy can be calculated by using equations (5.1) and (5.2). Equation 5.1 is applicable in calculating the energy input due to the injection of cold air through the inlet vents; it does not account for the energy input in the chilled radiation slab.

$$\int \dot{m} * C_p * (T_{outside} - T_{cold-jet}) dt \tag{5.1}$$

For the two systems with radiation slab, Equation 5.1 was used to calculate the energy input due to the injection of cold air through the inlet vent, which was then added to the energy input due to the chilled radiation slab to obtain the total energy input for the system. The energy input due to the radiation slab was calculated by Equation (5.2). *Flux* refers to the total amount of heat flux leaving the radiation slab from all the surfaces, and the *Area* in Equation (5.2) refers to the total surface area of the slab. The energy obtained from this calculation was negative due to the cooling effect of the slab, but these numbers were reversed in sign in order to correctly obtain the total energy required for the system.

$$\int Flux * Area * dt \tag{5.2}$$

Comparing the final energy input into the system in a 24 hour period, Figure 177 shows that the DV system with radiant cooling (Case 4) was the most energy efficient. Compared to this most efficient system, the DV system (Case 3) used 28% more energy, the VAV with radiant cooling system (Case 2) used 56% more energy, and the VAV system (Case 1) used 92% more energy. Thus the VAV system which is currently the most widely used HVAC system for cooling buildings is the least efficient of those tested.

5.4.8 Conclusions

Based on the results presented in this chapter, the following conclusions can be drawn about the relative energy efficiency of four ventilation systems. Out of the four ventilation systems considered, the Distributed Ventilation (DV) system with radiant cooling is definitely the most energy efficient. In the DV system, the vents are placed on the floor and therefore this system takes advantage of the natural convection of the air in the room, which rises as it heats up, thereby moving away from the area which needs to be cooled. The least efficient system tested is actually the most commonly deployed VAV system. The problem with the VAV system is that the single vent in the ceiling is not able to thoroughly mix the existing air in the room with the cold air injected by the vent. It is very expensive to retrofit the existing building with a DV system including the radiation slab. However, such an HVAC system should be seriously considered in the design of new buildings.

Chapter 6: Analysis of Ventilation Systems with the Inclusion of a Phase Change Material Layer in the Exterior Wall

6.1 3-D Room with PCM Included in Exterior Wall

In this study, we employ the same room model as described in Chapter 5 with changes in the exterior wall of the room to include a layer of PCM. In the exterior wall, a PCM layer was added between the air and plastic shade as shown in Figure 178. Table 2 shows the two types of PCM layers used, with their different thickness and material properties. In Table 2, PCM 1 is a cloth type PCM and PCM 2 is a panel type PCM, which are both commercially available PCM products. In the simulations reported in this chapter, the S-A turbulence model was employed instead of the realizable k-ε model used in Chapter 5. In addition, a different temperature curve was employed at the external wall in place of the ASHRAE curve shown in Figure 7. The new temperature curve was created for Sioux Falls, SD using the ASHRAE SolAir calculation which approximates all the heat transfer from convection, conduction and radiation on the surface of a building as an equivalent temperature.

To compare the effects of the addition of a PCM layer on the fluid flow and heat transfer in the room, five cases were run. The first three were VAV cases, the first of which

was without PCM, and the other two were with the two different types of PCM materials (PCM 1 and PCM 2) listed in Table 2. The last two cases were for a VAV system with radiant cooling, without and with the addition of a PCM layer. All the computational simulations utilized a mass flow rate of 0.0528 kg/s, a cold air temperature of 288.706 K (60F) and a computational time step of 10 seconds similar to the one employed in all the ventilation cases in Chapter 5. In the simulations, a PCM layer was added between the air and the plastic shade in the external wall.

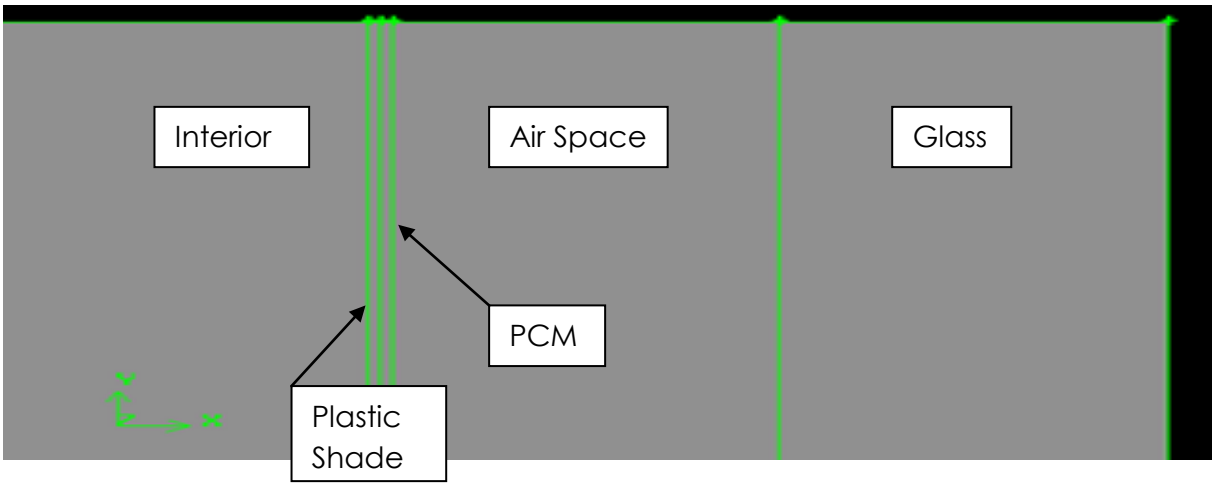

Figure 178: External Wall Treatment with PCM Layer

TABLE 2: Phase Change Material (PCM) Properties

Material	PCM 1	PCM 2
Thickness [in]	1/32	1/4
Cp [J/kg-K]	1700	2400
Melting Heat [kJ]	74.1	150
Melting Temperature [K]	297-305.3	304.2-306.2

6.2 Results

For all five cases ((a) VAV system without PCM, (b) VAV system with PCM 1 layer, (c) VAV system with PCM 2 layer, (d) VAV system with radiant cooling without PCM, and (e) VAV system with radiant cooling and PCM layer 1) detailed flow field and heat transfer calculations were performed using the methodology described in Chapter 5. Figures 179-183 show the mass flow rate through the vents for Cases (a)-(e) respectively. Figures 184-188 show the controller temperature and the average volume temperature throughout the day for Cases (a)-(e) respectively. Figures 189 and 190 show different ways of comparing the energy efficiency of the ventilation systems investigated with a PCM layer. By examining Figure 189, it is evident that the PCM 1 layer has a very minimal effect on the amount of cool air entering the room for the VAV system (Case (a)), and employing the PCM 1 layer results in a 4% reduction in cool air required for the VAV case with a Radiation Slab (Case (d)). However, for the VAV case with PCM 2 layer (Case(c)) a reduction of 42 % in cool air requirement is obtained for a 24 hour period.

Another interesting comparison to look at is the hot energy removed from the room in all cases (a)-(e). In order to calculate the hot energy removed from the room due to the injection of cold air, we numerically integrate the following equation (6.1):

$$\int \dot{m} * C_p * (T_{jet} - T_{Room-average}) dt \tag{6.1}$$

The energy removed by the radiation slab is calculated by numerically integrating equation (6.2):

$$\int flux * area * dt \tag{6.2}$$

where *flux* refers to the total surface heat flux transmitted from the radiation slab's surfaces into the room, and *area* refers to the total surface area of the radiation slab. The total energy removed from the room due to the cold air and the radiation slab is the sum of the above two equations (6.1) and (6.2) for the VAV system with radiation slab.

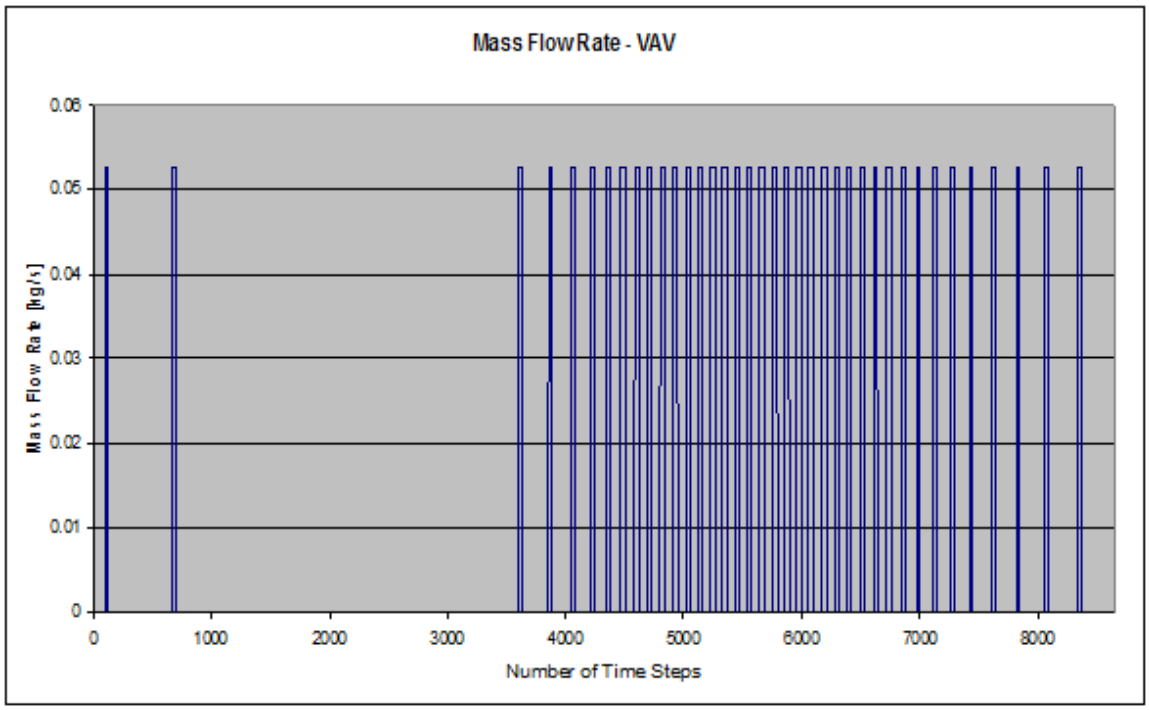

Figure 179: Mass Flow Variation for VAV System with 10 Second Time Steps

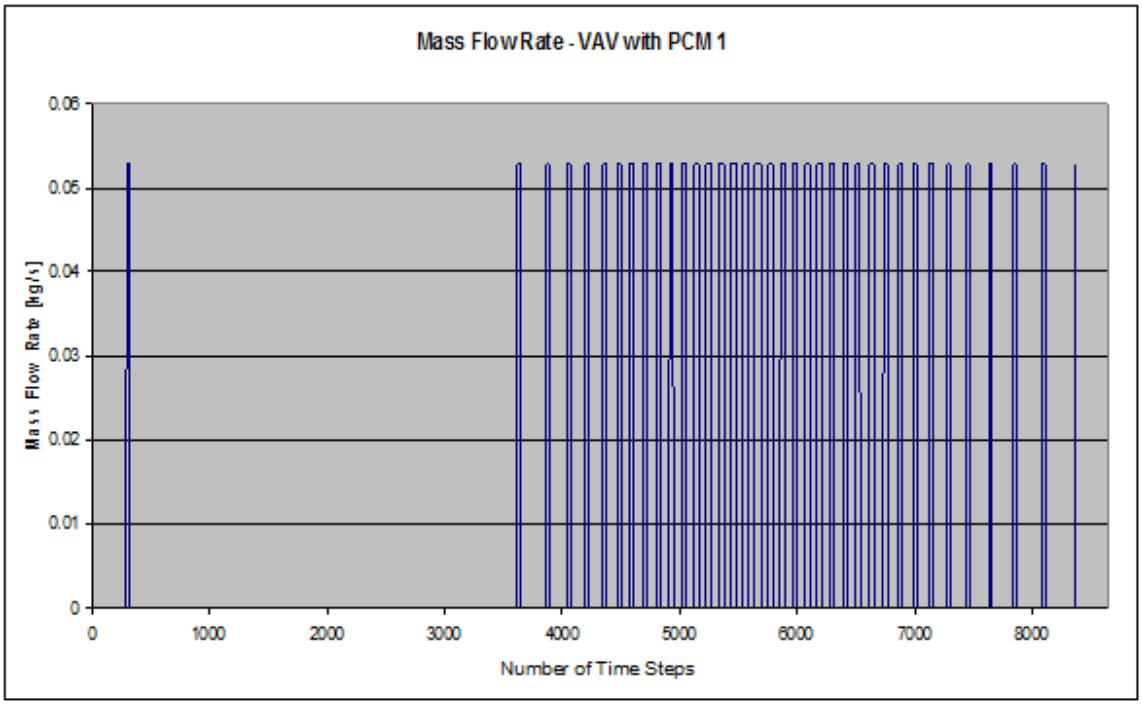

Figure 180: Mass Flow Variation for VAV System with PCM 1 with 10 Second Time Steps

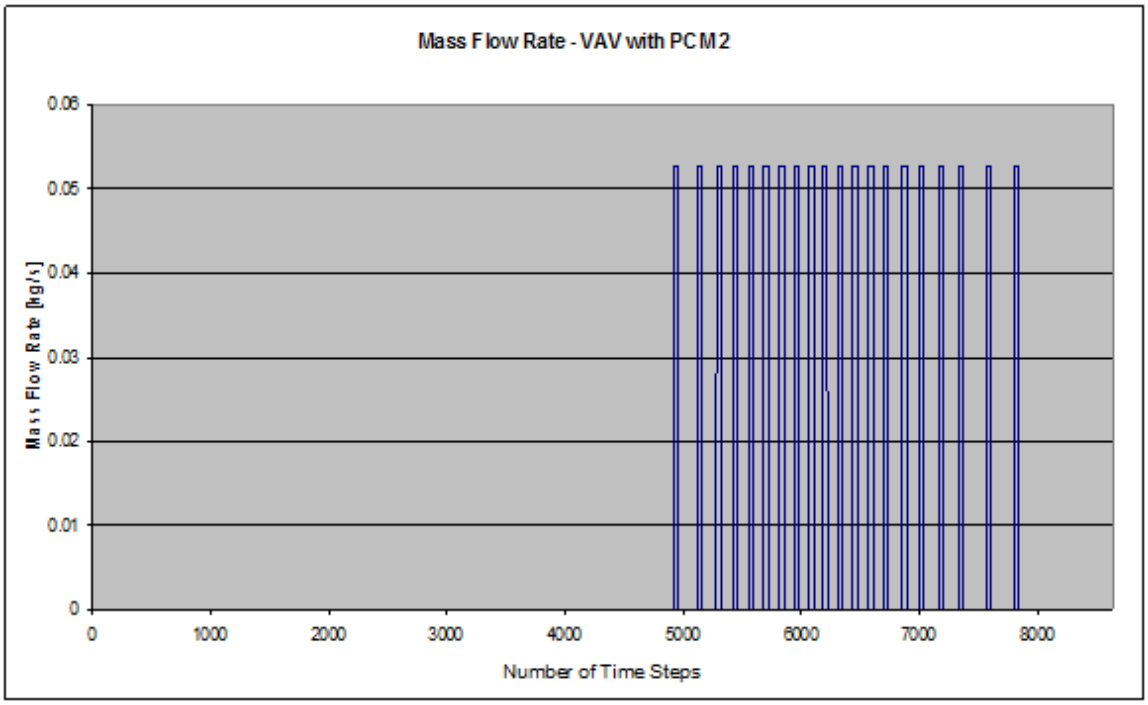

Figure 181: Mass Flow Variation for VAV System with PCM 2 with 10 Second Time Steps

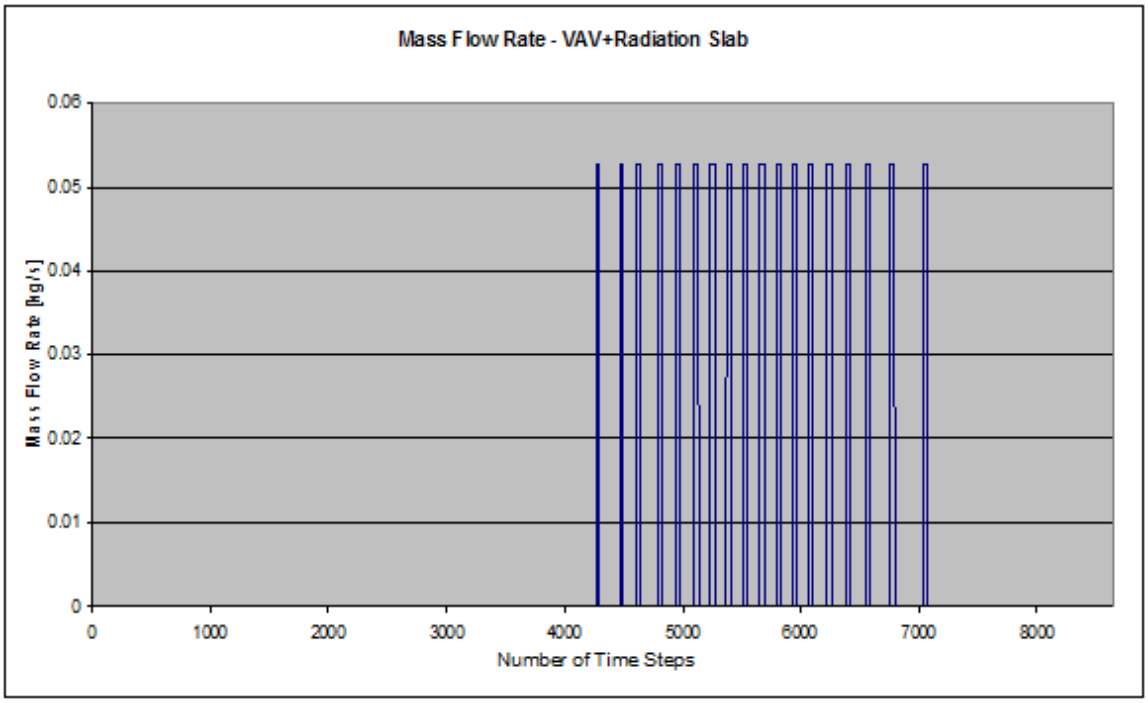

Figure 182: Mass Flow Variation for VAV System with Radiation Slab with 10 Second Time Steps

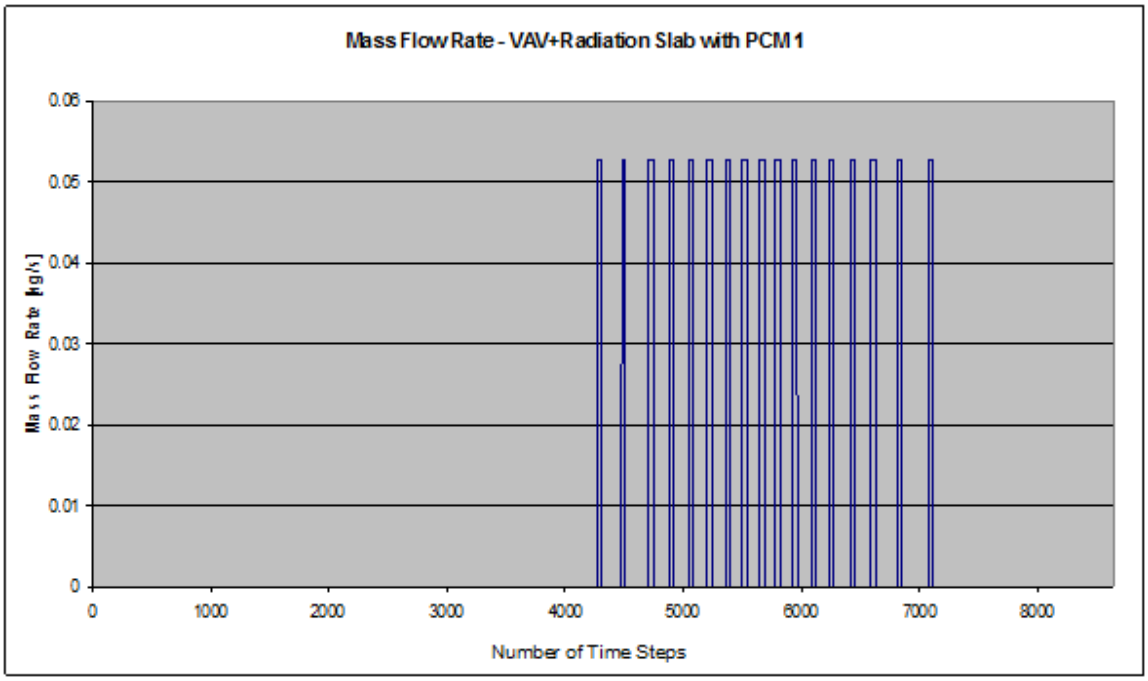

Figure 183: Mass Flow Variation for VAV System with Radiation Slab with PCM 1with 10 Second Time Steps

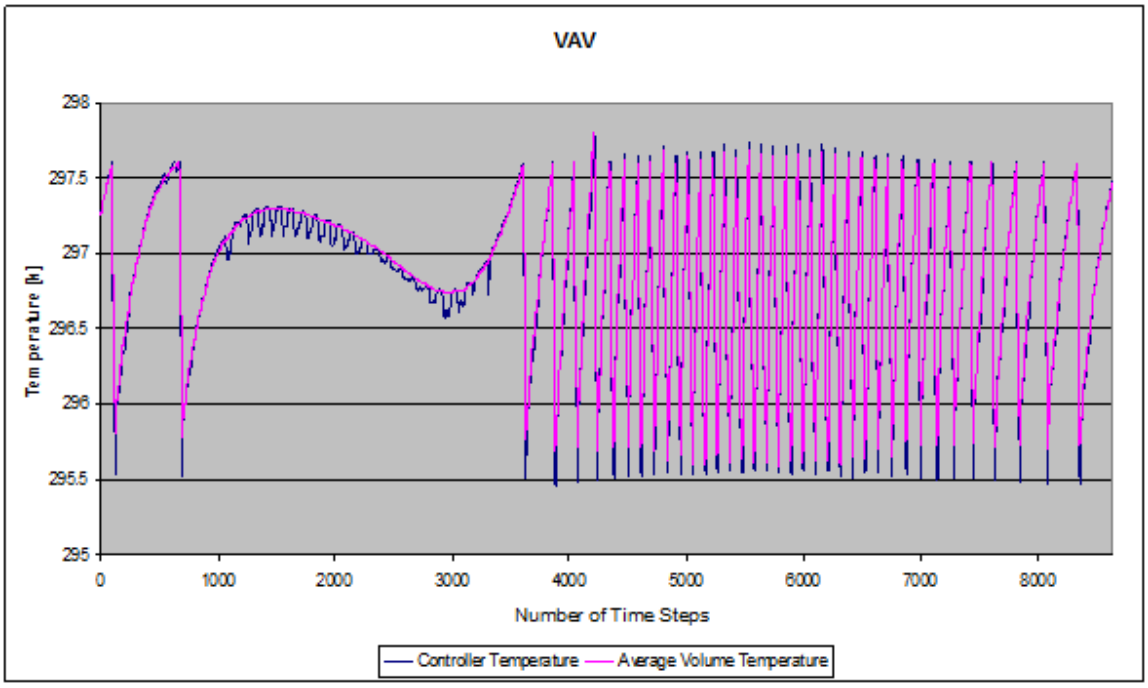

Figure 184: Controller and Average Room Temperature for VAV System with 10 Second Time Steps

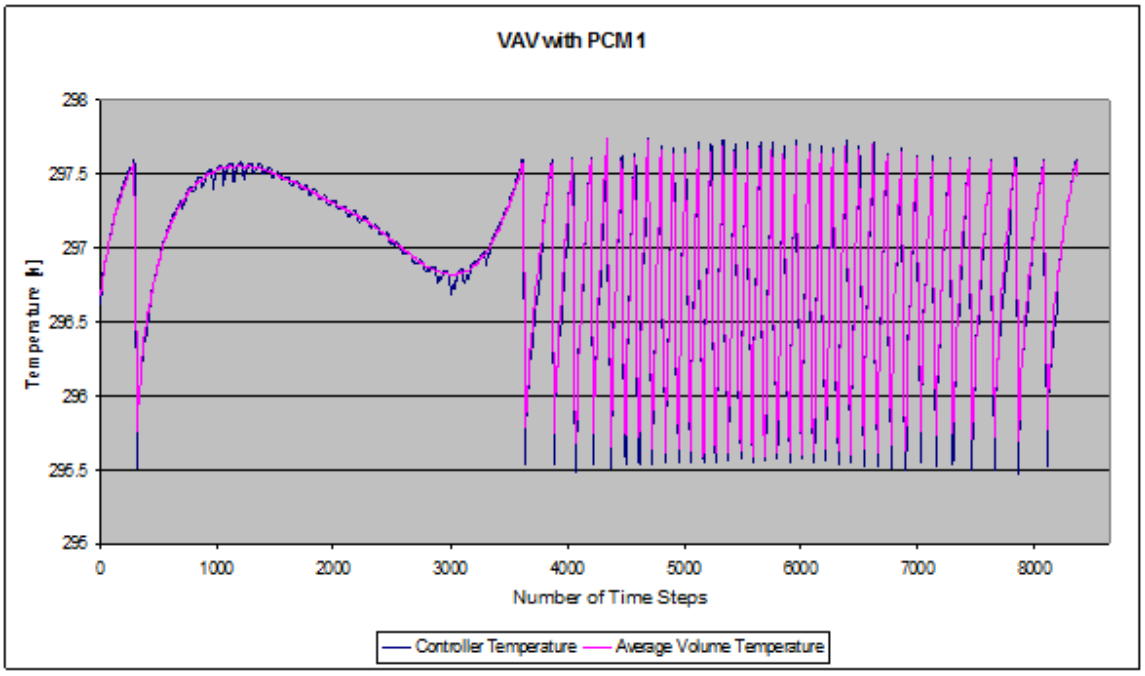

Figure 185: Controller and Average Room Temperature for VAV System with PCM 1 with 10 Second Time Steps

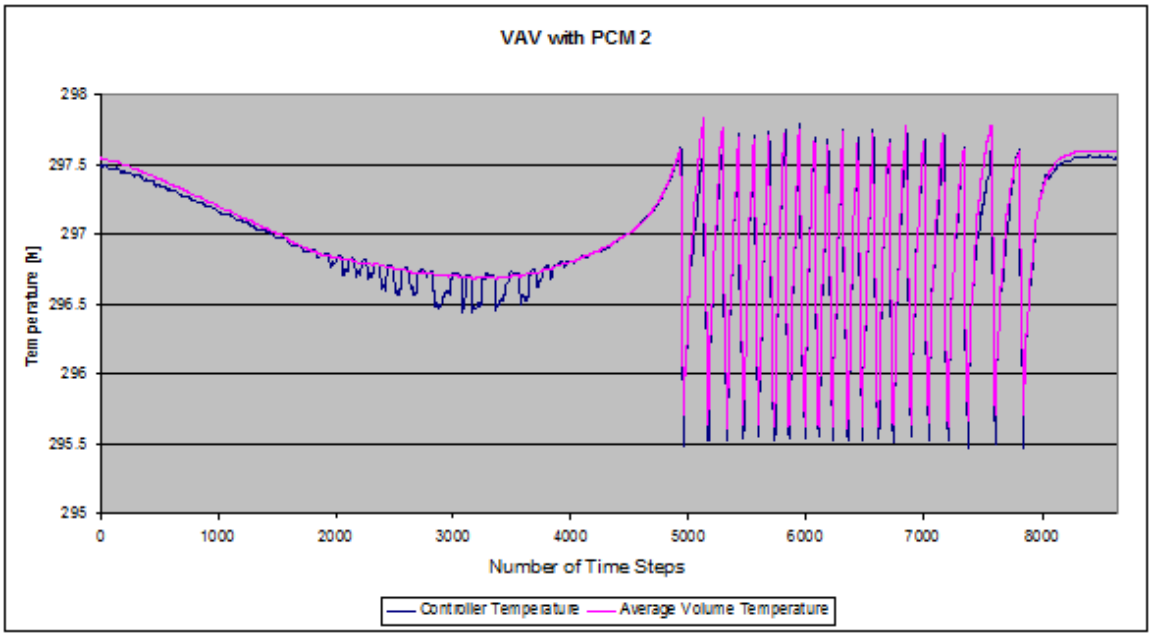

Figure 186: Controller and Average Room Temperature for VAV System with PCM 2 with 10 Second Time Steps

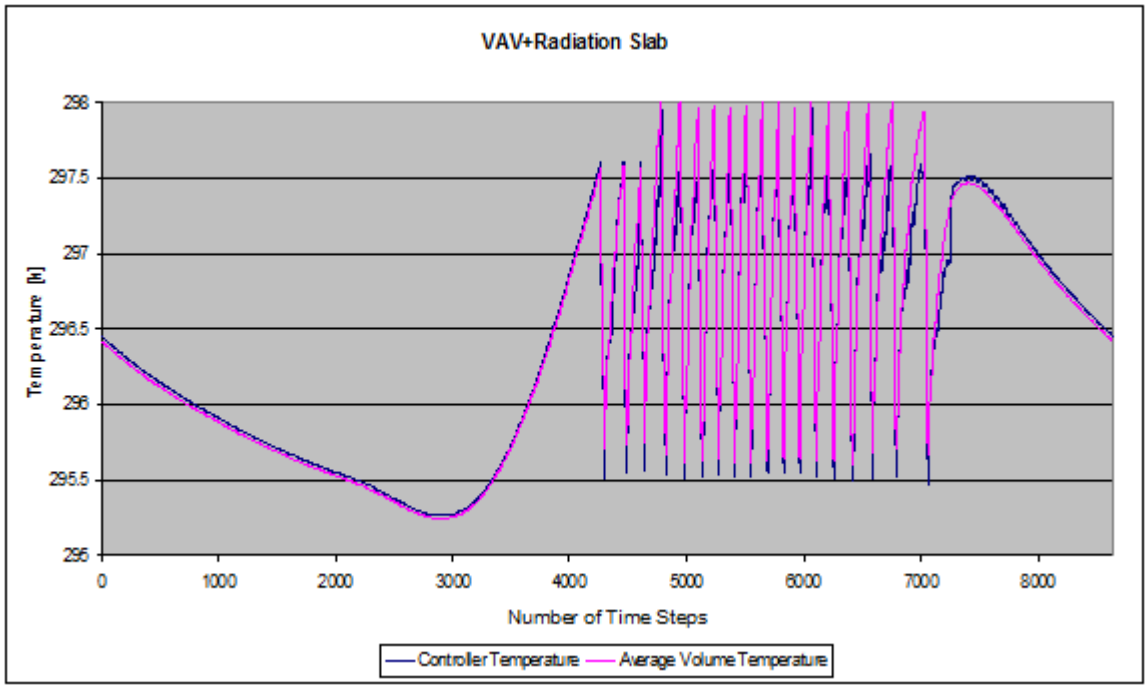

Figure 187: Controller and Average Room Temperature for VAV System with Radiation Slab with 10 Second Time Steps

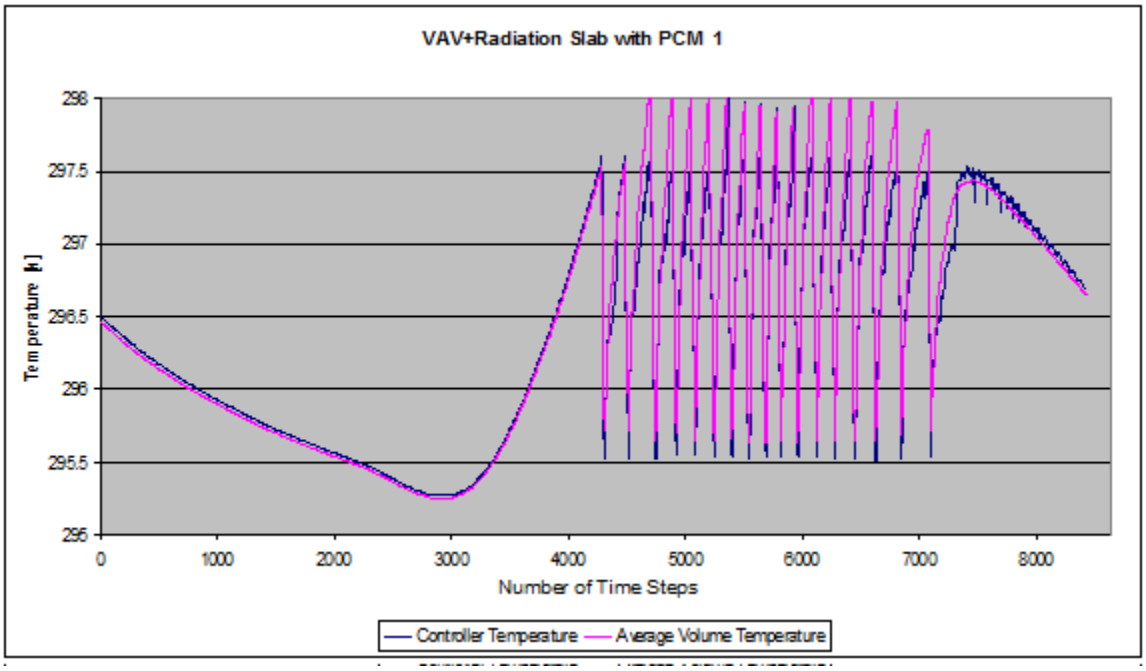

Figure 188: Controller and Average Room Temperature for VAV System with Radiation Slab with PCM 1 with 10 Second Time Steps

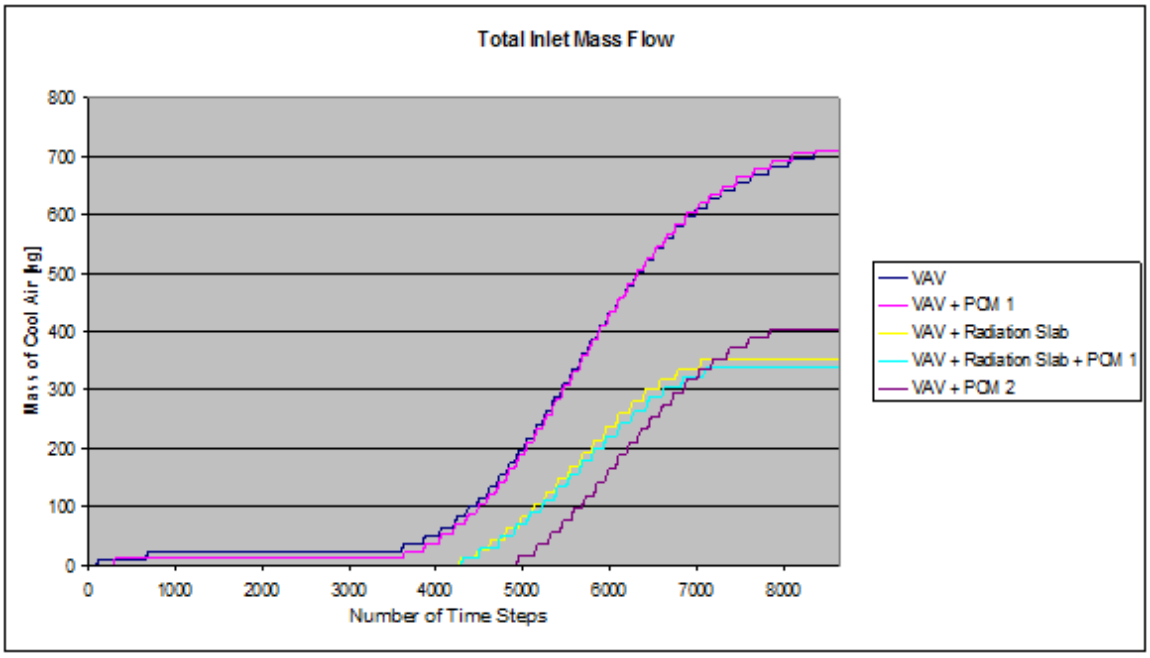

Figure 189: Total Mass Flow Comparison for Five Cases

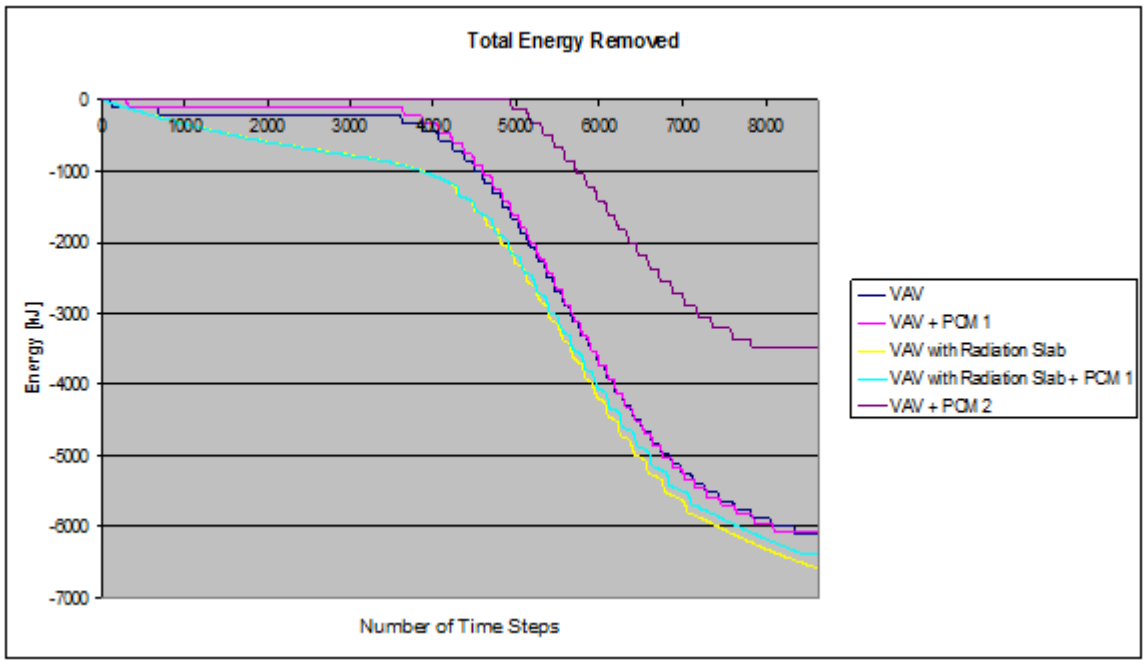

Figure 190: Total Hot Energy Removed from Room Comparison with 10 Second Time Steps

Figure 190 shows the energy removed from the room by various ventilation systems (a)-(e); this energy is removed by pushing the hot air through the outlet vent. These numbers are all negative; they show the amount of total energy needed to be removed from the room to maintain it within the desired temperature band. Therefore the VAV system (a) requires more hot energy removal by the system compared to the VAV system with a radiation slab, which requires less energy removal to maintain the desired temperature inside the room. The results also show that the PCM 1 layer has a minimal effect on the amount of energy required to be removed from the room with the VAV system. However when the PCM 1 layer is used with a VAV system with a radiation slab, there is a 3.2% reduction in energy needed to be removed from the room. On the positive side, the PCM 2 layer shows a significant reduction (43%) in the energy needed to be removed from the room to maintain the desired temperature.

6.3 Conclusions

Adding a layer of PCM in the external wall appears to be beneficial in all the five cases considered, however the energy savings appear to be linked to the thickness and properties of the PCM layer. A 1/32" thick layer of PCM material added into the exterior wall construction is just too thin to absorb enough heat to make it a worthwhile investment, however if a thicker PCM layer is used, the results are very encouraging. It is important to choose the PCM which has melting and solidifying temperatures close to the desired thermal comfort range of the room. This allows the PCM to fully melt and solidify during the 24-hour period at appropriate times, thus maximizing its effect and allowing it to perform at its full potential. The results with PCM layer do not seem to depend appreciably on the type of ventilation system used; they seem to depend primarily on the properties of the PCM chosen, and its placement in the exterior wall construction. Overall, inclusion of PCM in wall construction appears to have a positive effect on reducing the thermal loads on any HVAC system.

Chapter 7: Conclusions

The goal of the work presented in this thesis has been to determine the energy requirements for cooling a model 3-D office room using four different ventilation systems in order to determine their relative energy efficiency. The CFD simulation software FLUENT is used for this purpose.

In Chapter 3, two different turbulence models were analyzed: the one-equation Spalart-Allmaras (S-A) model and the two-equation k-ε model. It was determined that the difference in results obtained using these two different turbulence models was only about 1%. Although the S-A model is computationally more efficient, it requires a prior knowledge of turbulence length length scales inside the room which can result in inaccuracies in a complex 3-D flow environment. Therefore, the two equation realizable k-ε model was employed in the calculations since it calculates the turbulence length and time scales using k and ε which are modeled by the transport equations.

In Chapter 4, two different models for approximating the density inside the room were investigated, the constant density model and the Boussinesq model. By running two identical cases, only differing in the method of approximating the density, it was found that the solution with Boussinesq approximation required 5.4% more energy input compared to constant density approximation in order to maintain the same temperature inside the room. However, the Boussinesq approximation is more physically realistic for natural convective flow, therefore it was employed in all the calculations.

Four different ventilation systems were analyzed: Variable Air Volume (VAV) system, VAV with radiation slab, Displacement Ventilation (DV) system, and DV with radiation slab. Fluid flow and heat transfer variations inside the rooms during a 24 hour period were recorded and analyzed. The detailed temperature, velocity and turbulence quantities were calculated and used to determine the performance of the four ventilation systems for energy efficiency and thermal comfort. By examining the mass flow of air and energy required to keep the room within a comfortable band of temperature, it was found that the DV system with radiation slab was the most energy efficient, followed by the DV system, then the VAV system with radiation slab, and finally the VAV system was least energy efficient among the four. Retrofitting existing buildings with DV systems will be very expensive, and is not recommended. However, serious consideration should be given to the deployment of a DV system in new buildings to meet the HVAC requirements; furthermore this DV system could be augmented with the inclusion of a radiation slab for even better energy efficiency.

The energy efficiency performance of two of the four ventilation systems analyzed in Chapter 5 was further examined in Chapter 6 by including a PCM layer in the external wall of the model room. By running several cases with an actual ASHRAE SolAir curve and then examining both the mass flow and the energy removed from the room, it was determined that depending upon the properties of the PCM, the addition of the PCM layer in the external wall (window) of the room could result in significant energy savings. However, the correct PCM for a given climate must be chosen for it to be effective.

Finally, it is also important to note that the accuracy of the numerical solutions presented in this thesis is dependent upon a number of numerical parameters, namely the mesh size, the fluid flow model (we have employed the Unsteady Reynolds-Averaged Incompressible Navier-Stokes equations), the turbulence model (we have employed the two-equation realizable k-ε model), the density variation model (we have employed the Boussinesq approximation to account for the buoyancy effects) and the numerical scheme (we have used the first-order upwind scheme in a finite-volume framework). In addition, it is important to note that the solutions must be run over a number of 24 hour time cycles (at least a minimum of two) so that the effects of the initial conditions die down. In Chapter 3 and 4 respectively, we carefully examined the effects of various turbulence models and density models on the solution accuracy and concluded that the k-ε realizable turbulence model and the Boussinesq approximation for density variation should be employed in the calculations.

Chapter 8: Future Work

1. It was found that the average volume temperature in the room for four different ventilation systems differed from the temperatures recorded by the temperature controller at a single specified point in the room. Simulations should be conducted with the temperature controller reading the average volume temperature instead of temperature at a single specified point inside the room to determine the effect on the efficiency gains that can be obtained with different ventilation systems. In order to accomplish this, additional control points should be added in the room in order to bring the energy efficiency analysis closer to that based on the average volume temperature. This needs to be done during the hotter parts of the day.

2. Additional simulations should be conducted to determine the energy requirements for cooling in different climate conditions in different parts of the U.S and the world using the different ventilation systems. The influence of temperature controller setting on energy requirements should also be estimated since it is likely to be nonlinear. A more rigorous approach towards temperature control should be developed by creating a PID controller or a Model-Predictive Controller (MPC) for regulation of room temperature.

3. Additional simulations should be conducted to determine the effectiveness of different PCM in different climate conditions. It is likely that a PCM might effectively reduce the cooling energy requirements in one climate but not in another.

References

1) Linden, P. F., 1999, "The Fluid Mechanics of Natural Ventilation," Annu. Rev. Fluid Mech., 31, pp. 291-38.

2) Ürge-Vorsatz, D., Harvey, L.D., Mirasgedis, S., and Levine, M. D., 2007, "Mitigating CO_2 Emissions from Energy Use in the World's Buildings," Building Research and Information, 35, pp. 379-98.

3) Bourassa, N., Haves, P., and Huang, J., 2002, "A Computer Simulation Appraisal of Non-Residential Low Energy Cooling Systems in California," American Council for Energy Efficient Economy (ACEEE), Washington, DC, pp. 41–53.

4) Howe, M., Holland, D., and Livchak A., 2003, "Displacement Ventilation– Smart Way to Deal with Increased Heat Gains in the Telecommunication Equipment Room." ASHRAE Transactions, 109, pp. 323–327.

5) Harvey, L. D., 2009, "Reducing Energy Use in Buildings Sector: Measures, Costs, and Examples," Energy Efficiency, 2, pp.139-63.

6) Brandemuehl, M.J. and Braun, J.E., 1999, "The Impact of Demand-Controlled and Economizer Ventilation Strategies on Energy Use in Buildings." ASHRAE Transactions, 105, pp. 39–50.

7) Costelloe, B. and Finn, D., 2003, "Indirect Evaporative Cooling Potential in Air–Water Systems in Temperate Climates," Energy and Buildings, 35, pp. 573–591.

8) Harvey, L.D., 2006, *Handbook on Low-Energy Buildings and District-Energy Systems: Fundamentals*, *Techniques and Examples*, Earthscan, London.

9) Donnelly, P., Becker, R., and Dedorko, D., 2008, "PCM Membranes in Architectural Enclosures," Proc. of the Washington University McDonnell Academy Global Energy and Environment Partnership (MAGEEP), P. Biswas ed., pp.130-138.

10) Madireddi, S., 2009, "Meshing Techniques," Personal Communication.

11) Howell, R. H, Saur, H .J., and Coad, W. J., 1998, *Principles Of Heating Ventilation and Air Conditioning,* American Society of Heating, Refrigeration and Air-Conditioning, New York

12) Pérez-Lombard, L., Ortiz, J., and Pout, C., 2008, "A Review on Buildings Energy Consumption Information", *Energy and Buildings*, 40, pp. 394–398

13) Building Energy Codes Program. Web. 2008.
<http://www.energycodes.gov/why_codes/>.

14) Clean Energy. Web. 2008. < http://www.epa.gov/cleanenergy/energy-and-you/index.html>.

15) Energy Information Administration. "Emissions of Greenhouse Gases in the United States 2008," Washington, D.C.2008. Web. 22 Feb 2011.
http://www.eia.doe.gov/oiaf/1605/ggrpt/0573(2008).pdf

16) "Building Sector, Energy, CO2 Emissions - Current Situation - Architecture 2030." *Climate Change, Global Warming, and the Built Environment - Architecture 2030*. Web. 1 Feb. 2011.
<http://www.architecture2030.org/current_situation/building_sector.html>.

17) Korolija, I., "Influence of Building Parameters and HVAC System Coupling on Building Energy Performance." *Energy and Buildings* (2011). Web. 23 Feb 2011.
http://www.sciencedirect.com/science/articel/B6V2V-51YYNYM-3/2/cc56017a6cecf9e89af4a57e35730ffe.>

Vita

Jared T. Daiber

Date of Birth	April 10, 1988
Place of Birth	Breese, IL
Degrees	Washington University in St. Louis B.S./M.S., Mechanical Engineering May 2011